

**Modulations of Visual Cortex Organization Investigated with  
7 Tesla fMRI**

**Dissertation**

zur Erlangung des akademischen Grades

**Doctor rerum naturalium**

**(Dr. rer. nat)**

genehmigt durch die Fakultät für Naturwissenschaften  
der Otto-von-Guericke-Universität Magdeburg

von Master of Health Science, Aini Ismafairus Binti, Abd Hamid  
geb. am 17. Oktober 1985 in Perak (Malaysia)

Gutachter: Prof. Dr. rer. nat. habil. Oliver Speck  
Prof. Dr. med. Michael Nitsche

eingereicht am: 29. September 2015

verteidigt am: 12. Februar 2016

*To my family*

## ABSTRACT

Damage to the brain following trauma or stroke may result in neurological dysfunctions affecting visual perception, motor control, memory or language. With rehabilitation these deficits can improve. Alternating current stimulation (ACS) is a relatively new non-invasive brain stimulation technique that has been shown to alter brain rhythm activity in various experiments of motor, visual, somatosensory, and higher cognitive functions, but its effects on brain hemodynamic activation are not known. To gain more information about the ACS effect on brain activation, therefore in this thesis, the goal was to explore possible after-effects of transorbital ACS using high-resolution 7-Tesla functional magnetic resonance imaging (fMRI) based retinotopic mapping in patients with visual deficits and in normal subjects.

However, before the implementation of any fMRI paradigm, especially for the study of the effects of rehabilitation techniques, it is important to understand brain response patterns across time. Therefore in Study I, the goal was to assess the systematic changes in the activated cortical surface area, response amplitude and coherence in visual areas at three separate sessions in seven healthy subjects. The findings of the activated cortical surface areas, amplitude, and coherence showed that the initial scan (Session 1) introduced sequential effects and should be considered in future experiments.

In Study II, the goal was to explore the after-effects of repetitive transorbital ACS (rtACS) in visual areas in a patient with homonymous hemianopsia following a right posterior cerebral artery stroke. The findings of the activated cortical surface area, amplitude and coherence showed that rtACS may well have reorganized brain activity in the visual cortex. To further understand the changes of brain activity that underlie the transorbital ACS effects, a subsequent study, Study III, was done.

In Study III, the goal was to explore the after effects of transorbital ACS in visual cortex in five healthy subjects at two time points. All subjects randomly received both ACS and sham-transorbital ACS in different sessions. The transorbital ACS was delivered at the individual alpha frequency. The findings demonstrated that transorbital ACS modulates the activated cortical surface area, fMRI response amplitude, and coherence over time in visual cortex which outlasted the stimulation period.

In conclusion, these findings showed that transorbital ACS is able to alter plasticity in visual cortex in healthy subjects and in patient with visual deficits which out-last the time of stimulation.

# ZUSAMMENFASSUNG

Nach einem Trauma oder Schlaganfall kann es im Gehirn zu Schädigungen kommen, die zu neurologischen Störungen der visuellen Wahrnehmung, der Bewegung, des Gedächtnisses oder der Sprache führen. Durch Therapien können manche Defizite behandelt werden. Die ACS (Wechselstrom-Stimulation) ist eine relativ neue nicht-invasive Stimulationstechnik des Gehirns, die eine Änderung der rhythmischen Aktivität des Gehirns bei motorischen, visuellen, somatosensorischen und höheren kognitiven Funktionen in verschiedenen Experimenten gezeigt hat, jedoch sind hämodynamische Effekte nicht bekannt. Das Ziel dieser Dissertation war es, mehr Informationen über die Auswirkungen der ACS auf die Aktivität des Gehirns zu erhalten. Dazu wurden mögliche Folgeerscheinungen der transorbitalen ACS mit der Methode der funktionellen Magnetresonanztomografie im 7 Tesla MRT an Patienten mit visuellen Ausfällen und gesunden Probanden untersucht und der visuelle Kortex retinotop kartiert.

Zuerst war es notwendig das zeitliche Antwortmuster des Gehirns zu verstehen. Deshalb war das Ziel im ersten Teil der Arbeit (Studie I) die systematischen Veränderungen in den aktivierten Gebieten, sowie der Amplitude und der Kohärenz der Reaktion im visuellen Kortex festzustellen. Zu diesem Zweck wurden sieben Probanden an drei separaten Terminen im 7 Tesla MRT gemessen und retinotope Karten erstellt. Die Ergebnisse von Studie I zeigten sequentielle Effekte, die in zukünftigen Experimenten berücksichtigt werden müssen.

Im zweiten Teil der Arbeit (Studie II) wurden die Auswirkungen der wiederholten transorbitalen ACS an einem Patienten mit einer homonymen Hemianopsie, als Folge eines Schlaganfalls untersucht. Die Ergebnisse zeigten nach wiederholter transorbitaler ACS eine reorganisierte Gehirnaktivität im visuellen Kortex. Die Änderungen der Gehirnaktivität, die der transorbitalen ACS zugrunde liegen, wurden im letzten Teil der Arbeit (Studie III) untersucht.

In Studie III, war das Ziel, die Auswirkungen der transorbitalen ACS im visuellen Kortex an fünf gesunden Probanden zu zwei Zeitpunkten zu untersuchen. Alle Probanden erhielten randomisiert sowohl transorbitale ACS als auch pseudo-ACS in verschiedenen Sitzungen. Die Frequenz der transorbitalen ACS wurde für jeden Probanden individuell an Hand der alpha-Frequenz ermittelt. Die Ergebnisse zeigten, dass die Aktivierung im visuellen Kortex die Stimulationsperiode überdauert.

Generell wurde nachgewiesen, dass die transorbitale ACS eine andauernde Veränderung der Plastizität im visuellen Kortex induziert, sowohl bei gesunden Probanden als auch bei Patienten mit visuellen Defekten.



## ACKNOWLEDGEMENT

All praise to god who is the most gracious, most merciful. This thesis may never have been successful without the help of many generous people. My sincere gratitude must go to my supervisor, Prof. Dr. Oliver Speck. Many thanks for his guidance, advice, support and encouragement. I am very thankful to Prof. Dr. Michael B. Hoffmann from the Visual Processing Laboratory, Department of Ophthalmology for your guidance and advice especially in the data processing and knowledge of retinotopic mapping. Thanks to Dr. Carolin Gall and Prof. Dr. Berhanrd A. Sabel from Institute of Medical Psychology for your cooperation in the REVIS project, and guidance and advice especially regarding the non-invasive brain stimulation techniques.

I would like to thank the Malaysian Ministry of Education and the Universiti Sains Malaysia for a fellowship grant. With this fellowship grant, I managed to pursue my study at this level. Thanks to ERA-net neuron project “Restoration of Vision after Stroke (REVIS),” BMBF (grant nr: 01EW1210) for research funding.

I am also thankful to Astrid Wollrab for conducting the fMRI scans. Thanks to all members of the Department of Biomedical Resonance for sharing your knowledge and experience.

Special thanks to my father Abd Hamid Hanafi and mother Norlida Ahmad Yudin in Malaysia for your constant support and prayers for me. Their sacrifice in raising me and providing the best education possible is greatly appreciated, which I can never repay. Thanks to my sisters Aimi Noremezan, Alya Norasyikin and Amni Norwafiy who are always supporting me from behind.

I would like to thank Prof. Dr. Jafri Malin Abdullah from Universiti Sains Malaysia for his support, encouragement and valuable insight on science in Malaysia.

Last but not least, to those who have made contributions directly or indirectly thank you.

Courtesy and kindness from everyone will always be remembered. I will never forget all the priceless experience that I received during my PhD journey.

Finally thank you, terima kasih, danke, for everything.

# TABLE OF CONTENTS

ABSTRACT.....	iii
ZUSAMMENFASSUNG .....	iv
ACKNOWLEDGEMENT .....	v
TABLE OF CONTENTS.....	vi
LIST OF FIGURES .....	x
LIST OF TABLES.....	xvi
ABBREVIATIONS .....	xvii
CHAPTER 1 .....	1
INTRODUCTION .....	1
1.1    MOTIVATION .....	1
1.2    RESEARCH OBJECTIVE.....	4
1.3    ORGANISATION OF THE THESIS .....	4
CHAPTER 2 .....	5
BACKGROUND .....	5
2.1    THE VISUAL SYSTEM.....	5
2.1.1    Structure and Function of the Eye .....	5
2.1.2    Retina .....	7
2.1.3    Visual Pathway: Projection of Retinal Output to the Visual Cortex .....	9
2.1.4    Visual Field Representation.....	17
2.2    FUNCTIONAL MAGNETIC RESONANCE IMAGING .....	20
2.2.1    Magnetic Resonance Imaging.....	20
2.2.2    Functional Magnetic Resonance Imaging.....	28
2.2.3    Retinotopic Mapping .....	32
2.3    EFFECTS OF ALTERNATING CURRENT STIMULATION IN THE HUMAN BRAIN .....	40
2.3.1    Introduction.....	40
2.3.2    Basic Principle of ACS.....	41
2.3.3    Mechanism of Action.....	42

2.3.4	Neuromodulation by ACS and Effect on Behavior .....	46
2.3.5	Safety Issues.....	58
2.3.6	Summary and Future Direction.....	58
CHAPTER 3 .....		60
STUDY I: QUANTITATIVE ASSESSMENT OF VISUAL CORTEX FUNCTION WITH 7 TESLA fMRI: TEST-RETEST VARIABILITY .....		60
3.1	INTRODUCTION.....	60
3.2	MATERIAL AND METHODS .....	62
3.2.1	Subjects.....	62
3.2.2	Visual Stimulation for fMRI.....	62
3.2.3	fMRI Acquisition .....	63
3.2.4	Cortical Flattening .....	64
3.2.5	Preprocessing of Functional Images .....	64
3.2.6	Head Motion Assessment .....	66
3.2.7	Statistical Analysis.....	66
3.3	RESULTS.....	67
3.3.1	BOLD Signals.....	72
3.3.2	Reproducibility of Phase Maps.....	82
3.3.3	Head Motion .....	82
3.4	DISCUSSION .....	86
CHAPTER 4 .....		89
STUDY II: RETINOTOPIC MAPS IN EARLY VISUAL AREAS AFTER TRANSORBITAL REPETITIVE ALTERNATING CURRENT STIMULATION: A SINGLE CASE STUDY IN fMRI.....		89
4.1	INTRODUCTION.....	89
4.2	MATERIAL AND METHODS .....	90
4.2.1	Subject.....	90
4.2.2	Visual Field Measurement .....	91
4.2.3	Stimulation Protocol .....	91
4.2.4	Retinotopic Mapping For fMRI.....	92
4.2.5	fMRI Acquisition .....	92
4.2.6	Data Processing.....	93

4.3	RESULTS.....	94
4.3.1	Visual field tests.....	94
4.3.2	Functional Magnetic Resonance Imaging.....	98
4.4	DISCUSSION .....	103
CHAPTER 5 .....		110
STUDY III: VISUAL CORTEX ORGANIZATION AFTER TRANSORBITAL ALTERNATING CURRENT STIMULATION IN HEALTHY SUBJECTS WITH 7 TESLA fMRI.....		110
5.1	Introduction .....	110
5.2	Material and Methods.....	112
5.2.1	Subjects.....	112
5.2.2	Experiment Overview .....	112
5.2.3	Visual Stimulation for fMRI.....	113
5.2.4	fMRI Acquisition .....	114
5.2.5	Cortical Flattening .....	116
5.2.6	Preprocessing of Functional Images .....	116
5.2.7	Transorbital ACS Procedure.....	117
5.2.8	Statistical Analysis.....	118
5.3	RESULTS.....	118
5.3.1	Effects of ACS condition (ACS vs. sham).....	119
5.3.2	Effect of time (post-1 vs. post-2).....	119
5.3.3	Effects of brain hemisphere (left vs. right).....	119
5.3.4	Effects of tasks (eccentricity, polar angle, and full field).....	122
5.3.5	Interaction effects between ACS condition and time .....	122
5.3.6	Interaction effects between ACS condition and tasks.....	122
5.3.7	Interaction effects between ACS condition, time and tasks .....	122
5.3.8	Interaction effects between ACS condition and hemisphere .....	127
5.4	DISCUSSION .....	127
CHAPTER 6 .....		133
SUMMARY AND FUTURE DIRECTIONS.....		133
6.1	SUMMARY .....	133

6.2	CONCLUSIONS.....	138
6.3	FUTURE DIRECTIONS.....	139
	BIBLIOGRAPHY .....	140
	SELBSTÄNDIGKEITSERKLÄRUNG .....	159
	CURRICULUM VITAE.....	160
	PUBLICATIONS.....	162

## LIST OF FIGURES

Figure 1. Anatomy of the human eye (adapted from Prasad and Galetta (2011) and Purves et al. (2012))..... 6

Figure 2. The anatomy of the retina (Webvision, <http://webvision.med.utah.edu/book/part-i-foundations/simple-anatomy-of-the-retina/>)..... 7

Figure 3. Visual field information in the eye and the brain. Projections on the retinas are transmitted to the left and right visual cortices through the lateral geniculate nuclei. The red and green portions of the diagram represent the level of neural activity communicated between sections of the receptive fields in the eyes and other parts of the visual system (from Pinel (2011))..... 11

Figure 4. The six layers of the lateral geniculate nucleus and their projection to the striate cortex (from Purves et al. (2012))..... 11

Figure 5. The primary visual cortex contains discrete anatomical layers featuring individually-distinguished synapse connections. (A) Input from LGN neurons. M cell axons terminate in layer 4C $\alpha$ , P cell axons terminate in layers 4C $\beta$  and 4A, and K (I) cell axons terminate in layers 2 and 3. (B) Resident neural cells. Spiny stellate cells receive signals from LGN neurons. Smooth stellate cells comprise a local neuronal circuit and are not excitatory. Pyramidal cells emit axons to other areas of the brain and contribute to the overall inner-processing. (C) Processing circuitry originating from LGN axons and resident neural cells. Layers 2, 3 and 4B send signals to other cortical areas, layer 5 sends signals to the superior colliculus, and layer 6 sends signals to the LGN, ultimately forming a loop (From Lund (1988), via Teller ( 2013))..... 13

Figure 6. Representation of a cortical module. The primary visual cortex is arranged into modules which feature orientation columns arranged orthogonally to the ocular dominance columns. All cells behave similarly with respect to their receptive fields, in that they are responsive to the same part of the visual field. However, the cells vary in signal input (left or right eye), receptivity to orientation, color (blobs), and size (not shown) (from (Goebel et al., 2004). ..... 15

Figure 7. The 305 proposed feed-forward connections among the 32 visual areas. The colored rectangles represent the visual areas. Retinal input originates from the base of the diagram with V4 and MT in the middle. The parietal stream and ventral stream are situated to the left and right, respectively, though they are highly interconnected to one another. The represented connections as stipulated are feed-forward, but the majority of them are also capable of feedback signaling (from Van Essen et al. (1992)). ..... 16

Figure 8. The pathway is comprising the visual system. Different colors demarcate the different quadrants of the visual pathway and the paths taken by the visual impulses to reach the primary visual cortex, where the image is first perceived. The figure does not depict the fovea (from Wison-Pauwels et al. (2013))..... 19

Figure 9. Protons spin randomly when they are not under the influence of a magnetic field. The net sum of all the random movements equals zero. When the protons are influenced by a magnetic field, most move in the direction of the field and precess around an axis. The vector  $M$ , the so-called sum of magnetic moments, no longer equals zero (from <http://fontrcalculus.tumblr.com/post/70201405968/mri-basics>). ..... 22

Figure 10. Once under the influence of a magnetic field, the proton precesses in that field. The axis of precession and the main magnetic field (denoted by  $B$ ) are parallel to each other. The component of interest is the z component, which indicates the magnitude of rotation and maintains a constant direction irrespective of the proton's precession). Both the x and y components are dependent on time with a frequency  $\omega_0$  which relates to  $B_0$  as in equation (1-1) (from Brown and Semelka (2003))..... 23

Figure 11. Absorption of energy. In a rotating frame of reference, the RF pulse emitted at resonance frequency  $\omega_0$  produces an additional magnetic field  $B_1$  which is perpendicular to the main magnetic field  $B_0$ . If the protons are activated by a proper amount of energy at the required frequency, they then absorb that energy and rotate ( $M$ ) in the transverse plane, perpendicular to  $B_1$  and  $B_0$ . The pulse flip angle is the total amount of rotation performed by  $M$  (from Brown and Semelka (2003))..... 25

Figure 12. T1 Relaxation Curve. After a  $90^\circ$  RF pulse, no longitudinal magnetization is observed. A short time later, the protons begin to release their energy, resulting in longitudinal magnetization. With more and more energy being released,  $M_z$  begins to re-established. Once this process is completed,  $M_0$  returns to its original equilibrium orientation. The change of  $M_z / M_0$  over time  $\tau$  follows an exponential growth process. T1 denotes the time-constant, the so-called spin-lattice relaxation time, representing the time it takes for  $M_z$  to regain 63% of the original value (from Brown and Semelka (2003))..... 26

Figure 13. T2 decay curve. (a) This panel is applicable to a frame which rotates at a frequency slower than  $\omega_0$ . (1) Before the RF pulse is transmitted, net magnetization ( $M$ , arrow) is oriented parallel to  $B_0$  (not depicted in the plane). (2) After a  $90^\circ$  RF pulse, the protons initially precess in the transverse plane. (3) A short time later, the protons begin to lose their coherence and precess at varying frequencies. (4, 5) The synchronicity of protons in the transverse plane decreases gradually over time, (6) finally reaching a random configuration of the transverse component. (b) Depicts the  $M_{XY}$  component over time. The change in  $M_{XY} / M_{Xy\max}$  over time  $\tau$  follows an exponential decay process. T2 denotes the time-constant for this process, the so-called spin-spin

relaxation time, representing the time it takes for  $M_{XY}$  to decay to 37% of the original value (from Brown and Semelka (2003)).

Figure 14. BOLD fMRI. (a) Under normal conditions, the amount of deoxygenated hemoglobin is higher than the amount of oxygenated hemoglobin within the capillary bed. (b) In the active condition, increased neuronal activity leads to increased oxygenation of hemoglobin in the blood, which in turn leads to increased levels of oxygenated hemoglobin in the capillary bed. The corresponding decrease in the amount of deoxygenated hemoglobin caused this MRI image to brighten (from Hill and Wyse (2012), via Moseley and Glover (1995)).

Figure 15. The BOLD hemodynamic response function (HRF) (from Francis and Panchuelo (2014)).

Figure 16. T2\* curve: the relationship between the amount of T2\*-weighting and TE. A short TE results in a small difference between the activated state and the resting state, while a long TE results in no difference between the activated state and the resting state (from Stuart (1997)).

Figure 17. Visual fields and their corresponding areas in the cortex. (A) A visual field is described in terms of a fixation point denoted by F, a horizontal meridian denoted by HM, and upper and lower meridians in a vertical direction denoted by UVM and LVM. The polar angle increases in the clockwise direction and eccentricity increases from the fixation point towards the periphery of the visual field. (B) The occipital lobe is depicted in a medial cross-section, with abbreviations for parieto-occipital sulcus (PO), corpus callosum (CC) and calcarine sulcus (C). Dashed lines are used to depict both the upper and lower vertical meridians which mark the boundaries of visual areas V1 and V2. A part of the horizontal meridian runs along the calcarine sulcus but is not depicted in this view. The horizontal meridian also demarcates the boundaries between the dorsal and ventral parts of visual areas V2. (from Engel et al. (1997)).

Figure 18. Travelling-wave stimulation. Frames from sequences of expanding rings (A) and rotating wedges (B) are shown. The arrows show the moving direction of the sequences and are not included in the frames. (C) Visual field maps in the right hemisphere of a single subject, measured using expanding rings (left) or rotating wedges (right). The color mapping denotes eccentricity (left) or polar angle (right). The stimuli covers the center 20° radius (adapted from Wandell et al. (2007)).

Figure 19. Examples of stimulation electrode placements and neural oscillation. (A) Transcranial ACS: electrodes were placed over the parieto-occipital region (P09 (target) and PO10 (reference), according to the 10-10 system). (B) Transorbital ACS: four stimulation electrodes were positioned at or near the eyeballs (with eyes closed), and one electrode was positioned at the occipital pole as the reference electrode. (C) The model prediction of neural oscillation and neural firing patterns induced by ACS (adapted from Zaehla et al. (2010), Gall et al. (2011) and Battleday et al. (2014); from Abd Hamid et al. (2015a)).



Figure 20. The activated cortical surface area (mm <sup>2</sup> ) across sessions in V1, V2 and V3 for all visual stimulation conditions for subjects 1-7 (from Abd Hamid et al. (2015b) .....	68
Figure 21. The response amplitude (%) across sessions in V1, V2 and V3 for all visual stimulation conditions for subjects 1-7 (from Abd Hamid et al. (2015b).....	69
Figure 22. The coherence (Z-transformed values) across sessions in V1, V2 and V3 for all visual stimulation conditions for subjects 1-7 (from Abd Hamid et al. (2015b).....	70
Figure 23. The head motion (mm) across sessions for all visual stimulation conditions for subjects 1-7 (from Abd Hamid et al. (2015b).....	71
Figure 24. Projection of the response phases onto the flattened representation of the occipital pole for the left and right hemisphere for all subject during (a) eccentricity mapping, (b) polar angle mapping and (c) full field stimulation (response threshold: $p=0.05$ ). Typical eccentricity and polar angle maps were evident that covered the cortical expand activated during full field stimulation. There is a high degree of correspondence for the topographies across the three sessions within each stimulation condition (from Abd Hamid et al. (2015b)). .....	77
Figure 25. Quantitative comparison of the activated cortical surface area (mean $\pm$ SEM) across sessions in V1, V2 and V3 for all visual stimulation conditions. Significant effects were observed for the factors session and visual area as detailed in Results (from Abd Hamid et al. (2015b). ..	78
Figure 26. Quantitative comparison of the response amplitude (mean $\pm$ SEM) across sessions in V1, V2, and V3 for all visual stimulation conditions. Significant effects were observed for the factors session, stimulation condition, and visual area, and for the interaction of stimulation condition and visual area as detailed in Results (from Abd Hamid et al. (2015b))......	79
Figure 27. Quantitative comparison of coherence (re-transformed mean $\pm$ SEM of Z-transformed value) across sessions in V1, V2 and V3 for all visual stimulation conditions. Significant effects were observed for the factors session and stimulation condition as detailed in Results (from Abd Hamid et al. (2015b))......	80
Figure 28. Quantitative comparison of correlation of phase maps (re-transformed mean $\pm$ SEM of Z-transformed value) of between session 1 and session 2, and between session 2 and session 3 within defined visual for eccentricity and polar angle. No significant effects were observed as detailed in Results (from Abd Hamid et al. (2015b))......	83
Figure 29. Quantitative comparison (mean $\pm$ SEM) of head movement across sessions for all visual stimulation conditions. No significant effects were observed as detailed in Results (from Abd Hamid et al. (2015b). .....	84

Figure 30. Results of campimetric and perimetric visual field tests before and after 10-days rtACS. ....	96
Figure 31. Detection performance in visual field tests pre- and post-rtACS in (a) binocular computer-based campimetry (HRP) and (b) monocular static automated threshold perimetry (Twinfield Oculus).....	97
Figure 32. Structural magnetic resonance images in sagittal, coronal and axial view indicating the location of the patient’s occipital lesion. The white circle shows the location of lesion.....	98
Figure 33. Retinotopic maps before and after rtACS for eccentricity, polar angle and full field with the definition of ROIs on the (a) intact hemisphere and (b) damaged hemisphere at threshold $p=0.05$ . The black color shape shows the location of the lesion and the ROI2 showed the widespread spatial activation after rtACS.....	99
Figure 34. Zoom-in of selected visual areas in the retinotopic map before and after rtACS for eccentricity, polar angle and full field at threshold $p=0.05$ . ....	100
Figure 35. Experimental design. The fMRI scanned started with the initial session. Subsequently, in separate sessions, the subjects completed two blocks of visual stimulation tasks during fMRI scanning before and after stimulation (ACS- or sham-transorbital ACS). At each blocks three visual stimulation tasks were give: eccentricity, polar angle, and full field. All of the subjects received both ACS- and sham-transorbital ACS randomly in different sessions. To assess the effects of transorbital ACS in the early visual areas, the time series from visual cortex signals was inverted in time of one of the counter directions in the three visual stimulation types. ....	115
Figure 36. Retinotopic maps of sham- and ACS-transorbital ACS in the left hemisphere of a single subject. Maps of eccentricity, polar angle, and full field were projected onto the flattened surfaces of the occipital pole of the left hemisphere (response threshold: $p=0.05$ ).....	120
Figure 37. Retinotopic maps of sham- and ACS-transorbital ACS in the right hemisphere of a single subject. Maps of eccentricity, polar angle, and full field were projected onto the flattened surfaces of the occipital pole of the left hemisphere (response threshold: $p=0.05$ ).....	121
Figure 38. Quantitative comparison of the percent change over baseline for activated cortical surface area (mean±standard error of the mean) across time in the ACS- and sham-transorbital ACS for all of the visual tasks. Statistically significant interaction effects were observed for the factors of ACS condition, time, and tasks, as detailed in the Results section. ....	124
Figure 39. Quantitative comparison of the percent change over baseline for fMRI response amplitude (mean±standard error of the mean) across time in the ACS- and sham-transorbital ACS for all of the visual tasks. Statistically significant interaction effects were observed for the factors of ACS condition, time, and tasks, as detailed in the Results section. ....	125

Figure 40. Quantitative comparison of the percent change over baseline for coherence (mean±standard error of the mean) across time in the ACS- and sham-transorbital ACS for all of the visual tasks. Statistically significant interaction effects were observed for the factors of ACS condition, time, and tasks, as detailed in the Results section. .... 126

## LIST OF TABLES

Table 1. Examples of ACS studies in the healthy and diseased brain (from Abd Hamid et al. (2015a)) .....	49
Table 2. Results from repeated measures analyses for (a) the activated cortical surface area, (b) the responses amplitude and (c) coherence (from Abd Hamid et al. (2015b)). .....	81
Table 3. Results from repeated measures analyses of the head movement for (a) eccentricity, polar angle and full field and (b) eccentricity and polar angle (from Abd Hamid et al. (2015b)).	85
Table 4. The effect of rtACS on the percentage change over baseline of the activated voxels, amplitude and coherence in the different visual areas in the left and right hemisphere at threshold $p=0.05$ .....	102

## ABBREVIATIONS

ACS	Alternating current stimulation
BART	Balloon analog risk take
BOLD	Blood-oxygen-level-dependent
CSF	Cerebrospinal fluid
DLPFC	Dorsolateral prefrontal cortex
EEG	Electroencephalography
EPI	Echo planar imaging
FID	Free induction decay
fMRI	Functional magnetic resonance imaging
HH	Homonymous hemianopsia
HRF	Hemodynamic response function
LGN	Lateral geniculate nucleus
LTD	Long-term depression
LTP	Long-term potentiation
MEP	Motor evoked potential
MRI	Magnetic resonance imaging
NMR	Nuclear magnetic resonance
NMV	Net magnetization vector
PD	Parkinson's disease
PTZ	Pentylentetrazole
RAPM	Raven's Advances Progressive Matrices
RF	Radio frequency

rtACS	Repetitive transorbital alternating current stimulation
SNR	Signal-to-noise ratio
STDP	Spike-timing-dependent plasticity
tACS	Transcranial alternating current stimulation
TBI	Traumatic brain injury
TE	Echo time
tDCS	Transcranial direct current stimulation
TMS	Transcranial magnetic stimulation
tRNS	Transcranial random noise stimulation
TR	Repetition time
TS	Time series
TTCT	Torrance Test of Creative Thinking
V1	Primary visual cortex
V2	Visual area two
V3	Visual area three
V4	Visual area four

# CHAPTER 1

## INTRODUCTION

### 1.1 MOTIVATION

The visual cortex of the brain is the part of the cerebral cortex that processes visual information. The human visual cortex is divided into several functional areas with distinct local neural properties (Zeki and Shipp, 1988; Van Essen et al., 1992; Engel et al., 1994; Slotnick and Yantis, 2003; Warnking et al., 2002). The receptive fields of neurons in the visual cortex are organized retinotopically (Serenio and Allmann, 1991; Sereno et al., 1994), i.e., different parts of the visual field are laid out in an organized manner in the visual cortex, e.g., as a stimulus moves from the fovea to the periphery, the locus of responding neurons varies from the posterior to the anterior portions of the calcarine sulcus, the site of human primary visual cortex (Engel et al., 1994; Warnking et al., 2002). Therefore, retinotopic mapping on individual subjects is the gold standard method of defining visual areas and investigating brain responses in different regions. Thus, the knowledge of retinotopy, mapped by functional magnetic resonance imaging (fMRI) (Engel et al., 1994), allows for precise delineation of some low-order retinotopic visual areas (Serenio et al., 1995). The ability to measure visual field maps in the human brain using fMRI offers an exciting opportunity to locate the maps, see their overall spatial arrangement, and clarify their computational functions. One of the classical ways of doing this is to show the subjects two kinds of travelling wave stimuli, which are (1) a wedge that rotates around a central fixation point, and (2) a ring that expands out from the central fixation, and then look at the activation in the visual cortex (Engel et al., 1994).

The basic principle of fMRI retinotopic mapping using travelling wave (also called phase-encoding) stimuli has been the subject of several publications (Engel et al., 1994; DeYoe et al., 1996; Sereno et al., 1995). From these publications, many publications have revealed a great deal about human retinotopic maps and fMRI retinotopic mapping procedures (Engel et al., 1997; Dumoulin et al., 2003; Dumoulin and Wandell, 2008; Huk et al., 2002; Hagler et al., 2007;

Larsson and Heeger, 2006; Pitzalis et al., 2006; Schluppeck et al., 2005; Sereno et al., 2001; Silver et al., 2005; Swisher et al., 2007a; Schneider et al., 2004; Schneider and Kastner, 2005; Dougherty et al., 2003; Wandell and Wade, 2003; Wandell et al., 2000, 2007; Wandell and Winawer, 2011). Therefore, several years after fMRI-based retinotopic mapping procedures were well-established, several laboratories started exploring cortical visual responses in subjects with various types of visual dysfunction (Morland et al., 2001; Slotnick et al., 2002; Hoffmann et al., 2003, 2012a; Hadjikhani et al., 2004; Conner et al., 2007; Reitsma et al., 2013a). These visual dysfunction studies provide a unique opportunity to examine how the human visual cortex deals with abnormal visual inputs and experience. The application of the fMRI-based retinotopic mapping procedure in the studies of visual dysfunction holds promise toward furthering our understanding of plasticity in the human visual cortex. This could lead, in turn, to the development of a rehabilitation program with probable beneficial effects to improve the quality of life.

Research has demonstrated that patients suffering from neurodevelopment disorders or cortical damage may develop visual, language, and memory dysfunctions, depending on the parts of the brain affected. These dysfunctions prevent the patients from performing their daily activities and eventually affect their quality of life (Gall et al., 2011; Dimyan and Cohen, 2011; Shah et al., 2013; Morland et al., 2001; Conner et al., 2007). There is substantial evidence, however, showing that invasive and non-invasive and behavior therapy techniques can achieve the recovery of affected regions and ensure that the patients can regain functionality, although not as before (Sabel et al., 2011a; Dimyan and Cohen, 2011; Shah et al., 2013; Hamilton et al., 2011). These techniques have both advantages and disadvantages (see chapter 1.3 for further discussion). In the work of this thesis, a non-invasive method, namely transorbital alternative current stimulation (ACS), was explored. The non-invasive techniques are inexpensive and have the potential to influence both cortical and sub-cortical areas, to the extent that they provide neuroplastic changes in the brain (Nardone et al., 2014). Currently, there are only a limited number of researches that have reported beneficial effects of ACS on the clinical population, for example, patients with Parkinson's disease (Brittain et al., 2013; Krause et al., 2013) or patients with visual impairment (Sabel et al., 2011a; Gall et al., 2011; Fedorov et al., 2011; Bola et al., 2014). The ACS technique could become the best option in the therapeutic field of brain stimulation because of its low incidence of side effects. Although many studies have reported the



beneficial effects of ACS, only a few have reported the mechanism and functional reorganization achieved by the technique. The current evidence remains sparse and more knowledge and scientific evidence is required to be better able to apply ACS therapeutically. Therefore, incorporating neuroimaging techniques such as fMRI is suggested to evaluate the effects of the ACS brain stimulation technique. To date, there have been a few recent studies using combined experiments such as transcranial direct current stimulation (Antal et al., 2011; Holland et al., 2011; Clark et al., 2012; Meinzer et al., 2014) and transcranial random noise stimulation (Chaieb et al., 2009). This is a particularly interesting approach because it provides information regarding functional activations and ACS modulation.

In this thesis, the reorganization of early visual areas following hemianopia after repetitive transorbital ACS (rtACS) was explored by using high resolution 7T fMRI-based retinotopic mapping. However due to stringent inclusion and exclusion criteria for 7T-fMRI, only one patient was suitable after screening a total of 78 potential patients. To provide more information about the application of transorbital ACS as a rehabilitation program, the after-effects in the early visual areas of five healthy subjects were explored. However, a longitudinal fMRI study should carefully evaluate activation across sessions to determine the eligibility of inclusion of all time points. Therefore, the quantitative assessment of systematic variations in activated cortical surface area, amplitude, and coherence across sessions were determined by using fMRI-based retinotopic mapping in order to provide guidance in the methodological issues of longitudinal fMRI-studies.

## **1.2 RESEARCH OBJECTIVE**

A number of studies showed the benefits of a high resolution 7 Tesla in fMRI studies (Hoffmann et al., 2009; Beisteiner et al., 2011). Previous studies demonstrated that high-resolution 7 Tesla fMRI allows higher functional sensitivity (Hoffmann et al., 2009; Beisteiner et al., 2011). Therefore, the present study used high-resolution 7 Tesla fMRI to explore the visual cortex organization in the healthy subjects and a patient.

There were three specific objectives of this thesis.

- (1) To evaluate inter-session systematic variations in spatial activation, response amplitude and coherence in the early visual areas by using 7 T fMRI-based retinotopic mapping.
- (2) To explore the effect of transorbital ACS in the early visual areas of a patient with homonymous hemianopia by using 7 T fMRI-based retinotopic mapping.
- (3) To explore the effect of transorbital ACS in the early visual areas of healthy subjects by using 7 T fMRI-based retinotopic mapping.

## **1.3 ORGANISATION OF THE THESIS**

This thesis starts with an introduction in Chapter 1. In this introduction, I highlight the motivation of doing the present study, research objectives and the thesis organization. Chapter 2 provides background including these three topics: (1) the visual system pathways to provide a background on visual processing, (2) the basic theory of MRI and fMRI, and also retinotopic mapping with fMRI, (3) the mechanism of action and the evidence for ACS modulated brain activity. Chapter 3 discussed the first study (Study I), which is the quantitative assessment of visual cortex function with 7 Tesla fMRI – test-retest variability. Chapter 4 discussed the second study (Study II), which is the reorganization of the visual cortex after repetitive transorbital ACS in a homonymous hemianopsia patient measured with 7 Tesla fMRI. Chapter 5 discussed the third study (Study III), which is the reorganization of the visual cortex after transorbital ACS in the healthy subjects measured with 7 Tesla fMRI. The final part of this thesis is chapter 6. In chapter 6, I summarize the present findings and highlight a few suggestions that are worth to be considered particularly to improve future studies.

## **CHAPTER 2**

### **BACKGROUND**

#### **2.1 THE VISUAL SYSTEM**

The visual system is the sensory system that is responsible for collecting and processing images of the things we see around us. The visual system begins with the eye. The eye collects information in the form of light that is reflected from objects that we see. The light information is in the form of electromagnetic energy in the visible spectrum, which can be detected by the human eye and has wavelengths in the range from about 390 nm to 700 nm (Starr et al., 2006). The retina initially processes visual information and relays it via visual system pathways to the primary visual cortex for further visual processing. In this section, these visual system pathways are discussed to provide a background to visual processing.

##### **2.1.1 Structure and Function of the Eye**

The visual pathway begins in the eye. The eye is the primary organ in the visual system that is responsible for collecting visual information, namely, light, from reflected images or objects and converting the information into neural signals in the retina (Prasad and Galetta, 2011) for further visual processing.

Figure 1 shows the structure of the human eye. The human eye has three layers: the sclera, the choroid and the retina (Purves et al., 2012). The sclera is the outermost layer of the eye, also known as the white of the eye, and comprises tough and fibrous tissue (Purves et al., 2012) that serves to maintain the shape of the eye and protect it from injury. The choroid is the middle layer that lies between the sclera and the retina, which contains blood vessels to nourish the retina. The retina is the innermost layer, which contains light-sensitive nerve cells that transmit visual information via optic nerves to the visual cortex for further visual processing.

Light enters the eye through the cornea, the front part of the eye that is covered by transparent tissue. The light then passes through the pupil, the small circular opening in the iris. The iris is the colored part of the eye that controls the amount of light entering the eye and reaching the retina. The size of the pupil adjusts according to the brightness of the light and is controlled by the pupillary sphincter and dilator muscles in the iris. The iris constricts (shrinks) the pupil in bright light to allow less light to enter the eye and dilates (enlarges) the pupil in dim light so that more light can enter the eye. The lens of the eye is located behind the iris and is responsible for focusing refracted light onto the retina. The lens is encircled by the ciliary muscles, which enable control of the shape of the lens during the focusing process. The lens is made thicker for focusing on nearby objects and thinner to focusing on distant objects. Apart from the above-described eye structures, the eye is also filled with a fluid environment called the aqueous and vitreous humor. The aqueous humor is a clear fluid found in the anterior chamber, the space between the back of the cornea and in front of the lens. The aqueous humor plays a role in refracting light rays and maintaining intraocular pressure. The vitreous humor is a clear and thick glutinous substance found in the posterior chamber, the space between the back of the lens and the retina. The vitreous humor is responsible for light transmission, holding the retina in position, and giving shape to the eye.

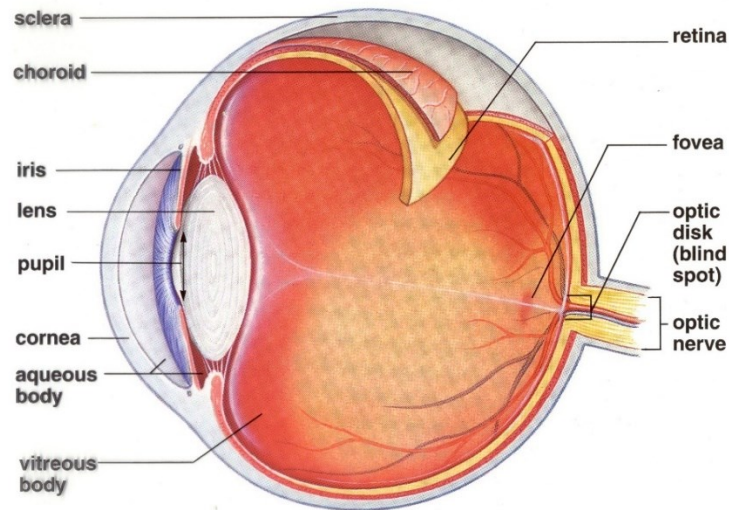


Figure 1. Anatomy of the human eye (adapted from Prasad and Galetta (2011) and Purves et al. (2012))

### 2.1.2 Retina

The retina is a light-sensitive tissue containing photoreceptors that line the inside of the back of the eye. Light rays focus onto the retina after passing through the cornea, pupil, lens and vitreous humor. The purpose of the retina is to convert the received photons into electrical or neural signals to transmit to the brain.

Figure 2 shows the anatomy of the retina. The retina is structured into several layers. Photons must travel through all layers of cells in the retina to reach the layer of photoreceptors, cells that play a role in converting the received photons into neural signals for further visual processing. Therefore, photons must pass through the nerve fiber layer, the ganglion cell layer, the inner plexiform layer (in which the layer of retinal ganglion cells synapse with bipolar and amacrine cells), the inner nuclear layer (containing bipolar cells, amacrine cells and horizontal cell bodies), the outer plexiform layer (where the bipolar cells and horizontal cells synapse with the photoreceptor cells) and the outer nuclear layer (containing cells bodies and nuclei of rods and cones). The layer of cells after the photoreceptors is the retinal pigment epithelium. The retinal pigment epithelium is responsible for nourishing cells in the retina and absorbing any scattered light (intraocular light) that has passed through the photoreceptor layer to improve the quality of vision (Prasad and Galetta, 2011; Purves et al., 2012).

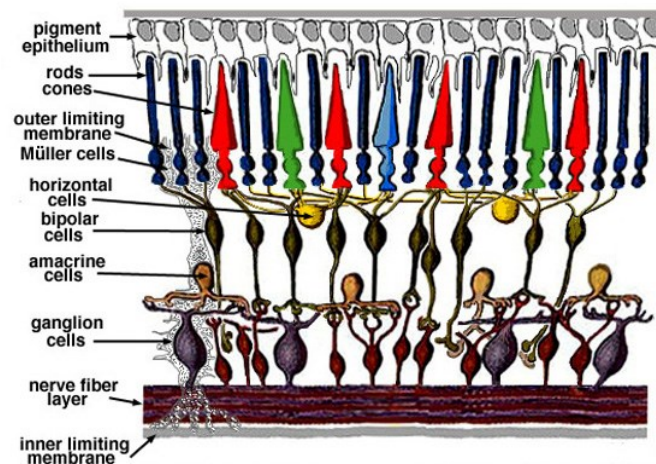


Figure 2. The anatomy of the retina (Webvision, <http://webvision.med.utah.edu/book/part-i-foundations/simple-anatomy-of-the-retina/>)

Photoreceptors consist of two types of cells, rods, and cones. In humans, photoreceptors contain about 120 million rods and 6 million cones (Goebel et al., 2004). Each type of photoreceptor is sensitive to different wavelengths of lights. Rods are more sensitive to low light and are responsible for night vision (scotopic vision). Anatomically, rods are concentrated towards the outer edges of the retina, making them important in peripheral vision. Unlike rods, cones are less sensitive to low light but more sensitive to color, thus contributing to color vision (photopic vision). Anatomically, cones are concentrated at the center of the retina (fovea), making them responsible for providing high spatial acuity. In humans, there are three types of cone cells, each responsible for specific wavelengths of light: (1) S cones, which are sensitive to short wavelengths (420 nm, blue); (2) M cones, which are sensitive to middle wavelengths (531 nm, green); and (3) L cones, which are sensitive to long wavelengths (559 nm, red). Therefore, each type of photoreceptor uniquely processes and responds to the light intensity at a specific wavelength.

After the light information has been uniquely extracted and processed, the produced signals are then projected from the retina onto the brain. There are four major types of neurons in the retina that are involved in these processes: horizontal cells, bipolar cells, amacrine cells and ganglion cells. In the retina, ganglion cells are the final output neurons that collect electrical messages regarding the visual signal and transmit information to the brain. To relay visual information to ganglion cells, there are two types of connections or pathways involved: (1) straight-through connections, or vertical pathways, in which photoreceptors connect to bipolar cells and convey the information to retinal ganglion cells, and (2) lateral pathways, in which information from photoreceptor cells is transmitted to ganglion cells via horizontal cells and amacrine cells, which allows other elements in the retinal layers to relay information for further processing. Additionally, before the electrical signals corresponding to visual information are conveyed to the brain, such visual information undergoes extensive additional processing in the ganglion cells. Kuffler (1953) found that each ganglion cell has a different response pattern, either “on”- center or “off”-center. The response patterns reflect the receptive field structure or retinotopic map differences of illumination levels or local changes in light intensity. Another process that is also involved is the splitting of the visual information into specific ganglion cells. There are three types of ganglion cells: midget cells (80% of ganglion cells), parasol cells (10% of ganglion cells), and other types (10% of ganglion cells). Each ganglion cell type has different

functions in the detection of visual input and also forms a separate pathway to reach its target in the lateral geniculate nucleus (LGN). Midget cells receive inputs from cones conveyed by bipolar cells that presume color-opponent response properties with a spectral selection of red-green or blue-yellow. According to De Monasterio and Gouras (1975), midget cells have small receptive fields and allow relatively high visual acuity. In the retina, the fovea is the region that contains a high concentration of midget ganglion cells and therefore exclusively provides high acuity and high color sensitivity. The anatomical features of midget cells allow them to specialize in color vision and high spatial resolution (e.g., object recognition features such as pattern and texture, but with low temporal resolution). Midget cells form a projection to parvocellular layers of the LGN, the so-called “P” pathway. Parasol cells receive inputs from a relatively large number of rods and cones. Parasol cells have relatively larger receptive fields that give a low spatial resolution. The anatomical features of parasol cells allow them to specialize in low spatial resolution and provide high temporal resolution (e.g., motion detection). Parasol cells form a projection to magnocellular layers of the LGN, the so-called “M” pathway. Another type of ganglion cell has been identified, the small bistratified cells (Yamada et al., 2005; Martin, 1998), which form a projection to koniocellular layers of the LGN, the so-called “K” pathway. Bistratified cells received inputs from intermediate numbers of rods and cones and are presumed to have a moderate spatial resolution and moderate temporal resolution. They are likely to be involved in color vision (Dacey, 1993; Martin, 1998).

### **2.1.3 Visual Pathway: Projection of Retinal Output to the Visual Cortex**

As discussed above, light energy from photons is converted into neural signals in the retina. Additionally, there are other processes that are also involved in sending a neural signal to the visual cortex for further processing. Neural signals corresponding to visual information are delivered by ganglion cell axons leaving the retina through the optic disk, the point of exit for ganglion cell axons leaving the eyeball. The optic disk is also called a blind spot because it does not have any receptors. Then, neural signals from the optic disk travel through the optic nerve and are conveyed to the optic chiasm, where the optic nerves partially cross. The crossing over of optic nerves at the optic chiasm enables the gathering of information from the same hemifield of the visual field from both eyes. Figure 3 shows the visual field projection from the eye to the brain via the optic chiasm. The total area of surrounding images entering both eyes while they

are focused on a central point is generally called the visual field. The visual field can be divided into the left hemifield and the right hemifield. The objects from the left and right hemifields fall on the temporal and nasal halves of both eyes. The objects in the left visual hemifield fall on the nasal retina of the left eye and the temporal retina of the right eye, while objects in the right visual hemifield fall on the nasal retina of the right eye and temporal retina of the left eye. At the optic chiasm, visual information from the two nasal hemiretinas cross, while those from the two temporal hemiretinas (that see opposite halves of the visual field) do not cross. Information from the nasal hemiretina of the left eye crosses and joins information from the temporal hemiretina of the right eye, while information from the nasal hemiretina of the right eye crosses and joins information from the temporal hemiretina of the left eye.

Next, information that partially crosses at the optic chiasm relays neural signals to the LGN via optic tracts. The LGN is the main central structure of the brain that relays visual information from the optic nerve to the visual cortex. In primates, the LGN is arranged in six neuronal layers. Figure 4 show the layers of the LGN, which are numbered from 1 to 6. Layers 1 and 2 are magnocellular (M) layers that contain relatively large cells that receive inputs from parasol ganglion cells. Layers 3-6 are parvocellular (P) layers that contain relatively small cells that receive inputs from midget ganglion cells. In addition, in between the six major layers of the LGN are intercalated or koniocellular layers that contain relatively tiny or dust-like cells. In the LGN, inputs of visual information relayed from retinal ganglion cells are highly organized. Each left and right LGN receives inputs from both eyes. Inputs from the ipsilateral eye (temporal retina) are projected to layers 2, 3 and 5, while inputs from the contralateral eye (nasal retina) are projected to layers 1, 4 and 6. Moreover, each layer of the LGN accommodates an organized topographic map: the upper visual field projects inferior laterally in the LGN, and the lower visual field projects superior medially in the LGN. Additionally, magnocellular layers contain neurons that are more sensitive to contrast and responsive to motion or movement, making them responsive to the “where” properties of visual information. In contrast, the parvocellular layers contain neurons that respond weakly to motion or movement but are sensitive to color vision, making them responsive to the “what” properties of visual information. Neural signals that are carried from each layer in the LGN is relayed through the optic radiation to the visual cortex.



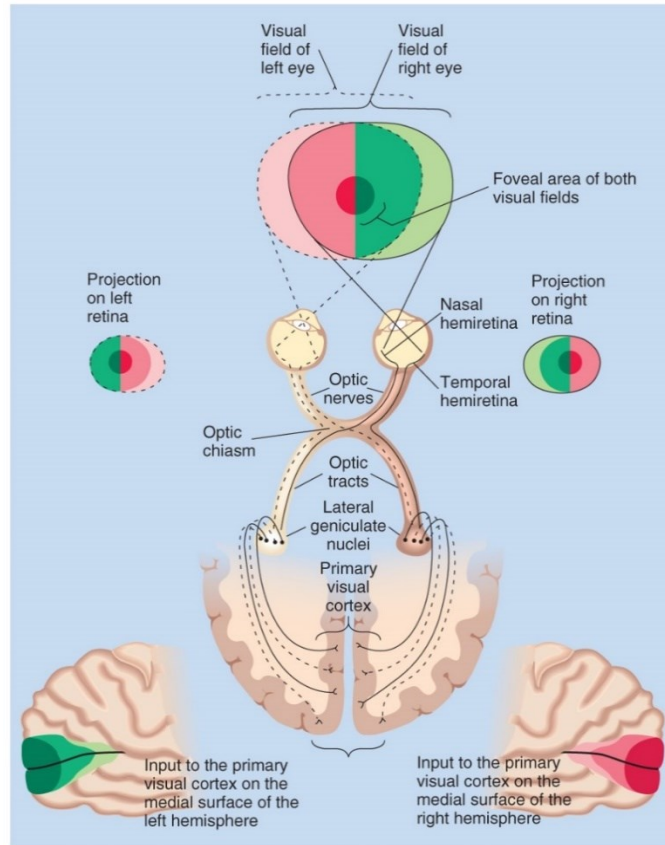


Figure 3. Visual field information in the eye and the brain. Projections on the retinas are transmitted to the left and right visual cortices through the lateral geniculate nuclei. The red and green portions of the diagram represent the level of neural activity communicated between sections of the receptive fields in the eyes and other parts of the visual system (from Pinel (2011)).

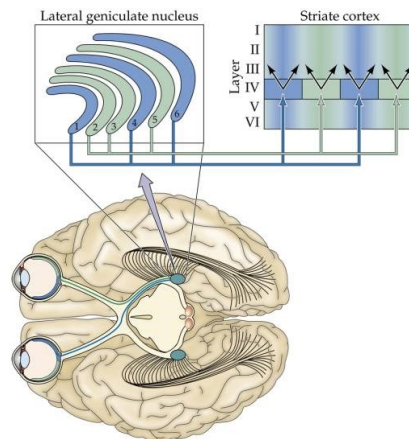


Figure 4. The six layers of the lateral geniculate nucleus and their projection to the striate cortex (from Purves et al. (2012))

The visual cortex is located at the back of the head. In the brain, both the left and right hemispheres contain a visual cortex. Generally, the visual cortex in the left hemisphere receives neural signals from the right visual hemifield, and the visual cortex in the right hemisphere receives neural signals from the left visual hemifield. The primary visual cortex, also known as V1, is the part of the visual cortex that receives the main signals from the LGN and conveys the main outputs to extrastriate areas (e.g. V2, V3, V4, etc.) (Goebel et al., 2004). The primary visual cortex is constituted by a thin sheet of grey matter composed mainly of neuronal cell bodies and unmyelinated axons. The primary visual cortex also has a large number of neurons, approximately 350 million neurons (Prasad and Galetta, 2011). Additionally, the primary visual cortex is structured into six functionally distinct layers, layer 1 to layer 6. Most of the input signals from the LGN are relayed to the primary visual cortex in layer 4. Layer 4 is subdivided into layers 4A, 4B, 4C $\alpha$ , and 4C $\beta$ . Layers 4C $\alpha$  and 4C $\beta$  are the major sublayers that receive input signals from the LGN (Hubel and Wiesel, 1972; Lund, 1988). The magnocellular layers (M-pathway) send input signals to cortical layer 4C $\alpha$ , and the parvocellular layers (P-pathway) send input signals to cortical layers 4B and 4C $\beta$ . However, the koniocellular layers (K-pathway) send direct input signals to layers 2 and 3.

Within V1, there are special connections to process the input signals received from the LGN. Lund (1988) reported that V1 consists of resident cells called spiny stellate cells, smooth stellate cells and pyramidal cells that are involved in internal input and output processing. Spiny stellate cells are excitatory cells that receive and process input signals from the magnocellular and parvocellular layers of the LGN. Smooth stellate cells are inhibitory cells that process input signals locally, within V1 cells. Pyramidal cells provide outputs from V1 to other cortical areas and subcortical structures; these cells can be found in layers 2, 3, 4B, 5 and 6. Figure 5 shows the summary diagram for inputs to, resident cells in, and outputs from V1. The following is an example of the simple circuits or interactions between neurons within V1. The magnocellular and parvocellular layers of the LGN send input signals to layer 4 in V1, which then relays the information to layers 2 and 3 via excitatory spiny stellate cells. Next, the pyramidal cells (output) in layers 2 and 3 pass the information to higher cortical areas. There are also pyramidal cells in layers 5 and 6. Layer 5 projects to the superior colliculus, while layer 6 projects back to the LGN.

Furthermore, Hubel and Wiesel (1979) discovered that neurons in the primary visual cortex possess distinct categories of receptive field structures. V1 cells are classified into three categories: simple cells, complex cells and hypercomplex cells (also called end-stopped cells). Simple cells respond to an edge or a bar of a certain orientation and produce responses with defined “on” and “off” regions in the retina, similar to center-surround cells. Complex cells also respond to an edge or a bar of a certain orientation but without the arrangement of “on” and “off” regions. Complex cells respond selectively to a particular width of an edge or bar, whereas hypercomplex cells respond selectively to a particular length of edge or bar. These types of neurons possess a preference to respond optimally to a selective or specific stimulus in the early cortical processing.

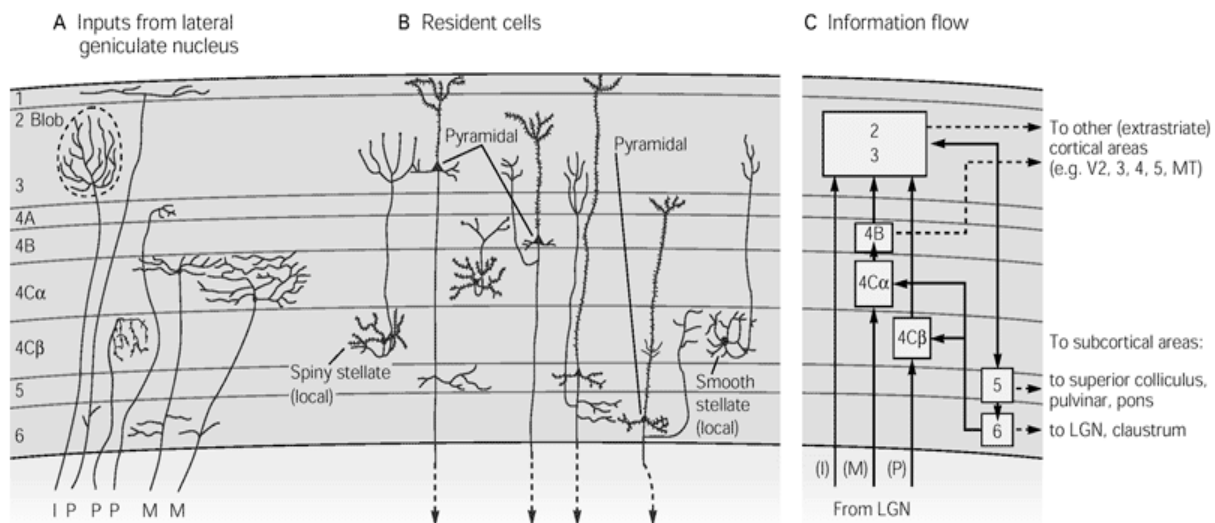


Figure 5. The primary visual cortex contains discrete anatomical layers featuring individually-distinguished synapse connections. (A) Input from LGN neurons. M cell axons terminate in layer 4C $\alpha$ , P cell axons terminate in layers 4C $\beta$  and 4A, and K (I) cell axons terminate in layers 2 and 3. (B) Resident neural cells. Spiny stellate cells receive signals from LGN neurons. Smooth stellate cells comprise a local neuronal circuit and are not excitatory. Pyramidal cells emit axons to other areas of the brain and contribute to the overall inner-processing. (C) Processing circuitry originating from LGN axons and resident neural cells. Layers 2, 3 and 4B send signals to other cortical areas, layer 5 sends signals to the superior colliculus, and layer 6 sends signals to the LGN, ultimately forming a loop (From Lund (1988), via Teller (2013)).

Moreover, Hubel and Wiesel (1962) demonstrated that cells in V1 are organized systematically according to receptive field properties. Figure 6 shows the architecture of the cortical module in the primary visual cortex. The cortical module of V1 consists of a set of columns that are sensitive to a specific orientation; these columns are also called orientation columns. Cells in the visual cortex that receive inputs from the left and right eyes are also organized into ocular dominance columns. Hubel and Wiesel (1962) demonstrated that the position of the stimulus in the retina maps precisely in the visual space across the surface of the cortex (retinotopic maps). Moreover, when V1 is stained for the enzyme cytochrome oxidase, blob structures are revealed. These blobs are clearly seen in layers 2 and 3. Livingstone and Hubel (1984) found that these blobs do not respond to orientation but do contain neurons that are sensitive to color perception. Livingstone and Hubel (1984) also applied the same method in the second visual area, V2. When V2 is stained for the enzyme cytochrome oxidase, parallel stripes or subareas called thin stripes, thick stripes, and pale stripes are revealed. They also found anatomical connections between V1 and V2. According to Sincich and Horton (2005), neurons in blob columns of V1 project to the thin stripes in V2, and neurons in interblob columns of V1 project to the thick stripes and pale stripes in V2. The connections between neurons in V1 and subareas of V2 show that the projections are organized into two pathways of functional specialization, the ventral stream, and the dorsal stream. Neurons in V1 projecting to the thick stripes of V2 relay via the dorsal stream, while neurons in V1 are projecting to the thin and pale stripes relay via the ventral stream. The ventral stream is also called the “what” system because it processes information for object recognition, i.e., color and form, while the dorsal stream is also called the “where” system because it processes information for motor actions, i.e., locations and motions of objects (Milner and Goodale, 2006). The following are examples of simple projections in the ventral and dorsal streams: (1) ventral stream:  $V1 \rightarrow V2 \rightarrow V3 \rightarrow V4 \rightarrow \text{inferiortemporal}$ , and (2) dorsal stream:  $V1 \rightarrow V2 \rightarrow V3 \rightarrow \text{medialtemporal} \rightarrow \text{medial superior temporal}$ . Figure 7 shows the proposed 305 feedforward connections between 32 visual areas according to Van Essen et al. (1992).

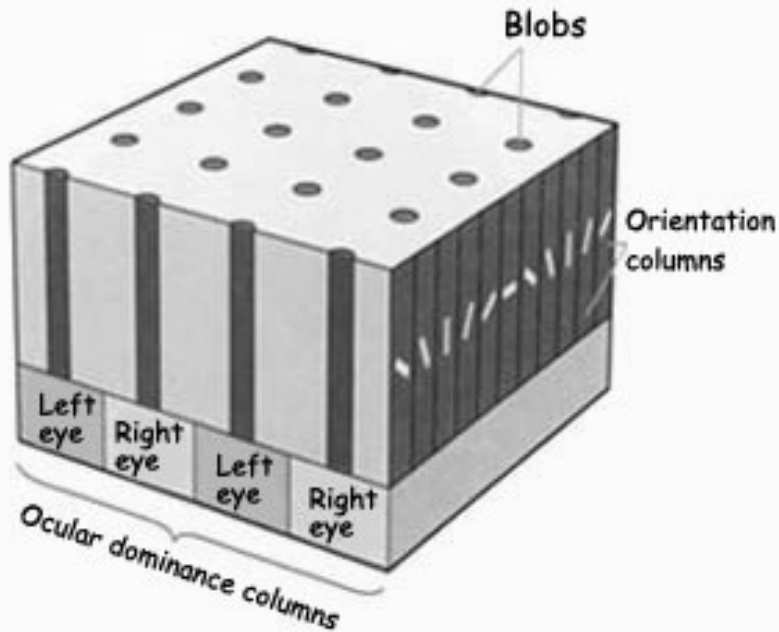


Figure 6. Representation of a cortical module. The primary visual cortex is arranged into modules which feature orientation columns arranged orthogonally to the ocular dominance columns. All cells behave similarly with respect to their receptive fields, in that they are responsive to the same part of the visual field. However, the cells vary in signal input (left or right eye), receptivity to orientation, color (blobs), and size (not shown) (from (Goebel et al., 2004).



#### 2.1.4 Visual Field Representation

As discussed above, there are spatial relationships between the ganglion cells in the retina and the visual space across the surface of the cortex. Visual input perceived from the retina is organized into visual field maps in the visual cortex. The visual field maps are also called retinotopic maps or visuotopic maps. The visual field is the total area of surrounding images that enter both eyes while they are focused on a central point. Additionally, each eye has a separate visual field called a monocular visual field. The monocular visual field is the part of the visual field that only can be seen with the left or right eye (i.e., the peripheral part of the visual field). According to Spector (1990), the portion of the visual field, or visual angle, that a normal eye of human is able to see for each left or right eye separately is about 100 degrees laterally, 60 degrees medially, 60 degrees upward and 75 degrees downward while both eyes are focused on a central fixation point. The visual fields of both eyes (the right and left visual fields) overlap extensively to create a binocular visual field. Therefore, the binocular visual field consists of two monocular visual fields.

To understand projections from the visual field, the left and right visual fields may also be further subdivided vertically into nasal and temporal divisions and horizontally into inferior and superior divisions. Figure 8 shows the divisions of the left and right hemifields and their related projections to the brain. When light rays reflected from an object pass through both eyes, the surfaces of the left and right retinas receive an image of the object that is inverted top-to-bottom and left-to-right after passing through the lens. Therefore, the image of an object in the left hemifield is projected onto the right hemifield of the retina, with the superior division of the left eye falling onto the inferior division of the right retina, the inferior division of the left eye falling onto the superior division of the right retina, the temporal division of the left eye falling onto the nasal division of the right retina, and the nasal division of the left eye falling onto the temporal division of the right retina. Meanwhile, the image of an object in the right hemifield is projected onto the left hemifield of the retina, with the superior division of the right eye falling onto the inferior division of the left retina, the inferior division of the right eye falling onto the superior division of the left retina, the temporal division of the right eye falling onto the nasal division of the left retina, and the nasal division of the right eye falling onto the temporal

division of the left retina. As noted, each point in real space is represented onto some point on the surface of the retina.

Next, visual information forming on the retina passes through optic nerves and crosses in the optic chiasm. At the optic chiasm, the visual information from two nasal hemiretinas crosses, while those from the two temporal hemiretinas do not cross. Hence, the left optic tract carries visual information from the temporal division of the left retina and the nasal division of the right retina, while the right optic tract carries visual information from the nasal division of the left retina and temporal division of the right retina. When visual information reaches the LGN, the visual information is organized according to the contralateral field of view of both eyes: the left LGN receives visual information from the left hemifield, and the right LGN receives visual information from the right hemifield. The retinotopic maps on the left and right LGN then project onto the visual cortex. The superior (upper) visual field maps dorsal (below) to the calcarine sulcus, and the inferior (lower) visual field maps ventral (above) to the calcarine sulcus (see Figure 8). The posterior part of the striate cortex corresponds to the fovea, and the anterior part of the striate cortex corresponds to the peripheral regions of the retina. The extent of the cortical area represented is reflected in the number of neurons in the retina. Notice that the posterior part of the striate cortex is overrepresented compared to the anterior part of it. This is because more neurons are concentrated in the central portion of the retina (fovea) than in the peripheral areas. Therefore, the convergence is higher on the posterior part of the striate cortex (fovea) than on the anterior part of the striate cortex (peripheral).

Visual dysfunction or impairment may affect the projection of visual information to the brain. Visual dysfunction may be associated with disease in or damage to one or more parts of the eye or within the visual pathways or visual cortex. Individuals with visual dysfunction may have difficulties in daily activities such as reading, driving or walking. Therefore, individuals with visual dysfunction usually have different visual responses (i.e. reorganization) in the brain. Functional magnetic resonance imaging (fMRI) can be used to understand visual cortical responses either in a normal individual or in an individual with visual dysfunction. Therefore, a basic theory to MRI and fMRI is provided in the next section (2.2). Additionally, a few examples of visual cortical responses using functional magnetic resonance imaging (fMRI) and retinotopy



maps in subjects with visual dysfunction are discussed in section 2.2.3 (Retinotopic Mapping). See section 2.2 for further discussion.

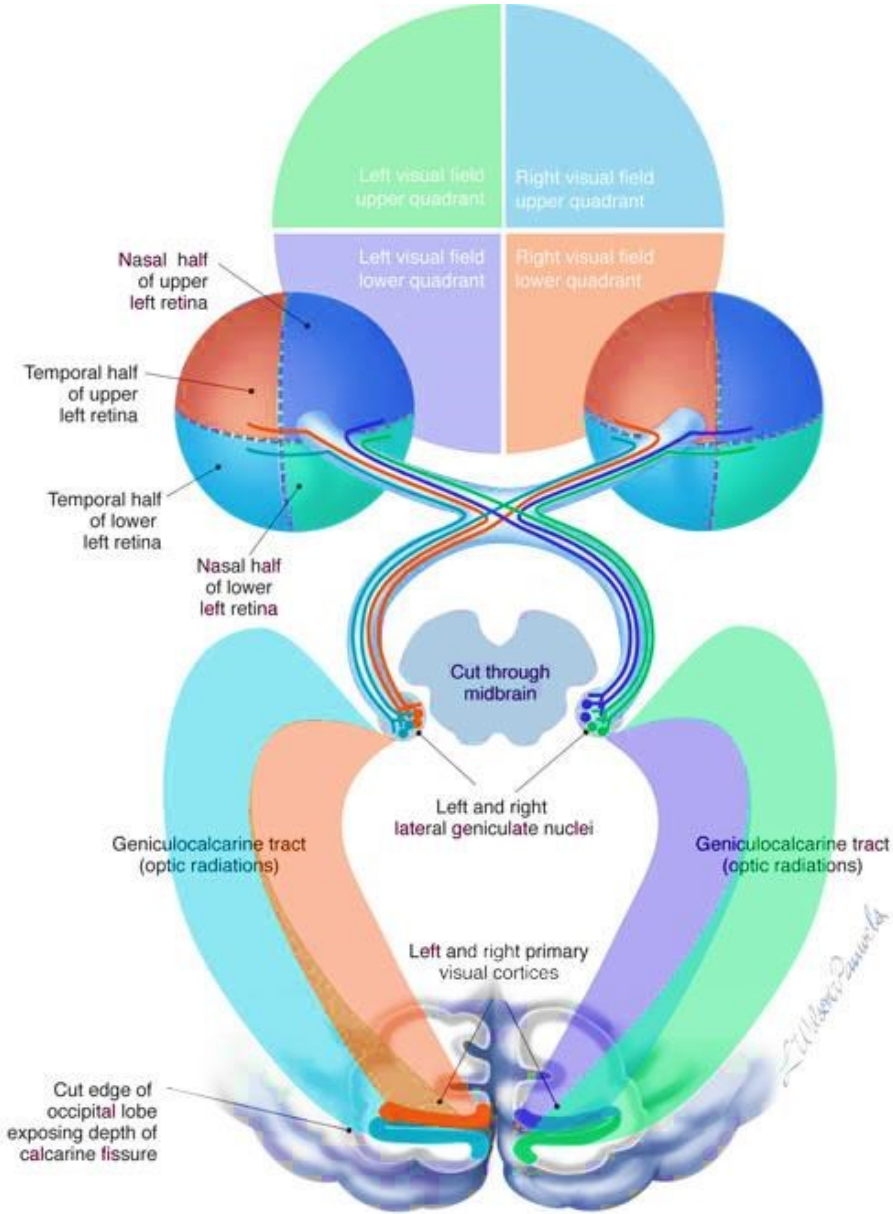


Figure 8. The pathway is comprising the visual system. Different colors demarcate the different quadrants of the visual pathway and the paths taken by the visual impulses to reach the primary visual cortex, where the image is first perceived. The figure does not depict the fovea (from Wilson-Pauwels et al. (2013)).

## **2.2 FUNCTIONAL MAGNETIC RESONANCE IMAGING**

In 1946, Felix Bloch discovered nuclear magnetic resonance (NMR) (Bloch, 1946). He found that the proton has its own nuclear magnetic momentum: the spin of the proton around its own axis has a magnetic field (Bloch, 1946). In 1952, Felix Bloch and Edward M. Purcell were awarded the Nobel Prize for their discovery of NMR by describing the underlying physicochemical phenomenon. This discovery triggered the development of NMR in various fields: physics, chemistry, biology, physiology, and medicine. The story of NMR use in medical imaging started when Raymond Vahan Damadian discovered that tumors and normal tissue had different NMR parameters (Damadian, 1971).

NMR, or magnetic resonance imaging (MRI), is a safe and non-invasive method to examine structural images of the human body. Basically, MRI produces a maps of the distribution of hydrogen nuclei in the body. MRI is a widely used imaging technique that has evolved both in the clinic and in research. In the early 1990s, a physicist named Seiji Ogawa discovered a new way to apply this imaging technique called functional magnetic resonance imaging (functional MRI or fMRI) (Ogawa et al., 1990a, 1990b; Ogawa and Lee, 1990). He found that molecules in the blood that are oxygen-rich (oxygenated) have different magnetic properties than those that were oxygen-poor (deoxygenated), and that this difference in magnetic properties results in a small change in the local MR signal (Ogawa et al., 1990a). Therefore, Ogawa used blood-oxygen-level-dependent (BOLD) contrast to map brain activity (Ogawa et al., 1990a, 1990b; Ogawa and Lee, 1990)(Ogawa et al., 1990a). By using an MRI scanner, it was thus possible to obtain information about both brain structure and function (Ogawa et al., 1990b, 1992; Kwong et al., 1992). This section provides a basic theory to MRI and fMRI. Additionally, this section also discusses an application of fMRI called retinotopic mapping (see section 2.2.3). A discussion of retinotopic mapping is included because this thesis is about brain activation in the visual cortex imaged with high-resolution 7 Tesla fMRI.

### **2.2.1 Magnetic Resonance Imaging**

MRI is a method to produce detailed images of internal body structures, e.g. organs, bones, tissues, blood vessels and nerves. MRI uses hydrogen nuclei, which are abundant in water and fat in the human body, to emit signals that allow visualization of internal body structures. The

hydrogen nucleus has one proton that spins around its own axis. This spinning induces a magnetic field called a magnetic moment. The magnetic moment of each hydrogen nucleus in the body has a specific vector quantity and direction, resulting the variations in signals detectable by an MRI scanner.

Without an external magnetic field, the protons (the nuclei of the hydrogen atoms) in the body spin randomly about their axes (see Figure 9), and the sum of the magnetic moments of all of the protons, also known as the net magnetization vector (NMV), is zero. Therefore, without an external magnetic field, the protons do not constitute any coherent magnetization. When the human body is placed in an MRI scanner with a strong constant magnetic field,  $\mathbf{B}_0$  (e.g., 1.5 tesla, 3.0 Tesla or 7.0 Tesla), the magnetic field causes the individual protons to precess and align. By convention, the individual protons are aligned in the z-direction, along the bore of the MR scanner. As the protons precess, the spin vector in the z-axis (parallel with  $\mathbf{B}_0$ ) is constant with time (no change in magnitude or direction), and the component in the x and y directions (perpendicular and transverse, respectively, with  $\mathbf{B}_0$ ) vary with time. The change in orientation for each proton can be described by a unique set of Cartesian x-y-z-coordinates (see Figure 10) that are perpendicular (x and y) and parallel (z) to  $\mathbf{B}_0$ . Each proton precesses with a certain frequency rate proportional to the strength of the magnetic field. This relationship is expressed by the Larmor equation:

$$\omega_0 = \gamma B_0 \tag{1-1}$$

where  $\omega_0$  is the Larmor frequency in megahertz (MHZ),  $\gamma$  is the gyromagnetic ratio, which is constant for each nucleus, e.g., approximately 42.58 MHz/Tesla for protons, and  $\mathbf{B}_0$  is the magnetic field strength in Tesla.

Additionally, the externally applied  $\mathbf{B}_0$  forces the individual protons to align either parallel or anti-parallel to  $\mathbf{B}_0$ . These two orientations have different energy states: the protons that align parallel to  $\mathbf{B}_0$  are in a low energy state, while the protons that align anti-parallel to  $\mathbf{B}_0$  are in a high-energy state. In essence, the protons oriented parallel to  $\mathbf{B}_0$  are slightly preferred. Therefore, there are more protons oriented parallel to  $\mathbf{B}_0$  than protons that are oriented anti-parallel to  $\mathbf{B}_0$ . This phenomenon is governed by the Boltzmann distribution:

$$N_{\text{upper}} / N_{\text{lower}} = e^{-\Delta E/kT} \quad (1-2)$$

where  $N_{\text{upper}}$  and  $N_{\text{lower}}$  are the number of protons in the upper and lower energy levels respectively,  $k$  is Boltzmann's constant ( $1.381 \times 10^{-23} \text{ JK}^{-1}$ ),  $\Delta E$  is the energy difference between the two states proportional to  $B_0$ , and  $T$  is the temperature of the proton at body temperature. The Boltzmann distribution explains the magnitude of the NMV.

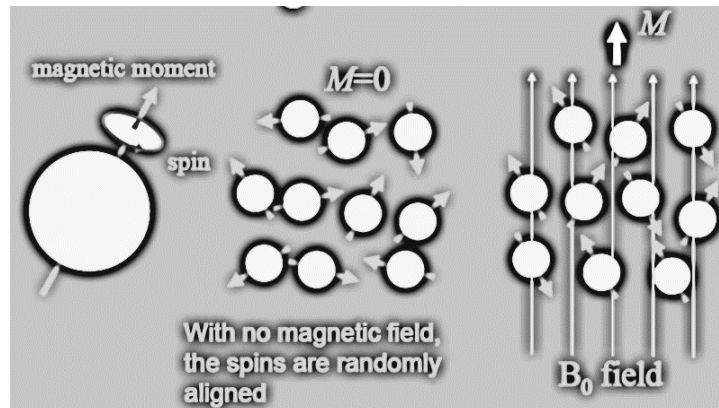


Figure 9. Protons spin randomly when they are not under the influence of a magnetic field. The net sum of all the random movements equals zero. When the protons are influenced by a magnetic field, most move in the direction of the field and precess around an axis. The vector  $M$ , the so-called sum of magnetic moments, no longer equals zero (from <http://fontralculus.tumblr.com/post/70201405968/mri-basics>).

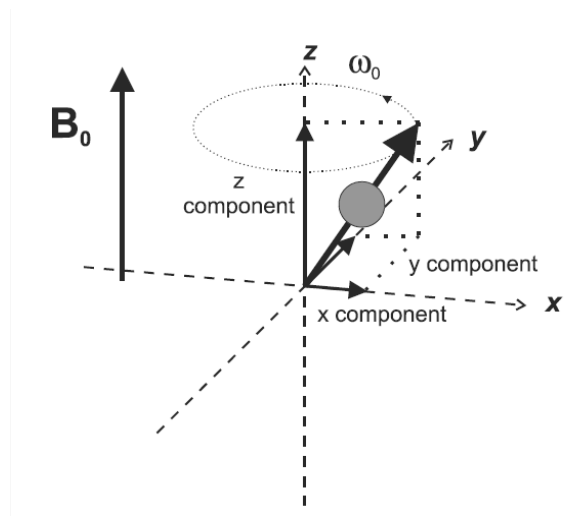


Figure 10. Once under the influence of a magnetic field, the proton precesses in that field. The axis of precession and the main magnetic field (denoted by  $B$ ) are parallel to each other. The component of interest is the z component, which indicates the magnitude of rotation and maintains a constant direction irrespective of the proton's precession). Both the x and y components are dependent on time with a frequency  $\omega_0$  which relates to  $B_0$  as in equation (1-1) (from Brown and Semelka (2003)).

The unequal numbers of protons in a low- vs. high-energy state induce a non-zero net magnetization aligned with  $B_0$ ; the tissue in the body becomes magnetized in the presence of  $B_0$ . Therefore, the net magnetization  $M_0$  is directly related to the magnetic field strength  $B_0$ , which can be explained by the equation:

$$M_0 = \chi B_0 \tag{1-3}$$

where  $\chi$  is the magnetic susceptibility and  $M_0$  is the source of the signals for MRI. The higher the strength of the magnetic field, the greater the potential the MR signals will produce.

During image acquisition, a radio-frequency (RF) pulse is applied to manipulate the net magnetization vector. The RF pulse is transmitted from a coil of wire called the RF coil. The application of the RF pulse allows the magnetic component of RF energy (RF magnetic field,  $B_1$ ) to interact with the magnetic moment of protons in the body. Here, the RF pulse establishes an RF magnetic field,  $B_1$ . By transmission of RF energy at a particular resonance frequency  $\omega_0$ , the protons start to precess around the axis of  $B_1$  oriented perpendicular to  $B_0$  (Figure 11). In the coordinate system, the perpendicular RF pulse is in the x-y plane if  $B_0$  is taken to be in the z

direction, along the bore of the MR scanner. Conceptually, turning on an RF pulse results in: (1) the protons absorbing energy at a particular resonance frequency, thus causing  $M_z$  to flip into the x-y plane (transverse plane; i.e. a 90° flip), and (2) the magnetic moments of protons becoming synchronized and moving in phase, thereby causing  $M_z$  to precess in the transverse plane. Additionally, the protons induce a voltage across the RF coil of the MRI scanner during the precession. Subsequently turning off the RF pulse results in: (1) the protons emitting the absorbed RF energy at a particular resonance frequency, (2) the protons beginning to return to their original magnetization orientation, and (3) the magnetic moment of protons beginning to lose their coherence and move out of phase (dephase). Therefore, when the RF pulse is turned off, the absorbed RF energy is emitted and processed by the receiver coil in the transverse plane, thereby producing an MR signal. The MR signal that is generated is known as the free induction decay (FID). This term denotes that, when the RF pulse is turned off, the magnetic moment of the protons begin to move out of phase, which causes  $M_z$  to precess “freely” in  $B_0$  and the associated signal to decay or decrease over time (Brown and Semelka, 2003). The process by which the magnetization returns to its resting state after RF excitation is called relaxation. The relaxation process or the process of signal change over time is unique for each type of tissue. The differences in tissue relaxation properties provide a contrast that allows imaging of anatomy and function. There are two types of relaxation processes: T1 relaxation and T2 relaxation.

T1 relaxation, also known as spin-lattice relaxation or longitudinal relaxation (recovery), is the process by which the magnetic moments of the protons return to their original or initial equilibrium orientations, thus resulting in recovery of longitudinal magnetization ( $M_{x-y}$  or  $M_z$  return to  $M_z$ ). The time course for the system returning to its original equilibrium orientation can be described by an exponential curve. The recovery rate or the time required for the magnetization to return to 63% of its original magnetization value following an excitation pulse is characterized by the time constant T1. Figure 12 shows an example of a T1 relaxation curve. In general, T1 values are related to the main magnetic field  $B_0$ : T1 values increase with increasing values of  $B_0$ . T1 values are tissue-specific, which provides an advantage in generating high T1-dependent contrast obtained by modifying the sequence parameters of MRI acquisition. Thus, T1-weighted imaging, which provides good contrast between grey matter and white matter tissue, is applied to differentiate anatomical structures.

T2 relaxation, also known as spin-spin relaxation or transverse relaxation, is the process by which the transverse component of magnetization decays as the protons release the absorbed energy, lose their coherence and reorient along  $B_0$ . Similar to T1, the time course of signal decay in the system can be described by an exponential curve. The decay rate, or the time required for the magnetization of the transverse component to decay to 37% of its original value following an excitation pulse, is characterized by the time constant T2. Figure 13 shows an example of a T2 relaxation curve. Unlike T1, T2 values are not related to the main magnetic field  $B_0$ . As a result, the loss of coherence produces FID, which provides an MR signal. Similar to T1, T2 values are also tissue-specific. The application of T2-weighted imaging provides good contrast between brain tissue and cerebrospinal fluid (CSF). Thus, functional MRI takes advantage of loss in magnetization (T2\* decay or T2\* dephasing) following an RF pulse to extract the underlying signal and produce an image of brain activity.

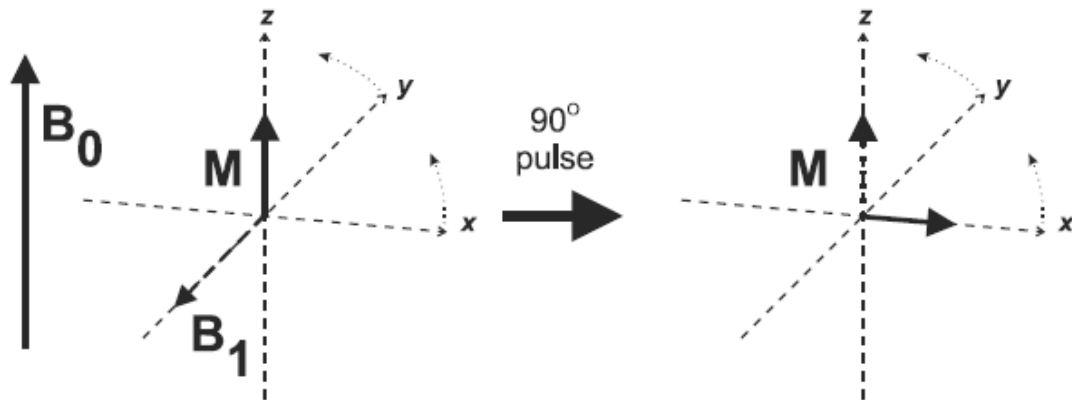


Figure 11. Absorption of energy. In a rotating frame of reference, the RF pulse emitted at resonance frequency  $\omega_0$  produces an additional magnetic field  $B_1$  which is perpendicular to the main magnetic field  $B_0$ . If the protons are activated by a proper amount of energy at the required frequency, they then absorb that energy and rotate ( $M$ ) in the transverse plane, perpendicular to  $B_1$  and  $B_0$ . The pulse flip angle is the total amount of rotation performed by  $M$  (from Brown and Semelka (2003)).

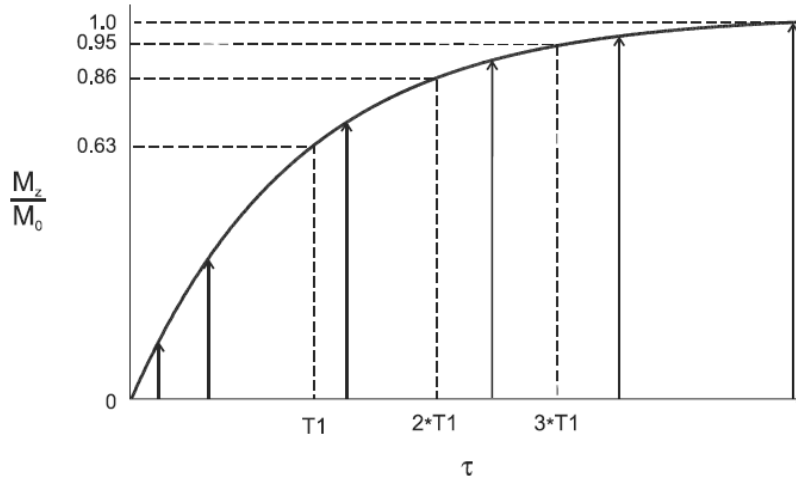


Figure 12. T1 Relaxation Curve. After a  $90^\circ$  RF pulse, no longitudinal magnetization is observed. A short time later, the protons begin to release their energy, resulting in longitudinal magnetization. With more and more energy being released,  $M_z$  begins to re-established. Once this process is completed,  $M_0$  returns to its original equilibrium orientation. The change of  $M_z / M_0$  over time  $\tau$  follows an exponential growth process. T1 denotes the time-constant, the so-called spin-lattice relaxation time, representing the time it takes for  $M_z$  to regain 63% of the original value (from Brown and Semelka (2003)).



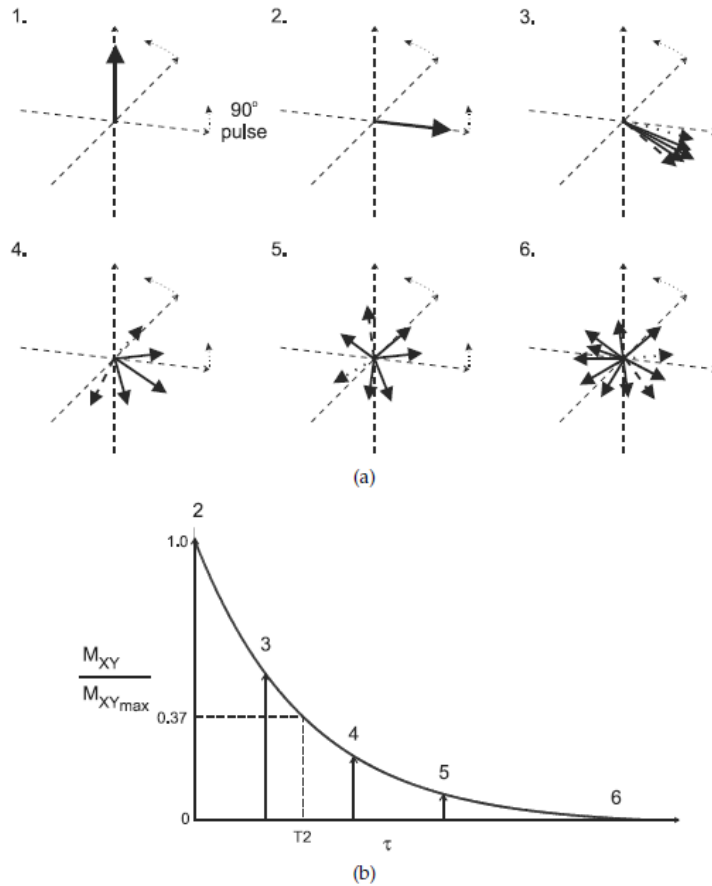


Figure 13. T2 decay curve. (a) This panel is applicable to a frame which rotates at a frequency slower than  $\omega_s$ . (1) Before the RF pulse is transmitted, net magnetization ( $M$ , arrow) is oriented parallel to  $B_0$  (not depicted in the plane). (2) After a  $90^\circ$  RF pulse, the protons initially precess in the transverse plane. (3) A short time later, the protons begin to lose their coherence and precess at varying frequencies. (4, 5) The synchronicity of protons in the transverse plane decreases gradually over time, (6) finally reaching a random configuration of the transverse component. (b) Depicts the  $M_{XY}$  component over time. The change in  $M_{XY} / M_{XYmax}$  over time  $\tau$  follows an exponential decay process.  $T_2$  denotes the time-constant for this process, the so-called spin-spin relaxation time, representing the time it takes for  $M_{XY}$  to decay to 37% of the original value (from Brown and Semelka (2003)).

### 2.2.2 Functional Magnetic Resonance Imaging

Functional magnetic resonance imaging is a non-invasive technique for studying human brain function. In essence, fMRI expands the use of MRI to measure changes in the magnetic properties of blood in the brain (Ogawa et al., 1990a, 1990b; Ogawa and Lee, 1990). Blood-oxygen-level-dependent (BOLD) contrast is the most commonly used contrast mechanism to map brain activity (Ogawa et al., 1990a, 1990b).

Theoretically, the brain needs the same nutrients as every cell in the body does. Therefore, a constant supply of oxygen to the neuron is essential to maintain the unique system in the brain. In an active state, i.e. during a visual task, motor task or cognitive task, neurons of activated brain regions demand more oxygen than they do in the normal state (without task) to process information; oxygen consumption increases with the demand of the task. This changes the magnetic properties of oxygenated and deoxygenated hemoglobin in the blood vessels within the activated brain regions. Consequently, the deoxygenated hemoglobin is paramagnetic to the magnetic field, and the oxygenated hemoglobin is diamagnetic to the magnetic field. Therefore, fMRI takes advantage of the presence of paramagnetic deoxyhemoglobin, which induces magnetic susceptibility differences between the blood and the surrounding tissue to obtain MR signals in the brain. This results in an endogenous contrast agent called blood-oxygen-level-dependent or BOLD in fMRI (Ogawa et al., 1990a, 1990b, 1992; Kwong et al., 1992). Figure 14 shows the BOLD mechanism of fMRI.

The essential observation in fMRI is of neural activity. This means the content of oxygenated hemoglobin in the tissue of a particular brain region is actually directly linked to neural activation. A task or stimulus increases neural activity, which also results in an increase in the content of oxygenated hemoglobin in the tissue within an activated brain region. This change might also affect the MR signal changes that allow the study of brain function. The process by which the BOLD signal changes over time in response to neural activity can be termed the hemodynamic response function (HRF). Figure 15 show the BOLD signal curve or hemodynamic response to brain activation. The BOLD response comprises several processes in response to the stimulus (e.g., a visual discrimination task) relative to a baseline condition (e.g., a blank screen). In general, the BOLD signal experiences (1) an initial decrease, also known as an

initial dip, approximately 2 seconds after onset of the stimulus, reflected in increases in oxygen consumption due to an initial increase in the blood flow (Francis and Panchuelo, 2014), (2) a slow rise and subsequent peak approximately 5-8 seconds after stimulus onset (in, e.g., the primary visual cortex), and (3) a gradual decay back to the initial value or baseline over a certain period (e.g., approximately 12-24 seconds). The decay process is often accompanied by a post-stimulus undershoot (an undershoot slightly below the baseline) due to an increase in oxygen consumption that is sustained even after cessation of the stimulus (Buxton et al., 1998). According to Aguirre et al. (1998), the HRF actually depends on the properties of the stimulus and on the underlying neural response. The authors also reported that there are HRF differences across individuals and across regions within individuals, although the hemodynamic response is stable across sessions using the same task or condition.

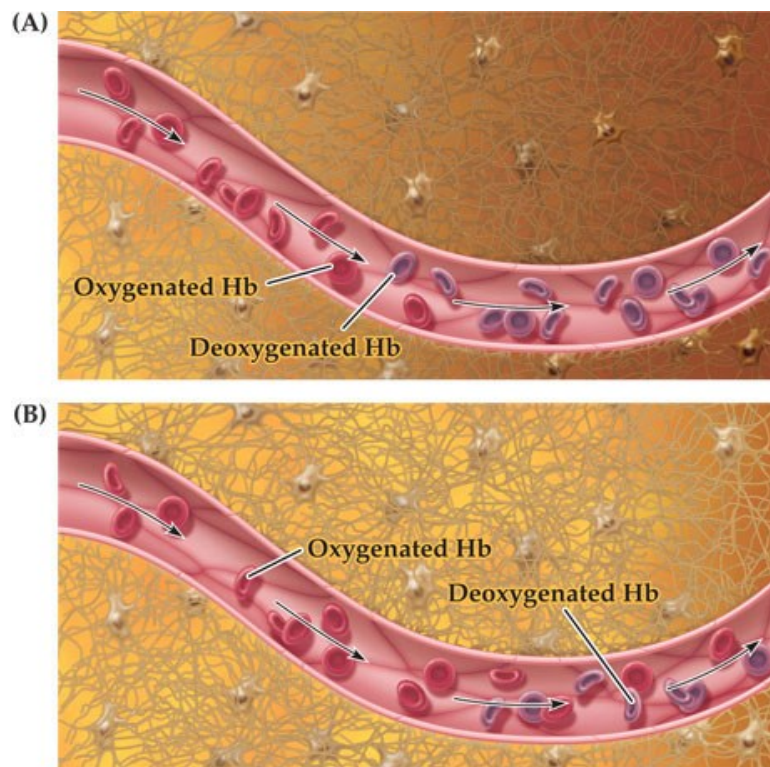


Figure 14. BOLD fMRI. (a) Under normal conditions, the amount of deoxygenated hemoglobin is higher than the amount of oxygenated hemoglobin within the capillary bed. (b) In the active condition, increased neuronal activity leads to increased oxygenation of hemoglobin in the blood, which in turn leads to increased levels of oxygenated hemoglobin in the capillary bed. The corresponding decrease in the amount of deoxygenated hemoglobin caused this MRI image to brighten (from Hill and Wyse (2012), via Moseley and Glover (1995)).

As mentioned earlier, levels of neural activity correspond to changes in oxygenated and deoxygenated hemoglobin in the brain. Such changes in magnetic properties cause protons to lose coherence and move out of phase (dephasing), leading to a small difference in the magnetic susceptibility, which results in T2\*-sensitivity to the BOLD effect. More demand for oxygenated hemoglobin within the activated brain region results in more intensity in T2\*-weighted images. In contrast, less demand for oxygenated hemoglobin within the activated brain region results in less intensity in T2\*-weighted images. T2\* contrast, therefore, forms the basis of BOLD-fMRI.

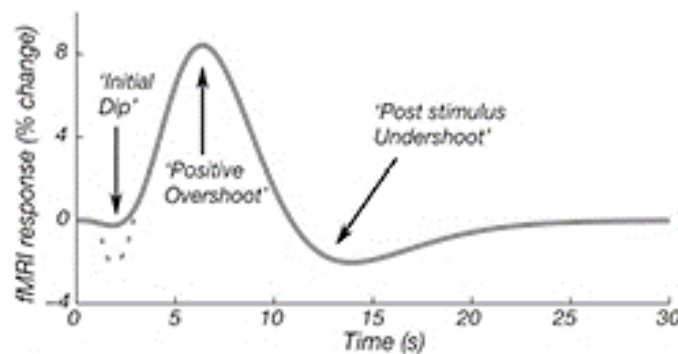


Figure 15. The BOLD hemodynamic response function (HRF) (from Francis and Panchuelo (2014)).

To extract the MR signal within the activated brain region, there are several MRI pulse sequence techniques available for imaging such as gradient echo (GE), spin-echo and inversion recovery. Of the various available imaging sequences, the GE imaging sequence is the most commonly used in fMRI because an optimum MR signal can be obtained with maximum susceptibility to the BOLD contrast from T2\*-weighted images. The amount of T2\*-weighting shown in the image is dependent on an acquisition parameter, namely the echo time (TE). The echo time is the time between the application of the RF excitation pulse and the maximum signal induced in the RF coil (or between excitation and data acquisition). Figure 16 shows a T2\* curve showing the relationship between T2\*-weighting and TE. Short TE results in a little difference between the activated state and the resting state, as shown in the T2\* curve (Figure 16). On the other hand, a TE that is too long results in no difference between the activated state and the resting state, as shown in the T2\* curve (Figure 16), which implies no signal due to all signals

having decayed to zero. Therefore, an optimal value of TE is important for acquiring the maximum signal change represented by a particular value of T2\*. Aside from the optimum value of TE, the optimum voxel size and slice thickness are also required to enhance the detection of the BOLD signal. Larger voxels contain more protons that can produce signals than do small voxels. Therefore, the signal-to-noise ratio (SNR) is higher in larger voxels than in small voxels. Additionally, the voxel volume is related to the slice thickness. Doubling the slice thickness doubles the voxel volume and the SNR. In contrast, reducing the slice thickness by half halves the voxel volume and the SNR. The SNR is therefore proportional to the selected parameters. Although it is true that larger voxel volumes increase the SNR, they also lead to more artifacts than do small voxel volumes. Therefore, a good combination of parameters is necessary to maximize BOLD sensitivity.

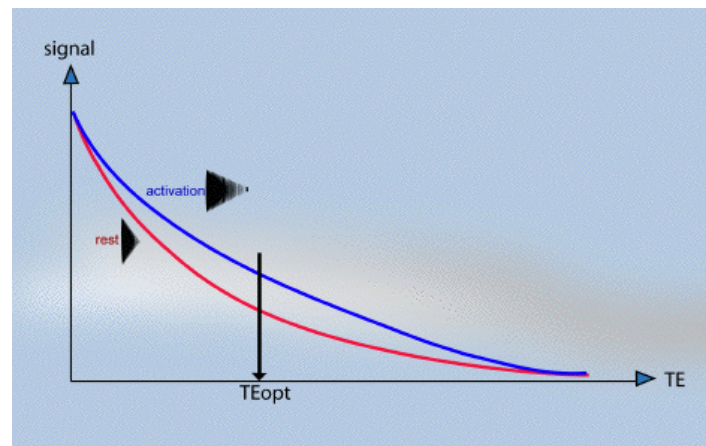


Figure 16. T2\* curve: the relationship between the amount of T2\*-weighting and TE. A short TE results in a small difference between the activated state and the resting state, while a long TE results in no difference between the activated state and the resting state (from Stuart (1997)).

Additionally, most fMRI studies apply an image acquisition technique called echo-planar imaging (EPI) to acquire fMRI data. This is because EPI allows rapid, continuous acquisition of a series of images with a single repetition time (TR, the time between excitation pulses) in response to a stimulus. Despite the benefits of EPI for fast and robust imaging, it has the disadvantages of geometry and intensity distortions especially at high magnetic field strength (In and Speck, 2012; In et al., 2015). This is because EPI is very sensitive to magnetic field inhomogeneity caused by magnetic susceptibility differences between structures in the brain (e.g. between air and tissue interfaces) (Zeng and Constable, 2002; Morgan et al., 2004). According to Zeng & Constable (2002), magnetic field inhomogeneity results in severe voxel shifts and signal loss in the phase-encoding direction. Additionally, it also may result in poor image quality. Therefore, promising methods for correcting distortion in EPI are required. Point-Spread-Function (PSF) mapping is one of the recent techniques available for distortion correction (Zeng and Constable, 2002; In and Speck, 2012; In et al., 2015). The PSF method uses additional phase-encoding to encode the spatial information about the geometry and intensity distortions (Zeng and Constable, 2002; Hoffmann et al., 2012a; In et al., 2015). Then the additional phase-encoding is added to the original EPI sequence for distortion correction processes (refer Zeng and Constable, 2002; Hoffmann et al., 2012; In et al., 2015 for further explanations). In addition, previous reports show that PSF is reliable at high magnetic field strengths.

In summary, BOLD contrast is a widely used contrast mechanism for mapping brain activation (Ogawa et al., 1990a, 1990b, 1992; Kwong et al., 1992). The optimum selection of image acquisition techniques and parameters might improve activation detection in fMRI.

### **2.2.3 Retinotopic Mapping**

By the early nineties, fMRI methods became fairly well-developed, enabling a leap forward in various fields, i.e. visual, memory, auditory and motor studies. Some of the first fMRI studies showed increased signaling in the visual cortex following visual stimulation (Bandettini et al., 1992; Belliveau et al., 1991; Kwong et al., 1992; Ogawa et al., 1992). Eventually, fMRI was used to identify visual field maps in healthy subjects and patients (Wandell and Winawer, 2011). In the past two decades, fMRI has produced a great amount of data on human visual field maps. A comprehensive knowledge of human vision has been achieved through experimentation,

elucidating the organization of cortical visual areas and various aspects of visual function including development, plasticity, and perceptual functions.

Visual areas in the primate cortex are believed to be retinotopically-structured (Serenio and Allmann, 1991; Sereno et al., 1994). By stimulating adjacent parts of the visual field, visual areas can be revealed using fMRI methods. The retinotopic organization of the human primary visual cortex, located in the sulcus has been known for over 100 years (Henschen, 1893; Holmes, 1918; Lister and Holmes, 1916). Figure 17 shows a schematic illustration of the visual cortex and its corresponding retinotopic map of the visual space. Each visual neuron features a receptive field which responds to input from a particular region of retinotopic space. Neighboring neurons within this cortical sheet demonstrate receptive fields that overlap in the visual space.

Soon after functional visual responses in humans were presented and understood, a number of research groups developed experimental techniques to identify and delineate the human visual field map. To measure the activity in the visual cortex effectively, Engel et al. (1993, 1994) developed a method based on the discovery of stimuli which generate a travelling wave of activity in the primary visual cortex. This travelling wave method used the least complex and most powerful retinotopic techniques for describing the distribution of neural activity from fixation (fovea) to the periphery (i.e., eccentricity mapping). The human visual cortex can be progressively stimulated by flickering checkerboard rings or wedges of increasing radii. The wedges originate at the midpoint and extend towards the periphery, whereas the rings encircle the midpoint. Ring and wedge stimuli produce accurate mapping because the cortical locations on the map are extremely sensitive to every small area of the visual field. Figure 18 shows how travelling-wave rings and wedges identify visual field maps at different eccentricities and angles. The eccentricity and polar angle espouse accurate visual field position in polar coordinates (Wandell et al., 2007). Several laboratories have used data from travelling-wave stimuli (DeYoe et al., 1996; Dumoulin et al., 2003; Engel et al., 1997; Sereno et al., 1995; Wandell et al., 2005; Warnking et al., 2002) to construct visual field maps. The travelling-wave method, also called phase-encoded retinotopy, has become a standard technique for identifying cortical visual areas. The response phase at the stimulation frequency can be calculated using algorithms aided by computer processing, such as Fourier transform (Engel, 1997; Warnking et

al., 2002). The phasing of the Fourier transform component facilitates a highly accurate spatial distribution in the visual cortex over the stimulation cycle (Engel, 1997; Warnking et al., 2002; Greenlee and Tse, 2008). Therefore, maps of the human visual cortex can be produced precisely and reproducibly, whereby boundaries among V1, V2, and other visual areas are explained by the phase sequences from vertical and horizontal meridians (Greenlee and Tse, 2008) (Figure 18).

The travelling-wave fMRI method clearly reveals visual areas, i.e. V1, V2, and V3, in the occipital lobe (Engel et al., 1997; Sereno et al., 1995) (Figure 18). The visual areas in the left hemisphere form a topographic map of the right half of the visual field, with the fovea being represented at the posterior edge of the occipital lobe and increasingly eccentric retinal regions being represented at more anterior locations within the calcarine sulcus. Moreover, the lower visual field projects to the upper bank of the calcarine sulcus, and the upper visual field to the lower bank. These maps are repeated, with variations, in areas V2 and V3. The primary visual cortex (V1), which receives direct input from retinogeniculate pathways, occupies the calcarine cortex and is represented as a hemifield of visual space.

In addition to healthy or control subjects, individuals with visual deficits have revealed much about functional brain imaging. These deficits – cortical, retinal or ocular – help to reveal how the cortex reorganizes after changes in the nature of everyday visual stimulation. In addition, the deficits can be used to test theories regarding the existence, function, and overlap of different visual pathways (Wandell and Wade, 2003). The application of fMRI in individuals with visual disorders provides many opportunities for helpful insights into the visual pathways and visual development. Several fMRI studies are listed below which used retinotopic mapping to explore cortical visual responses in subjects with visual dysfunction.



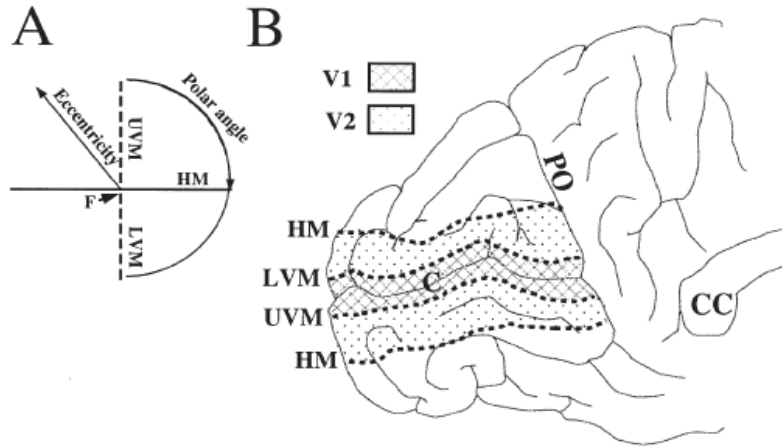


Figure 17. Visual fields and their corresponding areas in the cortex. (A) A visual field is described in terms of a fixation point denoted by F, a horizontal meridian denoted by HM, and upper and lower meridians in a vertical direction denoted by UVM and LVM. The polar angle increases in the clockwise direction and eccentricity increases from the fixation point towards the periphery of the visual field. (B) The occipital lobe is depicted in a medial cross-section, with abbreviations for parieto-occipital sulcus (PO), corpus callosum (CC) and calcarine sulcus (C). Dashed lines are used to depict both the upper and lower vertical meridians which mark the boundaries of visual areas V1 and V2. A part of the horizontal meridian runs along the calcarine sulcus but is not depicted in this view. The horizontal meridian also demarcates the boundaries between the dorsal and ventral parts of visual areas V2. (from Engel et al. (1997)).

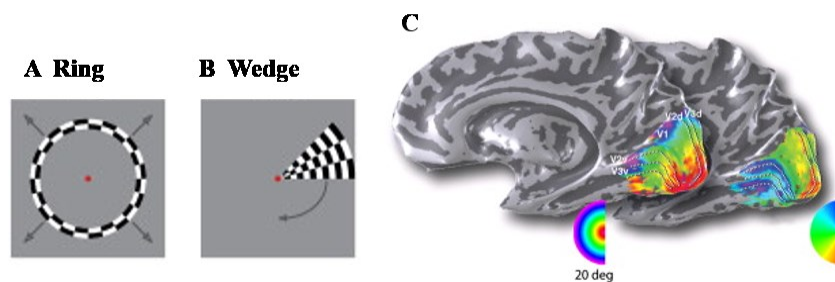


Figure 18. Travelling-wave stimulation. Frames from sequences of expanding rings (A) and rotating wedges (B) are shown. The arrows show the moving direction of the sequences and are not included in the frames. (C) Visual field maps in the right hemisphere of a single subject, measured using expanding rings (left) or rotating wedges (right). The color mapping denotes eccentricity (left) or polar angle (right). The stimuli covers the center 20° radius (adapted from Wandell et al. (2007)).

Morland et al. (2001) investigated the impact of visual dysfunction on cortical visual responses in three different studies. Each study had different subjects with different levels of visual deficits. In the first study, the authors described the effect of abnormal retinal receptor distributions in rod monochromacy onto cortical visual maps. Subject KN, 56 years-old, had a complete absence of cone photoreceptors and also had a central scotoma between 10 min and 1°, although estimations are prone to inaccuracy due to nystagmus. KN's cortex had reorganized: the regions normally represented by central fields were reassigned to more peripheral positions in the visual cortex. The authors believed that this reorganization occurred due to abnormal signaling from the retina to the cortex. In the second study, the group assessed how the input signals from each left and right hemifield are presented in the visual cortex of human albino. In human albinism, the primary defects are found in the optic chiasm, where the visual information from the two nasal hemiretinas and the two temporal hemiretinas cross. (In normal subjects, the visual information from the nasal hemiretinas, but not the temporal hemiretinas, cross – see Figure 3 for the visual field projection from the eye to the brain via the optic chiasm.) The authors presented the stimulus separately for left and right hemifields to an albino subject viewing monocularly. This subject was female, 55 years-old, tyrosinase-positive, with best-corrected acuity of 0.33 and nystagmus not exceeding more than 3° in amplitude. Monocular stimulation of each hemifield resulted in activations in the hemisphere contralateral to the eye being stimulated. This is consistent with abnormal decussation at the optic chiasm in albinos. The authors believed that reorganization is a probable outcome of developmental, not genetic, factors, as found in the Boston pattern (Guillery, 1986). In the third study, the authors described how visual field deficits can be ascertained through retinotopic mapping in the case of cortical lesions. Subject SA, 43-years old, had a unilateral lesion of the white matter of the left occipital lobe. SA was faced with problems in reading, but standard perimetry revealed a questionable central scotoma. Retinotopic mapping performed with fMRI showed an absence of cortical activity in response to small stimuli ( $< 3^\circ$ ) in the lower-right quadrant of the visual field, which was relative to the subject's field defects.

Slotnick et al. (2002) determined the retinotopic organization of a patient with congenital dysgenesis but with normal visual function. The subject was 32 years-old, female, and left-handed. At age 30 she underwent a partial right lobectomy to treat medically-intractable seizures. The perimetry maps within the central 60° of the visual field demonstrated normal visual

function. The retinotopic map of the upper-right visual field on the ventral left hemisphere was relatively normal, but the retinotopic map of the lower-right visual field on the dorsal left hemisphere was shifted in location. The primary aspect of the patient's dysgenesis was restricted to the right hemisphere, which contained a zone of abnormal cortical migration disruptive to the white matter tracts delivering retinotopic information from the left visual field. This atypical neural reorganization may have caused the changes in the retinotopic maps, using multiple islands of spared cortex in the left and right hemispheres. This reorganization was shown to involve shifts in locations with spared topography and, in other forms, to involve shifts in both location and topography. These results show that retinotopic maps can be shifted in both location and topography and that cortical reorganization is likely due to cortical dysgenesis or a functional displacement.

Hoffmann et al. (2003) examined visual cortex topographically maps in four female albinos aged 23-32 years-old and two control subjects. The input from the temporal retina was not substantially suppressed and formed a retinotopic map that was superimposed on the nasal retina map in the striate and extrastriate cortex. The abnormal routing of the temporal fibers was not total, with the line of decussation shifting 6-14° into the temporal retina. This indicates that the abnormal input to the visual cortex in human albinism does not undergo topographic reorganization between the thalamus and cortex and is not significantly suppressed in either striate or extrastriate areas. The human albino exhibits a topographical representation of the visual field that is rarely observed in hypopigmented mammals, although the mapping in this study is consistent with the map from the only other primate study (Guillery et al., 1984).

Autism is a neurodevelopment disorder characterized by preserved visual abilities as well as a special profile for visual cognition. Hadjikhani et al. (2004) examined the visual system of high-ability autistic individuals to determine whether their unusual pattern of visual cognitive abilities was due to the presence of abnormalities at the primary sensory level. Eight autism spectrum disorder patients with high-ability, and four non-autistic controls were studied. The authors reported that the subjects with autism had retinotopic maps in the visual cortex that were similar in all manners to the maps in controls. This indicates that the differences in local versus global processing in autism do not arise from early visual areas, but likely have a basis in other areas of the brain that function in attention and cognition, such as the parietal or frontal cortices.

Amblyopia is a developmental visual disorder associated with loss of monocular acuity, sensitivity, and profound alterations in binocular integrations. Abnormal connections in the visual cortex are known to underlie the loss of acuity, but the extent to which these abnormalities are regionally or retinotopically specific is not fully known. Corner et al. (2007) used fMRI to examine the retinotopic specificity of cortical activity and to compare multiple visual areas under monocular and binocular viewing conditions. The authors compared the retinotopic maps in the visual cortex produced by each eye in 19 adults (7 esotropic strabismus, 6 anisometropic, and 6 controls). In the standard viewing condition, the non-tested eye viewed a dichoptic homogeneous mid-level grey stimulus, thereby permitting some degree of binocular interaction. The authors measured fMRI signals in the V1, V2 and foveal regions in each subject. In general, the brain signal was reduced for the amblyopic eye, in comparison with the fellow eye, in some subjects. In addition, the amblyopic eye exhibited a significant shift toward greater preferred eccentricity in the field of view, indicating that foveal eccentricities in the amblyopic eye were represented in the same cortical region. Interestingly, occlusion of the fellow eye caused an expanded foveal representation for the amblyopic eye in one early-onset strabismic subject with binocular suppression, indicating real-time cortical remapping. In addition, several subjects showed increased activity in the parietal and temporal cortices when viewing with the amblyopic eye. The authors concluded that, even in a heterogeneous population, abnormal early visual experience commonly leads to regionally specific cortical adaptations.

In most brains, signals from one eye are sent to two places by partial crossing at the optic chiasm. At the optic chiasm, visual information from the two nasal hemiretinas cross, whereas visual information from two temporal hemiretinas do not cross (see Figure 3 for a visual field projection from the eye to the brain via the optic chiasm). Hoffmann et al. (2012) investigated the organization of the visual cortex in two male achiasmic subjects, one (22 years-old) at Magdeburg University, Germany, with 4 controls, and the second (30 years-old) at Stanford University, USA, with 34 controls. The visual hemifield representations on the cortical surface were obtained separately for each visual hemifield and eye, through retinotopic mapping. In the first subject, stimulation of the right eye revealed orderly eccentricity maps of both hemifields in the right hemisphere only, whereas opposite visual hemifields were represented as a cortical superposition of mirror-symmetrical visual field position. Similar results were obtained in the left hemisphere for stimulation of the left eye. The authors found a highly-atypical organization

of the visual cortex, consisting of overlapping visual hemifield maps with bilateral population receptive fields. In addition, visual pathway connectivity, including the occipital callosal connections, was investigated using diffusion tensor imaging and tractography. In the achiasmatic subjects, the gross topography of the geniculate-striate and callosal occipital connections was largely unaltered. Therefore, the authors proposed that reorganization of intra-cortical architecture in the visual system underlies the subjects' ability to cope with the abnormal visual input.

Impairment of the visual cortex is a common occurrence in cases of stroke, tumor, and trauma. Specific damage to the visual cortex creates pathological deletions of retinotopic maps. To evaluate the damage-associated plasticity of retinotopic maps, Reitsma et al. (2013) investigated the retinotopic organization in patients with diverse central brain pathologies (e.g. stroke, tumor, surgery-associated pathology). The 55 subjects in the initial experiment included 25 patients with clear anatomical evidence of pathology involving visual cortex and/or underlying white matter tracts. Of these patients, three (two with adult-onset damage and one with congenital cerebral malformation) exhibited abnormal retinotopic organization including an expanded ipsilateral visual field representation. The expanded representations were found to be located at the vertical meridian borders between visual areas V1 and V2. Two of these three subjects had a topographically-inconsistent (ectopic) representation of the ipsilateral field within the lateral occipital cortex which is normally associated with visual areas V2 and V3. The two adult-onset cases had direct damage to the early visual cortex itself rather than to the efferent drive, resulting in a mostly-nonfunctional hemisphere. The congenital case had a severe cortical malformation of the visual cortex and was acallosal. The other 22 subjects showed normal retinotopic organizations, aside from the presence of retinotopic deletions caused by the pathologies. These results are consistent with a competitive model whereby unilateral damage to the visual cortex or disruption of the transcallosal connections destroys interhemispheric suppression from retinogeniculate afferent in the intact visual cortex that represents the vertical meridian and ipsilateral visual field.

The above-mentioned studies describe how the visual cortex deals with abnormal inputs. In subjects with visual cortex damage or neurodevelopment disorders, i.e. autism, albinism, or amblyopia, the cortex appears to have very different visual representations or organization. The

application of fMRI-based retinotopic mapping in visual dysfunction research can deepen our understanding of the plasticity of the human visual cortex. This could lead to the development of rehabilitation programs for these patients, with therapeutic effects and improvements in the quality of life. Therefore, in chapter 2.3, the effects of alternating current stimulation (ACS) on the healthy and diseased brain are discussed.

## **2.3 EFFECTS OF ALTERNATING CURRENT STIMULATION IN THE HUMAN BRAIN**

The work presented in this chapter has been accepted for publication:

**Aini Ismafairus Abd Hamid**, Carolin Gall, Oliver Speck, Andrea Antal, and Bernhard Sabel. 2015. Effects of alternating current stimulation on the healthy and diseased brain. *Front. Neurosci.* 9, 391. doi:10.3389/fnins.2015.00391.

### **2.3.1 Introduction**

Research has demonstrated that patients suffering from a stroke or traumatic brain injury (TBI), neurodegeneration of the brain or the retina, or genetic predispositions may develop visual, language and memory dysfunctions depending on the parts of the brain that are affected. These dysfunctions prevent patients from performing their daily chores and eventually affect the quality of life of these people (Gall et al., 2011; Dimyan and Cohen, 2011; Shah et al., 2013). However, there is substantial evidence showing that invasive, non-invasive and behavior therapy techniques can support the recovery of the affected regions. Patients can accordingly again regain functionality, although not as before (Sabel et al., 2011b; Dimyan and Cohen, 2011; Hamilton et al., 2011; Shah et al., 2013). The techniques have both advantages and disadvantages (Nizard et al., 2012; Nardone et al., 2014) that will be discussed below.

Behavior therapy is one of the techniques that has been found to promote the recovery of affected brain regions (Sabel et al., 2011b; Perrey, 2013; Dobkin, 2005). The method involves the use of repetitive training programs that stimulate the surviving regions to promote neuroplastic changes (Sabel and Kasten, 2000; Breier et al., 2009; Mang et al., 2013; Perrey, 2013; Dobkin, 2005; Musso, 1999). Some of the trainings conducted by practitioners include cognitive training such as motor skills and strength training (Jensen et al., 2005), visual training

(Kasten et al., 1998, 2006; Sabel and Gudlin, 2014), language comprehension training (Rogde et al., 2013) and neuropsychological trainings related to daily activities (Ávila et al., 2004).

Non-invasive brain stimulation (NIBS), specifically transcranial electrical stimulation (tES) (i.e., tDCS, tACS, and tRNS), have intriguing capabilities that were recently identified: improvement of brain function or cognitive abilities in both the healthy and diseased brain with the help of separate physiological mechanisms that vary by tES type (Filmer et al., 2014; Miniussi et al., 2013; Santarnecchi et al., 2015). Substantially, tES methods are based on the exertion of weak electrical currents, via electrodes placed on the scalp, to the targeted brain area. The most commonly used application of tES is tDCS; neuronal membrane potential is modulated by tDCS presumably via stimulation polarity, as anodal tDCS and cathodal tDCS instigate membrane depolarization and membrane hyperpolarization, respectively (Bindman et al., 1964; Creutzfeldt et al., 1962). Very recently, tRNS and tACS were proposed as eligible tES methods to modulate brain activity, whereby tRNS delivered random electrical frequencies over the cortex to modulate neural oscillations (Miniussi et al., 2013; Santarnecchi et al., 2015; Terney et al., 2008) and tACS delivered specific electrical frequencies to modulate neural oscillations (Miniussi et al., 2013; Santarnecchi et al., 2015). Additionally, transorbital ACS delivered at a specific electrical frequencies also allows modulation of neuronal activity (Bola et al., 2014; Gall et al., 2010a, 2011; Fedorov et al., 2011; Sabel et al., 2011a; Schmidt et al., 2013); however, all NIBS methods can induce changes in cortical plasticity. In this sub-chapter, I aimed to summarize the effects of transorbital and transcranial ACS in the brain.

### **2.3.2 Basic Principle of ACS**

Studies have demonstrated that ACS is a non-invasive technique used in brain stimulation, but ACS is not much studied as compared with tDCS and TMS. Although ACS and tDCS use the same device, as well as montages, these two techniques use different current waves: ACS uses alternating current; tDCS uses direct current to stimulate the brain (Zaghi et al., 2010). Research of ACS stimulation shows that the current wave stimulating the brain changes cyclically over time with the sinus pulses or square pulses penetrating the skull through the electrodes placed on the surface of the scalp (Zaghi et al., 2010; Gall et al., 2011). Researchers conducting non-invasive ACS stimulation place the stimulation electrodes according to target location (i.e., transcranial placement) [e.g., Zaehle et al. (2010)] or near the eyeball (i.e., transorbital

placement) [e.g., Gall et al. (2011)] (see Figure 1). The effects of ACS at the neuronal level depend mainly on the parameters used such as current, density, frequency, electrode size, and the locations where the electrodes are placed.

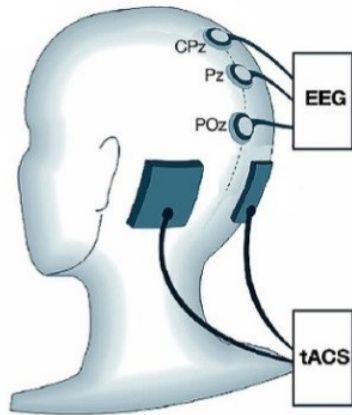
### **2.3.3 Mechanism of Action**

When conducting ACS techniques, researchers typically use a particular frequency band; however, these frequencies must be within the human EEG frequency range (for a review, see Miniussi et al. (2012)), although recently frequencies up to 5 kHz were also used (Chaieb et al., 2014). Recent studies (e.g., Kanai et al. (2008)) have shown that ACS can entrain frequencies within the EEG frequency range, including the local oscillatory activities of the stimulated area. For example, Pogosyan et al. (2009) showed that tACS increased the coherence of EEG at the beta frequency in the contralateral motor cortex. Zaehle et al. (2010) showed how EEG spectral power increased after tACS in the individual alpha frequency range, compared with the spectral power before ACS at the baseline (or sham stimulation). These results demonstrate a possible relationship between frequency-specific oscillations and specific brain functions.

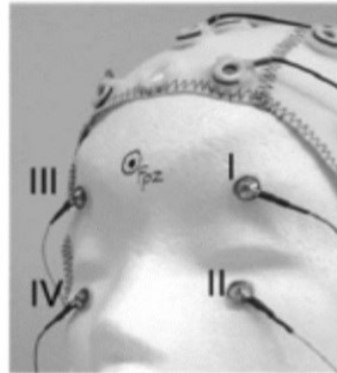
The after-effects induced by ACS are presumed to emerge from synaptic-level processes (Nardone et al., 2014). Synaptic plasticity refers to the efficiency achieved from synaptic strength or the experiences gained by the synapses over time (Citri and Malenka, 2008). Synaptic plasticity is involved in brain development and brain recovery (Citri and Malenka, 2008); however, for neuronal networks to function properly, two principal mechanisms are involved at the synaptic level: long-term potentiation (LTP), e.g., synchronous signals that allow synaptic transmission and improve the strength of synapses, and long-term depression (LTD), which decreases (weaken) synaptic strength (Citri and Malenka, 2008; Zaehle et al., 2010). Ideally, healthy brains work in a synchronous way; in contrast, patients with brain disorders suffer from brain asynchrony (“desynchronization”) and therefore require resynchronization for recovery.



(A) Transcranial ACS



(B) Transorbital ACS



(C) Neural oscillation and neural firing patterns induced by ACS

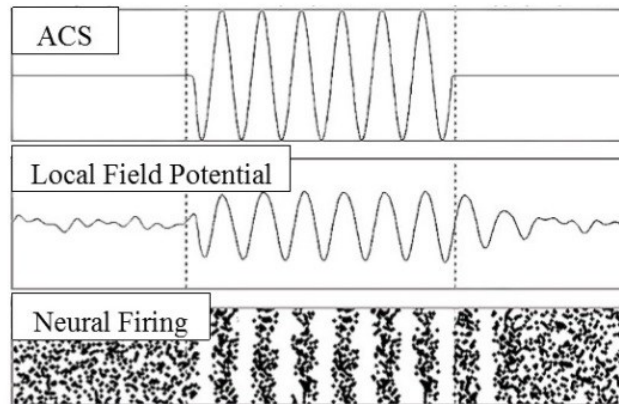


Figure 19. Examples of stimulation electrode placements and neural oscillation. (A) Transcranial ACS: electrodes were placed over the parieto-occipital region (P09 (target) and PO10 (reference), according to the 10-10 system). (B) Transorbital ACS: four stimulation electrodes were positioned at or near the eyeballs (with eyes closed), and one electrode was positioned at the occipital pole as the reference electrode. (C) The model prediction of neural oscillation and neural firing patterns induced by ACS (adapted from Zaehla et al. (2010), Gall et al. (2011) and Battleday et al. (2014); from Abd Hamid et al. (2015a)).

Resynchronization can be achieved by using an ACS frequency that matches the endogenous frequency of network oscillations (Herrmann et al., 2013; Zaehle et al., 2010; Reato et al., 2013; Battleday et al., 2014). For example, Zaehle et al. (2010) found that 10-Hz tACS increased synaptic strength in a simple spiking neuronal network. Recently, Vossen et al. (2015) demonstrated that the application of tACS frequencies at or above individual alpha power (IAF) resulted in increased EEG alpha power after tACS. The comparison of EEG alpha power after tACS between phase continuity condition (i.e., short, phase-continuous condition; long, term phase-continuous condition; and long, phase-discontinuous conditions) revealed no differences. Therefore, tACS after-effects were not related to phase continuity. Additionally, the phase-locked alpha oscillation during tACS did not last long after the end of stimulation. The author concluded that tACS induces short-term plasticity in alpha activity instead of entrainment activity.

In addition to the physiological mechanisms of tACS in humans observed by Zaehle et al. (2010) and Vossen et al. (2015), there are simultaneous reports of *in vitro* and *in vivo* tACS by Fröhlich and McCormick (2010), Reato et al. (2010), Ozen et al. (2010), and Ali et al. (2013). Fröhlich and McCormick (2010) reported the effects of intracranial ACS in ferrets, e.g., intracranial ACS applied to ferret cortical slices. In *in vitro* slice preparations, slow oscillations (up and down states of physiological activity) were spontaneously induced and persisted as *in vivo*. The recorded multi-unit activity demonstrated the ability of AC fields to modulate the neuronal membrane voltage, e.g., up and down states. The application of ACS fields at endogenous frequencies showed more periodicity than ACS at other frequencies. The open question here is whether the neuronal activity remains the same even if weak AC fields are applied on the surface of the skull; Ozen et al. (2010) answered this question by applying ACS at different frequency ranges (0.8-1.7 Hz) on the skull surface and simultaneously recording intracranial neural activity in anesthetized rats. They showed that ACS entrained 16% of the units in the cortical areas and 20% of the units in hippocampal areas. The spikes were successfully phase-locked at intracellular polarization values of 2-3 mV. Synchronization of neural spiking with an applied sinusoidal current could be sufficiently realized by very low intracranial electrical field values (1 V/m). Also, the recruited number of spiking neurons was affected by the stimulation intensity; increased stimulation intensity led to increased spike activity. Subsequently, the CA3 area of rat hippocampal slices was stimulated with ACS by

Reato et al. (2010). Twenty  $\mu\text{M}$  carbachol was used to induce brain activity in the gamma frequency range (25-35 Hz) in the CA3 area of the hippocampus. The oscillatory activity was modulated in a frequency-dependent manner, as revealed by the local field potentials; the gamma power was significantly modulated by ACS at a low frequency of 7 Hz (1 V/m), changing the rate of firing within the cycles of stimulation. Nevertheless, a net zero change in the rate of firing, e.g., systematic power modulation of the gamma cycles, showed rate-limiting property of the excitatory-inhibitory loop. Moreover, increased spike time coherence was noted when the ACS frequency delivered at the intrinsic frequency at low amplitude (0.2 V/m). These results implied that ACS can alter the spiking time, firing rate, and excitation-inhibition balance of neurons.

Later on, the modulation of the dynamics of space and time in a large-scale dynamic network of spiking neurons was revealed by Ali et al. (2013). The authors recorded multi-unit activity in anesthetized ferrets to validate the outcome obtained from a computational model. The neuronal oscillation was effectively entrained by tACS when the stimulation frequency matched the endogenous network frequency (3 Hz). Furthermore, the entrainment time was related to the onset phase of the oscillatory stimulation corresponding to the endogenous network oscillation; the noted minimum time for entrainment was at  $\pi$  onset phase. The authors concluded that tACS modulation in neuronal networks depends on frequency and phase.

The findings discussed above demonstrate the physiological mechanisms induced by tACS; however, the physiological mechanisms induced by transorbital ACS are still unclear. Foik et al. (2015) examined transorbital ACS' physiological mechanisms in rats. The authors demonstrated that transorbital ACS could induce neural activity, originating in the retina and eliciting visual information flow through visual pathways (Foik et al., 2015). Increased neural activity synchronization induced by transorbital ACS implies effectiveness in information transfer and fast processing (Lesica et al., 2007; Wang et al., 2010) from the retina towards cortical networks. The authors suggested that applying stimulation electrodes around the eyeball is more effective for increasing plasticity at the early stages of visual processing, in line with the findings of Sergeeva et al. (2012). Nevertheless, more investigation is required to identify problems with instigating the modulation of neural oscillation through transorbital ACS, e.g.,

effects on ongoing neural activity from other structures and stimulation electrode configuration like eye-neck and eye-eye (Foik et al., 2015).

Transcranial ACS modulates neuronal activity focally in various brain areas, while transorbital ACS modulates the neuronal activity of visual networks. Truly, each stimulation electrode placement (i.e., either transorbital placement or transcranial placement) can modulate brain activity. Nevertheless, to acquire complete comprehension regarding the mechanisms responsible for both types of stimulation electrode placement, more investigation must be pursued because to date no research has compared the physiological mechanisms of transorbital and transcranial ACS.

In this sub-chapter, the focus is on the evidence that exhibits the ability of ACS entraining activity of neuronal networks at various frequencies of stimulation (Zaehle et al., 2010; Vossen et al., 2015; Fröhlich and McCormick, 2010; Reato et al., 2010a); synchronization of neural oscillation was effectively acquired if the stimulation frequency was close to the endogenous network frequency (Zaehle et al., 2010; Fröhlich and McCormick, 2010; Reato et al., 2010a). One can conclude that ACS improves brain oscillatory activity by increasing the number of synchronously-firing neurons; additionally, the stimulating frequency may restore the damaged brain.

#### **2.3.4 Neuromodulation by ACS and Effect on Behavior**

As noted above, tACS works by modulating the oscillatory activity of the brain to a specific frequency (Herrmann et al., 2013; Antal and Paulus, 2013). Other stimulation parameters such as electrode size, stimulation time and intensity can also substantially affect cortical stimulations. Examples of ACS studies in the healthy and diseased brain are listed in Table 1. Below are the summary of previous findings from various experimental paradigms (e.g., motor, visual, somatosensory and higher cognitive function).

Primary motor context studies by Antal et al. (2008), Feurra et al. (2011a), Moliadze et al. (2010), and Chaieb et al. (2014) demonstrated that tACS modulates specific parts of the brain depending on the parameters of the ACS used. Antal et al. (2008) evaluated the effect of different frequencies of ACS and duration on left motor context. The authors used ACS for 2–10

minutes and frequencies of 1, 10, 15, 30 and 45 Hz. The data analysis revealed that 10 Hz tACS improved explicit motor learning but did not have any influence on cortical excitability. The authors evaluated the safety of the subjects by making them complete a questionnaire. The analysis of the questionnaires revealed that the subjects experienced minor side effects including light burning sensation and headaches, but none of them experienced transient side effects within two weeks of follow-up. Another study by Feurra et al. (2011a) used a shorter period of 90 seconds at different ACS frequencies (5, 10, 20 and 40 Hz) and sham stimulation in healthy subjects; stimulation was delivered over the left parietal cortex. For control stimulation, stimulation of 20 Hz and sham were delivered over the right parietal cortex, while, for peripheral control, stimulation of 5 and 20 Hz was delivered on the right forearm (ulnar nerve). The authors found that only frequencies at 20 Hz over the left parietal cortex achieved motor context excitability compared with other experimental conditions. Furthermore, the results also revealed that there were no significant differences in the compound muscle action potentials.

Schutter and Hortensius (2011) evaluated the associations between the brain rhythms and cortical excitability in healthy subject with different ACS frequencies such as delta (1–3 Hz), theta (4–7 Hz), alpha (8–12 Hz) and beta (13–30 Hz) on the right and left motor cortices. The regression analysis showed that the MEP amplitude was modeled by theta and beta frequency band in the primary motor cortex. The study was extended, and combined frequencies of theta-beta (5 and 20 Hz) were delivered for five minutes. The study was also modeled to alpha-alpha (10 Hz for 10 minutes), and both conditions were delivered over the primary motor cortex to examine the difference between the two conditions. The data analysis showed that only the theta-beta frequency stimulation increased the cortical excitability, but the exact excitability produced by a specific frequency was not known.

Interestingly, another study by Moliadze et al. (2010) evaluating the effect of higher ACS frequencies (140 and 250 Hz for 10 minutes) on cortical excitability. The frequencies were delivered on the right first dorsal interosseous muscle (MI) in healthy subjects. Specifically, the application of 140 Hz frequency was found to increase M1 excitability, and this after effect persisted for up to one hour. On the other hand, the application of a 250 Hz frequency revealed an increase of MEP amplitudes during the time of stimulation, and MI excitability was only

sustained for the first five minutes after stimulation. Additionally, the use of an 80 Hz frequency did not show any effects.

Chaieb et al. (2014) applied tACS at 5 kHz to healthy subjects. Although this frequency is beyond the EEG range, the application of the frequency for 10 minutes over the primary motor context showed a small reduction in delta activities. The reductions in delta-band oscillations were proposed to illustrate performance improvement (Chaieb et al., 2014; Wirth et al., 2011).

Pogosyan et al. (2009), Joundi et al. (2012) and Wach et al. (2013) focused on voluntary activities and reported that brain oscillations are specific to tasks. Joundi et al. (2012) evaluated go/no-go activities using 20 and 70 Hz frequencies over the left motor cortex in healthy subjects and found that an opposite effect persisted at these frequencies. For example, the use of 70 Hz tACS over the motor cortex was found to increase the performance of the go trial and be ineffective with the no-go trials. On the other hand, 20 Hz tACS yielded opposite results. Additionally, the use of 20 Hz tACS was also correlated with slower movements of participants during the application of tACS; this finding has also been reported in two other studies: Pogosyan et al. (2009) and Wach et al. (2013).

Table 1. Examples of ACS studies in the healthy and diseased brain (from Abd Hamid et al. (2015a))

	Article	Stimulation frequency	Stimulation intensity	Stimulation duration	Location of stimulation electrode	Location of reference electrode	Experiment	
Healthy Brain	Motor	Antal et al. (2008)	1, 10, 15, 30, and 45 Hz	400 $\mu$ A	5-10 min	left motor cortex (4 x 4 cm)	contralateral orbit (5 x 10 cm)	Motor learning
		Moliadze et al. (2010)	140 and 250 Hz	1000 $\mu$ A	10 min	Right first dorsal interosseous (FDI) (4 x 4 cm)	forehead (14 x 6 cm)	Motor Cortex excitability
		Feurra et al. (2011a)	5, 10, 20, and 40 Hz	1000 $\mu$ A	90 sec	left motor cortex (5 x 7 cm) and right parietal cortex (P4)	Pz according to 10-20 system (5 x 7 cm)	Motor Cortex excitability
		Schutter and Hortensius (2011)	delta (1-3 Hz), theta (4-7 Hz), alpha (8-12 Hz) and beta (13-30 Hz)	1000 $\mu$ A	10 min	Left motor cortex (C3) (5 x 7 cm)	Right motor cortex (C4) (5 x 7 cm)	Motor Cortex excitability
		Chaieb et al. (2014)	5 kHz	1000 $\mu$ A	10 min	Left motor cortex (M1) (4 x 4 cm)	contralateral orbit (7.5 x 6 cm)	EEG power spectra
	Voluntary movement	Pogosyan et al. (2009)	5 and 20 Hz	580 $\pm$ 40 $\mu$ A	10 periods of stimulation were randomly interspersed with 10 periods of no stimulation within 3 blocks for each session (total duration is not available)	left motor cortex (4.5 x 3.2 cm)	contralateral side of the neck (7.6 x 5.5 cm)	Motor performance

Cont.

Healthy Brain	Voluntary movement	Joundi et al. (2012)	20 and 70 Hz	50 $\mu$ A	Stimulation was randomly applied in 50% of trials (total duration is not available)	left motor cortex (5 x 7 cm)	ipsilateral shoulder (5 x 10 cm)	Motor performance
		Wach et al. (2013)	10 and 20 Hz	1000 $\mu$ A	10 min	Left motor cortex (M1) (5 x 7 cm)	contralateral orbit (5 x 7 cm)	Motor performance
Visual		Kanai et al. (2008)	4, 8, 10, 12, 14, 16, 18, 20, 22, 24, 30 and 40 Hz	(125, 250, 500, 750 and 1000 $\mu$ A)	10 sec for each frequency/condition	visual cortex-4cm above inion (4 x 4 cm)	vertex (9 x 6 cm)	Phosephene perception
		Kanai et al. (2010)	5, 10, 20 and 40 Hz	750 $\mu$ A	5-8 min	Oz (7 x 5 cm)	vertex (7 x 5 cm)	Visual cortex excitibility
		Schutter and Hortensius (2010)	2, 10 and 20 Hz	1000 $\mu$ A	10 sec	Oz, Pz (5 x 7 cm)	vertex (Cz), right shoulder (5 x 7 cm)	Retinal contribution to cortex
		Zaehle et al. (2010)	(8–12 Hz)	1120 $\pm$ 489 $\mu$ A	10 min	P09, PO10 (7 x 5 cm)	Oz (7 x 5 cm)	EEG alpha power
		Neuling et al. (2013)	Individual alpha frequency	1500 $\mu$ A	20 min	Oz according to 10-20 system (7 x 5 cm)	vertex (Cz) according to 10-20 system (7 x 5 cm)	EEG alpha power
		Helfrich et al. (2014)	10 Hz	1000 $\mu$ A	20 min	Cz, Oz, according to 10-20 system (5 x 7 cm)	NA	EEG alpha power, EEG coherence
		Vossen et al. (2015)	Individual alpha frequency	Individual stimulation intensity	3 sec, 8 sec	PO8-PO10, PO7-PO9 according to 10-10 system (5 X 7 cm)	Oz according to 10-20 system (5 X 7 cm)	EEG alpha power

Cont.



Healthy Brain	Somatosensory	Feurra et al. (2011b)	2-70 Hz	1500 $\mu$ A	5 sec per trial	Right somatosensory cortex (3 x 4 cm)	Left posterior parietal cortex (5 x 7 cm)	Tactile sensation
	Higher cognitive functions	Polanía et al. (2012)	6 Hz	1000 $\mu$ A	14 $\pm$ 1.5 min	F3, P3 according to 10-20 system (5 x 5 cm)	vertex (Cz) according to 10-20 system (5 x 5 cm)	Cognitive performance
		Sela et al. (2012)	6.5 Hz	1000 $\mu$ A	15 min	left DLPFC (F3), left temporal (CP5) (5x 5 cm)	left temporal (CP5), right temporal (CP6)(5x 5 cm)	Cognitive performance
		Santarnecchi et al. (2013)	5 Hz, 10 Hz, 20 Hz, and 40 Hz	750 $\mu$ A	Duration of the task	left middle frontal gyrus (5 x 7 cm)	vertex (Cz) (5 x 7 cm)	Cognitive performance
		Lustenberger et al. (2015)	10 Hz and 40 Hz	2000 $\mu$ A	30 min	F3, F4 according to 10-20 system	vertex (Cz) (5 x 7 cm)	Cognitive performance
Diseased brain	Visual impairment	Fedorov et al., (2011)	5-20 Hz	417 $\pm$ 156 $\mu$ A	25-40 minutes of each session for two weeks (10 sessions in total)	upper eyelids (two electrodes for each eye)	wrist on the right hand	EEG power spectra, Visual field improvement
		Gall et al. (2011)	5-30 Hz	Individual stimulation intensity (< 500 $\mu$ A)	10-20 min for each eye/session for 10 days (10 sessions in total)	at or near eyeballs (two electrodes for each eye)	occipital pole	Vision-specific quality of life, visual field improvement
		Sabel et al. (2011)	Individual stimulation frequency	Individual stimulation intensity	15 min for each eye/session for 10 days (10 sessions in total)	upper eyelids (two electrodes for each eye)	wrist on the right hand	EEG power spectra, Visual field improvement

Cont.

Diseased brain	Visual impairment	Schmidt et al. (2013)	9-37 Hz	Individual stimulation intensity (< 500 $\mu$ A)	25 to 40 min of each session for 10 days (10 sessions in total)	superior and inferior to the eye (two electrodes for each eye)	occipital pole	EEG power, Visual field improvement
		Bola et al (2014)	Individual stimulation frequency	Individual stimulation intensity	40 min of each session for 10 days (10 sessions in total)	at or near eyeballs (two electrodes for each eye)	NA	EEG power spectra, functional connectivity, coherence
Parkinson disease		Brittain et al. (2013)	individual tremor frequency	2000 $\mu$ A	10 minutes	contralateral motor region (5 x 7 cm)	ipsilateral (to tremor) shoulder (5 x 11 cm)	phase alignments
		Krause et al. (2013)	10 and 20 Hz	1000 $\mu$ A	15 min	M1	contralateral orbit	Motor performance, Cortico-muscular coupling

In addition to motor studies, ACS techniques have also been used for examining brain rhythms and cortical excitability in visual processing (Herrmann et al., 2013). Kanai et al. (2008) evaluated the application of ACS. These authors used tACS to demonstrate how the visual cortex perceives phosphenes and how cortical oscillation can be manipulated when participants are in different light conditions (light and dark). The authors subjected participants to different tACS at various intensities including 125, 250, 500, 750 and 1000  $\mu$ A at different frequencies (4, 8, 10, 12, 14, 16, 18, 20, 22, 24, 30 and 40 Hz). The results revealed that perception of phosphenes in light conditions were only seen in the beta frequency range (14–20 Hz). On the other hand, in dark conditions the perceptions of phosphenes were only observed in the alpha frequency range (10–12 Hz). However, the study failed to clarify whether the stimulation was achieved by the retina or the cortex or both. However, recent studies have focused on addressing the concern noted by Paulus (2010) regarding the contribution of the retina in visual cortex excitability. For example, Schutter and Hortensius (2010) evaluated the potentiality of retinal influences on phosphenes by subjecting healthy participants to tACS at different frequencies (2, 10 and 20 Hz for a duration of 10 seconds) in a dimly lit room. The participants experienced more intense phosphenes during the frontalis-vertex montage than the occiput-vertex montage. The results led the authors to hypothesize a volume conduction effect of the scalp. This hypothesis prompted a second experiment examining voltage potentials when the electrodes were placed in different regions on the right eye such as the canthus, supra-orbital and sub-orbital regions. The results from the second experiment revealed that the electrodes placed near the eye showed greater voltage-related potentials than those placed further from the eye. The second experiment provided evidence that the retina influences cortical modulation. Kanai et al. (2010) additionally decided to examine the modulation of the visual cortical excitability during tACS by extending the study. The third experiment used different tACS frequencies (5, 10, 20 and 40 Hz) previously measured using TMS. The results revealed that only 20 Hz increased the excitability of the visual cortex. As a result, the authors concluded that retinal stimulation on the activation of the visual cortex was possible.

Zaehle et al. (2010) conducted the first study showing evidence of the electrophysiological effect of ACS on neuronal oscillatory activities in the visual cortex. The authors used healthy subjects and subjected them to ACS stimulation in the alpha range (8–12

Hz). Zaehle et al. (2010) found that alpha stimulation increased the alpha power. Additionally, Neuling et al. (2013) evaluated the effect of ACS and found that EEG after effects was directly related to the individual alpha power. tACS was only able to influence the alpha powers, especially in the condition with low endogenous individual alpha powers (open eyes), but not with high endogenous individual alpha powers (closed eyes). Recently, Vossen et al. (2015) observed increased EEG alpha power after tACS, particularly with long intermittent tACS (8 s) in comparison to short intermittent tACS (3 s). The EEG alpha power after tACS did not differ based on phase-continuity (short phase-continuous, long phase-continuous and long phase-discontinuous). However, the phase-locking results showed that the synchronization of neural oscillation was not long-lasting, indicating that tACS induced plasticity in neuronal networks. This finding may also have relevance for the application of transorbital ACS, which will be discussed later.

As a result of several studies that evaluated the effectiveness of non-invasive ACS in the treatment of visual problems (Chibisova et al., 2001; Fedorov et al., 2005, 2011; Sabel et al., 2011a; Gall et al., 2011), this methods cannot yet be adopted as therapeutic techniques because there is not enough evidence. Early studies (e.g., Chibisova et al. (2001) and Fedorov et al. (2005)) described how small currents were used to stimulate visual pathways via a non-invasive application. A later study by Fedorov et al. (2011) showed how a 10-day course of repetitive transorbital ACS (rtACS) in both eyes improved visual acuity and visual field of 446 patients with optic nerve lesions. During the application of rtACS, different frequency ranges were used, which were between the low alpha and flicker fusion frequencies. Flicker fusion frequencies refer to frequencies that allow continuous visual light rather than a distinct flickering of phosphenes. Furthermore, EEG analysis showed that there was an increase in alpha power at the occipital sites (Sabel et al., 2011a; Schmidt et al., 2013), which is a clear indication of increased synchronizations of neural networks after the application of rtACS.

A study comparing rtACS and sham stimulations revealed that the rtACS group experienced significant improvement in visual field detection deficit, reaction time, and visual acuity (Sabel et al., 2011a). According to the authors, only areas of residual vision showed improvement, which was consistent with the residual vision activation theory of Sabel et al. (2011b). The patients received a 10-day application of rtACS, which led to long-term changes to

the impaired visual fields; stable visual improvements were recorded after a two-month follow-up. Furthermore, Gall et al. (2011) reported improved visual functioning and visual-related quality of life after the application of rtACS.

Research shows that the effects of rtACS in functional networks are beneficial in understanding the underlying mechanism of ACS. Bola et al. (2014) evaluated alpha band functional connectivity and studied the effect of rtACS on perceptual functioning. These authors evaluated the effect of rtACS on the impairment caused by the presence of lesions, and they found lower power of oscillatory activity and decreased strength of short- and long-range connectivity compared with the healthy group. The study found that the use of rtACS increased the functional connectivity of alpha band; rtACS furthermore modified the network topology and showed that synchronization within non-affected network was beneficial since it improved visual perception (Bola et al., 2014).

Apart from improving the visual system, the ACS technique has also been found to have beneficial effects in people suffering from Parkinson's disease (PD). PD is defined as a progressive movement disorder manifested when neurons in the brain, especially in the substantia nigra, start to lose their capabilities (Beitz, 2014; Gröger et al., 2014). Neurons in the substantia nigra produce dopamine, which is a neurotransmitter chemical responsible for planning and regulation of body movements (Arias-Carrión et al., 2010) and which mediate reward (Ilango et al., 2014). The death of neurons in this regions causes a reduction in dopamine, which results in a reduction in the person's ability to regulate his or her body properly (Kourtidou et al., 2015). However, as a result of motor activities being associated with the changes of beta frequency oscillations, beta-band oscillations have been proposed to modulate oscillatory activity in people with PD (Schnitzler and Gross, 2005). Brittain et al. (2013) evaluated the effects of tACS on the motor cortex of patients with tremor-dominant PD and found that tACS at the individual tremor frequency was the most effective technique for inducing cortical phase cancelations. Krause et al. (2013) evaluated the effectiveness of 10 and 20 Hz ACS and sham ACS using healthy and patients with PD; these authors found that only the 20 Hz frequency was effective because it was the only one that produced the after effect. Specifically, 20 Hz tACS was found to reduce the beta band cortico-muscular coherence amplitude during the isometric contraction and amplitude variation in patients with PD but not in healthy subjects during fast

finger tapping. On the other hand, the results of Krause et al. (2013) from healthy people were discrepant from those found in previous studies; this difference can be attributed to the use of older people and smaller changes in the tACS methodology. The studies revealed that transcranial beta-band ACS is capable of modulating cortical motor oscillation in PD patients and that it, therefore, can be used as an intervention in PD control.

Apart from the motor and visual effects, the effects of ACS were also found in somatosensory modality (Feurra et al., 2011b). Feurra et al. (2011b) evaluated the effects of 35 different frequencies of tACS (2–70 Hz) delivered randomly. The subjects were instructed to rate the strength of tactile sensations. The results revealed that tACS had a stronger tactile sensation at the alpha frequency range (10–14 Hz) and the high gamma range (52–70 Hz).

Furthermore, there have also been some studies that have reported the ability of tACS to modify higher cognitive functions (Polanía et al., 2012a; Sela et al., 2012). To evaluate the effectiveness of tACS, Polanía et al. (2012) applied tACS at 6 Hz over the left prefrontal and parietal cortices (F3 and P3, respectively). The 6 Hz frequency was delivered to a sample with synchronized conditions (relative 0°) and desynchronized conditions (relative 180°), and these conditions were additionally compared with sham stimulations. The aim of the study was to investigate reaction time during a memory task in healthy people. The results showed that the reaction times of people with desynchronized conditions were longer than those of the sham conditions. Sela et al. (2012) also applied theta-band tACS to investigate risk-taking behavior in people using a balloon analog risk take (BART). BART refers to a conceptualized task that has been developed to understand how people react to real-work risk behaviors (e.g., gambling) that provide a risk of losing or winning. In this study, participants were typically presented with balloons and then given the opportunity of losing or winning a prize. The prize was given to individuals who obtained the largest number of points for inflating a balloon. As a result, points were garnered through cautious decisions of either to keep inflating and risk explosion or to stop after each pump. The study used tACS with a 6.5 Hz frequency delivered over both the left and right dorsolateral prefrontal cortex (DLPFC). The subjects was divided into three groups, and each group received different stimulations at the different electrode position: left DLPFC, right DLPFC and sham stimulation. The results did not show any effects of tACS for the right DLPFC and sham stimulations. However, the stimulation of left DLPFC showed sequential losses of the

chance to win. In the analysis, the authors found that subjects were not able to make a decision because of either negative feedback or error. As a result, they concluded that theta band ACS can be used to modulate decision making. Santarnecchi et al. (2013) applied transcranial ACS over the left middle frontal gyrus in healthy subjects while conducting Raven's Advances Progressive Matrices (RAPM). RAPM is a nonverbal intelligence test that decides the individual's fluid intelligence, the ability to identify and resolve issues. RAPM has the stimulus characteristics form a 3x3x3 matrix to present about 3000 matrices combining various orientations, colours, and shapes. For completing the pattern, subjects need to identify the absent component within a maximum of 60 seconds. On the basis of analogical operations (matrices with one, two, or three relations and logic trials), inferring the correct response is possible. The subjects received both ACS at different frequencies (such as 40, 20, 10, or 5 Hz) and sham stimulation in a random fashion during the intelligence test. The authors revealed that the application of tACS at 40 Hz improved performance (i.e., decreased the time of response), particularly for complex trials (logic trial), compared to sham and other stimulation frequencies. Therefore, the authors suggested that tACS in the gamma range increased fluid intelligence in cognitive tasks. Moreover, Lustenberger et al. (2015) applied 10 Hz ACS and sham stimulation over the bilateral frontal cortex while conducting the Torrance Test of Creative Thinking (TTCT) in healthy subjects. The authors aimed to investigate the effects of 10 Hz tACS on creative thinking. Ten Hz tACS increased creativity index scores and individual creativity subscales (i.e., fluency, originality, elaboration, abstractness of titles, and resistance to premature closures) compared to sham stimulation. Lustenberger et al. (2015) further decided to conduct extended experiments to eliminate the probable effects of modulation of frequency on creativity. In this context, the authors applied 40 Hz ACS over the bilateral frontal cortex while conducting the TTCT. The authors reported no enhancement in the creativity index or individual creativity subscales at 40 Hz ACS relative to sham stimulation. On the basis of these two experiments, the authors implied that creative thinking can be improved by applying transcranial ACS at alpha band frequencies (10 Hz).

As noted above, there is strong evidence showing that ACS can modulate cortical oscillation. Even so, most studies have been based on the after-effects of the stimulation. Recently, Helfrich et al. (2014) successfully indicated online electrophysiological effects of tACS on visual tasks. The authors used simultaneous EEG recording and 10 Hz tACS for 20

minutes delivered over the parietal-occipital cortex. The results revealed the capability of tACS to increase parieto-occipital alpha activities and enhance synchronization of cortical oscillations. Interestingly, long-lasting effects after the end of stimulation has been observed (e.g., a significant correlation between alpha power during stimulation and alpha power after stimulation). The results of the study also showed that tACS was capable of modulating targeted detection performance in a phase-dependent fashion and the causal role of alpha oscillations in visual perception.

### **2.3.5 Safety Issues**

Previous studies demonstrated that non-invasive brain stimulation, including ACS, is safe with a fairly low risk of side-effects if used within the allowed safety limits (Nitsche et al., 2003, 2008; Poreisz et al., 2007; Bikson et al., 2009; Brunoni et al., 2011). To limit the probability of side effects and adverse implications, various safety limits have been defined, such as the highest current density, charge density, stimulation duration and stimulation frequency (Nitsche et al., 2003, 2008; Poreisz et al., 2007; Bikson et al., 2009). Only minor side effects have been reported by subjects, including a light itching sensation under the electrode or sponge during stimulation, tingling, a burning sensation, mild headache, nausea, and fatigue (Nitsche et al., 2003, 2008; Poreisz et al., 2007; Bikson et al., 2009; Brunoni et al., 2011). In the case of transorbital ACS, no serious side effects were observed during clinical trials (Sabel et al., 2011a; Gall et al., 2011). Although the side effects of ACS are considered to be mild, the side effects of repetitive ACS application and even a single session of ACS have not been fully clarified. Therefore, future studies are needed to further investigate the safety of these methods, as few publications on this topic are currently available.

### **2.3.6 Summary and Future Direction**

In recent years, studies focusing on the use of non-invasive methods to stimulate the brain have rapidly increased in prevalence. Although it is a relatively new technique, ACS has been found to be an effective method in modulating brain rhythm activity. The studies discussed above have demonstrated the effectiveness of ACS in various experiments especially those dealing with motor (Antal et al., 2008; Moliadze et al., 2010; Feurra et al., 2011a; Chaieb et al., 2014; Schutter and Hortensius, 2011; Pogosyan et al., 2009; Wach et al., 2013), visual (Kanai et al.,



2008; Paulus, 2010; Schutter and Hortensius, 2010; Zaehle et al., 2010; Neuling et al., 2013; Fedorov et al., 2005; Sabel et al., 2011a; Gall et al., 2011; Schmidt et al., 2013; Bola et al., 2014), somatosensory (Feurra et al., 2011b) and higher cognitive functions (Polanía et al., 2012a; Sela et al., 2012).

Currently, there are only a limited number of studies that have reported the beneficial effects of ACS on a clinical population that includes patients with PD (Brittain et al., 2013; Krause et al., 2013) and patients with visual impairment (Sabel et al., 2011a; Gall et al., 2011; Fedorov et al., 2011; Bola et al., 2014). Although many studies have reported the beneficial effects of ACS, only a few have reported the mechanism and functional reorganization achieved by the technique. As a result, more research is required to understand the underlying mechanism and, at the same time, determine optimal protocols and parameters in both research and clinical practice.

The ACS technique has emerged as one of the potential options in the therapeutic field of brain stimulation because of its minimal side effects. Additional studies are needed to incorporate neuroimaging techniques such as functional magnetic resonance imaging to evaluate immediately and after effects of the ACS brain stimulation technique. There have been a few recent studies using combined experiments such as tDCS (Antal et al., 2011; Holland et al., 2011; Clark et al., 2012; Meinzer et al., 2014) and tRNS (Chaieb et al., 2009). This is a particularly interesting approach because it provides information regarding functional activations and ACS modulation. To increase the understanding of the ACS effect, knowledge of spatial intensity (activation area) and signal intensity (temporal or activation strength) are necessary; it is furthermore critical to examine their effect in different regions of the brain to complement our understanding gained from electrophysiological as well as behavioral measures. Therefore, in this thesis, the after effects of transorbital ACS in the early visual cortex was explored with 7 Tesla fMRI and will be discussed in chapters 4 and 5 of this thesis.

## CHAPTER 3

### **STUDY I: QUANTITATIVE ASSESSMENT OF VISUAL CORTEX FUNCTION WITH 7 TESLA fMRI: TEST-RETEST VARIABILITY**

The work presented in this chapter has been accepted for publication:

**Aini Ismafairus Abd Hamid**, Oliver Speck, and Michael B. Hoffmann. 2015. Quantitative assessment of visual cortex function with fMRI at 7 tesla – test-retest variability. *Frontiers in Human Neuroscience* 9. doi:10.3389/fnhum.2015.00477.

#### **3.1 INTRODUCTION**

Human brain function can be investigated through the application of a widely used neuroimaging method called functional magnetic resonance imaging (fMRI). Visual field locations in the occipital cortex are identified using retinotopic mapping. The application of fMRI and retinotopic mapping stimuli allows the identification of cortical visual areas and the functional specialization of the visual system. In addition to fMRI, the visual topography or retinotopic reorganization in the visual cortex can also be examined using positron emission tomography (PET) and event-related potentials (ERPs) (Woldorff et al., 1997). However, fMRI results are susceptible to the effects of various factors associated with the image signal-to-noise ratio, motion artefacts, magnetic field inhomogeneities, cognitive processes, and long-term cognitive strategies, among other issues (Krüger and Glover, 2001; Huettel et al., 2008; Bennett and Miller, 2010).

The test–retest design is widely used in the neuroscience field to understand the occurrence of response variabilities over time and the detection accuracy. For instance, the

application of a repeated measures design in clinical studies of neurological disorders can highlight the modification of brain activation, structure, and connectivity in association with disease development, treatment or recovery. Therefore, to understand the implications of treatment, it is crucial first to understand the repeated measures test-retest variability for the patterns of brain activation exhibited by normal subjects. Thus, insights into methodological issues, such as experience-based effects can be gained from test-retest studies of normal subjects (Kelly et al., 2006).

The results of fMRI test-retest studies were assessed by earlier studies in terms of various tasks pertaining to auditory, motor, visual and cognitive stimuli (Specht et al., 2003; Johnstone et al., 2005; Kong et al., 2007; Raemaekers et al., 2007; Friedman et al., 2008; Caceres et al., 2009; Bressler and Silver, 2010; Seibert et al., 2012). However, insufficient knowledge is available regarding visual areas and retinotopic mapping. In one study, Bressler and Silver (2010) observed that the fMRI retinotopic mapping signals in the occipital and parietal cortex became more reliable due to spatial attention tasks. Those authors derived this observation from an experiment involving the use of a rotating checkerboard wedge stimulus, with the subjects being requested to focus on the wedge (attention-to-wedge task) or the central fixation point (attention-to-fixation task).

Various methods have been applied to evaluate the test-retest validity of fMRI results, including the Pearson product-moment correlation coefficient (Pearson's  $r$ ) (Fernández et al., 2003), the maximum likelihood (Maitra et al., 2002), and the intra-class correlation coefficient (Raemaekers et al., 2007; Friedman et al., 2008; Caceres et al., 2009; Bressler and Silver, 2010; Seibert et al., 2012). However, there is currently no widely accepted gold standard. Given these considerations, the purpose of the present study is to investigate systematic variations in the fMRI response between sessions. Therefore, the inter-session activation were compared using several measures that were employed in earlier studies. Furthermore, the activation extent, response amplitude, and coherence were used to permit comparisons of this study with previous studies. The reproducibility of phase maps in early visual areas was also assessed to determine how similar those maps are across sessions.

Visual studies frequently use retinotopic mapping, but the understanding of brain activity modifications in the same subject, particularly with regard to test-retest paradigms, is limited. This study evaluates inter-session systematic variations in activated cortical surface area, fMRI signal amplitude and coherence using the standard retinotopic mapping techniques of eccentricity and polar angle mapping, as well as full-field tasks.

## **3.2 MATERIAL AND METHODS**

### **3.2.1 Subjects**

This study included seven subjects with no history of ophthalmological or neurological conditions. These subjects were  $29 \pm 4$  years of age, and three of the subjects were female. The experimental procedures were conducted in accordance with the principles of the Declaration of Helsinki (World Medical Association, 2000), and protocol approval was obtained from the ethics committee of the University of Magdeburg, Germany. The subjects were informed of the purposes of the study and provided their written consent for participation. All test-retest experiments were carried out at the same time of day. Sessions 1 and 2 were separated by an interval of  $51 \pm 5$  days, while Sessions 2 and 3 were separated by an interval of  $168 \pm 24$  days. Subjects 1 and 7 had no knowledge of the procedure while the remaining five subjects had already been involved in fMRI experiments. In fact, subject 6 had been involved in a retinotopic mapping study ten months before Session 1 of the present study.

### **3.2.2 Visual Stimulation for fMRI**

The visual stimuli were back projected with a video projector (DLA-G150CL, JVC Ltd.) onto a screen (horizontal viewing angle  $\sim 14.8^\circ$  and vertical viewing angle  $\sim 8.3^\circ$ ) behind the subject and viewed via a surface mirror mounted onto the head coil. The stimulus patterns were approximately m-scaled to compensate for the cortical magnification of the visual stimulus (width of the most central and most peripheral ring  $0.1^\circ$  and  $1.0^\circ$ ) and comprised a contrast inverting (with 8 reversals per second) circular checkerboard of  $7.4^\circ$  radius consisting of black and white checks with 24 segments and 26 rings (mean luminance  $62 \text{ cd/m}^2$ , contrast 99%). Identical presentation of the visual stimulation is necessary to allow comparability between the three-time points. The average stimulus luminance of  $62 \text{ cd/m}^2$  and 99% contrast were ensured at

all three points based on photometer calibration (CS-100A Konica Minolta). To produce the desired luminance and contrast of the stimuli, the gamma function, which relates numeric input and visual output for each projector colour channel, has been considered in the computed RGB-values.

The subjects were instructed to fixate on a central-fixation marker ( $0.34^\circ$  diameter) and to report any color changes (200 ms duration at intervals between 5–10 s) by pressing a button. Each experimental scan started with a 12 s scan dummy stimulation period and was followed by seven 36 s cycles of visual stimulation for rings and rotating wedges and ten 24 s cycles of visual stimulation for full field. Phase-encoded paradigms in retinotopic mapping stimulated different parts of the visual field during different stimulation epochs, i.e., increasing or decreasing polar angle for (i) polar-angle mapping and increasing or decreasing eccentricities for (ii) eccentricity mapping. Thus, only a section of the contrast-reversing checkerboard was presented at a time: (i) Polar angle mapping: Polar angle stimuli stepping through clockwise and counterclockwise direction were presented. The wedge was 6 segments ( $90^\circ$ ) wide and stepped 54 times by  $6.7^\circ$  in each of the 36 s cycles. (ii) Eccentricity mapping: The stimulus moved through the eccentricities as an expanding or contracting ring. The ring was  $0.97^\circ$  wide and stepped 54 times by  $0.32^\circ$  in each of the cycles. It expanded uniformly beyond the maximum extent of the screen for 5 s and then wrapped around to the fovea. This stimulation gap helped to distinguish peripheral from fovea responses in the eccentricity mapping data (Hoffmann et al., 2009). For the third type of visual stimulation, i.e., full field stimulation, subjects viewed 12 s checkerboard reversal (8 reversals per second) followed by 12 s gray (same mean luminance in both epochs) in a block design. Altogether, the fMRI measurements took around 30 minutes.

### **3.2.3 fMRI Acquisition**

For functional imaging, T2\*-weighted echo-planar images (EPI) were acquired with a 7 Tesla whole body MRI scanner (Siemens Healthcare, Erlangen, Germany) using a 32 channel head coil (Nova Medical, Wilmington, MA). The gradient-echo EPI pulse sequence had the following parameters: repetition time (TR) = 3000 ms, echo time (TE) = 21 ms, field of view (FOV) = 140mm, flip angle ( $\alpha$ ) =  $90^\circ$ , and voxel size = 1 mm x 1 mm x 1 mm. Forty-five slices were acquired perpendicular to the calcarine sulcus for a duration 264 s with 88 volumes (dummy

stimulation period and 7 cycles) for eccentricity and polar angle mapping, and 252 seconds with 84 volumes (dummy stimulation period and 10 cycles) for the full-field stimulation. In addition, high-resolution anatomical images of the occipital region were obtained using T1-weighted 3D-MPRAGE with the following parameters: acquisition time = 296 s, TR = 2300 ms, TE = 2.66 ms, inversion time = 1050 ms, FOV = 256 mm, isotropic resolution = 1 mm. 3D-MPRAGE inhomogeneity was corrected by division with 3D gradient echo (GE) reference data (Van de Moortele et al., 2009) without inversion and otherwise identical parameters but: acquisition time = 170 s, TR = 1340 ms. The functional images were corrected online for motion and spatial distortions (In and Speck, 2012).

Over the course of all the experiments, no MR system upgrade or modification took place and no auxiliary equipment had been installed or removed. The MR system performance for fMRI experiments has been tested at least once per week as part of the regular quality assurance procedure and no relevant parameters (SNR, signal stability, signal homogeneity, RF-parameters, EPI ghost level) showed any deviation from the established reference values.

### **3.2.4 Cortical Flattening**

In order to provide homogenous white and grey matter contrast for segmentation, T1-weighted inhomogeneity corrected MPRAGE images (Van de Moortele et al., 2009) were used to segment the cortex and to create a flattened representation of the cortical gray matter (Teo et al., 1997; Wandell et al., 2000). Gray and white matter were segmented using Freesurfer, ITK Gray, 1.6.0.1., and mrGray (VISTA) and were manually edited to minimize segmentation errors. The anatomical segmentation and flattening was done once per subject.

### **3.2.5 Preprocessing of Functional Images**

In the three scanning sessions, identical methods were used for fMRI data analysis. The functional images were analyzed using the Stanford VISTA-Tools (VISTA; <http://white.stanford.edu/software/>). The T2\*-weighted images were aligned to the T1-weighted images' coordinate frame to project the fMRI time series onto the flattened cortex representation. Each voxel's time series (TS) underwent the following analysis steps: (1) dummy stimulation period (12 s or 4 volumes) of each functional run was discarded to avoid transient-onset artifact;

(2) final single cycle (36 s, i.e. 12 volumes) at the end of each functional run was also discarded for eccentricity and polar angle due to a reconstruction failure and an incorrect volume setting for two subjects in one of the sessions. These two scans were not excluded because only a few volumes at the end of the scans were involved. Thus, six stimulation cycles were retained for eccentricity and polar angle mapping and 10 stimulation cycles for full-field analysis for each subject; (3) TS were divided by their mean intensity; (4) for one of the opposing directions in the three types of visual stimulation (contracting vs expanding rings, clockwise vs counter clockwise rotating wedges, and on vs off start of full field stimulation) the TS were flipped in time. Then the hemodynamic delay of the flipped TS was corrected by shifting the TS by six seconds (i.e., two TR). (5) TS of opposing directions were averaged to remove or cancel the residual phase lags caused by residual hemodynamic delays of the two stimulus directions. This technique allows examining the true phase of the eccentricity and polar angle (Serenio et al., 1995; Larsson and Heeger, 2006; Silver et al., 2005; Smith et al., 1998); (6) data were Fourier transformed to calculate the amplitude and the response phase for the stimulus frequency; (7) the correlation, technically coherence, was measured (Engel, 1997). The coherence is calculated from the time series with a sinusoid with the frequency having the same value as the fundamental frequency (i.e. 1/36 Hz for 36 s stimulus described above) of the visual stimulation (Engel, 1997). The coherence value was determined independently for each voxel in the functional scan. The coherence value represents the strength of the response of that voxels to each visual stimulation condition.

For qualitative assessment and presentation of the response maps in the flattened representation, the coherence and phase values were smoothed by convolving a Gaussian Kernel (full width at half maximum: 4 mm) with the complex-vector representation of the BOLD response. The statistical significance levels, or  $p$ -values, for associated coherence values were estimated according to Silver et al. (2005). For all repeated measures of individual results, a threshold of  $p=0.05$  was applied for multiple comparison (Zandbelt et al., 2008; Plichta et al., 2012): only voxels with coherence values exceeding 0.18 were considered for further analysis. No spatial or temporal filtering was applied for any quantitative analyses (amplitude, coherence, or any responses in the EPI planes) to avoid loss of resolution. Data quality evaluation was performed through direct visual inspection and did not show signal dropouts due to local susceptibility artefact.

The identification of the visual areas V1, V2, and V3 was performed on the data averaged across all three sessions in order to avoid the intrusion of systematic inter-session effects. The boundaries between the visual areas were delineated manually on the cortical flat maps based on the response phase reflected in the false-colour maps for polar angle and eccentricity (Engel, 1997; Engel et al., 1994; Wandell et al., 2007). The borders of the visual areas were representations of the vertical and horizontal meridians in the visual field according to established procedures (Wandell et al., 2007). Subsequently, visual area definitions were used to examine the correlation of phase maps and fMRI signal difference between sessions (Swisher et al., 2007b).

### **3.2.6 Head Motion Assessment**

The uncorrected functional images were used to quantify head movement during the fMRI acquisitions (i.e., without the online motion and distortions correction). McFlirt version 5.0 (motion correction using FMRIB's Linear Image Registration Tool) (Jenkinson et al. 2002) and FSL (FMRIB's Software Library, [www.fmrib.ox.ac.uk/fsl](http://www.fmrib.ox.ac.uk/fsl)) were used to quantify head movement for every scan, with 72 volumes in the case of eccentricity and polar angle and 80 volumes in the case of full-field. Three translation (x, y, and z in mm) and three rotation (x, y, and z in rad) parameters were applied for the assessment of head motion metrics. Subsequently, the root mean square (RMS) of the six parameters enabled the calculation of the head motion index (in mm) (Silver et al., 2005).

### **3.2.7 Statistical Analysis**

Intra- and inter-subject factors were investigated to determine the causes of data variance. The variation in the activated cortical surface area, amplitude and coherence was examined using a repeated measures analysis of variance (ANOVA) by session as the intra-subject factors, while the inter-subject factors were the visual area and stimulation conditions. Fisher transformation was applied to convert the coherence values, which lacked a normal distribution, into normally distributed values. Furthermore, for the obtained 95% confidence intervals, an evaluation was conducted regarding the minimal effect sizes to be identified with the existing design. In addition, as recommended by Philipp (2009), circular correlation (circular Statistic toolbox in Matlab) was employed to investigate the reproducibility of the phase maps in early visual areas



and thus to determine the extent of similarity between the maps attained for different sessions. Fisher's z-transformation was applied to the obtained correlations to convert the values for additional statistical analysis. Independent t-tests were conducted for quantitative comparisons of phase correlation for each of the three visual areas, as well as visual stimulation (eccentricity and polar angle). Finally, repeated measures ANOVA was used to assess modifications in head movement across the sessions.

### **3.3 RESULTS**

Figures 20-22 show the between-sessions patterns for the activated cortical surface area, the response amplitude and coherence for all subjects. All subjects in this study had previous experience participating in fMRI scans, except for subjects 1 and 7. Subject 6 had previous experience with retinotopic mapping. In general, subject 7, who was inexperienced, followed the global patterns, while the inexperienced subject 1 exhibited small increases in response amplitude and coherence. The distinct patterns observed in subject 1 were assumed to be caused by head movement because larger head movements were noticed in this subject than in the other subjects, except for subject 3. Subject 3, who was experienced, also had large values for head movement (Figure 23). Despite the large movement values of those two subjects, their movement values were less than 1 mm; thus, those subjects were not excluded from this study, as the data were uncorrupted according to the present study definition. Additionally, a difference in the head movement pattern for subject 3 was only seen in the first session for eccentricity and full field stimulation. In conclusion, the present study shows that the head motion differences between inexperienced and experienced subject are of marginal importance.

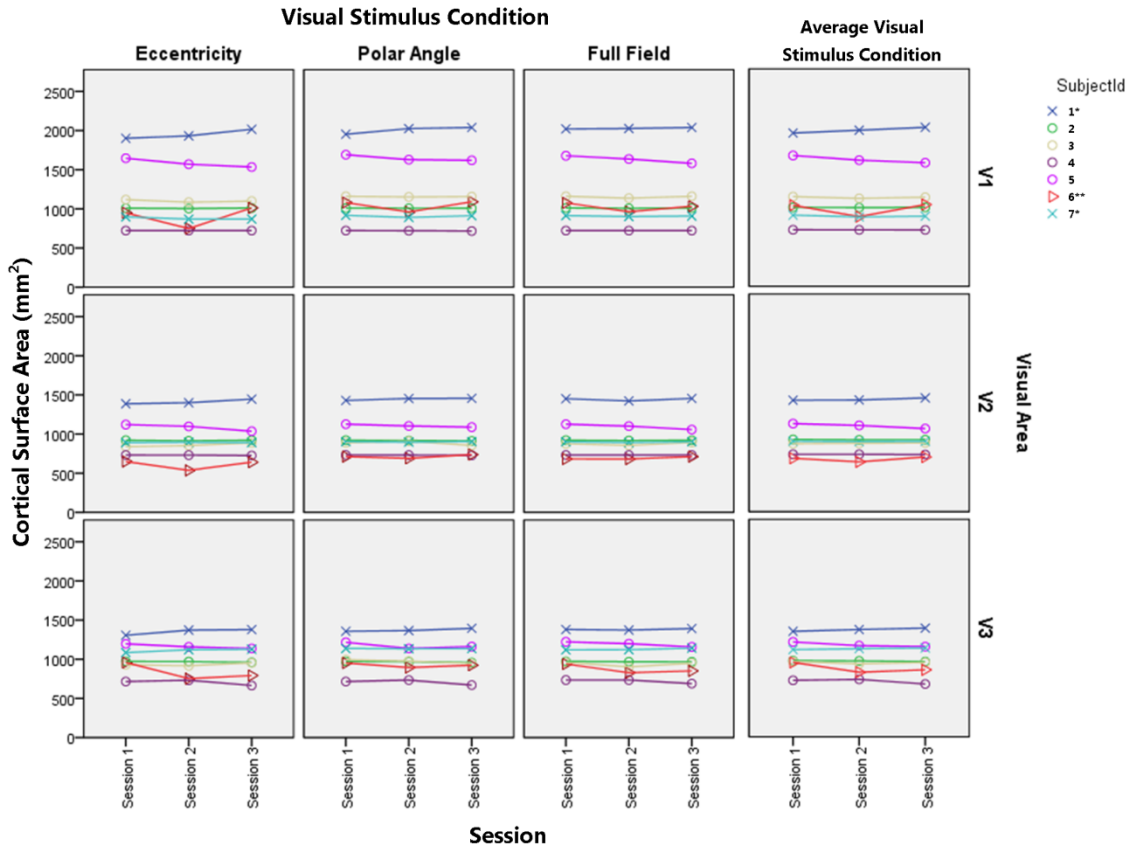


Figure 20. The activated cortical surface area (mm<sup>2</sup>) across sessions in V1, V2 and V3 for all visual stimulation conditions for subjects 1-7 (from Abd Hamid et al. (2015b) ).

Note: \* Inexperienced subject; \*\* Experienced subject in retinotopic experiment (in different study)

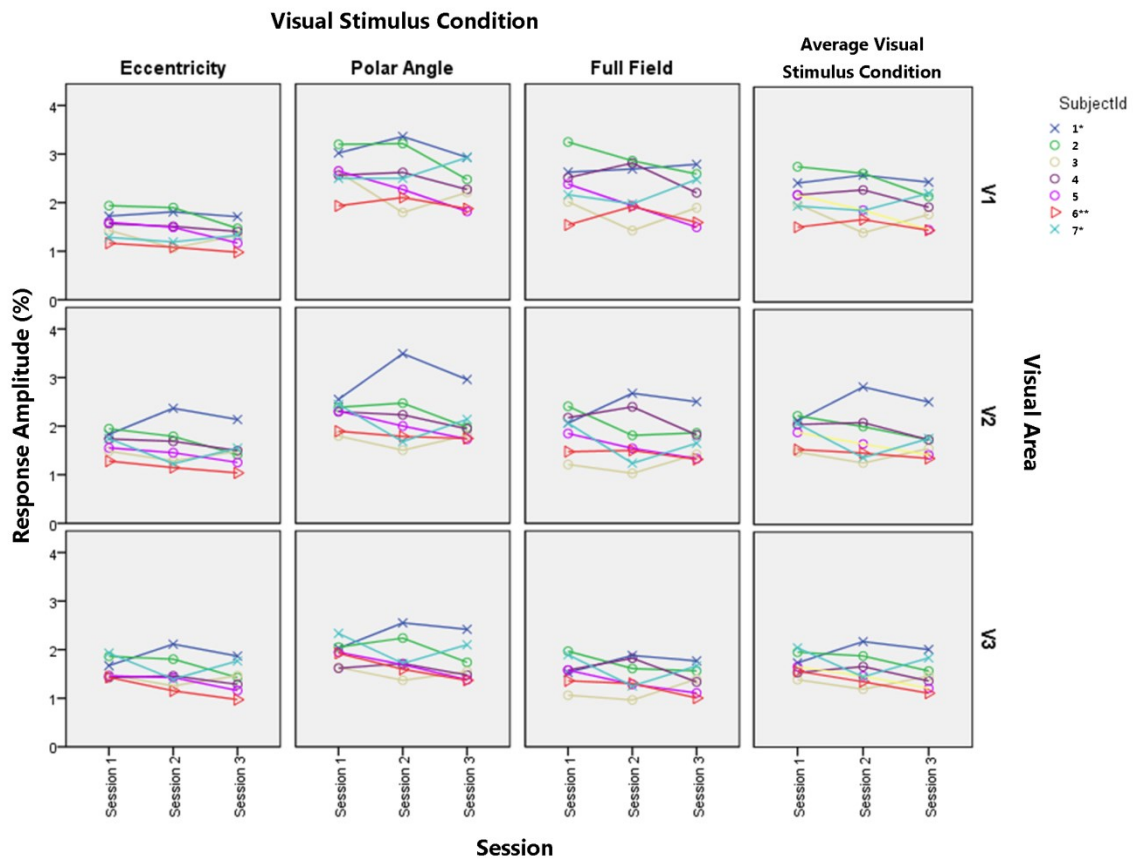


Figure 21. The response amplitude (%) across sessions in V1, V2 and V3 for all visual stimulation conditions for subjects 1-7 (from Abd Hamid et al. (2015b).

Note: \* Inexperienced subject; \*\* Experienced subject in retinotopic experiment (in different study)

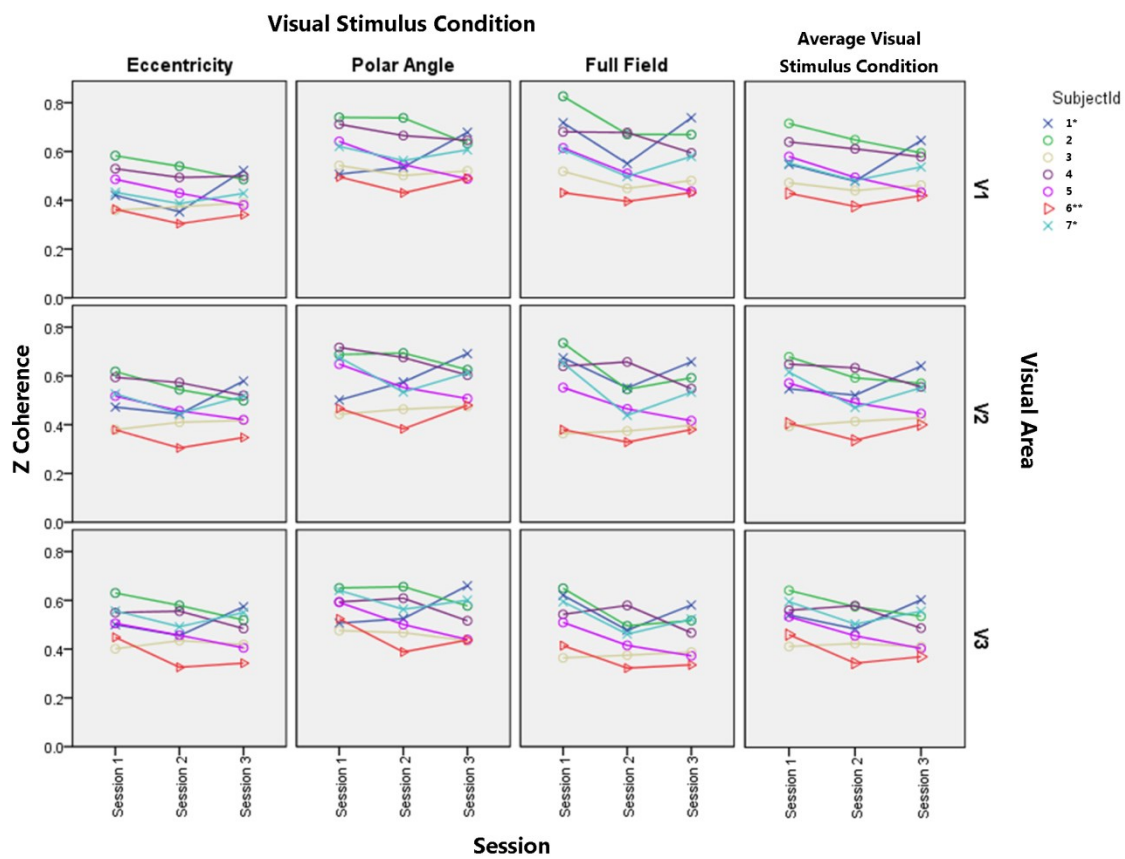


Figure 22. The coherence (Z-transformed values) across sessions in V1, V2 and V3 for all visual stimulation conditions for subjects 1-7 (from Abd Hamid et al. (2015b).

Note: \* Inexperienced subject; \*\* Experienced subject in retinotopic experiment (in different study)

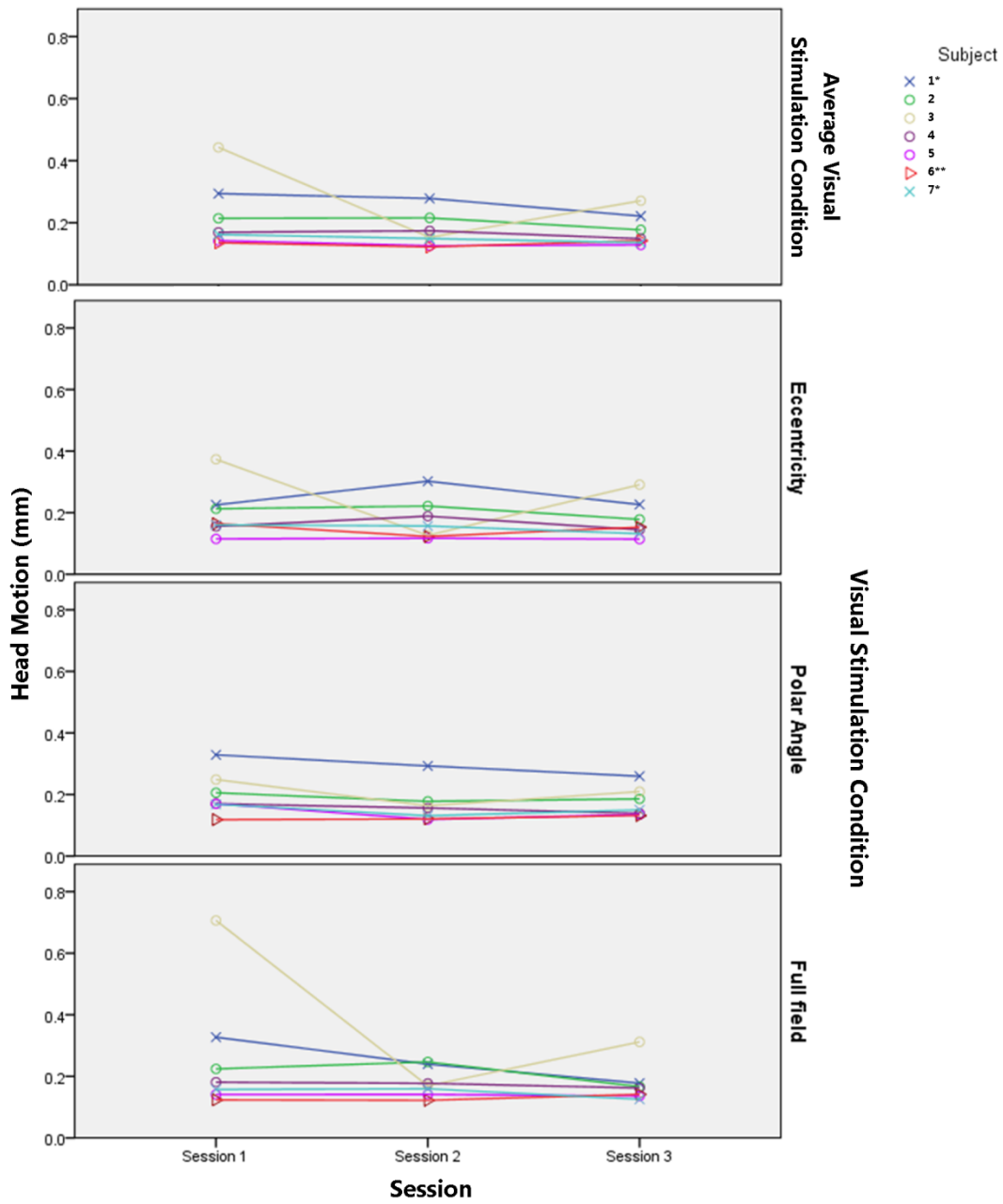


Figure 23. The head motion (mm) across sessions for all visual stimulation conditions for subjects 1-7 (from Abd Hamid et al. (2015b)).

Note: \* Inexperienced subject; \*\* Experienced subject in retinotopic experiment (in different study)

### 3.3.1 BOLD Signals

The response topography associated with eccentricity, polar angle mapping and full-field stimulation is shown by the flat maps of the occipital pole in Figure 24, which pertain to all subjects. It is clear that the response patterns for all three sessions were highly consistent. To quantify the effects, the activated cortical surface area (i.e. voxels with significant fMRI responses ( $p < 0.05$ ; Figure 25)) was identified for each visual area. Afterward, as shown in Figures 26 and 27, the mean amplitude and coherence associated with these super-threshold regions were determined for every visual area and session. A separate three-way repeated measures ANOVA investigations were undertaken to determine the effect significance based on the factors of the session, stimulation condition and visual area (see Table 2). No significant effects (individual and interaction factors) on the activated cortical surface area, the response amplitude and coherence were highlighted by initial three-way repeated measures ANOVA investigations that compared the dorsal and ventral portions of the early visual areas ( $p > 0.05$ ). Hence, the dorsal and ventral portions of the early visual areas V1, V2 and V3 were merged together for further analysis.

*Activated Cortical Surface Area:* Of the three factors of session, visual area, and stimulation condition, only the first two factors were found by repeated measures ANOVA to have significant effects ( $p = 0.05$  and  $p = 0.046$ , respectively). These factors were not observed to have any significant interactions. To further examine the effect of the session and visual area, post-hoc tests were conducted. With respect to the factor of the session, between Sessions 1 and 2, the activated area decreased slightly but significantly ( $1066 \pm 40 \text{ mm}^2$  vs.  $1044 \pm 42 \text{ mm}^2$ ;  $p = 0.006$ ). In the case of the factor visual area, a considerable difference was observed in V1 and V2 ( $1196 \pm 71 \text{ mm}^2$  vs.  $946 \pm 71 \text{ mm}^2$ ;  $p = 0.045$ ), which was also reported by Dougherty et al. (2003).

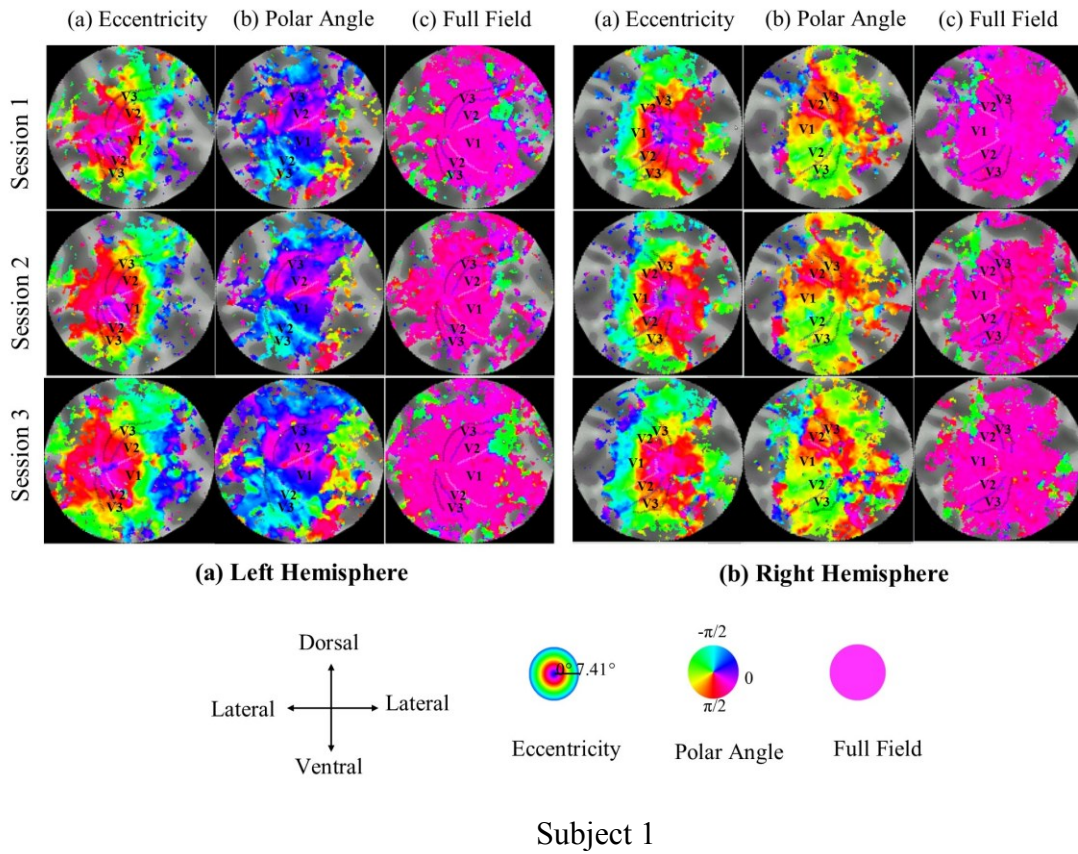
*Response amplitude:* Response amplitude: The repeated measures ANOVA revealed that the response amplitude was affected significantly by the factors of session ( $p < 0.001$ ), visual stimulation condition ( $p < 0.001$ ), and visual area ( $p < 0.001$ ). However, only the visual stimulation condition and the visual area exhibited a significant interaction ( $p = 0.019$ ). Between Sessions 1 and 3, post-hoc tests indicated that the amplitude decreased substantially ( $1.94 \pm 0.04\%$  vs.

1.74±0.05%;  $p<0.001$ ). Additionally, in the case of the visual stimulation factor, post-hoc tests revealed that the amplitude increased for (1) polar angle in comparison to eccentricity (2.17±0.08% vs. 1.51±0.08%;  $p<0.001$ ), (2) full-field in comparison to eccentricity (1.83±0.08% vs. 1.51±0.08%;  $p=0.012$ ), and (3) polar angle in comparison to full-field (2.17±0.08% vs. 1.83±0.08%;  $p=0.010$ ). It was not surprising that considerable discrepancies were observed between the response amplitudes of visual stimulation conditions, given that their stimulation duty cycles are distinct, which influences how the response amplitudes and coherences are quantified based on Fourier analysis (see Methods). Post-hoc tests also revealed that the amplitudes in V1 were greater than those in V3 for the factor visual area (2.07±0.08% vs. 1.61±0.08%;  $p<0.001$ ), consistent with the results obtained by Hoffmann et al. (2009).

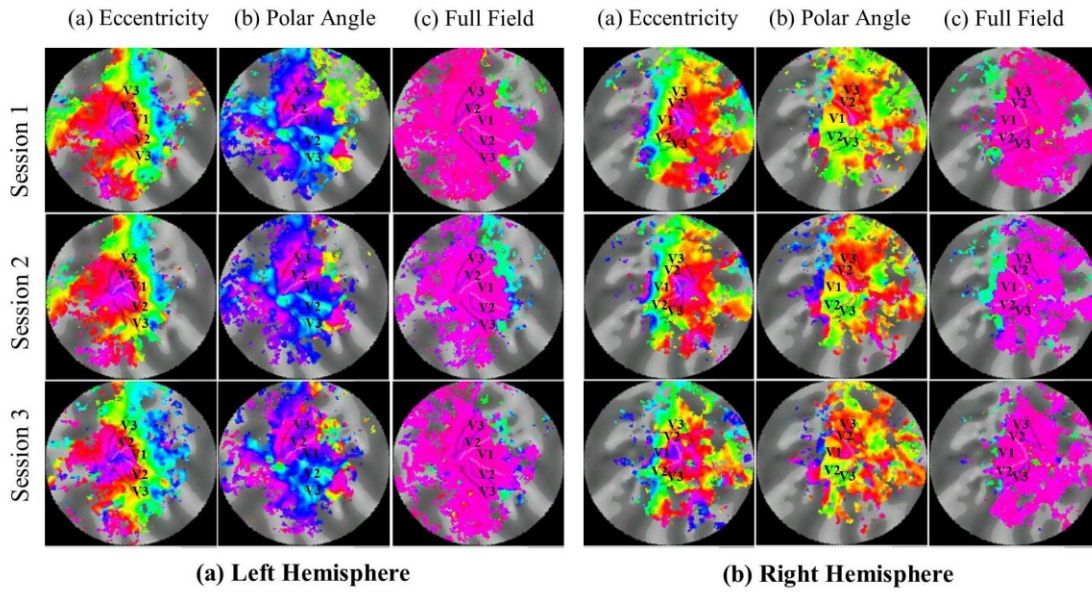
*Coherence:* Important differences were revealed by repeated measures ANOVA concerning the factors of the session and visual stimulation, with no marked interaction between factors. Post-hoc tests indicated that in the case of the factor session, the coherence decreased considerably (1) between Sessions 1 and 2 (0.55±0.01 vs. 0.50±0.01  $p<0.001$ ) and (2) between Sessions 1 and 3 (0.55±0.01 vs. 0.51±0.01  $p<0.001$ ). In contrast, post-hoc tests revealed that in the case of the factor visual stimulation, the coherence was higher for polar angle in comparison to eccentricity (0.57±0.02 vs. 0.46±0.02;  $p=0.001$ ). As was the case with the influence of stimulation on the BOLD signal amplitude, these differences are considered to occur because the different conditions have distinct stimulation duty cycles that affect the assessment of BOLD signals based on Fourier analysis (see Methods and above).

Overall, each of the tested measures was affected by the factor session and exhibited a decrease in Sessions 2 and 3 in comparison to Session 1, regardless of the visual area under investigation. Thus, between Sessions 1 and 2, a 2% reduction in activated cortical surface area was observed ( $p<0.006$ ), between Session 1 and 3, the response amplitude decreased by 11.5% ( $p<0.001$ ), and between Sessions 2 and 3, the coherence decreased by 8% ( $p<0.001$ ). It is worth noting that between Sessions 2 and 3 no session effects were observed. This finding implies that the obtained measures were determined by a “novelty effect” in Session 1. For this study design, which included seven subjects, repeated measures and initial scanning for the elimination of novelty effects, the minimal effect sizes that are identifiable with a 5% significance threshold ( $p<0.05$ ) can be deduced from the scatter of data, especially the 95% confidence interval in

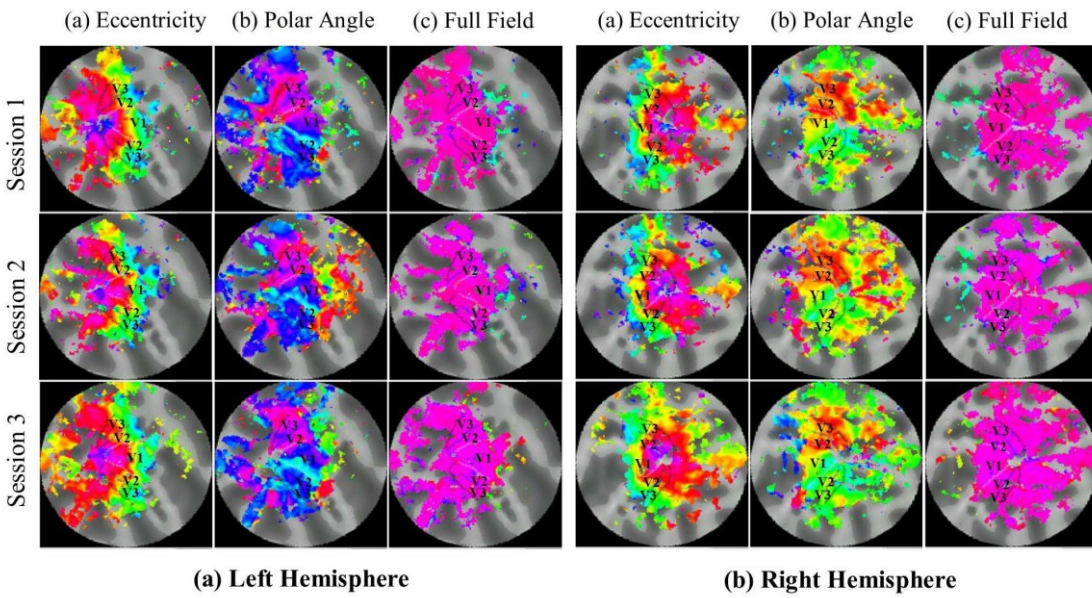
Session 2. This confidence level exhibits variability in the cortical surface area, response amplitude and coherence, on the order of  $\pm 1.5\%$  for the mean cortical surface area,  $\pm 6\%$  for the mean percentage of the amplitude modulation, and  $\pm 5\%$  for the Z-transformed coherence.



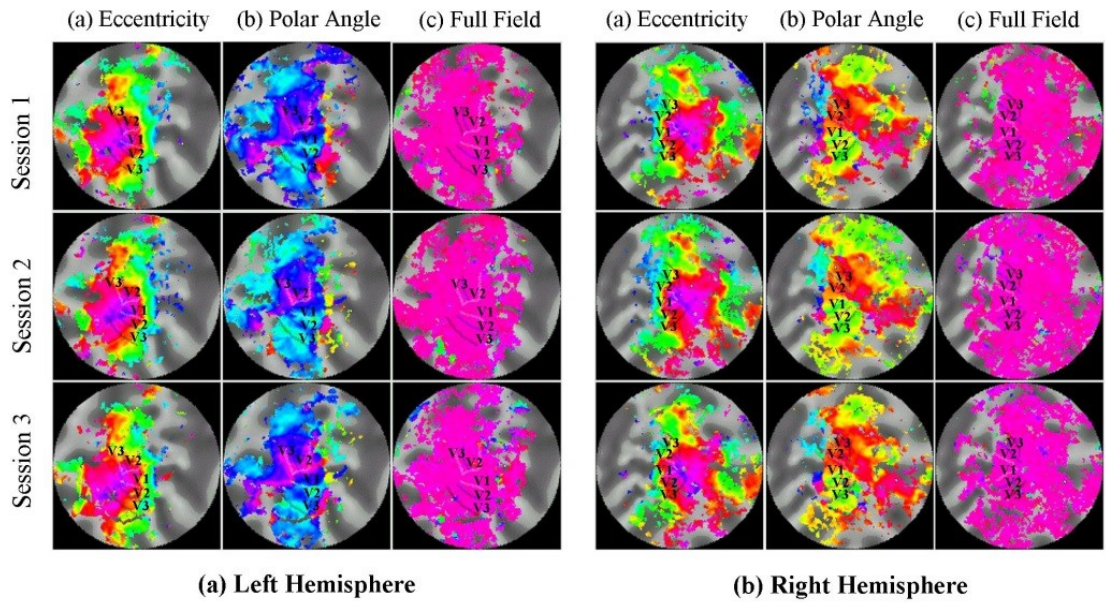




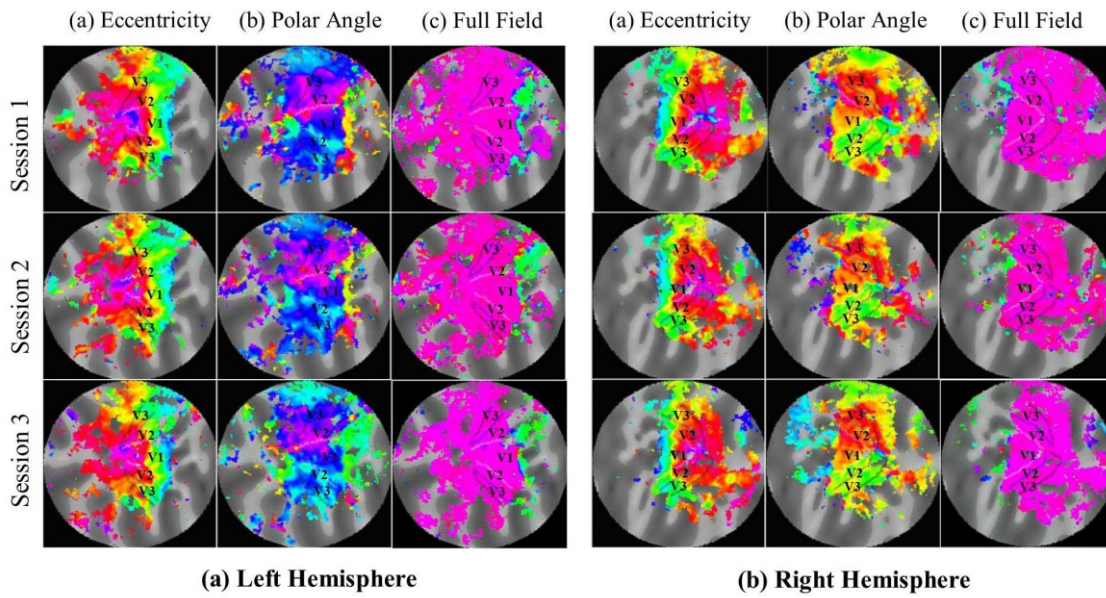
Subject 2



Subject 3

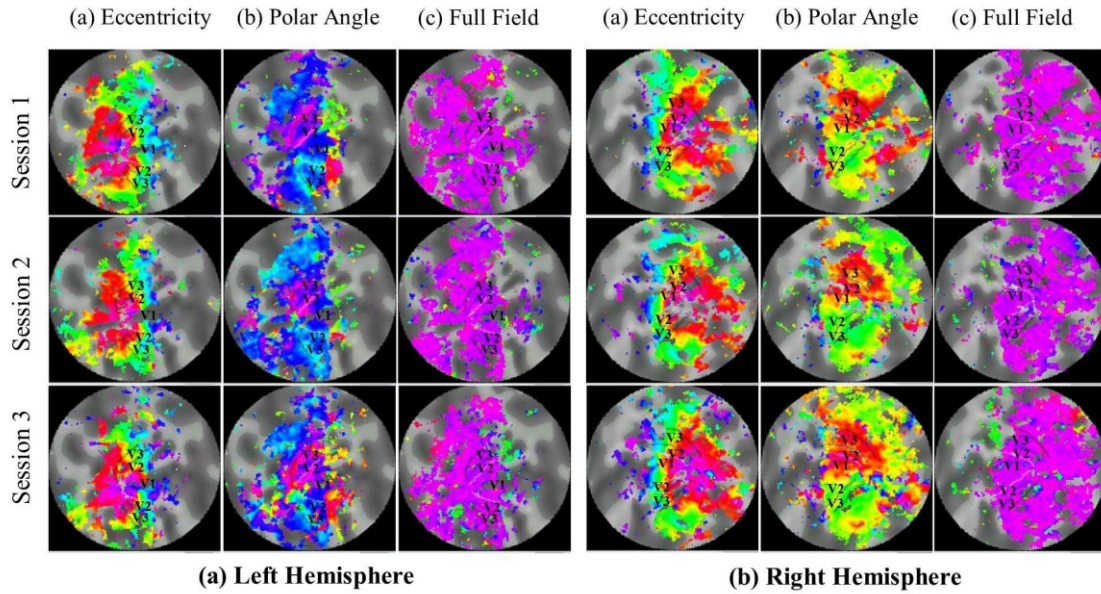


Subject 4

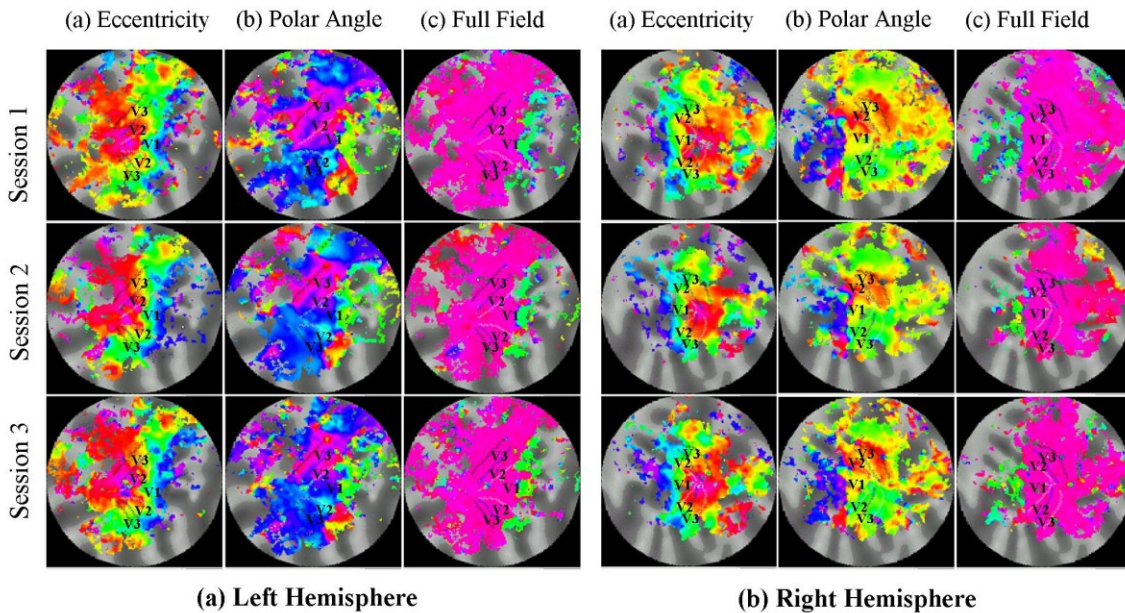


Subject 5





Subject 6



Subject 7

Figure 24. Projection of the response phases onto the flattened representation of the occipital pole for the left and right hemisphere for all subject during (a) eccentricity mapping, (b) polar angle mapping and (c) full field stimulation (response threshold:  $p=0.05$ ). Typical eccentricity and polar angle maps were evident that covered the cortical expand activated during full field stimulation. There is a high degree of correspondence for the topographies across the three sessions within each stimulation condition (from Abd Hamid et al. (2015b)).

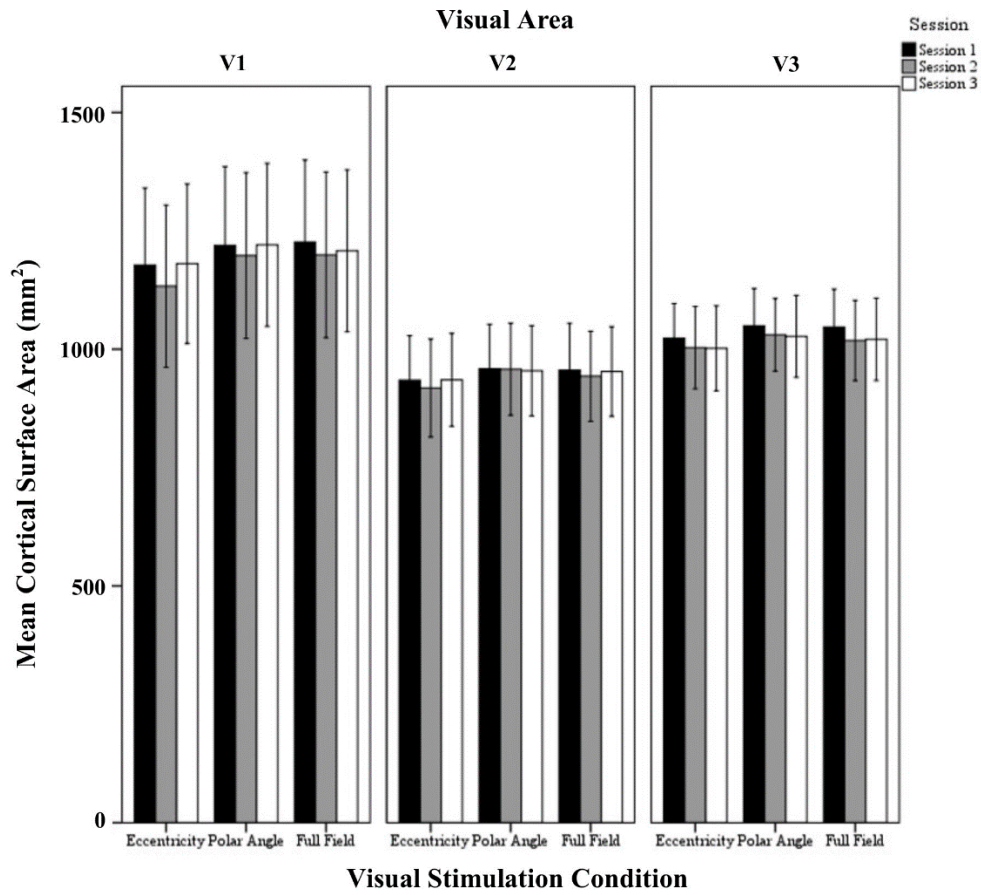


Figure 25. Quantitative comparison of the activated cortical surface area (mean  $\pm$  SEM) across sessions in V1, V2 and V3 for all visual stimulation conditions. Significant effects were observed for the factors session and visual area as detailed in Results (from Abd Hamid et al. (2015b)).

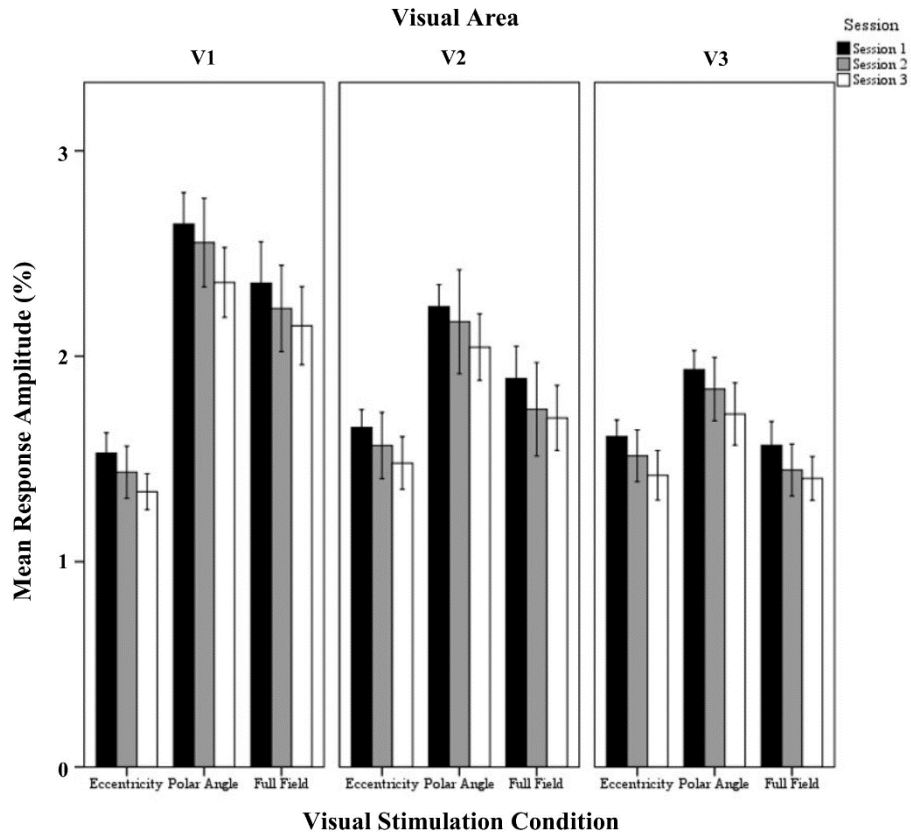


Figure 26. Quantitative comparison of the response amplitude (mean  $\pm$  SEM) across sessions in V1, V2, and V3 for all visual stimulation conditions. Significant effects were observed for the factors session, stimulation condition, and visual area, and for the interaction of stimulation condition and visual area as detailed in Results (from Abd Hamid et al. (2015b)).

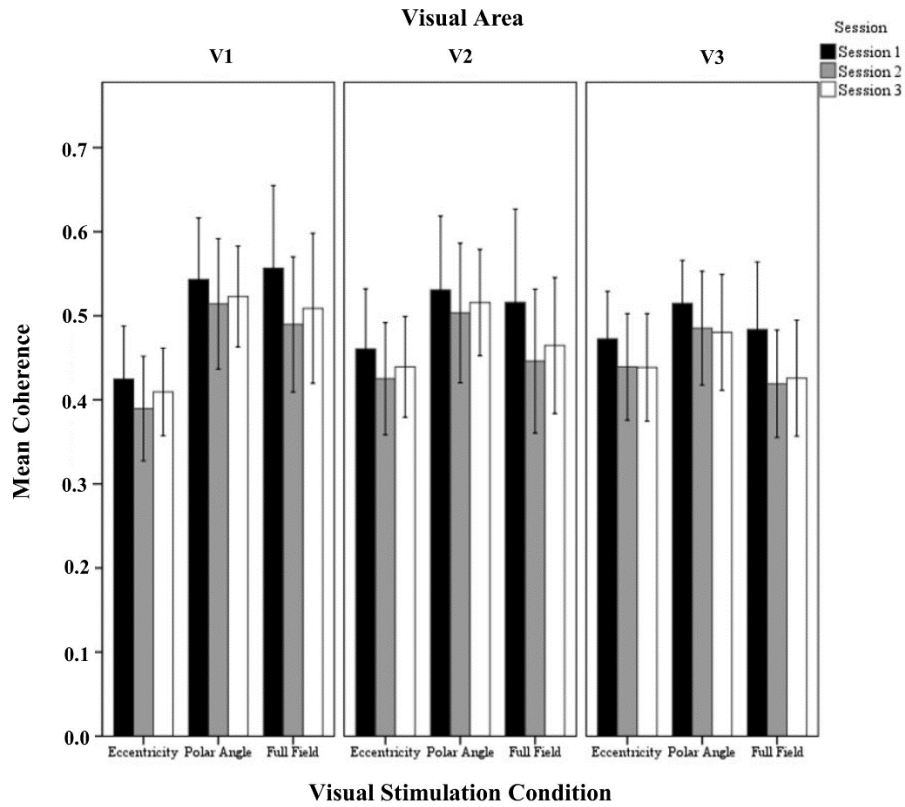


Figure 27. Quantitative comparison of coherence (re-transformed mean  $\pm$  SEM of Z-transformed value) across sessions in V1, V2 and V3 for all visual stimulation conditions. Significant effects were observed for the factors session and stimulation condition as detailed in Results (from Abd Hamid et al. (2015b)).

Table 2. Results from repeated measures analyses for (a) the activated cortical surface area, (b) the responses amplitude and (c) coherence (from Abd Hamid et al. (2015b)).

Factor	(a) Activated cortical surface area	(b) Amplitude	(c) Coherence
	F-ratio (df1,df2), <i>p</i> -value	F-ratio (df1,df2), <i>p</i> -value	F-ratio (df1,df2), <i>p</i> -value
Session	F (2, 108) = 5.590, <i>p</i> = 0.005 *	F (2, 108) = 10.184, <i>p</i> < 0.001 *	<sup>a</sup> F (1.785, 96.417) = 19.607, <i>p</i> < 0.001 *
Visual stimulation condition	F (2, 54) = 0.068, <i>p</i> = 0.934	F (2, 54) = 18.467, <i>p</i> < 0.001 *	F (2, 54) = 7.242, <i>p</i> = 0.002 *
Visual area	F (2, 54) = 3.272, <i>p</i> = 0.046 *	F (2, 54) = 8.933, <i>p</i> < 0.001 *	F (2, 54) = 0.673, <i>p</i> = 0.514
Session x Visual area	F (4, 108) = 1.198, <i>p</i> = 0.316	F (4, 108) = 0.057, <i>p</i> = 0.994	<sup>a</sup> F (3.571, 96.417) = 0.266, <i>p</i> = 0.881
Session x Visual stimulation condition	F (4, 108) = 0.405, <i>p</i> = 0.804	F (4, 108) = 0.192, <i>p</i> = 0.942	<sup>a</sup> F (3.571, 96.417) = 1.609, <i>p</i> = 0.184
Visual stimulation condition x Visual area	F (4, 54) = 0.005, <i>p</i> = 1.000	F (4, 54) = 3.247, <i>p</i> = 0.019 *	F (4, 54) = 1.381, <i>p</i> = 0.253
Session x Visual stimulation condition x Visual area	F (8, 108) = 0.210, <i>p</i> = 0.989	F (8, 108) = 0.023, <i>p</i> = 1.000	<sup>a</sup> F (7.142, 96.417) = 0.027, <i>p</i> = 1.000

Note: <sup>a</sup> Greenhouse-Geisser correction. \* The effect factor is significant at the 0.05 level (*p* < 0.05).

### 3.3.2 Reproducibility of Phase Maps

Phase map reproducibility within defined visual areas for polar angle and eccentricity was determined between Sessions 1 and 2 (S1S2) and between Sessions 2 and 3 (S2S3). The threshold for every visual area in both sets of sessions was established as  $p=0.05$ . The mean correlation coefficient of S1S2 and S2S3 in the polar angle and eccentricity within defined visual areas is indicated in Figure 27. A high correlation was observed on the phase maps in V1, V2, and V3 for eccentricity and for polar angle, with the mean correlation coefficient exceeding 0.70. This result is consistent with the findings of Hoffmann et al. (2012) on intra-session variability; the present experiment generated a higher value than that obtained by Swisher et al. (2007) in their study of inter-session variability.

The effect of variability on the Z-transform correlation for S1S2 and S2S3 was subsequently determined separately for each visual area (V1, V2, and V3) and type of visual stimulation (eccentricity and polar angle). According to the obtained findings, there was no significant difference between the mean correlation coefficients in the two pairs of sessions for eccentricity mapping within visual areas V1 ( $t(12) = 0.388$ ,  $p=0.705$ ), V2 ( $t(12) = -1.404$ ,  $p=0.186$ ), and V3 ( $t(12) = -0.211$ ,  $p=0.386$ ) and for polar angle mapping within visual areas V1 ( $t(12) = -0.484$ ,  $p=0.637$ ), V2 ( $t(12) = -0.938$ ,  $p=0.345$ ), and V3 ( $t(12) = -0.600$ ,  $p=0.560$ ). This result implies a high correlation between the phase maps for eccentricity and polar angle mapping across sessions, as well as the absence of a systematic effect between sessions on the resultant mapping.

### 3.3.3 Head Motion

The stability of the phase maps across sessions was clearly indicated by the results. Nevertheless, significant differences in inter-session activation were observed from Session 1 to Session 3, but no session effects were discerned between Sessions 2 and 3. Differences in the degree of head movement may explain why the BOLD responses in Session 1 are dissimilar to those observed in the other sessions. The mean head movement across sessions is indicated in Figure 28. Generally, in every stimulation condition, the average head motion did not exceed 0.3 mm. According to the results of repeated measures one-way ANOVA employing the factors of session and stimulation condition (Table 3), head motion was not significantly affected ( $p>0.05$ )



by either individual factors or interactions between factors. A non-significant trend was noted for the factor session ( $p=0.074$ ), with a 0.049 mm decrease in head motion between Sessions 1 and 2. The full-field stimulation condition was not included in the further analysis because it was associated with a particularly high scatter. An additional non-significant trend was discerned for the factor time ( $p=0.160$ ; a reduction of head movement by 0.030 mm). Based on these results, I can conclude that the novelty effect observed in the BOLD responses for Session 1 was not caused by head movement. The response patterns for individual subjects, which are provided above, support this conclusion (Figures 20-23).

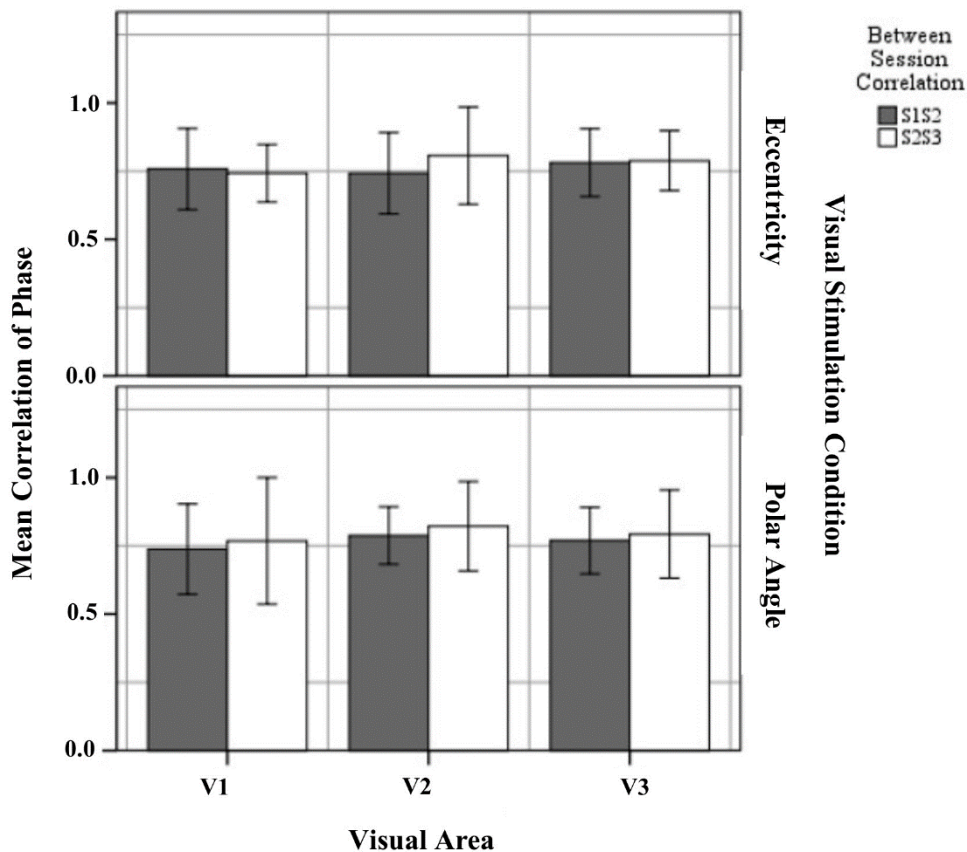


Figure 28. Quantitative comparison of correlation of phase maps (re-transformed mean  $\pm$  SEM of Z-transformed value) of between session 1 and session 2, and between session 2 and session 3 within defined visual for eccentricity and polar angle. No significant effects were observed as detailed in Results (from Abd Hamid et al. (2015b)).

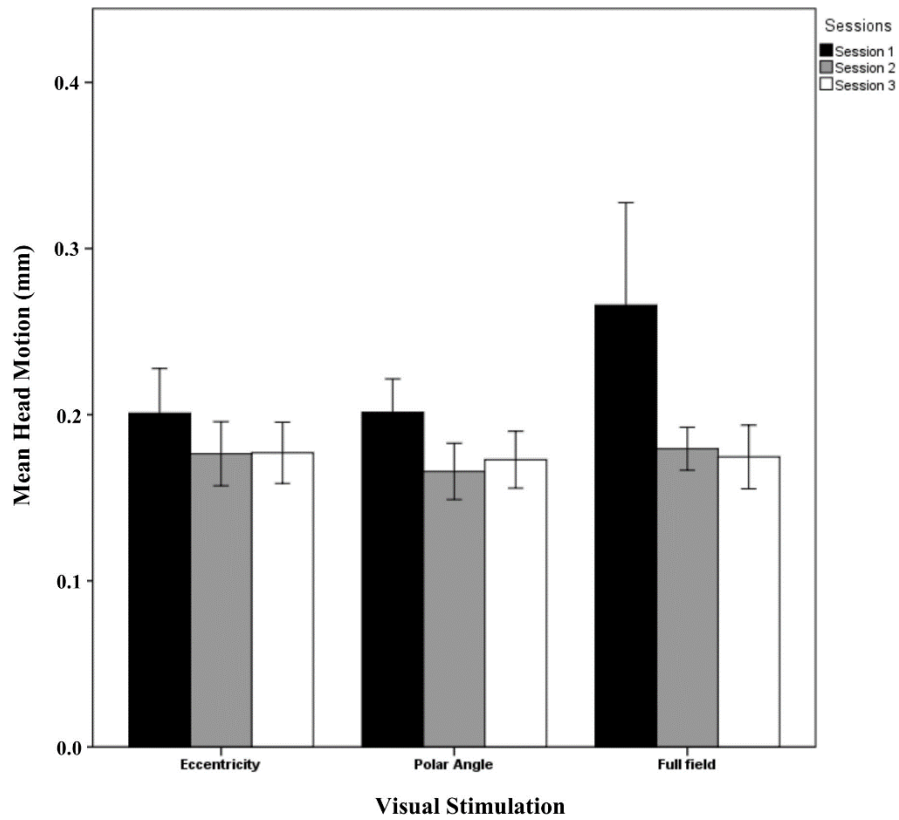


Figure 29. Quantitative comparison (mean  $\pm$  SEM) of head movement across sessions for all visual stimulation conditions. No significant effects were observed as detailed in Results (from Abd Hamid et al. (2015b)).

Table 3. Results from repeated measures analyses of the head movement for (a) eccentricity, polar angle and full field and (b) eccentricity and polar angle (from Abd Hamid et al. (2015b)).

Factor	(a)	(b)
	F-ratio (df1,df2), <i>p</i> -value	F-ratio (df1,df2), <i>p</i> -value
Session	<sup>a</sup> F (1.185, 21.322) = 3.377, <i>p</i> = 0.074	<sup>a</sup> F (1.128, 13.537) = 2.204, <i>p</i> = 0.160
Visual stimulation condition	F (2, 18) = 0.276, <i>p</i> = 0.762	F (1,12) = 0.024, <i>p</i> = 0.879
Sessions x Visual stimulation condition	<sup>a</sup> F (2.369, 21.322) = 0.615, <i>p</i> = 0.576	<sup>a</sup> F (1.128, 13.537) = 0.066, <i>p</i> = 0.830

Note: <sup>a</sup> Greenhouse-Geisser correction.

### 3.4 DISCUSSION

Based on an evaluation of fMRI variability between sessions for retinotopic mapping and full-field stimulation, this study found that after the initial session, BOLD responses were reduced, as indicated by comparisons between sessions 1 and 2 for the activated cortical surface area, between sessions 1 and 3 for the response amplitude, and between sessions 1 and 2 and sessions 1 and 3 for coherence. No session effect between Sessions 2 and 3 was revealed by the results, which also do not indicate that the higher BOLD responses observed in session 1 were induced by head motion. The phase map correlation coefficients between sessions 1 and 2 and between sessions 2 and 3 were also investigated. The findings confirmed the stability of the phase maps and cortical representations, based on both the high correlations for eccentricity and polar angle that were exhibited by the phase maps in the early visual areas and the similarities in correlation among the three sessions.

The current study reports reduced BOLD responses following the first session, which might be attributed to the occurrence of a “novelty effect” in the initial scan. A number of previous studies also highlighted this phenomenon. In an anti- and pro-saccade study, Raemaekers et al. (2007) found that activation decreased between Sessions 1 and 2, which were conducted one week apart. Those authors suggested that as the subjects familiarized themselves with the procedure, they became less alert in follow-up sessions, thus causing the amplitude to decrease. In the context of the motor activity with stop signal paradigm, although Zandbelt et al. (2008) did not observe changes in BOLD responses due to inter-session effects, those authors did note that the cortical surface area decreased between Sessions 1 and 2, which were conducted one week apart. In contrast, no session effect was evident between Sessions 2 and 3, which were again conducted one week apart. Other researchers have argued that increased neural efficiency due to accumulated experience may be the reason for a reduced response (Kelly et al., 2006; Zandbelt et al., 2008; Poldrack, 2000). As a result, a particular task would trigger the activation of fewer neurons (Poldrack, 2000) or recruit a more precise functional circuit (Garavan et al., 2000). Head movement discrepancies between sessions during MRI scans may also help to explain decreases in brain activation patterns. Savoy (2005) noted that even in the case of normal subjects, incorrect fMRI interpretations may be made due to head motion. However, in this study, the “novelty effect” explanation seems to be the most viable cause, as the head motion

was not found to have any impact on the sessions. It is important to bear in mind that fMRI data could be affected by a number of noise sources, including physiological sources, such as respiratory, cardiovascular or motion artefacts, and technical noise sources, such as differences in viewing distance and susceptibility. Although they increase the variability of fMRI data, such noise disruptions are unlikely to generate the systematic effects between sessions that have been reported in this study. As demonstrated by the head movement testing, noise effects are not related to the order of the sessions.

The data obtained in this study suggest that sequential effects, especially in the initial scan, may cause ambiguities in longitudinal studies of visually driven cortical activity. This finding is highly relevant in connection with existing therapeutic attempts to enhance or completely restore impaired visual function. The efficiency of such attempts has been shown to be denoted by visually driven fMRI responses (e.g. Ashtari et al. 2011, 2014; Baseler et al. 2011). According to this study, inherent errors occur in straightforward comparisons of fMRI responses at baseline and after treatment. As such, it is important for future longitudinal studies to assess the ability of the applied task to trigger stable activation measured on the basis of particular outcome measures. If this ability cannot be ascertained, then all of the time points cannot be included in the assessment. With respect to the applied visual stimulation paradigm, this study proves that the initial fMRI session may lack representativeness and may foster incorrect interpretations in longitudinal fMRI studies. One possible solution to this problem is the use of a control group to illustrate sequential effects similar to those observed in the subjects. However, aside from age and sex, the subject and control groups must also be similar in terms of familiarity with the scanning paradigm. Moreover, whether the level of visual impairment augments novelty effects is unknown. This uncertainty calls for the development of a different approach. The stability of the BOLD-fMRI signal may be increased through the introduction of initial scanning sessions. The usefulness of this test-retest study is underscored by the fact that despite the observation of a linear drop in amplitude from Session 1 to Session 3 (Figure 3), no inter-session effects in cortical surface area, coherence or amplitude were observed between Sessions 2 and 3. Although data consistency is not demonstrated by the lack of notable differences in average amplitude between Sessions 2 and 3, neither is a lack of response stability. It is important to note that the duration of this effect may be long, as the effect appears to endure for a number of months, which was the interval between sessions that was employed in the

present study. Hence, longitudinal studies would benefit from an initial fMRI session followed by a baseline scan (Sessions 1 and 2 in this study). Such an initial session could facilitate the acquisition of fMRI scans, such as anatomical scans and functional localizers that are needed a single time. Furthermore, this approach would ensure that every scan introduced in the actual longitudinal observation complies with the established order and protocol. In this case, the experimental design involved the scanning of seven subjects at 7 T, producing a sensitivity which permitted the identification of between-session modifications in cortical surface area (1.5%), response amplitude (6%) and coherence (5%).

To summarize, in comparison to the initial scanning session, the activated cortical surface area, amplitude and coherence of visually driven BOLD responses were observed to decrease in subsequent sessions, whilst the reproducibility of the phase maps was maintained throughout the sessions. The distinguished between-session effects might have been caused by cognitive effects, such as novelty, learning, and adaptation. Because of this possibility, data from the initial session in longitudinal studies may lack representativeness. Hence, all interpretations of fMRI findings from longitudinal studies must consider this issue.

## CHAPTER 4

### **STUDY II: RETINOTOPIC MAPS IN EARLY VISUAL AREAS AFTER TRANSORBITAL REPETITIVE ALTERNATING CURRENT STIMULATION: A SINGLE CASE STUDY IN fMRI**

The work presented in this chapter is currently submitted for publication:

**Aini Ismafairus Abd Hamid**, Carolin Gall, Oliver Speck, Mircea Ariel Schoenfeld, and Bernhard A. Sabel. Visual Cortex Reorganization after Repetitive Transorbital Alternating Current Stimulation following Stroke: A Single Case 7T-fMRI Study.

#### **4.1 INTRODUCTION**

Homonymous hemianopsia (HH) is among the frequent consequences associated with stroke. This condition typically results in the loss of binocular vision on one side of the field of vision. Approximately 30% of all stroke events result in HH due to damaged visual nerve pathways (Grunda et al., 2013). Damage in the visual fields may affect the day-to-day activities of the patient, for instance, body orientation, mobility aided by sight, and even reading (Gall et al., 2009, 2010b).

Patients may tend to encounter spontaneous, partial vision restoration after several weeks or months (Zhang et al., 2006), and further recovery can be achieved if techniques for restoring vision are used to treat patients to improve their sight perception and quality of life. One potential neurological basis for restoring vision are visual field areas that are not totally blind but have some residual potential that can be altered using various methods, such as behavioral visual field training and electrical brain stimulation (i.e., transcranial direct current stimulation (tDCS) and repetitive transorbital alternating current stimulation (rtACS)). These stimulation methods

may increase the excitability of brain tissue and the connectivity of long-range neuronal networks in the brain (Sabel et al., 2011b; Gall et al., 2013; Bola et al., 2014).

The stimulation of the brain with a direct current has been suggested as an adjuvant intervention for enhancing recovery following a stroke event (Bolognini et al., 2009). The application of anodal tDCS to the right posterior parietal cortex results in enhanced perceptual deficits in patients suffering from visual neglect (Ko et al., 2008; Sparing et al., 2009). tDCS methods may improve the effect of vision training in patients experiencing post chiasmatic visual field loss (Halko et al., 2011; Plow et al., 2012). With respect to the use of alternating current (AC), a daily course of rtACS for ten continuous days was shown to increase light perception within impaired visual fields among patients with damaged optic nerves (Sabel et al., 2011a). This method also resulted in an improvement in patient quality of life-related to vision capabilities that were shown to correlate with better visual fields (Gall et al., 2011). The probable modification of the visual system of adult patients by AC fields increases the probability that rtACS may be clinically significant for improving visual loss by stimulating residual tissue at or close to the lesion site in patients with HH.

The aim of this study was to investigate the possible use of high-resolution 7T-fMRI for monitoring the reorganization of early visual areas following hemianopsia after a patient has undergone rtACS. More importantly, this study aims to investigate whether functional changes induced by rtACS are reflected by activity modifications in the brain and whether the respective modifications occur only at or close to the lesion site or cover a large area due to the known reorganization of functional connections in wide neuronal networks (Bola et al., 2014).

## **4.2 MATERIAL AND METHODS**

### **4.2.1 Subject**

I studied a 53-year-old male patient with complete HH caused by right posterior cerebral artery stroke which occurred 14 months earlier. After screening a total of 78 potential patients, only one patient was suitable for 7T-fMRI (see Gall et al. (2015) for inclusion and exclusion criteria). The patient gave written and informed consent to participate in the study, in accordance with IRB approval by the Ethics Committee of the Otto-von-Guericke University of Magdeburg. His



medical history documented no signs of visual field recovery and he presented a nearly-complete hemianopsia with minor sparing near the vertical midline.

#### **4.2.2 Visual Field Measurement**

Visual fields were assessed with static standard-automated Twinfield Oculus perimetry (Oculus, Lynnwood, WA, USA) and high-resolution perimetry (HRP) (Kasten et al., 1998) while the head was stabilized with a chin-forehead rest. Monocular static perimetry was performed at a distance of 33 cm. The task was to press a button whenever a target was perceived (size: III/4 mm<sup>2</sup>, white, luminance: 318 cd/m<sup>2</sup>/0 db, duration: 0.2 s, fast threshold strategy). Targets with varying luminance were presented on a background with a constant luminance of 10 cd/m<sup>2</sup>. The mean threshold and the foveal threshold were measured.

A second method was employed to evaluate the central visual field with above-threshold light stimuli using a computer-based binocular high resolution perimetry (HRP, 25 × 19 grid of test positions; 16° vertical × 21.5° horizontal). HRP was carried out at a distance of 42 cm on a 17" monitor. The task was to press the space bar whenever a light stimulus or an isoluminant change in the colour of the fixation point (to control proper fixation) was detected. The detection accuracy was measured and the percentage of detected colour changes of the fixation point served as a reliability measure. To adjust for the size of the experimental set-up used for fMRI, only the central 9 × 5 HRP grid was analyzed to limit it to same visual field areas employed during the fMRI task.

For the statistical analysis, the detection accuracy improvement following rtACS in the full-field HRP and central visual field were assessed using dependent t-test. The reaction time in HRP and the average contrast sensitivity in the standard static perimetry following rtACS were evaluated using dependent t-test. The average contrast sensitivity in the central visual field was assessed using Wilcoxon signed rank test.

#### **4.2.3 Stimulation Protocol**

rtACS was applied on 2 × 5 consecutive weekdays. Biphasic square pulses given in bursts were generated by an MC4 stimulator (neuroConn, Germany) and applied to the surface of the face around the orbital cavity (eyes closed) via four Grass safelead gold electrodes (Astro-Med, Inc.,

USA). The return electrode (stainless steel plate; 32 × 30 mm) was placed above Oz according to the 10–20 system. The duration of each daily session ranged between 25 min on the first day to 50 min at the end of the treatment period. A current strength of 125% of phosphene threshold was used for stimulation. The mean current strength used for stimulation was 596  $\mu$ A. The range of stimulation frequencies was between the individual alpha peak (9 Hz) and the individual flicker fusion frequency (23 Hz). Side effects of the rtACS treatment were evaluated by a semi-structured daily interview.

#### **4.2.4 Retinotopic Mapping For fMRI**

Retinotopic mapping was carried out using visual stimuli which were back-projected with a video projector (DLA-G150CL, JVC Ltd.) onto a screen (horizontal visual angle  $\sim 14.8^\circ$  and vertical visual angle  $\sim 8.3^\circ$ ) behind the subject, and viewed via a surface mirror mounted onto the head coil. The stimulus patterns were based on a circular checkerboard with a radius of  $7.41^\circ$  consisting of black and white checks with a reversal frequency of 8 Hz; the patterns included 24 segments and 26 rings. The stimuli were projected with a mean luminance of 62  $\text{cd}/\text{m}^2$  and a contrast of 99%. The subject was instructed to focus on a central fixation marker ( $0.34^\circ$  diameter) and report any color changes by button pressing. The marker alternated color from green to red (200 ms duration) at intervals of 5–10 s. The paradigm consisted of a clockwise- or anti-clockwise-rotating wedge for polar angle mapping, expanding or contracting rings for eccentricity mapping, or full-field stimulation. A 12 s dummy period followed by seven 36 s cycles of the stimulus section polar angles or eccentricities were presented. For the full-field stimulation, a block design of 12 s dummy period and ten 24 s cycles of the stimulus (12 s checkerboard followed by 12 s mean luminance blank) were presented. The ring expanded uniformly beyond the maximum extent of the screen for 5 s and then wrapped around to the fovea. This stimulation gap aids in distinguishing peripheral from foveal responses in the eccentricity mapping data (Hoffmann et al., 2009). Altogether, the fMRI measurements took approximately 30 minutes.

#### **4.2.5 fMRI Acquisition**

For functional imaging, T2\*-weighted echo planar images (EPIs) were acquired on a 7 Tesla whole-body MRI (Siemens, Erlangen, Germany) using a 32-channel head coil (Nova Medical,

Wilmington, USA). The gradient echo EPI pulse sequence was characterized by the following parameters: repetition time (TR) = 3000 ms, echo time (TE) = 21 ms, field of view (FOV) = 140 mm, flip angle ( $\alpha$ ) = 90, voxel size = 1 mm  $\times$  1 mm  $\times$  1 mm and 45 slices were acquired perpendicular to the calcarine sulcus for a duration of 252 s with 84 volumes (7 cycles) for eccentricity and polar angle mapping and 240 s with 80 volumes (10 cycles) for the full-field stimulation. In addition, high-resolution anatomical images of the occipital region were obtained using T1-weighted 3D-MPRAGE with the following parameters: acquisition time = 296 s, TR = 2300 ms, TE = 2.66 ms, FOV = 256 mm, voxel size = 1 mm  $\times$  1 mm  $\times$  1 mm. In order to ensure more accurate registration, the acquired functional images were online-motion and distortion corrected (In and Speck, 2012). In addition, in order to control for the correct fixation, the eye movement were monitored online with a pupil tracking system for all tasks (Kanowski et al., 2007a).

## **4.2.6 Data Processing**

### *4.2.6.1 Cortical Flattening and Preprocessing of Functional Images*

T1-weighted anatomical MRI images with an isotropic resolution of 1 mm<sup>3</sup> were used to segment the cortex and create a flattened representation of the cortical gray matter (Teo et al., 1997; Wandell et al., 2000). The functional images were analyzed using the Stanford VISTA-Tools (VISTA) (<http://white.stanford.edu/software/>). The T2\*-weighted images were aligned with the T1-weighted image's coordinate frame to project the fMRI time series onto the flattened cortex representation. The first cycle of each functional run (12 volumes from eccentricity and polar angle mapping and 8 volumes from full-field stimulation) was discarded to avoid transient onset artifacts. The time series of repeated measurements were averaged after time reversal and time shifting to cancel any residual hemodynamic delay at each voxel. The signal time course of each voxel was divided by its mean. In order to calculate the amplitude and the response phase for the stimulus frequency, Fourier analysis was applied. The correlation, also known as coherence, was calculated for the fundamental frequency of the visual stimulation (1/36 Hz) (Engel, 1997). For qualitative assessment and presentation of the response maps in the flattened representation, the coherence and phase values were smoothed by convolving a Gaussian kernel (full width at half maximum: 4 mm) with the complex vector representation of the blood-oxygenation-level

dependent (BOLD) response. The smoothed responses were plotted in false color in the flattened representation of the occipital lobe. The statistical significance levels or p-value for the associated coherence values were estimated according to Silver et al. (Silver et al., 2005). In this study, no filtering method was applied to any of the quantitative analyses (amplitude, coherence or any responses in the EPI planes) to avoid loss of spatial resolution.

Phase-encoded retinotopy was used to analyze different regions of interest (ROI) which were defined by the boundaries of V1, dorsal V2 (V2d), ventral V2 (V2v), dorsal V3 (V3d) and ventral V3 (V3v) on the cortical surface (Engel, 1997; Engel et al., 1994; Sereno et al., 1995; Wandell et al., 2007) in the intact hemisphere, while for damaged hemisphere ROI1 was defined to explore the changes. The effect of rtACS was evaluated in these ROIs by calculating the percentage of change over baseline ( $((Post - rtACS - Pre - rtACS)/(Pre - rtACS) \times 100)$ ) for the activated voxels, amplitude and coherence.

### 4.3 RESULTS

The rtACS stimulation was well tolerated by the subject. The subject only reported transient mild headache (5/10 days) and nausea (1/10 days). However, the subject experienced these symptoms frequently before participating in the study. Therefore, these symptoms were not instinctively expected to represent side effects of rtACS. Additionally, the subject reported a tingling sensation below the stimulation electrodes on 5 days.

#### 4.3.1 Visual field tests

The results of the visual field tests before and after rtACS are shown in Figures 30 and 31. In HRP, two visual field assessment approaches were used: (1) the standard visual field test size (25 × 19 grid of test positions; 16° × 21.5°), and (2) a “central” visual field size (9 × 5 grid of test positions) to match the eccentricity that was used in fMRI retinotopy testing. The border shift observed in the left and right visual field was minimal (Figure 30). Specifically, the observed increases in the detection accuracy in full-field HRP (25\*19 grid of test position) after rtACS were 0.91% for the right eye and 2.11% (t=-3.93(473); p<0.001) for the left eye. Within the central visual field (9 × 5 grid of test positions), there was an improvement in detection accuracy of 4.55%, although this change was not statistically significant (t=-1.27(43); p<0.210). With

respect to reaction times in HRP, a decrease from 257 ms (SE=12ms) before rtACS to 237 ms (SE=10ms) ( $t=5.2(473)$ ;  $p<0.001$ ) after rtACS was observed; a significantly faster reaction was observed.

In the standard static perimeter, no significant change was observed after rtACS in the right eye (difference of 0.36 dB;  $t=0.95(61)$ ;  $p=0.345$ ), but for the left eye, the average contrast sensitivity (threshold full visual field) showed a significant increase from 11.05 dB to 11.95 dB (difference of 0.90 dB;  $t=2.3(61)$ ;  $p=0.028$ ). Similarly, the foveal threshold exhibited increments of 3 dB for the left eye and 1 dB for the right eye. The increase in contrast sensitivity was higher in the central visual field (8 tested positions) than for full-field perimetry (62 tested positions) but did not reach significance due to the higher standard errors and the smaller number of stimulus presentations within this area (left eye difference: 2.87 dB;  $p=0.109$ ; right eye difference: 1.88 dB;  $p=0.180$ ; Wilcoxon signed rank test).

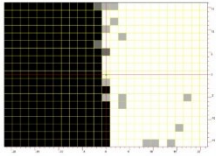
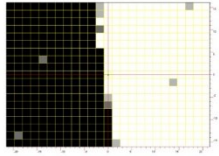
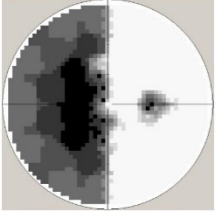
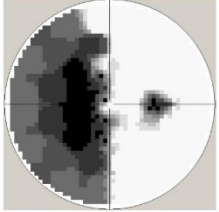
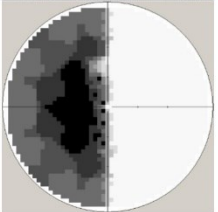
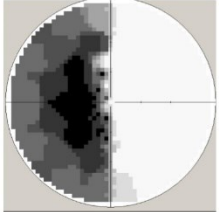
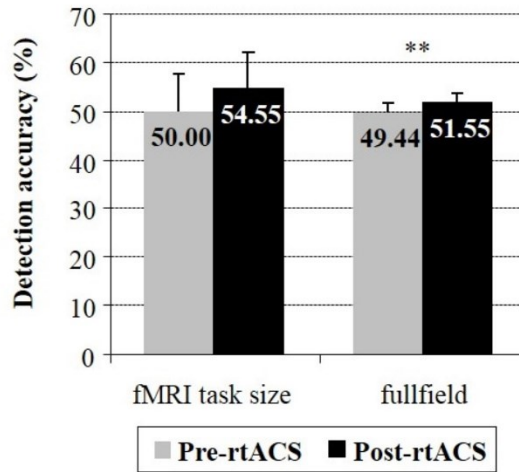
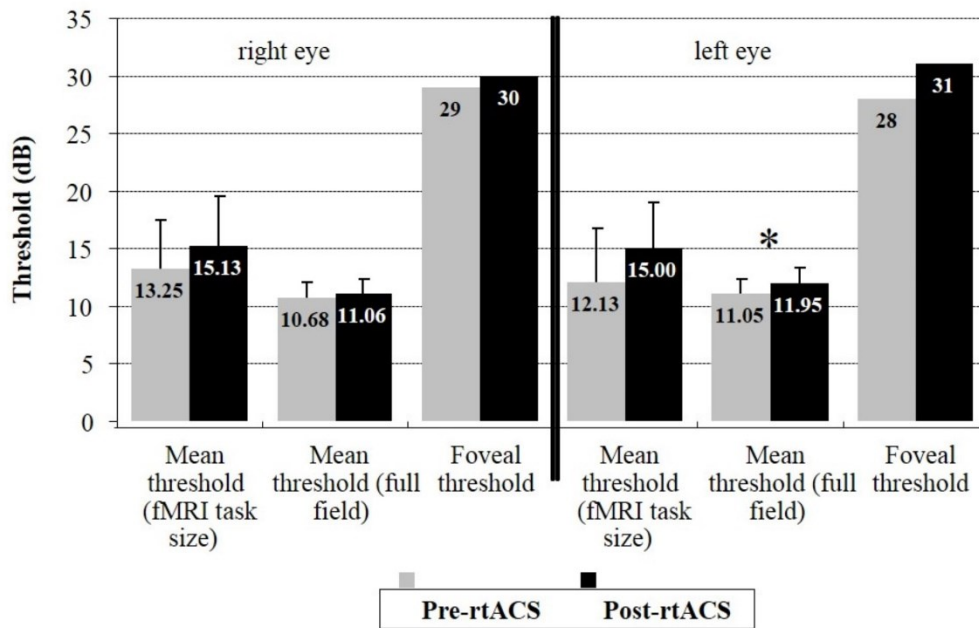
Visual field tests	Pre-rtACS	Post-rtACS (After 10 days)
Computer campimetry (binocular)	 <p>Detection accuracy 49.44% Fixation accuracy 98.16%</p>	 <p>Detection accuracy 51.55% Fixation accuracy 99.07%</p>
Twinfield Oculus perimetry (right eye, 30°)	 <p>Foveal threshold 29dB Fixation accuracy 100 % Mean threshold 10.68 dB</p>	 <p>Foveal threshold 30dB Fixation accuracy 100 % Mean threshold 11.06 dB</p>
Twinfield Oculus perimetry (left eye, 30°)	 <p>Foveal threshold 28dB Fixation 100 % Mean threshold 11.05 dB</p>	 <p>Foveal threshold 31dB Fixation 100 % Mean threshold 11.95 dB</p>

Figure 30. Results of campimetric and perimetric visual field tests before and after 10-days rtACS.

(a) Computer Campimetry (binocular)



(b) Twinfield Oculus Perimetry (monocular)



Note: \*\* p<0.001, \* p<0.05

Figure 31. Detection performance in visual field tests pre- and post-rtACS in (a) binocular computer-based campimetry (HRP) and (b) monocular static automated threshold perimetry (Twinfield Oculus).

### 4.3.2 Functional Magnetic Resonance Imaging

fMRI was performed twice, with the first scan ten days before the first rtACS and the second scan six days after the last rtACS. The locations of occipital lesions in the right hemisphere are shown in Figure 32. The subject had a complete right hemispheric HH, as indicated in the visual field tests. Figures 33 and 34 show the retinotopic visual cortex activation for eccentricity, polar angle, and full field in the left and right hemispheres, respectively (threshold p-value of 0.05). In the damaged hemisphere, only a small response area was detected in the dorsal location and defined as ROI1 (Figure 34). In the intact hemisphere, full hemifield responses were obtained and defined as early visual areas, namely V1, V2d, V2v, V3d and V3v.

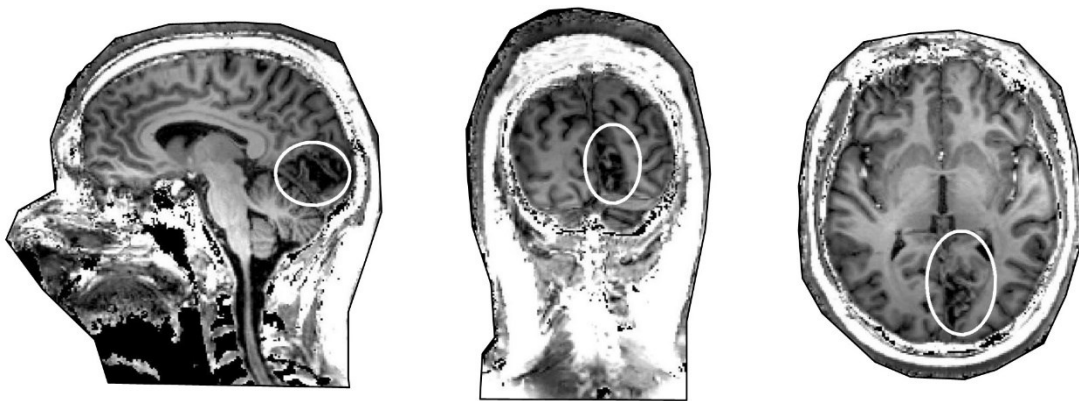


Figure 32. Structural magnetic resonance images in sagittal, coronal and axial view indicating the location of the patient's occipital lesion. The white circle shows the location of lesion.



### Retinotopic maps before and after rtACS

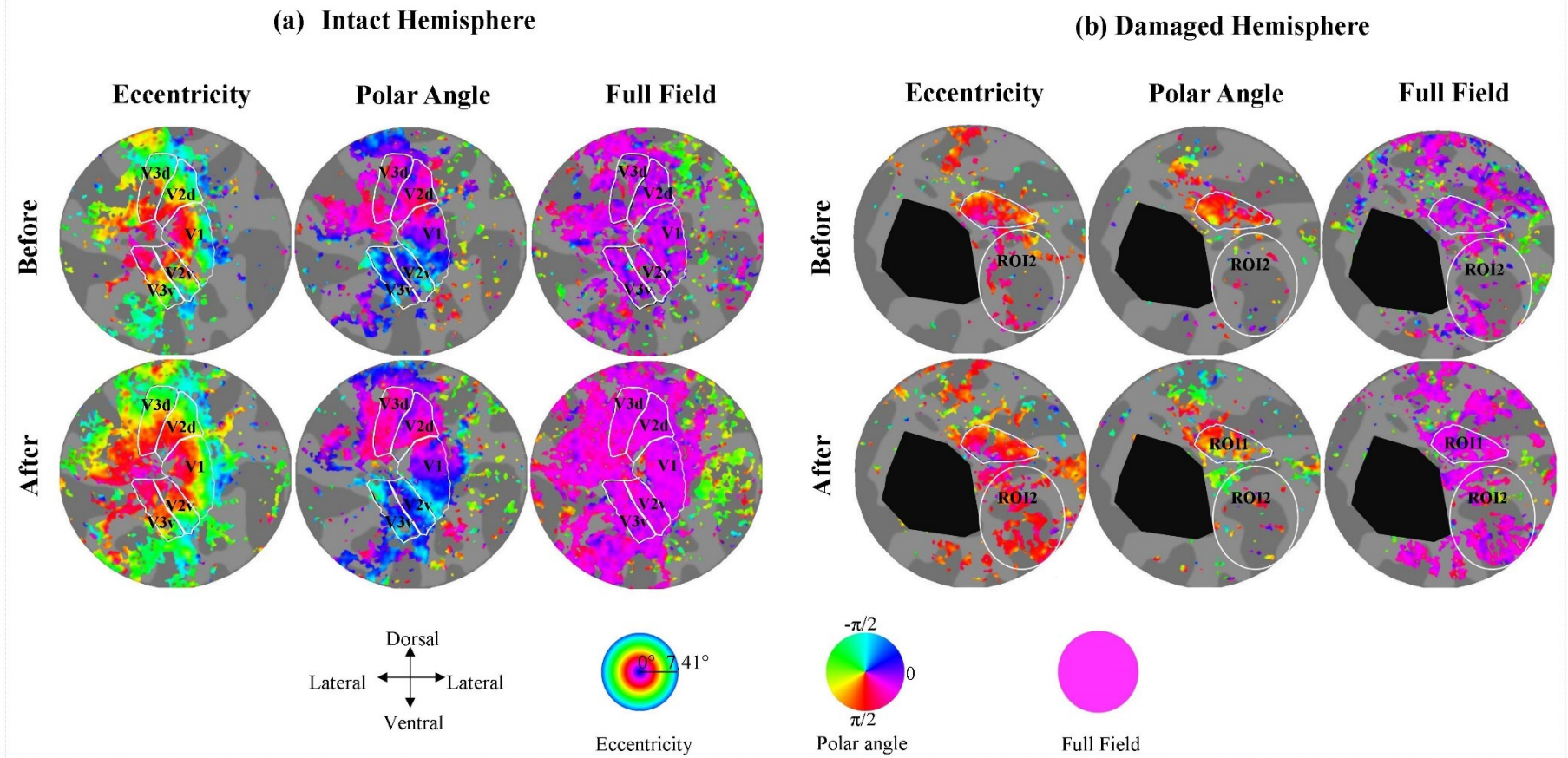


Figure 33. Retinotopic maps before and after rtACS for eccentricity, polar angle and full field with the definition of ROIs on the (a) intact hemisphere and (b) damaged hemisphere at threshold  $p=0.05$ . The black color shape shows the location of the lesion and the ROI2 showed the widespread spatial activation after rtACS.

### Zoom in Region of Interest

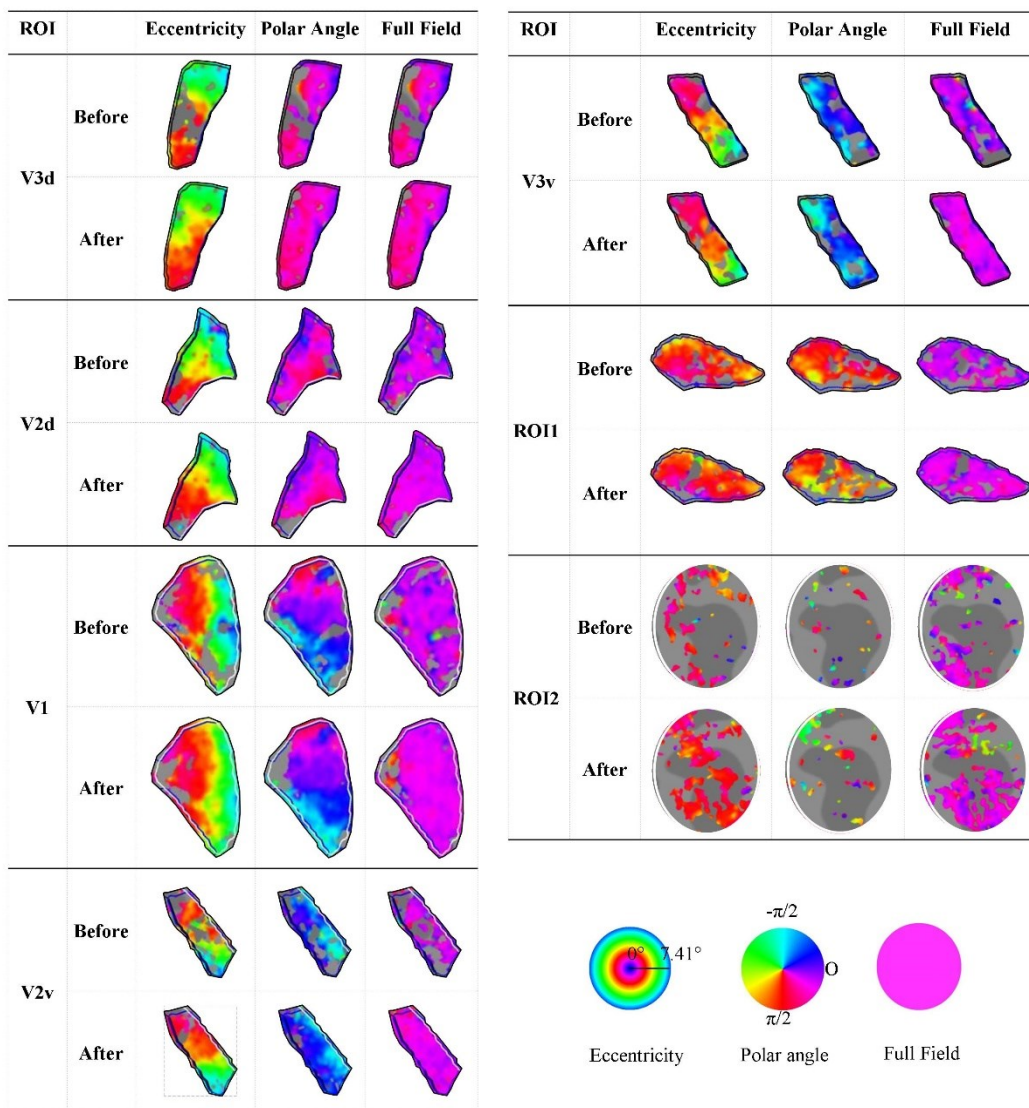


Figure 34. Zoom-in of selected visual areas in the retinotopic map before and after rtACS for eccentricity, polar angle and full field at threshold  $p=0.05$ .

Table 1 indicates the percentage change over baseline of the activated voxels within the functionally defined ROIs for the intact and the damaged hemisphere at  $p=0.05$ . In the *intact* hemisphere, the percentage change over baseline of the activated voxels after rtACS increased in all ROIs for all visual tasks except V2d for polar angle showed a small decrease (0.78%). Specifically, the ROI with the most pronounced increase was V2v when compared to those in all visual tasks (43%, 40% and 75% for eccentricity, polar angle and full field, respectively). In the *damaged* hemisphere, ROI1 showed an increase the percentage change over baseline of the activated voxels after rtACS for eccentricity and full-field stimuli; however, the the percentage change over baseline of the activated voxels were reduced by about 17.31% in polar angle stimulus. Additionally, widespread activation was also observed in the ventral part of the early visual areas of the damaged hemisphere for all visual tasks (represented as ROI2 in Figure 33b and 34). In fact, central visual stimulation activated sectors of the brain which represent more peripheral retinal locations, i.e. far outside their normal location. Eye movements might be a potential cause of an increased the activated voxels for eccentricity and full-field stimuli and the widespread activation in the ventral part of early visual areas. From the eye movements monitored online, however, the mean percentage of correct fixation (subject maintained fixation in the scanner) was  $>90\%$  in all stimulation condition and were not different before vs. after stimulation. Thus, eye movements are not a major cause of underlying changes in activation pattern after rtACS.

Regarding amplitude and coherence, the effect of rtACS on the percentage change over baseline was calculated from the cluster overlaps, which are the sets of voxels that remain active in both pre- and post-rtACS at threshold  $p=0.05$ . By using this approach, the brain signal changes associated with rtACS could be assessed effectively.

The percentage change over baseline of amplitude and coherence are shown in Table 4. The amplitude changes were not uniform: whereas some ROIs showed increased amplitude, others decreased in the intact hemisphere when different visual tasks were carried out. In the damaged hemisphere, the percentage change over baseline of amplitude for ROIs was decreased by approximately 12%, 17% and 11% for eccentricity, polar angle and full field task, respectively. Yet, the percentage change over baseline of coherence was increased in all ROIs for

all visual tasks in both intact and damaged hemisphere except for V3v in the polar angle coherence which showed no change (0.74%).

Table 4. The effect of rtACS on the percentage change over baseline of the activated voxels, amplitude and coherence in the different visual areas in the left and right hemisphere at threshold  $p=0.05$ .

Visual Stimulation Task	Hemisphere	Region of Interest	Percent change over baseline (%)		
			Voxels activated	Based on cluster overlap	
				Amplitude	Coherence
Eccentricity	Left (Intact)	V1	19,67	-3,88	18,92
		V2d	4,50	-1,06	23,59
		V2v	42,19	-3,58	21,41
		V3d	28,39	7,37	21,02
		V3v	13,55	-14,97	7,46
	Right (Damaged)	ROI1	1,63	-11,45	12,33
Polar Angle	Left (Intact)	V1	9,20	2,78	7,88
		V2d	-0,78	-3,36	2,44
		V2v	39,80	2,24	12,73
		V3d	35,19	9,59	0,39
		V3v	14,16	-6,99	-0,74
	Right (Damaged)	ROI1	-17,31	-17,00	0,76
Full Field	Left (Intact)	V1	14,70	7,66	52,95
		V2d	12,36	12,65	66,34
		V2v	75,14	-3,97	44,71
		V3d	46,49	28,50	67,41
		V3v	29,53	-4,04	39,19
	Right (Damaged)	ROI1	14,91	-10,49	7,42

## 4.4 DISCUSSION

The goal of this study was to determine whether the organization of early visual fields in a patient with HH would be altered by rtACS using high resolution 7T fMRI. Through the use of various visual field experiments, we determined that little improvement in the contrast sensitivity of static perimetry and the accuracy of detection in HRP in the central visual area occurred after rtACS. It was thought that this improvement could be accounted for by generalized perceptual learning because repeated measurements of visual areas before rtACS therapy were not associated with enhanced functionality. This improvement was only noted after rtACS in comparison with prior to rtACS, whereby a 14.19% improvement was observed with repeated perimetry measurements pre- and post-rtACS (before 13.25; after 15.13 dB) for the left eye and a 1.08% improvement (before 12.0 dB; after 12.13 dB) for the right eye, within the 7T measurement area. In comparison, with repeated measures of the visual field prior to rtACS, a 9.23% improvement was noted with repeated perimetry measurements prior to rtACS for the left eye (12.13 and 13.25 dB). The results of this study supported the suggestion that brain current stimulation may modify visual field function (Sabel et al., 2011a). Regarding healthy participants, a study performed by Kraft et al. (2010) demonstrated increased contrast sensitivity in perimetry following anodal tDCS, for which pre-post effects occurred at eccentricities less than two degrees but were absent in the additional peripheral visual areas. That finding agreed with the results of this study. These findings argue that the effects of different techniques for brain stimulation (rtACS and anodal tDCS) are topographically restricted on contrast sensitivity functions in the central visual field. In this study, a small number of testing positions in the visual field were applied. This approach reduced the statistical power of the study and could account for the observed statistical insignificance.

One limitation of this study is the observation of a single case. However, because the inclusion and exclusion criteria for 7T fMRI were stringent, only one subject was recruited out of 78 patients who were screened. This outcome reveals that screening a large number of stroke patients is crucial for obtaining a large sample size for a study.

The current findings concerning cortical reorganization are consistent with the results from other studies, which indicated that perimetric visual field training could modify contrast sensitivity functions. The results of static perimetry tests with 30 degrees of the visual field from a study performed by Heijl et al. (Heijl et al., 1989) suggested that training improves contrast sensitivity in peripheral visual areas at eccentricities beyond ten degrees. Additionally, studies performed by Mueller et al. (Mueller et al., 2007) indicated that repetitive testing with visual fields in subjects with brain damage improves perimetry performance.

High-resolution 7T fMRI was applied to explore the effects of rtACS in a patient with HH. Regarding feasibility, 7T fMRI is able to consistently separate activations between the two hemispheres, even though they are closely positioned. Interesting and relevant information was obtained from this single case study. Retinotopic mapping indicated that the retinotopic pattern in the left hemisphere (intact hemisphere) was normal, but a disturbed retinotopic pattern was evident in the right hemisphere, which was the damaged hemisphere. A lack of stimulation in the damaged hemisphere was anticipated due to diminished brain activity, which was caused by lesions induced by stroke. The retinotopic patterns in the damaged hemisphere roughly imply the V1 dorsal area. Moreover, in spite of the absence of a response in the damaged hemisphere, widespread activation in the ventral region was also noted. With respect to the distribution of activation in the damaged hemisphere, it is thought that retinotopic tasks involve signal transfer to residual cells in the primary visual cortex and are also capable of transferring signals to other residual cells in the visual cortex via alternative nerve pathways, as proposed in other studies (Zeki and Bartels, 1998, 1999). It was also suggested that the function of residual cells might be more or less normal (Zeki and Bartels, 1998, 1999).

Pioneering results from this study reveal that the two hemispheres showed noteworthy pattern changes after a ten-day course of continuous non-invasive rtACS. A significant change in the damaged hemisphere was observed in the ventral region (representing the upper visual field) of the retinotopic maps for all visual task conditions. Hence, following the ten-day course of rtACS, central visual stimulation activated brain regions that normally respond to only peripheral visual stimuli—that is, far outside their normal location (Fig. 33b and 34, shown by the ROI2).

This effect is a clear indication of extensive reorganization in the lesioned hemisphere, which had severe losses in retinotopic organization. Experiments conducted by Rosa et al. (2000), which focused on monkeys, entailed damaging a specific part of the visual field of V1 in one hemisphere, causing impairment of a particular visual function. That study demonstrated that several weeks after unilateral removal of V1, the recorded electrophysiology revealed that the residual cells found in V1 continued to respond, with indications of severe reorganization, which also involved other regions. In spite of the speed with which a novel network can arise during the spontaneous recovery process, as shown in the study performed by Rosa and colleagues (2000), it is thought that the use of rtACS may stimulate the residual cells and reconnect via alternative neuronal pathways. It is apparent that this reorganization was triggered by rtACS or that rtACS stimulated “dormant” areas that had reorganized initially after the event of stroke or during the spontaneous recovery period after the development of the lesions. Additionally, it is possible that the hemodynamic effect of ACS could account for the observations made in this study. Nevertheless, modifications also occurred in the “intact” hemisphere. In this hemisphere, different activation changes, some decreasing and others increasing, demonstrated the occurrence of retinotopic reorganization (Fig 33a). The outcomes of this study were consistent with the notion that rtACS restructured and developed new connections between undamaged cells, comprising the adjustment mechanism of the brain to correct damage. It appears that the transfer of initial functions from the damaged hemisphere to the intact hemisphere would be possible. Therefore, the brain can boost the functioning of other visual inputs, thus counterbalancing a dysfunctional visual input. The pattern of activation, particularly in the intact hemisphere, may also reflect an adaptation to fMRI in the subsequent measurement. In this study, we also used an extra baseline, which served as an introduction to sessions of fMRI scanning to reduce the effects of experience (Abd Hamid et al., 2015b). It is proposed that rtACS triggers a stable reorganization of the cortex in the visual system because the fMRI was organized four days after the sessions of rtACS activation. Additionally, the study outcomes revealed the relevance of activating neurons for maintaining their activity and generating new links, hence facilitating the recovery process.

In summary, increased the activated voxels was noted in the peripheral visual field in the intact (represented in light blue on the eccentricity maps; Figure 33a) and damaged hemispheres (represented in green on the eccentricity maps; Figure 33a). The findings of this study are

consistent with results of other studies. For instance, in a motion discrimination study of subjects with hemianopsia, vision restoration training combined with tDCS led to widely distributed fMRI activation in the lesioned area (Plow et al., 2011). Additionally, a study performed by Reamaekers et al. (2011) revealed that a widespread distribution of fMRI activation occurred in both hemispheres after ten weeks of visual stimulation training. The expansion of the activation pattern was larger in the damaged hemisphere than in the intact hemisphere. Although only a small expansion in the visual area was noted, the authors reported that this reorganization could facilitate the recovery process. In a study performed by Pleger et al. (Pleger et al., 2003), fMRI was applied to investigate alterations in brain activation following six months of visual stimulation training in subjects with partial cortical blindness. Those authors demonstrated a significant expansion of patterns of activation in both hemispheres. Hence, this study's experimental findings are consistent with the fact that changes triggered via rtACS can be seen in the early stages in visual regions using 7T fMRI and that those changes are also widespread (extensive) and affect both hemispheres. To my knowledge, no previous studies focused on fMRI, especially on the effects of ACS in a subject without visual field deficits. For further studies, this research has been extended to cover healthy subjects to gain more knowledge regarding the changes induced by rtACS.

Increased the activated voxels in the damaged structure may be indicative of a probable reactivation of residual visual fields (Plow et al., 2011; Sabel et al., 2011b), while increased the activated voxels in the intact structure may indicate further plastic changes of the extensive visual network. In this study, the expansion (enlargement) of the central visual area, as shown by the retinotopic mapping of both hemispheres (represented in purple and pink on the eccentricity maps), demonstrates increased activation following rtACS, which reflects the location of the visual improvements as demonstrated by static perimetry. This finding implies that activation changes occurred in the visual field sector that had shown functional improvement. Nevertheless, other activation changes do not match with changes in the perimetric visual field, suggesting that other visual system functions that cannot be measured with perimetry may be modified, although this hypothesis may require additional studies.

Nevertheless, visual field modifications in the patient with HH were slightly different from those observed in previous studies in which rtACS was used on subjects with optic



neuropathies (Gall et al., 2010a; Sabel et al., 2011a; Fedorov et al., 2011). This difference may be accounted for by lower levels of residual vision in patients with hemianopsia than in patients with lesions on the optic nerve, who appeared to have more diffuse (i.e., greater residual) vision. In the context of vision restoration, more diffuse vision appears to be a prognostic factor (Sabel et al., 2011b).

The observations made in this study show that rtACS influenced neuronal activation in the retina (Schutter and Hortensius, 2010) and can also modulate the activity of the brain cortex, as shown initially by electrophysiological markers (Schmidt et al., 2013; Bola et al., 2014; Sabel et al., 2011a). The respective activation patterns of the brain cortex are thought to be a result of the rhythmic firing of the retinal ganglion cells rather than the current reaching the cortex directly (Foik et al., 2015). Furthermore, it was suggested that visual field expansion following repetitive non-invasive electrical stimulation is linked to oscillatory function modulation in the visual cortex and changes in short-range and long-range functional connections, as observed in subjects with optic neuropathies damage (Sabel et al., 2011a; Bola et al., 2014). It is also possible that rtACS improves the hemodynamic status and hence helps in the activation of neurons.

In addition to the activated voxels and visual field improvement, rtACS also modified the amplitude and coherence of the brain signal in the early visual areas of this study's subject. Both excitation and inhibition of the brain signal amplitude were noted for every ROI and visual stimulation task. Every visual stimulus represented was observed independently, suggesting that the type of stimulus may also affect the manner in which neuronal activity may be altered. Different visual task conditions highlight different stimulation duty cycles, which influence the Fourier-based BOLD signals analysis. This finding is consistent with the hypothesis that rtACS triggers neuronal modifications, even though the interpretation of the precise mechanism for every ROI-excitation or inhibition may not yet be performed in a meaningful manner.

Nonetheless, rtACS is hypothesized to trigger increased neurophysiological activity in the residual structure of the damaged hemisphere, thus leading to the partial restoration of visual function (Sabel et al., 2011b). However, according to the observations made in this study, the outcomes differ with varying visual stimulation tasks. In spite of the reduced amplitude of the

brain signal in the damaged hemisphere following a ten-day course of rtACS, an increase in the coherence value for all visual stimulation tasks was noted. It was presumed that rtACS-triggered deactivation may be indicative of increasing neural efficiency, with neurons producing more synchronized functional connections following a ten-day course of rtACS. The increased coherence observed after rtACS is consistent with this proposal and may also account for the low variability of brain signals in the ROIs. In the intact hemisphere, similar pattern changes in brain signal amplitude and coherence were seen. Although certain ROIs exhibited reduced amplitude, other ROIs exhibited increased brain signal amplitude. Nevertheless, whether increased neurophysiological function in the intact hemisphere assists or distracts the process of vision restoration remains unclear.

Because the observations from this study, which are based on a single case study, demonstrated that changes in brain activation occur after rtACS in regions distant from the lesion areas, questions about the role of brain-wide modifications in hemianopic patients arise. Several previous research revealed that an “intact” visual field tends to be affected by a loss of vision. Whereby, disturbed functional connection networks of the brain are found all over the brain (Bola et al., 2013). More elusive visual loss, known as “sightblindness,” is present in a perimetrically “intact” visual field (Bola et al., 2013), and mono-hemispheric strokes may result in an interhemispheric inhibition imbalance (Oliveri et al., 1999; Corbetta et al., 2005). Regarding such a scenario, the intact hemisphere may be rendered “hyperactive” (Oliveri et al., 1999), thus inhibiting the damaged hemisphere even further. Hence, this study of 7T fMRI findings is consistent with the notion that a somewhat localized lesion may result in widespread reorganization all over the brain.

In conclusion, this study involving a single case demonstrated that changes in brain activation in the visual cortex, as measured by high-resolution 7T fMRI, reflect the perimetric improvements induced by rtACS. In addition, activation modifications occur in brain regions far from the lesions. Although the precise mechanisms that underlie the respective changes in brain activity currently remain unclear, the results of this study show that a ten-day course of daily rtACS therapy can trigger modifications in the activated voxels, amplitude and coherence in selected ROIs in the damaged and intact hemispheres. This study supports the design and

implementation of more studies focused on the plasticity of the visual system in the future and also offers justification for the use of a larger and more sufficient sample size in similar studies.

## CHAPTER 5

### **STUDY III: VISUAL CORTEX ORGANIZATION AFTER TRANSORBITAL ALTERNATING CURRENT STIMULATION IN HEALTHY SUBJECTS WITH 7 TESLA fMRI.**

The work presented in this chapter is currently submitted for publication:

**Aini Ismafairus Abd Hamid**, Oliver Speck, and Bernhard A. Sabel. Transorbital ACS modulates visual cortex activation in healthy subjects – 7 Tesla Fmri.

#### **5.1 Introduction**

Damage to the brain following trauma or stroke may result in neurological dysfunctions affecting visual perception, motor control, memory or language deficits (Gall et al., 2011; Dimyan and Cohen, 2011; Shah et al., 2013). With rehabilitation these deficits can improve. For example, in the field of vision disorders rehabilitation with vision restoration training can improve visual fields in hemianopia, optic nerve damage or glaucoma (Kasten et al., 1998, 2006; Sabel and Gudlin, 2014), but in recent years non-invasive brain stimulation (NIBS) was suggest as another method to improve brain recovery in different functional domains (Ameli et al., 2009; Pereira et al., 2013; Brittain et al., 2013; Gall et al., 2011; Nardone et al., 2014)

NIBS entails different methods such as transcranial random noise stimulation (tRNS) (Terney et al., 2008; Chaieb et al., 2009; Fertoni et al., 2011; Romanska et al., 2015), transcranial direct current stimulation (tDCS) (Nitsche and Paulus, 2000; Antal et al., 2004; Liebetanz et al., 2009; Liu et al., 2014; Miller et al., 2015), transcranial alternating current stimulations (ACS) (Antal et al., 2008; Moliadze et al., 2010; Feurra et al., 2011a; Chaieb et al., 2014; Schutter and Hortensius, 2011; Pogosyan et al., 2009; Wach et al., 2013; Kanai et al., 2008; Paulus, 2010; Schutter and Hortensius, 2010; Zaehle et al., 2010; Neuling et al., 2013; Sela

et al., 2012), and transorbital ACS (Fedorov et al., 2005; Sabel et al., 2011a; Gall et al., 2011; Schmidt et al., 2013; Bola et al., 2014). NIBS were shown to modify cortical plasticity, and an increasing number of studies have recently been published describing the use of transorbital and transcranial ACS to induce brain recovery in both animal (Fröhlich and McCormick, 2010; Reato et al., 2010b; Ozen et al., 2010; Ali et al., 2013) and human (Zaghi et al., 2010; Gall et al., 2011; Sabel et al., 2011a; Fedorov et al., 2011; Chaieb et al., 2014; Antal et al., 2008; Moliadze et al., 2010; Bola et al., 2014). Here, ACS is used to induce frequency modulation of specific regional activities with the aim to promote recovery of function. The application of different ACS frequencies that match the intrinsic frequency is suggested to increased synchronization of neural activity (Zaehle et al., 2010; Fröhlich and McCormick, 2010; Reato et al., 2010a) and transcranial or transorbital ACS has shown measurable changes in different functions including the motor (Antal et al., 2008; Moliadze et al., 2010; Feurra et al., 2011a; Chaieb et al., 2014; Schutter and Hortensius, 2011; Pogosyan et al., 2009; Wach et al., 2013), visual (Kanai et al., 2008; Paulus, 2010; Schutter and Hortensius, 2010; Zaehle et al., 2010; Neuling et al., 2013; Fedorov et al., 2005; Sabel et al., 2011a; Gall et al., 2011; Schmidt et al., 2013; Bola et al., 2014), somatosensory (Feurra et al., 2011b), and higher cognitive domains (Polanía et al., 2012a; Sela et al., 2012).

While a large body of research has emphasized the importance of transcranial or transorbital ACS, there have been only few studies to uncover the mechanism of action. While some recent studies used electrophysiological markers of recovery such as EEG power, coherence, and functional connectivity, there is still little information about effects of NIBS on functional neuroimaging parameters. Yet, especially functional magnetic resonance imaging (fMRI), coupled with NIBS, could provide further insight regarding the functional reorganization of the human brain. While some studies used fMRI are available on brain activation after tRNS (Chaieb et al., 2009) or tDCS (Antal et al., 2011; Holland et al., 2011; Amadi et al., 2013; Polanía et al., 2012b), none has been carried out using ACS. Therefore, I now explored the brain activation changes resulting from the application of transorbital ACS in healthy participants using fMRI-based retinotopic mapping. My hypothesis was that transorbital ACS might induce changes in the spatial activation and signal intensity (amplitude) compared with sham stimulation. As previous electrophysiological studies suggest that EEG patterns were changed beyond the stimulation period (“after-effects”), the goal of the present study was to explore

possible after-effects of transorbital ACS using fMRI-based retinotopic mapping in healthy participants.

## **5.2 Material and Methods**

### **5.2.1 Subjects**

Five subjects (2 females and 3 males; mean age:  $32.6 \pm 1.2$  years) without a history of ophthalmological or neurological disease participated in the study. The experimental procedures were conducted in accordance with the principles of the Declaration of Helsinki (World Medical Association 2000), and approval of the protocol was obtained from the ethics committee of the University of Magdeburg, Germany. The subjects were informed of the research purposes and provided their written consent to participate.

### **5.2.2 Experiment Overview**

All subjects received both ACS and sham randomly in different sessions separated by at least 3 days to prevent the carryover effects of the stimulation from affecting the measurements. The ACS condition was delivered according to a random block design to which the subjects were blinded (see Fig. 1 for a schematic of the experimental design). In this study, I applied an initial session as an introduction of the fMRI scanning sessions to decrease experience-based effects (Abd Hamid et al., 2015b). The initial session was conducted in a separate session which was independent of the transorbital ACS procedure. The initial sessions were discarded and not included in further analyses. Subsequently, the subjects were scanned with BOLD-fMRI-based retinotopic mapping at two time points before (baseline) and at two time points immediately after receiving ACS or sham (see section 2.3 for details of the visual stimulation). The two time points that were measured before the application of the ACS or sham was averaged and served as a baseline for further analyses. The two time points after the ACS or sham were measured at 15–32 minutes (post-1) and 37–54 minutes (post-2). At each of four time points (Pre-1, Pre-2, Post-1 and Post-2) three visual stimulation tasks had to be completed: eccentricity, polar angle, and full field testing which together took approximately 17 min. Immediately after being baseline scanned (fMRI scan session prior to ACS or sham), the subject received ACS or sham in a treatment room separate from the scanner room. After the transorbital ACS procedure, the

subjects went back into the scanner, so that the fMRI scan could be done within approximately 15 min thereafter.

### **5.2.3 Visual Stimulation for fMRI**

To prevent discrepancies in the order effects of visual tasks, all fMRI sessions followed an identical order of experiments: (1) eccentricity mapping with expanding rings, (2) polar-angle mapping with wedges rotating counterclockwise, (3) block design full-field stimulation starting with the stimulation on, (4) eccentricity mapping with contracting rings; (5) polar-angle mapping with wedges rotating clockwise, and (6) block design full-field stimulation starting with the stimulation off. A video projector (DLA-RS493 [Full HD, 1920 x 1080], JVC, Ltd.) was used to display the visual stimuli on a screen (horizontal and vertical viewing angles of  $\sim 12.8^\circ$  and  $\sim 7.3^\circ$ , respectively) located behind the subject and visualized with the help of a surface mirror mounted onto the head coil. To account for the cortical enhancement of the visual stimulus, the stimulus patterns were approximately m-scaled (the most central and most peripheral rings were  $0.1^\circ$  and  $1.0^\circ$  wide, respectively) and contained a contrast inverting (with 8 reversals per second) circular checkerboard with a radius of  $6.4^\circ$  comprising black and white checks with 24 segments and 26 rings. The average stimulus luminance and contrast were  $62 \text{ cd/m}^2$  and 99%, respectively, based on photometer calibrations (CS-100A Konica Minolta).

The subjects were instructed to focus on a central-fixation marker ( $0.32^\circ$  in diameter) and to press a button whenever they observed any transformations in color (200 ms duration at intervals between 5 and 10 s). Every experimental scan began with a 12-second dummy period, which was then followed by seven 36-second cycles of visual stimulation for rings and rotating wedges and ten 24-second cycles of full-field visual stimulation. During the different stimulation intervals, different areas of the visual field were stimulated by phase-encoded paradigms using retinotopic mapping. Thus, the polar angle and eccentricities were increased or decreased for polar-angle mapping and eccentricity mapping, respectively. In this way, the contrast-reversing checkerboard was displayed in distinct sections. The polar angle stimuli were displayed stepping through both the clockwise and counterclockwise directions. In every one of the 36-second cycles, the wedge had a width of 6 segments ( $90^\circ$ ) and was stepped 54 times by  $6.7^\circ$ . With regards to the eccentricity mapping, the movement of the stimulus through the eccentricities took

the form of an expanding or contracting ring that had a width of  $0.84^\circ$  and was stepped in every cycle 54 times by  $0.28^\circ$ . The ring continued to expand homogeneously beyond the maximum screen extent for a period of 5 seconds before covering the fovea. Due to this stimulation gap, it was possible to differentiate between peripheral responses and fovea responses in the eccentricity mapping data (Hoffmann et al., 2009). Full-field stimulation involved exposing subjects to 12-second checkerboard reversals (8 reversals per second) and then 12 seconds of grey (identical mean luminance in both epochs) in a block design. The total duration of all fMRI measurements was half an hour for the pre-stimulation (at two time points) and another half an hour for the post-stimulation (at two time points) in both stimulation-type conditions (i.e., transorbital ACS and the sham stimulation).

#### **5.2.4 fMRI Acquisition**

A 7-Tesla whole-body MRI scanner (Siemens Healthcare, Erlangen, Germany) employing a 32-channel head coil (Nova Medical, Wilmington, MA, USA) was used to obtain T2\*-weighted echo-planar images (EPI) for the purposes of functional imaging. The parameters of the gradient-echo EPI pulse sequence were as follows: repetition time (TR)=3000 ms, echo time (TE)=21 ms, field of view (FOV)=140 mm, flip angle ( $\alpha$ )= $90^\circ$ , and voxel size=1 mm  $\times$  1 mm  $\times$  1 mm. For an interval of 264 seconds with 88 volumes (dummy stimulation period and 7 cycles) for eccentricity and polar angle mapping and an interval of 252 seconds with 84 volumes (dummy stimulation period and 10 cycles) for the full-field stimulation, 45 slices were obtained orthogonal to the calcarine sulcus. Furthermore, T1-weighted 3D-MPRAGE was employed to acquire high-resolution anatomical images of the occipital area with the following parameters: acquisition time=296 s, TR=2300 ms, TE=2.66 ms, inversion time=1050 ms, FOV=256 mm, and isotropic resolution=1 mm. Three-dimensional gradient echo (GE) reference data were employed to rectify the 3D-MPRAGE inhomogeneity (Van de Moortele et al., 2009). GE without inversion was characterized by the same parameters with the exception of acquisition time and TR, which were 170 s and 1340 ms, respectively. The motion and spatial distortions of the functional images were rectified online (In and Speck, 2012). Additionally, eye movements were monitored online using a pupil tracking system (Kanowski et al., 2007b) for all visual stimulation tasks to control for the correct fixation.



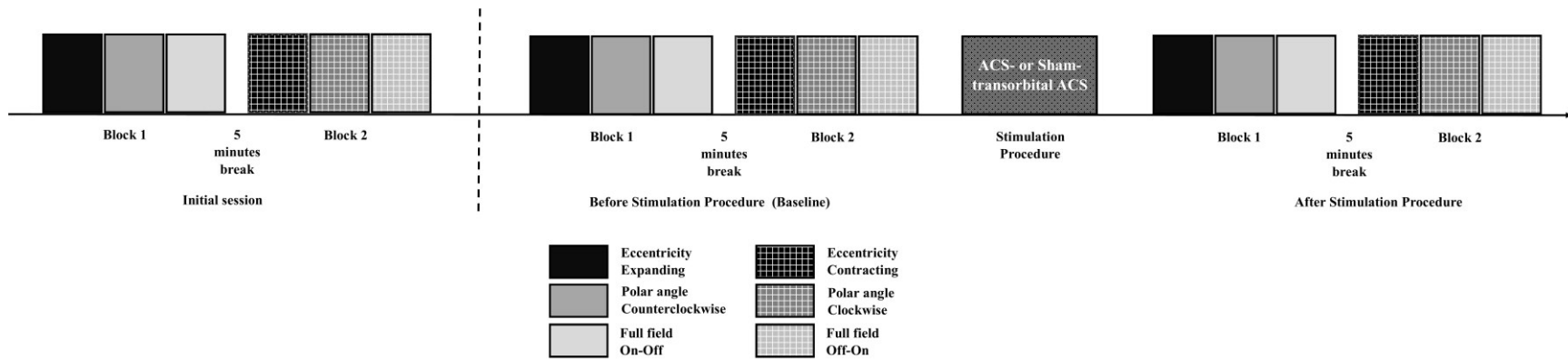


Figure 35. Experimental design. The fMRI scanned started with the initial session. Subsequently, in separate sessions, the subjects completed two blocks of visual stimulation tasks during fMRI scanning before and after stimulation (ACS- or sham-transorbital ACS). At each blocks three visual stimulation tasks were give: eccentricity, polar angle, and full field. All of the subjects received both ACS- and sham-transorbital ACS randomly in different sessions. To assess the effects of transorbital ACS in the early visual areas, the time series from visual cortex signals was inverted in time of one of the counter directions in the three visual stimulation types.

### **5.2.5 Cortical Flattening**

Cortex segmentation and the creation of a flattened depiction of the cortical grey matter were undertaken with the help of T1-weighted, inhomogeneity-corrected MPRAGE images (Van de Moortele et al., 2009) to ensure that the white and grey matter contrast for segmentation was uniform (Teo et al., 1997; Wandell et al., 2000). Freesurfer, ITK Gray, 1.6.0.1., and mrGray (VISTA) were used to segment the grey and white matter, which were subsequently subjected to manual editing to reduce segmentation errors. Anatomical segmentation and flattening were carried out once for every subject.

### **5.2.6 Preprocessing of Functional Images**

Analysis of fMRI data was conducted with the same methods in each sessions. The Stanford VISTA-Tools were employed to examine the functional images (VISTA; <http://white.stanford.edu/software/>). The fMRI time series were projected on the flattened cortex representation by aligning the T2\*-weighted images with the coordinate frame of the T1-weighted images. The analysis procedures applied to the time series (TS) of each voxel included the following: 1) for purposes of transient-onset artefact avoidance, the dummy stimulation interval (12 s or 4 volumes) of every functional run was eliminated; hence, for every subject, seven stimulation cycles were kept for eccentricity and polar angle mapping and ten stimulation cycles for full-field analysis; 2) the division of TS was done on the basis of their mean intensity; 3) the TS were inversed in time of one of the counter directions in the three visual stimulation types, namely, contracting versus expanding rings, clockwise versus counter-clockwise rotating wedges, and on versus off start of full-field stimulation. The TS were subsequently shifted by six seconds (two TR) in order to rectify the hemodynamic delay of the inversed TS; 4) the calculation of the amplitude and response phase of the stimulus frequency was undertaken by subjecting the data to Fourier transformation; 5) measurements of the correlation or coherence were carried out based on the TS with a sinusoid with frequency having the same value as the fundamental frequency of 1/36 Hz for 36 s stimulus of the visual stimulation (Engel, 1997). The coherence value was attributed to every voxel in the functional scan, which were indicative of the strength of the voxel response to every condition of visual stimulation.

A Gaussian kernel (4 mm wide at half maximum) was integrated with the complex-vector representation of the BOLD response in order to smooth the coherence and phase values to qualitatively evaluate the response maps and present them in a flattened manner. The approach proposed by Silver et al. (2005) was adopted to estimate the statistical significance levels ( $p$ -value) for related coherence values. For multiple comparison, a threshold  $p=0.05$  was applied for all repeated measures of distinct results (Zandbelt et al., 2008; Plichta et al., 2012), while additional analysis was undertaken solely on the voxels with coherence values higher than 0.18. To prevent resolution loss, no quantitative analysis included spatial or temporal filtering. Direct visual examination was undertaken to assess the quality of data, which did not exhibit signal dropouts as a result of local susceptibility artefacts.

To prevent any disruption from systematic inter-session effects, the visual areas V1, V2, and V3 were identified on the data averages for all sessions. The response phase indicated by the false-colour maps for polar angle and eccentricity was used to manually outline the boundaries between the visual areas on the cortical flat maps (Engel, 1997; Engel et al., 1994; Wandell et al., 2007). In keeping with standard procedures, the borders of the visual areas were representations of the vertical and horizontal meridians in the visual field (Wandell et al., 2007). Afterwards, the fMRI signal difference was investigated with visual area definitions (Swisher et al., 2007b). The effects of transorbital ACS was evaluated by normalized the post transorbital ACS output measurements to pre transorbital ACS by calculating the percentage of change with respect to individual pre transorbital ACS measurements (i. e.,  $(\text{Post\_ACS} - \text{Pre\_ACS})/(\text{Pre\_ACS}) \times 100$ ) for every post stimulation variables (post-1 and post-2).

### **5.2.7 Transorbital ACS Procedure**

NIBS was conducted using a battery-driven stimulator (NeuroConn GmbH, Ilmenau, Germany) through conductive-rubber electrodes placed in saline-soaked sponges. The center of the AC stimulation electrode ( $5 \times 7$  cm) was positioned at Fpz (center of electrode approximately 3–4 cm above nasion). The reference electrode ( $10 \times 10$  cm) was placed on the right upper arm. For ACS-transorbital ACS, stimulation was given for 20 minutes at 1.0 mA. The sinusoidal electrical current waveform was delivered at the individual alpha frequency range. The individual alpha

frequency was obtained based on the individual phosphene threshold measured prior to the stimulation procedure. For sham-transorbital ACS, only occasional current bursts (i.e., stimulation was given for 3 seconds every 2 minutes during the stimulation procedure) were given to create short but therapeutically ineffective phosphenes (Gall et al., 2015). This sham stimulation condition proved to be useful in a previous study since none of the study participants were able to tell for sure to which study arm they were part of (Gall et al., 2015).

### 5.2.8 Statistical Analysis

Here, I investigated which intra- and inter-subject factors or variables resulted in data variance. Two factors – *tasks* (eccentricity, polar angle, and full field) and *hemisphere*, which was the brain hemisphere for visual areas (left and right hemispheres) repeated-measures ANOVA with two within-subject factors of *ACS condition* (ACS and sham) and *time* (post-1 and post-2) – were used to determine the effects on the percent change over baseline of the cortical surface area (i.e., the number of voxels activated), the fMRI response amplitude (i.e., the amplitude of the BOLD signal modulation), and coherence separately. To enable additional statistical analysis, I applied a Fisher transformation to convert the coherence values that lacked a normal distribution into normally distributed values. In this study, I used the post-hoc Sidak correction to account for multiple testing to elucidate the factor effect. In this study, I was interested in understanding whether transorbital ACS affected changes in the output measurements over time.

## 5.3 RESULTS

To assess the effects of transorbital ACS, I determined the percent change over baseline of the cortical surface area, the fMRI response amplitude, and the coherence for each visual area (V1, V2, and V3) in each brain hemisphere. Figures 36 and 37 show the maps of eccentricity, polar angle, and full field on the flattened surfaces of the occipital pole in the left and right hemisphere, respectively. For the fMRI response amplitude and coherence analysis, the effect of ACS on the percent change over baseline was calculated using the cluster overlaps, which are the sets of voxels that remain active in all sessions at a threshold of  $p=0.05$ . By using this approach, the brain signal changes associated with ACS versus sham could be assessed effectively. fMRI activation, i.e., the activated cortical surface area, the fMRI response amplitude, and coherence, was tested with a repeated-measures ANOVA with the within-subject factors of *ACS condition*

(ACS and sham), *time* (post-1 and post-2), and the between-subject factors of *tasks* (eccentricity, polar angle, and full field), and *hemisphere* (left and right). Initial repeated-measures ANOVAs indicated no significant effect in the separately analyzed visual areas V1, V2, and V3 (individual and interaction factors) on the activated cortical surface area, fMRI response amplitude, or coherence ( $p>0.05$ ). Therefore, I combined the visual areas V1, V2, and V3 for further analyses.

Although the statistical analysis for the activated cortical surface area, fMRI response amplitude, and coherence was conducted separately, the findings were highlighted based on the significant outcomes to facilitate an understanding of the effects of transorbital ACS.

### **5.3.1 Effects of ACS condition (ACS vs. sham)**

Repeated-measures ANOVA revealed a significant difference between sham and ACS in terms of the percent change over baseline of the activated cortical surface area ( $F(1,24)=3.985$ ,  $p=0.05$ ), the fMRI response amplitude ( $F(1,24)=4.47$ ,  $p=0.03$ ), and coherence ( $F(1,24)=5.73$ ,  $p=0.02$ ). The post-hoc test revealed a greater percent change over baseline of the activated cortical surface area and coherence in ACS compared with sham (cortical surface area:  $7.22\pm 1.14$  vs.  $4.17\pm 1.16$ ,  $p=0.05$ ; coherence:  $7.69\pm 1.26$  vs.  $4.24\pm 0.91$ ,  $p=0.02$ ). In terms of amplitude, the post-hoc test revealed a decreased percent change over baseline amplitude in the ACS measurements compared with the sham measurements ( $-0.34\pm 0.79$  vs.  $2.46\pm 1.20$ ,  $p=0.03$ ).

### **5.3.2 Effect of time (post-1 vs. post-2)**

Repeated-measures ANOVA revealed a significant difference between post-1 and post-2 in terms of the percent change over baseline of the cortical surface area ( $F(1,24)=13.104$ ,  $p<0.001$ ), but not in terms of the percent change over baseline of the fMRI response amplitude ( $F(1,24)=0.30$ ,  $p=0.58$ ) and in coherence ( $F(1,24)=0.89$ ,  $p=0.35$ ). The post-hoc test exhibited a reduction in the percent change over baseline of activated cortical surface area in post-2 compared with post-1 ( $8.63\pm 1.50$  vs.  $2.76\pm 0.73$ ,  $p<0.001$ ).

### **5.3.3 Effects of brain hemisphere (left vs. right)**

Repeated-measures ANOVA revealed no significant difference between the left and right hemisphere in terms of percent change over baseline of the cortical surface area ( $F(1,24)=0.00$ ,

$p=1.00$ ), the fMRI response amplitude ( $F(1,24)=0.49$ ,  $p=0.48$ ), or coherence ( $F(1,24)=0.69$ ,  $p=0.41$ ).

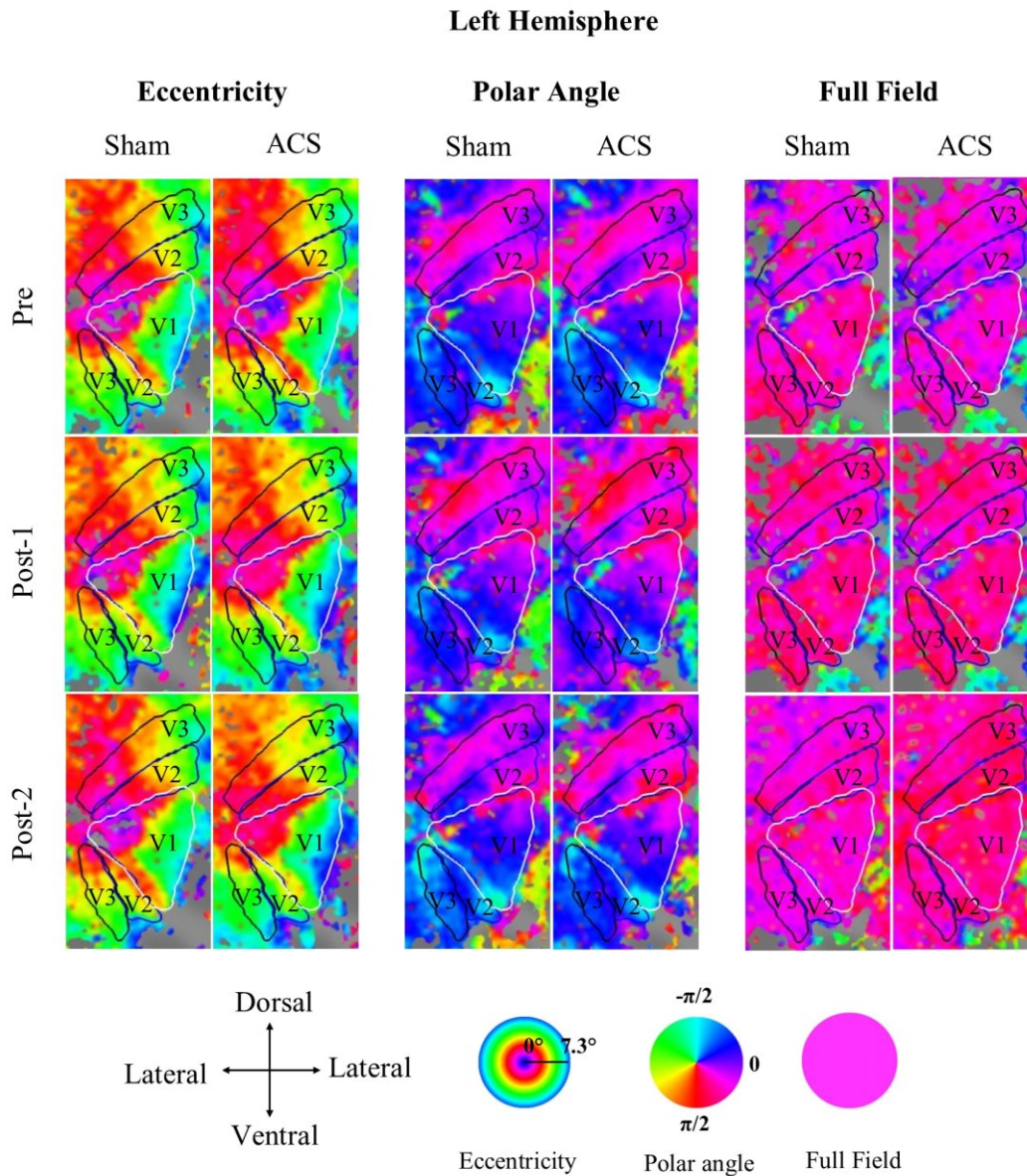


Figure 36. Retinotopic maps of sham- and ACS-transorbital ACS in the left hemisphere of a single subject. Maps of eccentricity, polar angle, and full field were projected onto the flattened surfaces of the occipital pole of the left hemisphere (response threshold:  $p=0.05$ ).



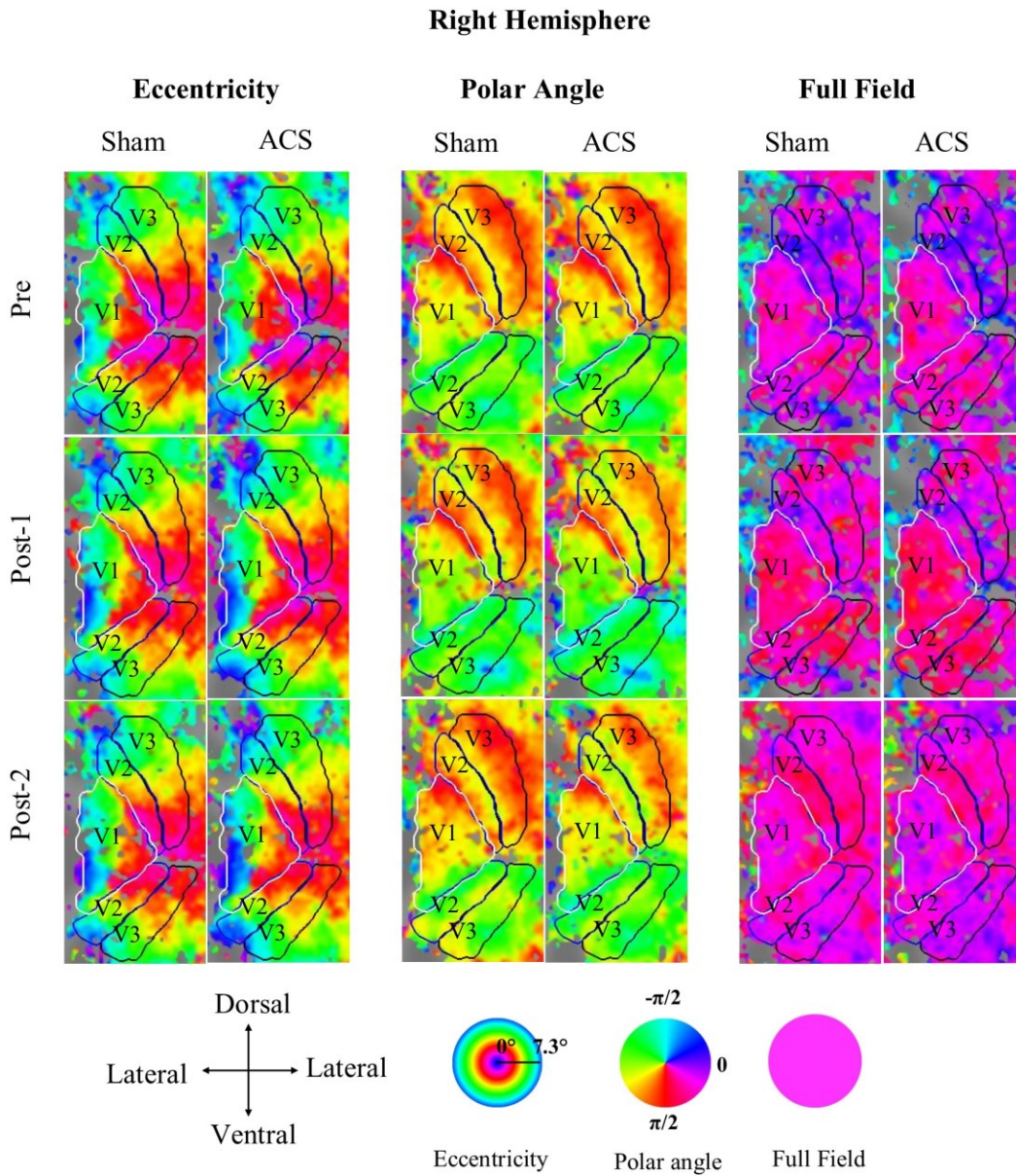


Figure 37. Retinotopic maps of sham- and ACS-transorbital ACS in the right hemisphere of a single subject. Maps of eccentricity, polar angle, and full field were projected onto the flattened surfaces of the occipital pole of the left hemisphere (response threshold:  $p=0.05$ ).

### **5.3.4 Effects of tasks (eccentricity, polar angle, and full field)**

Repeated-measures ANOVA revealed a significant difference between tasks for the percent change over baseline for the activated cortical surface area ( $F(1,24)=19.46, p<0.001$ ) but not for the fMRI response amplitude ( $F(1,24)=1.18, p=0.31$ ) or coherence ( $F(1,24)=0.78, p=0.47$ ). The post-hoc test showed larger percent changes over baseline for the activated cortical surface area for the full field compared with the eccentricity ( $13.21\pm 1.48$  vs.  $2.60\pm 1.48, p<0.001$ ), and the full field compared with the polar angle ( $13.21\pm 1.48$  vs.  $1.27\pm 1.48, p<0.001$ ).

### **5.3.5 Interaction effects between ACS condition and time**

Repeated-measures ANOVA revealed significant interactions between the factor *ACS condition* and *time* in terms of the percent change over baseline of the cortical surface area ( $F(1,24)=5.68, p=0.02$ ) and amplitude ( $F(1,24)=8.93, p=0.004$ ), but not for coherence ( $F(1,24)=1.68, p=0.20$ ). This interaction effect suggests that the time effects were different in the ACS condition for the percent change over baseline of the cortical surface area and amplitude.

### **5.3.6 Interaction effects between ACS condition and tasks**

Repeated-measures ANOVA revealed significant interactions between the factor *ACS condition* and *tasks* in terms of the percent change over baseline of the cortical surface area ( $F(1,24)=25.87, p<0.001$ ), amplitude ( $F(1,24)=8.61, p<0.001$ ), and coherence ( $F(1,24)=3.44, p=0.04$ ). This interaction effect suggests that the effect of ACS condition differs between visual tasks.

### **5.3.7 Interaction effects between ACS condition, time and tasks**

Repeated-measures ANOVA revealed significant interactions between the factor *ACS condition*, *time* and *tasks* in terms of the percent change over baseline of the cortical surface area ( $F(1,24)=16.95, p<0.001$ ), amplitude ( $F(1,24)=13.23, p<0.001$ ), and coherence ( $F(1,24)=32.75, p<0.001$ ). This interaction effect suggests that the effect of ACS condition differs between time and tasks in terms of the percent change over baseline of the cortical surface area, amplitude, and coherence. Figures 38–40 illustrate the variations in the percent change over baseline of the



cortical surface area, amplitude, and coherence resulting from different *ACS conditions, times,* and *tasks*.

In the sham condition, the results revealed a reduction trend between post-1 and post-2 in terms of the percent change over baseline of the cortical surface area and amplitude in eccentricity (activated cortical surface area:  $2.03 \pm 1.15$  vs.  $1.05 \pm 3.53$ ,  $t(9)=0.51$ ,  $p=0.61$ ; amplitude:  $5.86 \pm 1.90$  vs.  $2.68 \pm 2.67$ ,  $t(9)=2.57$ ,  $p=0.04$ ) and an increase trend between post-1 and post-2 in terms of the percent change over baseline of the cortical surface area and amplitude in polar angle (activated cortical surface area:  $1.21 \pm 1.15$  vs.  $2.19 \pm 3.53$ ,  $t(9)=1.64$ ,  $p=0.12$ ; amplitude:  $5.22 \pm 1.90$  vs.  $5.78 \pm 2.67$ ,  $t(9)=-0.38$ ,  $p=0.71$ ) and full field (activated cortical surface area:  $5.26 \pm 1.15$  vs.  $13.27 \pm 3.53$ ,  $t(9)=-1.45$ ,  $p=0.15$ ; amplitude:  $-0.63 \pm 1.90$  vs.  $-4.19 \pm 2.67$ ,  $t(9)=1.28$ ,  $p=0.21$ ; respectively). In terms of the percent change over baseline for coherence, the results showed an increase trend between post-1 and post-2 in eccentricity ( $3.85 \pm 1.71$  vs.  $6.46 \pm 2.19$ ,  $t(9)=-0.81$ ,  $p=0.42$ ) and polar angle ( $5.07 \pm 1.71$  vs.  $7.08 \pm 2.19$ ,  $t(9)=-2.77$ ,  $p=0.01$ ) and a reduction trend in full field ( $8.08 \pm 1.71$  vs.  $-5.08 \pm 2.19$ ,  $t(9)=-5.82$ ,  $p<0.001$ ).

In the ACS condition, the results revealed a reduction trend between post-1 and post-2 in terms of the percent change over baseline of the cortical surface area, amplitude, and coherence in eccentricity (activated cortical surface area:  $7.37 \pm 2.12$  vs.  $-0.04 \pm 3.30$ ,  $t(9)=2.14$ ,  $p=0.04$ ; amplitude:  $-2.04 \pm 1.74$  vs.  $-4.53 \pm 1.78$ ,  $t(9)=2.57$ ,  $p=0.02$ ; and coherence:  $9.61 \pm 3.17$  vs.  $-0.53 \pm 2.56$ ,  $t(9)=2.06$ ,  $p=0.05$ ) and polar angle (activated cortical surface area:  $1.76 \pm 2.12$  vs.  $-0.07 \pm 3.30$ ,  $t(9)=1.82$ ,  $p=0.11$ ; amplitude:  $1.04 \pm 1.74$  vs.  $-1.14 \pm 1.78$ ,  $t(9)=1.49$ ,  $p=0.15$ ; and coherence:  $11.91 \pm 3.17$  vs.  $5.19 \pm 2.56$ ,  $t(9)=2.42$ ,  $p=0.02$ ) and an increase trend between post-1 and post-2 in terms of the percent change over baseline of the cortical surface area, amplitude, and coherence in the full field (activated cortical surface area:  $-1.08 \pm 2.12$  vs.  $35.41 \pm 3.30$ ,  $t(9)=-6.43$ ,  $p<0.001$ ; amplitude:  $-4.59 \pm 1.74$  vs.  $9.20 \pm 1.78$ ,  $t(9)=-4.05$ ,  $p<0.001$ ; coherence:  $1.07 \pm 3.17$  vs.  $18.87 \pm 2.56$ ,  $t(9)=-5.72$ ,  $p<0.001$ ).

### Activated Cortical Surface Area

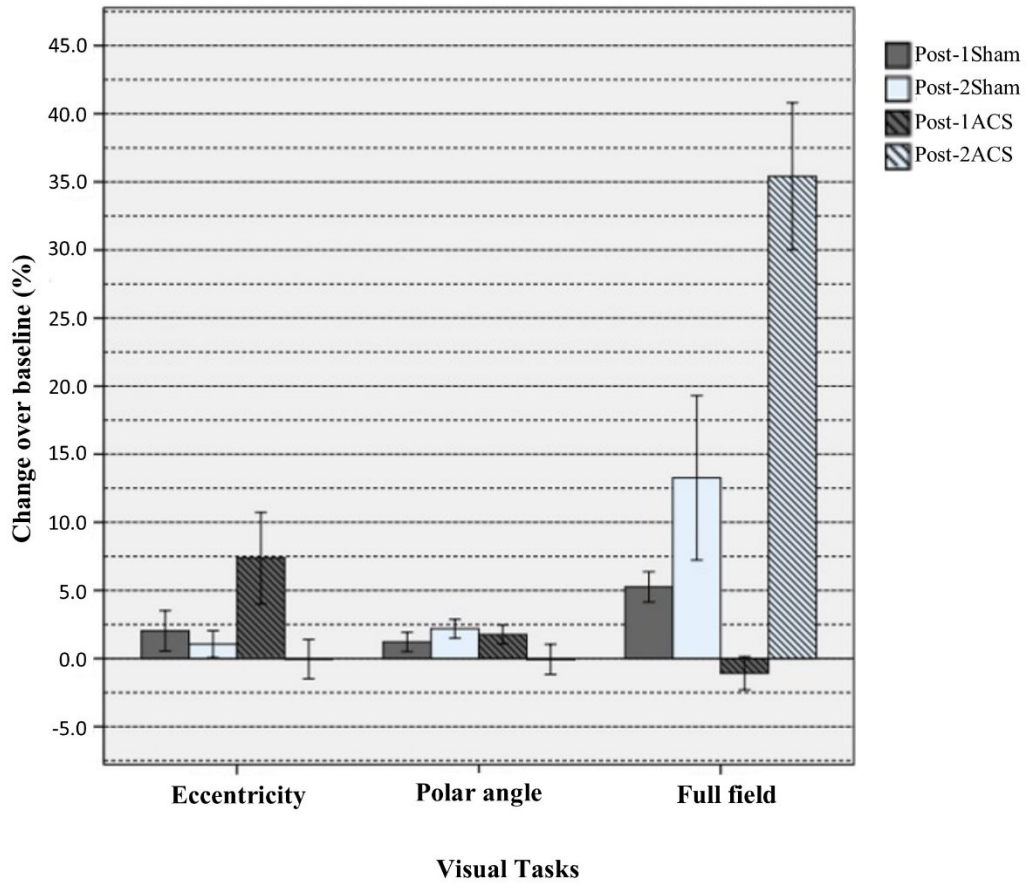


Figure 38. Quantitative comparison of the percent change over baseline for activated cortical surface area (mean±standard error of the mean) across time in the ACS- and sham-transorbital ACS for all of the visual tasks. Statistically significant interaction effects were observed for the factors of ACS condition, time, and tasks, as detailed in the Results section.

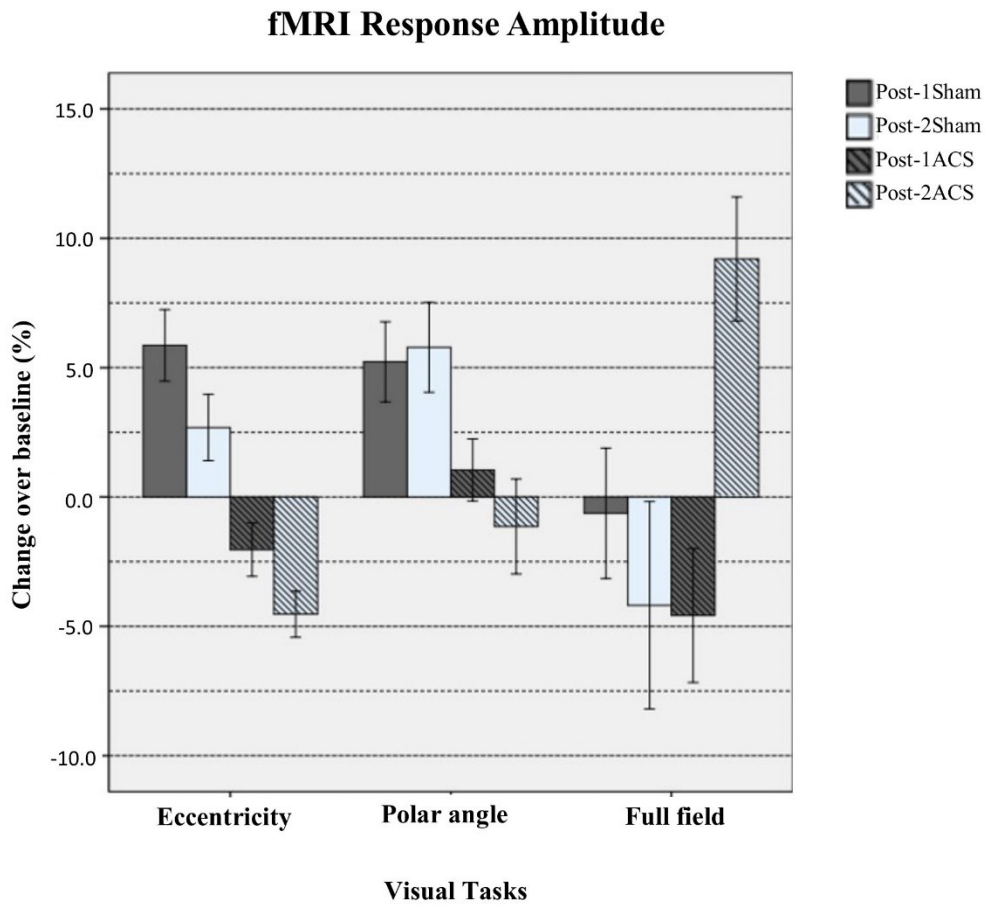


Figure 39. Quantitative comparison of the percent change over baseline for fMRI response amplitude (mean±standard error of the mean) across time in the ACS- and sham-transorbital ACS for all of the visual tasks. Statistically significant interaction effects were observed for the factors of ACS condition, time, and tasks, as detailed in the Results section.

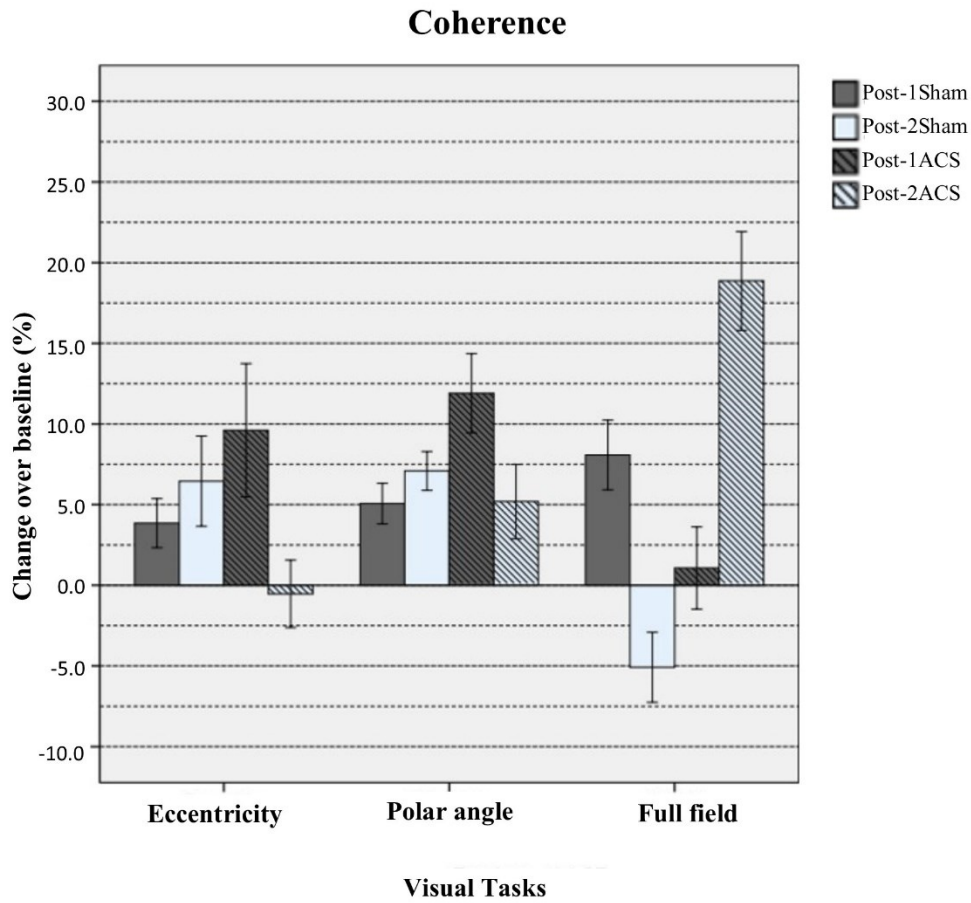


Figure 40. Quantitative comparison of the percent change over baseline for coherence (mean±standard error of the mean) across time in the ACS- and sham-transorbital ACS for all of the visual tasks. Statistically significant interaction effects were observed for the factors of ACS condition, time, and tasks, as detailed in the Results section.

### 5.3.8 Interaction effects between ACS condition and hemisphere

The repeated-measures ANOVA revealed significant interactions between the factor *ACS condition* and *hemisphere* in terms of the percent change over baseline of the amplitude ( $F(1,24)=4.68, p=0.03$ ) but not for the percent change over baseline of the cortical surface area ( $F(1,24)=1.54, p=0.22$ ) or coherence ( $F(1,24)=0.55, p=0.46$ ). This interaction effect suggests that the effect of ACS condition differs between left and right hemispheres in terms of the percent change over baseline of the amplitude. The results revealed a small increased percent change over baseline for the amplitude of the right hemisphere compared with the left hemisphere in the sham condition ( $3.31\pm 1.70$  vs.  $1.61\pm 1.70, t(28) = -0.72, p=0.47$ ) and the decreased percent change over baseline for the amplitude of the right hemisphere compared with the left hemisphere which showed some increased in the ACS condition ( $-2.29\pm 1.70$  vs.  $1.61\pm 1.70, t(28)=2.20, p=0.03$ ).

## 5.4 DISCUSSION

Here, I have explored the effects of transorbital ACS on the activated cortical surface area (activated voxels), the fMRI response amplitude, and stimulation-activation coherence. The findings demonstrated a greater increased of the activated cortical surface area and coherence in ACS compared with sham and a decreased amplitude in the ACS measurements compared with the sham measurements. The comparison of fMRI activation between two time points of post ACS procedure showed that ACS and sham changes the fMRI activation over time. The ACS condition modulates the fMRI activation in each visual task differently, whereby, the full field task demonstrated different fMRI activation patterns compared with eccentricity and polar angle. Moreover, the results showed that ACS condition modulates left and right hemisphere differently.

I included a sham condition, which served as a reference value. The sham condition was a very short ACS stimulation which was expected to be without any effects. As I now showed, sham and ACS conditions had different activated cortical surface areas, response amplitudes, and coherence. Specifically, ACS increased the activated cortical surface area and coherence compared with sham and decreased amplitude in the ACS measurements compared with the sham measurements. These modifications can be interpreted as signs of changes in brain cortical

activity following transorbital ACS. However, I observed also some minor changes in the sham condition as well which may be attributable to the minimal stimulation which was given during the sham block.

The present findings showed that the ACS condition was associated with more activated voxels than the sham condition. A larger number of activated voxels in the visual areas is consistent with the findings of an animal study conducted by Ozen et al. (2010) showed that transcranial electrical stimulation induced effects on neuronal activity in widespread cortical areas. According to Reato et al. (2013) and Battleday et al. (2014), transcranial ACS increased the number of neuron entrained in a particular or endogenous frequency. The application of non-invasive electrical stimulation close to the endogenous frequency has efficiently modified brain oscillations (Miniussi et al., 2012; Reato et al., 2013). Zaehle et al. (2010) demonstrated that stimulating a single neuron makes it more likely to stimulate other neurons that are connected to the driven neurons. It has been suggested that such increased spatial activation involves the modification of many neurons (Reato et al., 2013).

While most fMRI measures increased after ACS, the response amplitude was decreased in the ACS condition compared with the sham condition. The decreased response amplitude was assumed to be an indication of increased neural efficiency which fits with the current observation of an increased coherence and neuronal synchronization. In their studies of tDCS effects in the motor cortex with fMRI, Amadi et al. (2013) and Polanía et al. (2012b) proposed that increased coherence within the primary motor cortex was related to functional synchronization. Such an alteration in synchronization is the consequence of changes in the signal to noise ratio (SNR) (Amadi et al., 2013; Polanía et al., 2012b). Like previous authors, I propose that transorbital ACS can effectively reduce neuronal noise (Amadi et al., 2013), which would result in an increased SNR in the neuronal signal of the visual cortex. Because increased SNR may lead to, or be the result of, increased functional synchronization (Amadi et al., 2013; Polanía et al., 2012b), the current observation of increased coherence and reduced response amplitude following transorbital ACS suggests that visual cortical areas have altered to become more efficient.

Several previous studies have shown that the application of ACS can sustain entrainment of endogenous activity for up to 30 minutes (Neuling et al., 2013; Wach et al., 2013). It therefore seems that such “after-effects” of brain oscillation entrainment of a single ACS session is rather short lasting. In this study, the comparison of brain activation between two time points (15–32 minutes and 37–54 minutes after transorbital ACS) revealed significant differences which shows also that transorbital ACS induced short-duration changes in brain activation. Although the immediate effect of transorbital ACS was not sustained in the second time point, the current findings show that transorbital ACS was able to induce functional effects which are interpreted as a sign of altered neuroplasticity, although this was only short-lasting. I believe that by increasing the stimulation time and using an optimal combination of stimulation parameters, the effects – activated cortical surface area, response amplitude, and coherence – may last longer. Indeed Sabel et al. (2011) and Bola et al (2014) observed last lasting changes as late at 24-48 hrs.

The current findings show that brain signals are remarkably capable of modify in response to transorbital ACS. The brain signal changes induced by transorbital ACS is proposed to arise from synaptic plasticity (Zaehle et al., 2010). Synapses in the neuronal network can either strengthen or weaken their efficiency of input and output activity over time (Zaehle et al., 2010). Long-term potentiation (LTP) and long-term depression (LTD) are mechanisms of the synaptic level. The biological process that alters the connection strength between neurons is called spike timing-dependent plasticity (STDP) (Zaehle et al., 2010; Karabanov et al., 2015). Based on the STDP protocol, synapses in the neural network were strengthened if the external input was close to the endogenous frequency (Zaehle et al., 2010). The induction of LTP and LTD allow neurons to modify their synaptic strength, thereby enabling them to potentially adapt to the specific synaptic input (Neuling et al., 2013; Zaehle et al., 2010; Carlo Miniussi et al., 2012; Wach et al., 2013). Notably, the application of transorbital ACS close to the endogenous frequency could affect the entrainment of brain oscillations (Zaehle et al., 2010; Battleday et al., 2014; Kanai et al., 2010; Pogosyan et al., 2009), thereby modifying the synchronization of neural networks and its functions; the synchronization of the brain oscillation are also thought to continue after the end of the stimulus. Transorbital ACS presumably induces its effect via upregulation and or downregulation of synapses while maintaining a relatively balanced equilibrium of activity over time.

The variation of after-effects in the activated cortical surface area, the response amplitude, and coherence induced by transorbital ACS in visual tasks, i.e., the eccentricity, polar angle, and full field, is thought to be due to different response modulations involved. The full-field task has a larger stimulus segment compared with the eccentricity and polar angle. Therefore, full-field tasks activate a larger cortical region at one time than the eccentricity and polar angle. The changes in fMRI activations are task-related.

Additionally, these results reveal that the sham and ACS conditions modulated the left and right hemisphere of the fMRI response amplitude differently. The discrepancy may be due to the alteration of neuronal signals. Such alteration is suggested to maintain the internal balance of excitation and inhibition within the visual areas in both hemispheres. Moreover, the different effects seen in the left and right hemispheres might be due to the influence of the stimulation electrodes. Although the AC stimulation electrode (the active electrode) was positioned on the center forehead (Fpz), the reference (return) electrode was positioned on the right upper arm which may affect the pattern of the global current flow through the visual pathways and thus even may affect the modulation of the neural network under the active electrode. Therefore, I assumed that the position of the reference electrode could influence the which hemisphere was affected the most.

Moreover, the results presented here indicate that transorbital ACS can modulate neuronal activity in the retina (Schutter and Hortensius, 2010; Foik et al., 2015) and maintain the modulation of neuronal activity throughout the visual system, as shown previously by electrophysiological findings in patients with visual deficits (Schmidt et al., 2013; Bola et al., 2014; Sabel et al., 2011a). Foik et al. (2015) who studied rats, suggested that the enhanced synchronization of neural activity in the retina induced by transorbital ACS seemed to cause increased efficiency in the transfer of information and accelerate neuronal processing (Lesica et al., 2007; Wang et al., 2010), which subsequently influenced the neural network in the lateral geniculate nucleus, subcortical, and cortical areas. The application of a transorbital stimulation electrode could thus induce neural activity, originating in the retina and eliciting visual information flow through visual pathways (Foik et al., 2015). Consistent with previous findings, I believe that these cortical activation patterns are likely caused by the rhythmic firing of the retinal ganglion cells (Foik et al., 2015), which subsequently influence the modulation of



oscillatory activity in the visual cortex (Schmidt et al., 2013; Bola et al., 2014; Sabel et al., 2011a; Foik et al., 2015).

The present study has some limitations which may affect the interpretation of these results. One potential limitation is the relatively small sample size (n=5 subjects). Even so, I believe that by using a repeated-measures design in the same subjects with an identical procedure, and adequate control of the confounding factors was achieved. By increasing the sample size in future studies, I may be able to increase the confidence in evaluation and allow for more powerful inferences. Although the present study is characterized by a small sample size, this preliminary results demonstrate the potential of transorbital ACS to modify brain activity. Another limitation of the present study was the long time delay of approximately 15 minutes between the end of the stimulation procedure (ACS- and sham-transorbital ACS) and the start of the fMRI post-measurement. This long time delay arose because the stimulation procedure and fMRI measurement were conducted in different rooms. Moreover, I permitted subjects to have a short break after the stimulation procedure to go to washroom and relax. Recent results have indicated brain signal differences across time; therefore, the time delay may have influenced the effect of transorbital ACS on the visual cortex between the immediate and after-effects. For future studies, I suggest conducting the stimulation procedure inside the MR scanner using MR-compatible transorbital ACS to decrease the time delay between the stimulation procedure and the fMRI measurement. Additionally, by implementing the stimulation procedure inside the MR scanner it might be possible to also measure the online or direct effect of transorbital ACS and thus obtain additional information about the effect of transorbital ACS. Third, this study used different visual tasks to evaluate the effect of transorbital ACS in the visual cortex. For future studies I suggest using one visual stimulation task to enable a clearer transorbital ACS effect to be determined over time. Furthermore, I also suggest adding an additional time point to evaluate longer after effects in visual cortex.

In summary, while I have gained additional insight into the mechanism underlying transorbital ACS, this issue need further exploration. By combining transorbital ACS and fMRI, I expect to obtain more information about any acute effects on ACS brain activation. In any event, these findings are compatible with the proposal that transorbital ACS is able to alter

plasticity in the normal human brain which was observed already by electrophysiological techniques in normal subjects and in patients with vision loss.

## CHAPTER 6

### SUMMARY AND FUTURE DIRECTIONS

#### 6.1 SUMMARY

There are two themes in this thesis. The first is the quantitative assessment of visual cortex functions in the repeated measures design with fMRI at 7 Tesla. The second theme is an exploration of the effect of transorbital ACS in the visual cortex with fMRI at 7 Tesla.

In Study I, the systematic variation of brain response patterns in early visual areas over time was explored with fMRI. As we knew fMRI is one of the neuroimaging techniques that promise to advance our understanding of brain function in both healthy and diseased brains. Recently, fMRI has become one of the preferred techniques for investigating changes in brain activity, structure and connectivity induced by treatment or rehabilitation methods. The application of fMRI and retinotopic mapping stimuli enables the identification of visual cortical areas and the functional specialization of the visual system. Therefore, the changes of visual cortex activity underlying the effect of a rehabilitation method allow us to develop and provide more effective treatment approaches in patients. Therefore, before the implementation of any fMRI paradigm design, especially in the study of the effect of rehabilitation method, it is important to understand the brain response patterns across time. Test-retest or repeated measure design can be used to investigate how stable the fMRI responses are across time. So far, little is known about the stability of brain responses across time using retinotopic stimuli. What is known, however, is that spatial attention tasks increase the reliability of brain responses in the occipital and parietal cortex (Bressler and Silver, 2010). Therefore, I decided to start my research studies with an evaluation of the systematic changes in the cortical surface area, response amplitude and coherence across time. The study of seven healthy subjects was undertaken at three separate sessions ( i.e., an interval of  $51.4 \pm 5.4$  days between Session 1 and Session 2, and

167.9 ± 24.4 days between Session 2 and Session 3). The findings showed that the initial session, Session 1, indicated distinct fMRI activation, e.g. the activated cortical surface area, the response amplitude and coherence patterns as compared to other sessions. The head motion was hypothesised as the major effect in the initial session. However, the assessment of head motion on the data rejected that hypothesis. Additional analysis in the study of reproducibility of the phase maps in the early visual areas indicated a high phase correlation between sessions in eccentricity and polar angle mapping. This result showed that the phase maps were stable or consistent across the session. Although the phase maps were highly correlated between sessions, the activated cortical surface area, amplitude, and coherence differed in Session 1 as compared to Sessions 2 and 3. The reduction of brain activation from Sessions 1 and 2 suggested familiarity with the procedure (Raemaekers et al., 2007) and enhancement in neural efficiency with experience (Kelly et al., 2006; Zandbelt et al., 2008; Poldrack, 2000). The cognitive effects ( i.e., novelty, learning and adaptation) suggested influences on brain activation, especially in the initial session (Abd Hamid et al., 2015b). Therefore, because brain response patterns in the current work were not consistent at all time points, it was suggested that the initial session should introduce sequential effects (Abd Hamid et al., 2015b). It should be noted that if the sequential effects shown in the initial scan are not taken into account in the extended experiment or future studies, the result may be errors in inferences in the longitudinal studies on visually driven cortical activity (Abd Hamid et al., 2015b). Therefore, based on the results obtained in the test-retest study, the initial scanning session was implemented as an introduction to the two subsequent studies (i.e., Study II and Study III) to reduce experience-based effects (Abd Hamid et al., 2015b), whereby the initial scanning session was discarded for further analysis.

In the two subsequent studies, the effect of transorbital ACS was explored in the visual cortex using fMRI-based retinotopic mapping. Previous studies have demonstrated that the application of a 10-day course of transorbital ACS improved visual field size in patients with visual impairment (Sabel et al., 2011a; Fedorov et al., 2011; Schmidt et al., 2013). Increased alpha power at the occipital sites was observed after the application of repetitive transorbital ACS (rtACS) by Fedorov et al. (2011), Sabel et al. (2011a) and Schmidt et al. (2013), whereby the alpha power enhancement reflected increased synchronization of neural networks. Additionally, improved visual functioning and visual-related quality of life have been reported in the questionnaires study by Gall et al. (2011). In the study of functional connectivity by Bola et

al. (2014), the authors demonstrated that rtACS increased the alpha band functional connectivity. The findings indicated that rtACS was able to modulate network topology and synchronization within the non-affected network and was beneficial in improving visual perception (Bola et al., 2014). Notably, the visual outcome reported in the previous studies used HRP (Sabel et al., 2011a; Fedorov et al., 2011; Schmidt et al., 2013; Gall et al., 2011; Bola et al., 2014), EEG (Sabel et al., 2011a; Fedorov et al., 2011; Schmidt et al., 2013; Bola et al., 2014) and questionnaires (Gall et al., 2011) to investigate the effect of rtACS in patients with visual impairment (Sabel et al., 2011a; Fedorov et al., 2011; Schmidt et al., 2013; Gall et al., 2011; Bola et al., 2014). Although the previous study reported benefits of transorbital ACS, only a few studies have reported the mechanism and functional reorganization achieved by the technique (Sabel et al., 2011a; Fedorov et al., 2011; Schmidt et al., 2013; Gall et al., 2011; Bola et al., 2014). More research is required to provide such information. As mentioned before, a neuroimaging technique such as fMRI promises to advance our understanding of brain function in both healthy and diseased brains. I believe by incorporating NIBS (i.e., transorbital ACS) and neuroimaging technique (i.e., fMRI), more information can be obtained. Only a limited number of studies have reported the effect of the NIBS method using fMRI technique such as tDCS (Antal et al., 2011; Holland et al., 2011; Clark et al., 2012; Meinzer et al., 2014) and tRNS (Chaieb et al., 2009). Therefore, in Study II, the effects of transorbital ACS in a homonymous hemianopsia patient by using fMRI-based retinotopic mapping were explored. However, due to stringent inclusion and exclusion criteria (see Gall et al., (2015)) for 7T fMRI, only one subject out of 78 screened patients was a suitable candidate. Based on a single case study, the results showed that the 7T fMRI was reliably feasible for detecting the changes in brain activation in the early visual areas that underlie rtACS effect. Overall, rtACS increased the activated cortical surface area (4.5%–75.1%) and coherence (0.8%–67.4%) in most regions of interest in both intact and damaged hemispheres. For the fMRI response amplitude, rtACS caused a mix of increased and decreased amplitude in the region of interest of intact hemisphere and decreased amplitude in the damaged hemisphere.

In an animal study, Rosa et al. (2000) reported that the residual cells located in the damaged area (V1) remained responsive with an extended distribution in other areas as well during the spontaneous recovery. The extended distribution in the cortical areas showed the ability of the brain to form new nerve connections following brain injury even without any

rehabilitation methods. Based on the evidence of spontaneous recovery, I believe that the application of rehabilitation methods can facilitate neuroplasticity and induce recovery. Recently, Reato et al. (2013) proposed that increased spatial activation reflects modification of many neurons. While, Zaehla et al. (2010) demonstrated that the application of AC fields in a single neuron was capable of stimulating the other 2500 neurons that are linked to the driven neuron to fire synchronously. Previous findings showed that AC fields were capable of altering larger neuronal networks. In this work, the widespread activation in both intact and damaged hemispheres induced by transorbital ACS indicated a sign of massive reorganization. The widespread activation in the damaged regions shows that the rtACS is capable of reactivating residual cells (Plow et al., 2011; Sabel et al., 2011b) to keep them active and develop new neural links. The residual cells can still function more or less normally (Zeki and Bartels, 1998, 1999). Meanwhile, widespread activation in the intact regions indicates that rtACS is capable of forming plasticity in the larger neuronal network. Such changes suggest that there is a link to modification of neuronal oscillation and modification of short-range and long-range functional connections (Sabel et al., 2011a; Bola et al., 2014). Importantly, rtACS modifies not only visual cortex activity in the damaged areas but also in involved undamaged areas.

Several previous studies revealed that a lesion not only caused a disturbance signal in damaged areas but also involved undamaged areas (Rosa et al., 2000; Bola et al., 2013; Poggel et al., 2011). Poggel et al. (2011) reported that the interference of temporal processing not only involved damaged regions but also involved the “intact” regions. The disturbance event in the “intact” regions is known as “sightblindness” and has been discussed by Bola et al. (2013) (see Bola et al., (2013) for further discussion). This scenario rendered the intact hemisphere “hyperactive” (Oliveri et al., 1999) and inhibited the damaged hemisphere even further. Therefore, the lesion rendered an interhemispheric inhibition imbalance (Oliveri et al., 1999; Corbetta et al., 2005). The open question here is how the rtACS modifies the brain response amplitude. The current findings indicate mixed increased and decreased the fMRI response amplitude in the region of interest. These result denotes that rtACS-induced reorganization to compensate for a lesion (Rosa et al., 2000). The response amplitude of some regions of interest increased and others decreased, but the coherence value increased. I hypothesise that the increased coherence value denotes increased synchronization of the neuronal network. The rtACS might effectively reduce the variability of neuronal signals. Similar findings have been

shown by Amadi et al. (2013) and Polanía et al. (2012) in the application of tDCS in the motor cortex. However, the precise mechanism is still unclear. To date, there is still no report regarding ACS effects in the subject without visual field deficits by using the fMRI method. Therefore, an extended study that involved healthy subjects with fMRI was suggested to gain more knowledge of the underlying rtACS effects.

Therefore, a subsequent study (Study III) was conducted to explore the changes in brain activation that underlie the transorbital ACS in five healthy participants using fMRI-based retinotopy mapping. In this work, I hypothesize that transorbital ACS can induce changes in the activated cortical surface area, fMRI response amplitude and coherence. The results demonstrated that transorbital ACS increased the activated cortical surface area, decreased the fMRI response amplitude and increased coherence in the early visual cortex. The comparison of fMRI activation between two time points showed differences. These results demonstrated that transorbital ACS modulates the activated cortical surface area, fMRI response amplitude, and coherence over time in the visual cortex which outlasted the stimulation period.

Increased spatial activation has been observed in the activated cortical visual areas, which is similar to the findings in the single case study (Study II). The results showed that transorbital ACS can stimulate a large neural network (Zaehle et al., 2010; Reato et al., 2013). Furthermore, transorbital ACS induced decreased response amplitude and increased coherence in the early visual areas. I believe that decreased response amplitude may be an indication of increased neural efficiency as also indicated by increased coherence. Interestingly, the patterns of increased coherence value in this work are similar to the findings in the single patient study (study II). These findings showed that transorbital ACS might effectively increase the SNR of the neural signals in the visual cortex (Amadi et al., 2013; Polanía et al., 2012b). I believe that the increased coherence denotes increased functional synchronization (Amadi et al., 2013; Polanía et al., 2012b). In the damaged brain, the neuronal network may experience desynchronization or disturbances of synchronous firing. Therefore, the goal here is to resynchronize the oscillation of brain activity for functional improvement. Based on the findings, the transorbital ACS not only modified the brain activity in the patient study but also modified brain activity in the healthy subjects. Such brain changes show that transorbital ACS has the potential to improve visual function.

The next open question is whether the changes in brain response induced by transorbital ACS may last longer—that is, beyond the period of stimulation. In this work, Study III, the changes in brain response were compared at two time points of 15–32 minutes (Post-1) and 37–54 minutes (post-2). Neuling et al. (2013) and Wach et al. (2013) revealed that transcranial ACS can entrain intrinsic activity for up to 30 minutes. In the present study, the comparison of brain activation between two time points (15–32 minutes and 37–54 minutes after transorbital ACS) revealed significant differences which shows the effect of transorbital ACS did not last long-short duration changes. From this finding, I believe that transorbital ACS induced short-term plasticity.

Synaptic plasticity is proposed as the underlying the alteration or reorganization of brain signals induced by transorbital ACS (Zaehle et al., 2010; Vossen et al., 2015). LTP and LTD are the two mechanisms that occur at the synaptic level. These two mechanisms may play a crucial role in modifying the brain activity in a damaged brain (Neuling et al., 2013; Zaehle et al., 2010; Carlo Miniussi et al., 2012; Wach et al., 2013; Bliss and Cooke, 2011). The decreased response amplitude after transorbital ACS perhaps denotes reduced cortical excitability, which suggests LTD-like plasticity, while increased response amplitude after transorbital ACS perhaps denotes increased cortical excitability, which would suggest LTP-like plasticity. The mixed increased and decreased amplitude in the single case study is assumed to show LTP- and LTD-like synaptic plastic changes; reorganization following lesion. In the healthy subjects, decreased response amplitude was observed, thereby showing LTD-like plasticity. The distinct synaptic plasticity mechanism in the healthy subject and patient is possibly due to the distinct efficiency of synaptic transmission between these two groups. The induction of LTP and LTD permits neurons to alter the synaptic strength and thereby improve the functional brain activity (Neuling et al., 2013; Zaehle et al., 2010; Carlo Miniussi et al., 2012; Wach et al., 2013). The healthy subjects and patients maintain the internal balance by different mechanisms.

## **6.2 CONCLUSIONS**

The findings in the Study I showed that the initial scan (Session 1) introduced sequential effects and should be considered in future experiments. In the Study II and III, the findings revealed that transorbital ACS modulates the activated cortical surface area, the fMRI response amplitude, and coherence in the visual cortex. One can conclude from these findings that transorbital ACS has



the ability to alter plasticity in the visual cortex which out-last the time of stimulation in normal subjects and in patients with vision loss.

### **6.3 FUTURE DIRECTIONS**

Here, I highlight a few suggestions that are worthy of consideration in planning future studies. First, the sample size should be increased to boost confidence in evaluation and inferences. Despite the transorbital ACS-induced changes in brain activity in the visual cortex, the interpretation of the current findings is based on a small sample size. Second, a future study should have a control group and a patient group whose members match in terms of age and sex. I believe by using this study design, more information can be obtained, especially involving the precise mechanisms. Third, the implementation of a stimulation procedure inside the MR-scanner is needed. As mentioned before in Study III (Chapter 5), this implementation not only can lessen the time delay between the stimulation procedure and fMRI measurement, but we could also obtain additional information regarding the online or direct effect of transorbital ACS. Fourth, more time points of fMRI measurement are needed to obtain more information about the lasting effects. Fifth, only one visual task should be used; this would produce a clearer effect of transorbital ACS over time. Finally, simultaneous EEG-fMRI recording might reveal benefits in both spatial and temporal resolution. These methods would enable researchers to learn more about the synaptic plasticity mechanisms.

## BIBLIOGRAPHY

- Abd Hamid, A. I., Gall, C., Speck, O., Antal, A., and Sabel, B. A. (2015a). Effects of alternating current stimulation on the healthy and diseased brain. *Front. Neurosci.* 9, 391. doi:10.3389/fnins.2015.00391.
- Abd Hamid, A. I., Speck, O., and Hoffmann, M. (2015b). Quantitative assessment of visual cortex function with fMRI at 7 Tesla – test-retest variability. *Front. Hum. Neurosci.* 9. doi:10.3389/fnhum.2015.00477.
- Aguirre, G. K., Zarahn, E., and D’esposito, M. (1998). The variability of human, BOLD hemodynamic responses. *Neuroimage* 8, 360–9. doi:10.1006/nimg.1998.0369.
- Ali, M. M., Sellers, K. K., and Fröhlich, F. (2013). Transcranial alternating current stimulation modulates large-scale cortical network activity by network resonance. *J. Neurosci.* 33, 11262–75. doi:10.1523/JNEUROSCI.5867-12.2013.
- Amadi, U., Ilie, A., Johansen-Berg, H., and Stagg, C. J. (2013). Polarity-specific effects of motor transcranial direct current stimulation on fMRI resting state networks. *Neuroimage* 88C, 155–161. doi:10.1016/j.neuroimage.2013.11.037.
- Ameli, M., Grefkes, C., Kemper, F., Riegg, F. P., Rehme, A. K., Karbe, H., Fink, G. R., and Nowak, D. A. (2009). Differential effects of high-frequency repetitive transcranial magnetic stimulation over ipsilesional primary motor cortex in cortical and subcortical middle cerebral artery stroke. *Ann. Neurol.* 66, 298–309. doi:10.1002/ana.21725.
- Antal, A., Boros, K., Poreisz, C., Chaieb, L., Terney, D., and Paulus, W. (2008). Comparatively weak after-effects of transcranial alternating current stimulation (tACS) on cortical excitability in humans. *Brain Stimul.* 1, 97–105. doi:10.1016/j.brs.2007.10.001.
- Antal, A., Kincses, T. Z., Nitsche, M. A., Bartfai, O., and Paulus, W. (2004). Excitability changes induced in the human primary visual cortex by transcranial direct current stimulation: direct electrophysiological evidence. *Invest. Ophthalmol. Vis. Sci.* 45, 702–707. Available at: <http://www.iovs.org/cgi/doi/10.1167/iovs.03-0688>.
- Antal, A., and Paulus, W. (2013). Transcranial alternating current stimulation (tACS). *Front. Hum. Neurosci.* 7, 317. doi:10.3389/fnhum.2013.00317.
- Antal, A., Polania, R., Schmidt-Samoa, C., Dechent, P., and Paulus, W. (2011). Transcranial direct current stimulation over the primary motor cortex during fMRI. *Neuroimage* 55, 590–6. doi:10.1016/j.neuroimage.2010.11.085.
- Arias-Carrión, O., Stamelou, M., Murillo-Rodríguez, E., Menéndez-González, M., and Pöppel, E. (2010). Dopaminergic reward system: a short integrative review. *Int. Arch. Med.* 3, 24. doi:10.1186/1755-7682-3-24.
- Ashtari, M., Cyckowski, L. L., Monroe, J. F., Marshall, K. A., Chung, D. C., Auricchio, A., Simonelli, F., Leroy, B. P., Maguire, A. M., Shindler, K. S., et al. (2011). The human visual cortex responds to gene therapy-mediated recovery of retinal function. *J. Clin. Invest.* 121, 2160–8. doi:10.1172/JCI57377.

- Ashtari, M., Cyckowski, L., Yazdi, A., Viands, A., Marshall, K., Bókkon, I., Maguire, A., and Bennett, J. (2014). fMRI of retina-originated phosphenes experienced by patients with leber congenital amaurosis. *PLoS One* 9, e86068. doi:10.1371/journal.pone.0086068.
- Ávila, R., Bottino, C. M. C., Carvalho, I. A. M., Santos, C. B., Seral, C., and Miotto, E. C. (2004). Neuropsychological rehabilitation of memory deficits and activities of daily living in patients with Alzheimer's disease: a pilot study. *Brazilian J. Med. Biol. Res.* 37, 1721–1729. doi:10.1590/S0100-879X2004001100018.
- Bandettini, P. A., Wong, E. C., Hinks, R. S., Tikofsky, R. S., and Hyde, J. S. (1992). Time course EPI of human brain function during task activation. *Magn. Reson. Med.* 25, 390–397. doi:10.1002/mrm.1910250220.
- Baseler, H. A., Gouws, A., Crossland, M. D., Leung, C., Tufail, A., Rubin, G. S., and Morland, A. B. (2011). Objective visual assessment of antiangiogenic treatment for wet age-related macular degeneration. *Optom. Vis. Sci.* 88, 1255–61. doi:10.1097/OPX.0b013e3182282f13.
- Battleday, R. M., Muller, T., Clayton, M. S., and Cohen Kadosh, R. (2014). Mapping the Mechanisms of Transcranial Alternating Current Stimulation: A Pathway from Network Effects to Cognition. *Front. psychiatry* 5, 162. doi:10.3389/fpsy.2014.00162.
- Beisteiner, R., Robinson, S., Wurnig, M., Hilbert, M., Merksa, K., Rath, J., Höllinger, I., Klinger, N., Marosi, C., Trattnig, S., et al. (2011). Clinical fMRI: evidence for a 7T benefit over 3T. *Neuroimage* 57, 1015–21. doi:10.1016/j.neuroimage.2011.05.010.
- Beitz, J. M. (2014). Parkinson's disease: a review. *Front. Biosci. (Schol. Ed.)* 6, 65–74. Available at: <http://www.ncbi.nlm.nih.gov/pubmed/24389262> [Accessed January 19, 2015].
- Belliveau, J. W., Kennedy, D. N., McKinstry, R. C., Buchbinder, B. R., Weisskoff, R. M., Cohen, M. S., Vevea, J. M., Brady, T. J., and Rosen, B. R. (1991). Functional mapping of the human visual cortex by magnetic resonance imaging. *Science* 254, 716–9. Available at: <http://www.ncbi.nlm.nih.gov/pubmed/1948051> [Accessed July 12, 2015].
- Bennett, C. M., and Miller, M. B. (2010). How reliable are the results from functional magnetic resonance imaging? *Ann. N. Y. Acad. Sci.* 1191, 133–55. doi:10.1111/j.1749-6632.2010.05446.x.
- Bikson, M., Datta, A., and Elwassif, M. (2009). Establishing safety limits for transcranial direct current stimulation. *Clin. Neurophysiol.* 120, 1033–4. doi:10.1016/j.clinph.2009.03.018.
- Bindman, L. J., Lippold, O. C., and Redfearn, J. W. (1964). The action of brief polarizing currents on the cerebral cortex of the rat (1) during current flow and (2) in the production of long-lasting after-effects. *J. Physiol.* 172, 369–82. Available at: <http://www.pubmedcentral.nih.gov/articlerender.fcgi?artid=1368854&tool=pmcentrez&rendertype=abstract> [Accessed June 29, 2015].
- Bliss, T. V. P., and Cooke, S. F. (2011). Long-term potentiation and long-term depression: a clinical perspective. *Clinics* 66, 3–17. doi:10.1590/S1807-59322011001300002.
- Bloch, F. (1946). Nuclear Induction. *Phys. Rev.* 70, 460–474. doi:10.1103/PhysRev.70.460.
- Bola, M., Gall, C., Moewes, C., Fedorov, A., Hinrichs, H., and Sabel, B. A. (2014). Brain functional connectivity network breakdown and restoration in blindness. *Neurology* 83, 542–51. doi:10.1212/WNL.0000000000000672.

- Bola, M., Gall, C., and Sabel, B. A. (2013). “Sightblind”: perceptual deficits in the “intact” visual field. *Front. Neurol.* 4, 80. doi:10.3389/fneur.2013.00080.
- Bolognini, N., Pascual-Leone, A., and Fregni, F. (2009). Using non-invasive brain stimulation to augment motor training-induced plasticity. *J. Neuroeng. Rehabil.* 6, 8. doi:10.1186/1743-0003-6-8.
- Breier, J. I., Juranek, J., Maher, L. M., Schmadeke, S., Men, D., and Papanicolaou, A. C. (2009). Behavioral and neurophysiologic response to therapy for chronic aphasia. *Arch. Phys. Med. Rehabil.* 90, 2026–33. doi:10.1016/j.apmr.2009.08.144.
- Bressler, D. W., and Silver, M. a (2010). Spatial attention improves reliability of fMRI retinotopic mapping signals in occipital and parietal cortex. *Neuroimage* 53, 526–33. doi:10.1016/j.neuroimage.2010.06.063.
- Brittain, J.-S., Probert-Smith, P., Aziz, T. Z., and Brown, P. (2013). Tremor suppression by rhythmic transcranial current stimulation. *Curr. Biol.* 23, 436–40. doi:10.1016/j.cub.2013.01.068.
- Brown, M. A., and Semelka, R. C. (2003). *MRI Basic Principles and Applications*. 3rd ed. Hoboken, New Jersey: John Wiley & Sons doi:10.1002/0471467936.
- Brunoni, A. R., Amadera, J., Berbel, B., Volz, M. S., Rizzerio, B. G., and Fregni, F. (2011). A systematic review on reporting and assessment of adverse effects associated with transcranial direct current stimulation. *Int. J. Neuropsychopharmacol.* 14, 1133–45. doi:10.1017/S1461145710001690.
- Buxton, R. B., Wong, E. C., and Frank, L. R. (1998). Dynamics of blood flow and oxygenation changes during brain activation: The balloon model. *Magn. Reson. Med.* 39, 855–864. doi:10.1002/mrm.1910390602.
- Caceres, A., Hall, D. L., Zelaya, F. O., Williams, S. C. R., and Mehta, M. A. (2009). Measuring fMRI reliability with the intra-class correlation coefficient. *Neuroimage* 45, 758–68. doi:10.1016/j.neuroimage.2008.12.035.
- Carlo Miniussi, Paul, W., and Rossini, P. M. (2012). *Transcranial brain stimulation*. Boca Raton, FL: CRC Press.
- Chaieb, L., Antal, A., Pisoni, A., Saiote, C., Opitz, A., Ambrus, G. G., Focke, N., and Paulus, W. (2014). Safety of 5 kHz tACS. *Brain Stimul.* 7, 92–6. doi:10.1016/j.brs.2013.08.004.
- Chaieb, L., Kovacs, G., Cziraki, C., Greenlee, M., Paulus, W., and Antal, A. (2009). Short-duration transcranial random noise stimulation induces blood oxygenation level dependent response attenuation in the human motor cortex. *Exp. brain Res.* 198, 439–44. doi:10.1007/s00221-009-1938-7.
- Chibisova, A. N., Fedorov, A. B., and Fedorov, N. A. (2001). Neurophysiological characteristics of compensation-recovery processes in the brain during rehabilitation of the neurosensory impairment of the visual and acoustic systems. Available at: <http://pubget.com/paper/11548421>.
- Citri, A., and Malenka, R. C. (2008). Synaptic plasticity: multiple forms, functions, and mechanisms. *Neuropsychopharmacology* 33, 18–41. doi:10.1038/sj.npp.1301559.
- Clark, V. P., Coffman, B. A., Mayer, A. R., Weisend, M. P., Lane, T. D. R., Calhoun, V. D.,

- Raybourn, E. M., Garcia, C. M., and Wassermann, E. M. (2012). TDCS guided using fMRI significantly accelerates learning to identify concealed objects. *Neuroimage* 59, 117–28. doi:10.1016/j.neuroimage.2010.11.036.
- Conner, I. P., Odom, J. V., Schwartz, T. L., and Mendola, J. D. (2007). Retinotopic maps and foveal suppression in the visual cortex of amblyopic adults. *J. Physiol.* 583, 159–73. doi:10.1113/jphysiol.2007.136242.
- Corbetta, M., Kincade, M. J., Lewis, C., Snyder, A. Z., and Sapir, A. (2005). Neural basis and recovery of spatial attention deficits in spatial neglect. *Nat. Neurosci.* 8, 1603–10. doi:10.1038/nn1574.
- Creutzfeldt, O. D., Fromm, G. H., and Kapp, H. (1962). Influence of transcortical d-c currents on cortical neuronal activity. *Exp. Neurol.* 5, 436–452. Available at: <http://www.ncbi.nlm.nih.gov/pubmed/13882165>.
- Dacey, D. M. (1993). Morphology of a small-field bistratified ganglion cell type in the macaque and human retina. *Vis. Neurosci.* 10, 1081–98. Available at: <http://www.ncbi.nlm.nih.gov/pubmed/8257665> [Accessed July 12, 2015].
- Damadian, R. (1971). Tumor Detection by Nuclear Magnetic Resonance. *Science (80- )*. 171, 1151–1153. doi:10.1126/science.171.3976.1151.
- DeYoe, E. A., Carman, G. J., Bandettini, P., Glickman, S., Wieser, J., Cox, R., Miller, D., and Neitz, J. (1996). Mapping striate and extrastriate visual areas in human cerebral cortex. *Proc. Natl. Acad. Sci. U. S. A.* 93, 2382–6. Available at: [http://www.pubmedcentral.nih.gov/articlerender.fcgi?artid=39805&tool=pmcentrez&render\\_type=abstract](http://www.pubmedcentral.nih.gov/articlerender.fcgi?artid=39805&tool=pmcentrez&render_type=abstract) [Accessed May 1, 2015].
- Dimyan, M. A., and Cohen, L. G. (2011). Neuroplasticity in the context of motor rehabilitation after stroke. *Nat. Rev. Neurol.* 7, 76–85. doi:10.1038/nrneuro.2010.200.
- Dobkin, B. H. (2005). Clinical practice. Rehabilitation after stroke. *N. Engl. J. Med.* 352, 1677–84. doi:10.1056/NEJMcp043511.
- Dougherty, R. F., Koch, V. M., Brewer, A. A., Modersitzki, J., and Wandell, B. A. (2003). Visual field representations and locations of visual areas V1 / 2 / 3 in human visual cortex. *Area*, 586–598. doi:10.1167/3.10.1.
- Dumoulin, S. O., Hoge, R. D., Baker, C. L., Hess, R. F., Achtman, R. L., and Evans, A. C. (2003). Automatic volumetric segmentation of human visual retinotopic cortex. *Neuroimage* 18, 576–87. Available at: <http://www.ncbi.nlm.nih.gov/pubmed/12667835> [Accessed July 12, 2015].
- Dumoulin, S. O., and Wandell, B. A. (2008). Population receptive field estimates in human visual cortex. *Neuroimage* 39, 647–60. doi:10.1016/j.neuroimage.2007.09.034.
- Engel, S. (1997). Retinotopic organization in human visual cortex and the spatial precision of functional MRI. *Cereb. Cortex* 7, 181–192. doi:10.1093/cercor/7.2.181.
- Engel, S. A., Glover, G. H., and Wandell, B. A. (1997). Retinotopic organization in human visual cortex and the spatial precision of functional MRI. *Cereb. Cortex* 7, 181–192. doi:10.1093/cercor/7.2.181.
- Engel, S. A., Rumelhart, D. E., Wandell, B. A., Lee, A. T., Glover, G. H., Chichilnisky, E. J.,

- and Shadlen, M. N. (1994). fMRI of human visual cortex. *Nature* 369, 525. doi:10.1038/369525a0.
- Engel, S. A., Rumelhart, D. E., Wandell, B. A., Lee, A. T., Glover, G. H., Chichilnisky, E. J., Shadlen, M. N., and Newsome, W. T. (1993). Functional MRI measurements of human striate cortex topography. *Soc. Neurosci. Abs.*, 335.
- Van Essen, D., Anderson, C., and Felleman, D. (1992). Information processing in the primate visual system: an integrated systems perspective. *Science* (80-. ). 255, 419–423. doi:10.1126/science.1734518.
- Fedorov, A. B., Chibisova, A. N., and Tchibissova, J. M. (2005). Impulse modulating therapeutic electrical stimulation (IMTES) increases visual field size in patients with optic nerve lesions. *Int. Congr. Ser.* 1282, 525–529. doi:10.1016/j.ics.2005.05.007.
- Fedorov, A., Jobke, S., Bersnev, V., Chibisova, A., Chibisova, Y., Gall, C., and Sabel, B. A. (2011). Restoration of vision after optic nerve lesions with noninvasive transorbital alternating current stimulation: a clinical observational study. *Brain Stimul.* 4, 189–201. doi:10.1016/j.brs.2011.07.007.
- Fernández, G., Specht, K., Weis, S., Tendolkar, I., Reuber, M., Fell, J., Klaver, P., Ruhlmann, J., Reul, J., and Elger, C. E. (2003). Intrasubject reproducibility of presurgical language lateralization and mapping using fMRI. *Neurology* 60, 969–75. Available at: <http://www.ncbi.nlm.nih.gov/pubmed/12654961> [Accessed December 14, 2014].
- Fertonani, A., Pirulli, C., and Miniussi, C. (2011). Random noise stimulation improves neuroplasticity in perceptual learning. *J. Neurosci.* 31, 15416–23. doi:10.1523/JNEUROSCI.2002-11.2011.
- Feurra, M., Bianco, G., Santarnecchi, E., Del Testa, M., Rossi, A., and Rossi, S. (2011a). Frequency-dependent tuning of the human motor system induced by transcranial oscillatory potentials. *J. Neurosci.* 31, 12165–70. doi:10.1523/JNEUROSCI.0978-11.2011.
- Feurra, M., Paulus, W., Walsh, V., and Kanai, R. (2011b). Frequency specific modulation of human somatosensory cortex. *Front. Psychol.* 2, 13. doi:10.3389/fpsyg.2011.00013.
- Filmer, H. L., Dux, P. E., and Mattingley, J. B. (2014). Applications of transcranial direct current stimulation for understanding brain function. *Trends Neurosci.* 37, 742–53. doi:10.1016/j.tins.2014.08.003.
- Foik, A. T., Kublik, E., Sergeeva, E. G., Tatlisumak, T., Rossini, P. M., Sabel, B. A., and Waleszczyk, W. J. (2015). Retinal origin of electrically evoked potentials in response to transcorneal alternating current stimulation in the rat. *Invest. Ophthalmol. Vis. Sci.* 56, 1711–8. doi:10.1167/iovs.14-15617.
- Francis, S., and Panchuelo, R. S. (2014). Physiological measurements using ultra-high field fMRI: a review. *Physiol. Meas.* 35, R167–85. doi:10.1088/0967-3334/35/9/R167.
- Friedman, L., Stern, H., Brown, G. G., Mathalon, D. H., Turner, J., Glover, G. H., Gollub, R. L., Lauriello, J., Lim, K. O., Cannon, T., et al. (2008). Test-retest and between-site reliability in a multicenter fMRI study. *Hum. Brain Mapp.* 29, 958–72. doi:10.1002/hbm.20440.
- Fröhlich, F., and McCormick, D. A. (2010). Endogenous electric fields may guide neocortical network activity. *Neuron* 67, 129–43. doi:10.1016/j.neuron.2010.06.005.

- Gall, C., Antal, A., and Sabel, B. A. (2013). Non-invasive electrical brain stimulation induces vision restoration in patients with visual pathway damage. *Graefes Arch. Clin. Exp. Ophthalmol.* 251, 1041–3. doi:10.1007/s00417-012-2084-7.
- Gall, C., Fedorov, A. B., Ernst, L., Borrmann, A., and Sabel, B. A. (2010a). Repetitive transorbital alternating current stimulation in optic neuropathy. IOS Press doi:10.3233/NRE-2010-0617.
- Gall, C., Franke, G. H., and Sabel, B. A. (2010b). Vision-related quality of life in first stroke patients with homonymous visual field defects. *Health Qual. Life Outcomes* 8, 33. Available at: <http://www.pubmedcentral.nih.gov/articlerender.fcgi?artid=2859371&tool=pmcentrez&rendertype=abstract>.
- Gall, C., Lucklum, J., Sabel, B. A., and Franke, G. H. (2009). Vision- and health-related quality of life in patients with visual field loss after postchiasmatic lesions. *Invest. Ophthalmol. Vis. Sci.* 50, 2765–2776. doi:10.1167/iovs.08-2519.
- Gall, C., Sgorzaly, S., Schmidt, S., Brandt, S., Fedorov, A., and Sabel, B. A. (2011). Noninvasive transorbital alternating current stimulation improves subjective visual functioning and vision-related quality of life in optic neuropathy. *Brain Stimul.* 4, 175–88. doi:10.1016/j.brs.2011.07.003.
- Gall, C., Silvennoinen, K., Granata, G., de Rossi, F., Vecchio, F., Brösel, D., Bola, M., Sailer, M., Waleszczyk, W. J., Rossini, P. M., et al. (2015). Non-invasive electric current stimulation for restoration of vision after unilateral occipital stroke. *Contemp. Clin. Trials* 43, 231–236. doi:10.1016/j.cct.2015.06.005.
- Garavan, H., Kelley, D., Rosen, A., Rao, S. M., and Stein, E. A. (2000). Practice-related functional activation changes in a working memory task. *Microsc. Res. Tech.* 51, 54–63. doi:10.1002/1097-0029(20001001)51:1<54::AID-JEMT6>3.0.CO;2-J.
- Goebel, R., Muckli, L., and Kim, D.-S. (2004). “Visual system,” in *The human nervous system*, eds. J. K. Mai and G. Paxinos (Elsevier Inc.: Academic Press), 1280–1304.
- Greenlee, M. W., and Tse, P. U. (2008). “Functional neuroanatomy of the human visual system: A review of functional MRI studies,” in *Essential in Ophthalmology: Pediatric Ophthalmology, Neuro-Ophthalmology, Genetics*, eds. B. Lorenz and F.-X. Borruat (Leipzig: Springer), 119–138.
- Gröger, A., Kolb, R., Schäfer, R., and Klose, U. (2014). Dopamine reduction in the substantia nigra of Parkinson’s disease patients confirmed by in vivo magnetic resonance spectroscopic imaging. *PLoS One* 9, e84081. doi:10.1371/journal.pone.0084081.
- Grunda, T., Marsalek, P., and Sykorova, P. (2013). Homonymous hemianopia and related visual defects: Restoration of vision after a stroke. *Acta Neurobiol. Exp. (Wars)*. 73, 237–49. Available at: <http://www.ncbi.nlm.nih.gov/pubmed/23823985> [Accessed November 12, 2014].
- Guillery, R. W., Hickey, T. L., Kaas, J. H., Felleman, D. J., Debruyn, E. J., and Sparks, D. L. (1984). Abnormal central visual pathways in the brain of an albino green monkey (*Cercopithecus aethiops*). *J. Comp. Neurol.* 226, 165–83. doi:10.1002/cne.902260203.
- Hadjikhani, N., Joseph, R. M., Snyder, J., Chabris, C. F., Clark, J., Steele, S., McGrath, L.,

- Vangel, M., Aharon, I., Feczko, E., et al. (2004). Activation of the fusiform gyrus when individuals with autism spectrum disorder view faces. *Neuroimage* 22, 1141–50. doi:10.1016/j.neuroimage.2004.03.025.
- Hagler, D. J., Riecke, L., and Sereno, M. I. (2007). Parietal and superior frontal visuospatial maps activated by pointing and saccades. *Neuroimage* 35, 1562–77. doi:10.1016/j.neuroimage.2007.01.033.
- Halko, M. A., Datta, A., Plow, E. B., Scaturro, J., Bikson, M., and Merabet, L. B. (2011). Neuroplastic changes following rehabilitative training correlate with regional electrical field induced with tDCS. *Neuroimage* 57, 885–91. doi:10.1016/j.neuroimage.2011.05.026.
- Hamilton, R. H., Chrysikou, E. G., and Coslett, B. (2011). Mechanisms of aphasia recovery after stroke and the role of noninvasive brain stimulation. *Brain Lang.* 118, 40–50. doi:10.1016/j.bandl.2011.02.005.
- Heijl, A., Lindgren, G., and Olsson, J. (1989). The effect of perimetric experience in normal subjects. *Arch. Ophthalmol.* 107, 81–6. doi:10.1001/archophth.1989.01070010083032.
- Helfrich, R. F., Schneider, T. R., Rach, S., Trautmann-Lengsfeld, S. A., Engel, A. K., and Herrmann, C. S. (2014). Entrainment of brain oscillations by transcranial alternating current stimulation. *Curr. Biol.* 24, 333–9. doi:10.1016/j.cub.2013.12.041.
- Henschen, S. E. (1893). ON THE VISUAL PATH AND CENTRE. *Brain* 16, 170–180. doi:10.1093/brain/16.1-2.170.
- Herrmann, C. S., Rach, S., Neuling, T., and Strüber, D. (2013). Transcranial alternating current stimulation: a review of the underlying mechanisms and modulation of cognitive processes. *Front. Hum. Neurosci.* 7, 279. doi:10.3389/fnhum.2013.00279.
- Hill, R. W., and Wyse, G. A. (2012). *Animal Physiology*. 3rd ed. Sunderland, Massachusetts U.S.A: Sinauer Associates Available at: sites.sinauer.com/animalphys3e.
- Hoffmann, M. B., Kaule, F. R., Levin, N., Masuda, Y., Kumar, A., Gottlob, I., Horiguchi, H., Dougherty, R. F., Stadler, J., Wolynski, B., et al. (2012a). Plasticity and stability of the visual system in human achiasma. *Neuron* 75, 393–401. doi:10.1016/j.neuron.2012.05.026.
- Hoffmann, M. B., Kaule, F. R., Levin, N., Masuda, Y., Kumar, A., Gottlob, I., Horiguchi, H., Dougherty, R. F., Stadler, J., Wolynski, B., et al. (2012b). Plasticity and stability of the visual system in human achiasma. *Neuron* 75, 393–401. doi:10.1016/j.neuron.2012.05.026.
- Hoffmann, M. B., Stadler, J., Kanowski, M., and Speck, O. (2009). Retinotopic mapping of the human visual cortex at a magnetic field strength of 7T. *Clin. Neurophysiol.* 120, 108–16. doi:10.1016/j.clinph.2008.10.153.
- Hoffmann, M. B., Tolhurst, D. J., Moore, A. T., and Morland, A. B. (2003). Organization of the Visual Cortex in Human Albinism. *J. Neurosci.* 23, 8921–8930. Available at: <http://www.jneurosci.org/content/23/26/8921.full> [Accessed July 12, 2015].
- Holland, R., Leff, A. P., Josephs, O., Galea, J. M., Desikan, M., Price, C. J., Rothwell, J. C., and Crinion, J. (2011). Speech facilitation by left inferior frontal cortex stimulation. *Curr. Biol.* 21, 1403–7. doi:10.1016/j.cub.2011.07.021.
- Holmes, G. (1918). DISTURBANCES OF VISION BY CEREBRAL LESIONS. *Br. J. Ophthalmol.* 2, 353–84. Available at:



- <http://www.pubmedcentral.nih.gov/articlerender.fcgi?artid=513514&tool=pmcentrez&rendertype=abstract> [Accessed June 27, 2015].
- Hubel, D. H., and Wiesel, T. N. (1979). Brain mechanisms of vision. *Sci. Am.* 241, 150–162. doi:10.1038/scientificamerican0979-150.
- Hubel, D. H., and Wiesel, T. N. (1972). Laminar and columnar distribution of geniculo-cortical fibers in the macaque monkey. *J. Comp. Neurol.* 146, 421–50. doi:10.1002/cne.901460402.
- Hubel, D. H., and Wiesel, T. N. (1962). Receptive fields, binocular interaction and functional architecture in the cat's visual cortex. *J. Physiol.* 160, 106–54. Available at: <http://www.pubmedcentral.nih.gov/articlerender.fcgi?artid=1359523&tool=pmcentrez&rendertype=abstract> [Accessed December 15, 2014].
- Huettel, S. A., Song, A. W., and McCarthy, G. (2008). *Functional Magnetic Resonance Imaging: Data Acquisition and Analysis | Health Sciences and Technology | MIT OpenCourseWare*. 2nd ed. Sinauer Associates, Sunderland Massachusetts U.S.A Available at: <http://ocw.mit.edu/courses/health-sciences-and-technology/hst-583-functional-magnetic-resonance-imaging-data-acquisition-and-analysis-fall-2008/readings/> [Accessed October 7, 2014].
- Huk, A. C., Dougherty, R. F., and Heeger, D. J. (2002). Retinotopy and Functional Subdivision of Human Areas MT and MST. *J. Neurosci.* 22, 7195–7205. Available at: <http://www.jneurosci.org/content/22/16/7195.full> [Accessed July 12, 2015].
- Ilango, A., Kesner, A. J., Keller, K. L., Stuber, G. D., Bonci, A., and Ikemoto, S. (2014). Similar roles of substantia nigra and ventral tegmental dopamine neurons in reward and aversion. *J. Neurosci.* 34, 817–22. doi:10.1523/JNEUROSCI.1703-13.2014.
- In, M.-H., Posnansky, O., and Speck, O. (2015). PSF mapping-based correction of eddy-current-induced distortions in diffusion-weighted echo-planar imaging. *Magn. Reson. Med.* doi:10.1002/mrm.25746.
- In, M.-H., and Speck, O. (2012). Highly accelerated PSF-mapping for EPI distortion correction with improved fidelity. *MAGMA* 25, 183–92. doi:10.1007/s10334-011-0275-6.
- Jensen, J. L., Marstrand, P. C. D., and Nielsen, J. B. (2005). Motor skill training and strength training are associated with different plastic changes in the central nervous system. *J. Appl. Physiol.* 99, 1558–68. doi:10.1152/jappphysiol.01408.2004.
- Johnstone, T., Somerville, L. H., Alexander, A. L., Oakes, T. R., Davidson, R. J., Kalin, N. H., and Whalen, P. J. (2005). Stability of amygdala BOLD response to fearful faces over multiple scan sessions. *Neuroimage* 25, 1112–23. doi:10.1016/j.neuroimage.2004.12.016.
- Joundi, R. A., Jenkinson, N., Brittain, J.-S., Aziz, T. Z., and Brown, P. (2012). Driving oscillatory activity in the human cortex enhances motor performance. *Curr. Biol.* 22, 403–7. doi:10.1016/j.cub.2012.01.024.
- Kanai, R., Chaieb, L., Antal, A., Walsh, V., and Paulus, W. (2008). Frequency-dependent electrical stimulation of the visual cortex. *Curr. Biol.* 18, 1839–43. doi:10.1016/j.cub.2008.10.027.
- Kanai, R., Paulus, W., and Walsh, V. (2010). Transcranial alternating current stimulation (tACS) modulates cortical excitability as assessed by TMS-induced phosphene thresholds. *Clin. Neurophysiol.* 121, 1551–1554. Available at: <http://discovery.ucl.ac.uk/120681/>.

- Kanowski, M., Rieger, J. W., Noesselt, T., Tempelmann, C., and Hinrichs, H. (2007a). Endoscopic eye tracking system for fMRI. *J. Neurosci. Methods* 160, 10–5. doi:10.1016/j.jneumeth.2006.08.001.
- Kanowski, M., Rieger, J. W., Noesselt, T., Tempelmann, C., and Hinrichs, H. (2007b). Endoscopic eye tracking system for fMRI. *J. Neurosci. Methods* 160, 10–5. doi:10.1016/j.jneumeth.2006.08.001.
- Karabanov, A., Ziemann, U., Hamada, M., George, M. S., Quartarone, A., Classen, J., Massimini, M., Rothwell, J., and Siebner, H. R. (2015). Consensus Paper: Probing Homeostatic Plasticity of Human Cortex With Non-invasive Transcranial Brain Stimulation. *Brain Stimul.* 8, 442–454. doi:10.1016/j.brs.2015.01.404.
- Kasten, E., Bunzenthal, U., and Sabel, B. A. (2006). Visual field recovery after vision restoration therapy (VRT) is independent of eye movements: an eye tracker study. Available at: <http://www.ncbi.nlm.nih.gov/pubmed/16970999>.
- Kasten, E., Wüst, S., Behrens-Baumann, W., and Sabel, B. A. (1998). Computer-based training for the treatment of partial blindness. *Nat. Med.* 4, 1083–7. doi:10.1038/2079.
- Kelly, C., Foxe, J. J., and Garavan, H. (2006). Patterns of normal human brain plasticity after practice and their implications for neurorehabilitation. *Arch. Phys. Med. Rehabil.* 87, S20–9. doi:10.1016/j.apmr.2006.08.333.
- Ko, M.-H., Han, S.-H., Park, S.-H., Seo, J.-H., and Kim, Y.-H. (2008). Improvement of visual scanning after DC brain polarization of parietal cortex in stroke patients with spatial neglect. *Neurosci. Lett.* 448, 171–4. doi:10.1016/j.neulet.2008.10.050.
- Kong, J., Gollub, R. L., Webb, J. M., Kong, J.-T., Vangel, M. G., and Kwong, K. (2007). Test-retest study of fMRI signal change evoked by electroacupuncture stimulation. *Neuroimage* 34, 1171–81. doi:10.1016/j.neuroimage.2006.10.019.
- Kourtidou, P., Kasselimis, D., Potagas, C., Zalonis, I., and Evdokimidis, I. (2015). Effects of Mental Flexibility and Motor Dysfunction on Cognitive Performance in Patients With Parkinson’s Disease. *Arch. Neurosci.* 2. doi:10.5812/archneurosci.21087.
- Kraft, A., Roehmel, J., Olma, M. C., Schmidt, S., Irlbacher, K., and Brandt, S. A. (2010). Transcranial direct current stimulation affects visual perception measured by threshold perimetry. *Exp. brain Res.* 207, 283–90. doi:10.1007/s00221-010-2453-6.
- Krause, V., Wach, C., Südmeyer, M., Ferrea, S., Schnitzler, A., and Pollok, B. (2013). Cortico-muscular coupling and motor performance are modulated by 20 Hz transcranial alternating current stimulation (tACS) in Parkinson’s disease. *Front. Hum. Neurosci.* 7, 928. doi:10.3389/fnhum.2013.00928.
- Krüger, G., and Glover, G. H. (2001). Physiological noise in oxygenation-sensitive magnetic resonance imaging. *Magn. Reson. Med.* 46, 631–7. Available at: <http://www.ncbi.nlm.nih.gov/pubmed/11590638> [Accessed October 7, 2014].
- Kuffler, S. W. (1953). DISCHARGE PATTERNS AND FUNCTIONAL ORGANIZATION OF MAMMALIAN RETINA. *J Neurophysiol* 16, 37–68. Available at: <http://jn.physiology.org/content/16/1/37> [Accessed July 12, 2015].
- Kwong, K. K., Belliveau, J. W., Chesler, D. A., Goldberg, I. E., Weisskoff, R. M., Poncelet, B. P., Kennedy, D. N., Hoppel, B. E., Cohen, M. S., and Turner, R. (1992). Dynamic magnetic

- resonance imaging of human brain activity during primary sensory stimulation. *Proc. Natl. Acad. Sci. U. S. A.* 89, 5675–9. Available at: [http://www.pubmedcentral.nih.gov/articlerender.fcgi?artid=49355&tool=pmcentrez&render\\_type=abstract](http://www.pubmedcentral.nih.gov/articlerender.fcgi?artid=49355&tool=pmcentrez&render_type=abstract) [Accessed May 20, 2015].
- Larsson, J., and Heeger, D. J. (2006). Two retinotopic visual areas in human lateral occipital cortex. *J. Neurosci.* 26, 13128–42. doi:10.1523/JNEUROSCI.1657-06.2006.
- Lesica, N. A., Jin, J., Weng, C., Yeh, C.-I., Butts, D. A., Stanley, G. B., and Alonso, J.-M. (2007). Adaptation to stimulus contrast and correlations during natural visual stimulation. *Neuron* 55, 479–91. doi:10.1016/j.neuron.2007.07.013.
- Liebetanz, D., Koch, R., Mayenfels, S., König, F., Paulus, W., and Nitsche, M. A. (2009). Safety limits of cathodal transcranial direct current stimulation in rats. *Clin. Neurophysiol.* 120, 1161–1167. doi:10.1016/j.clinph.2009.01.022.
- Lister, W. T., and Holmes, G. (1916). Disturbances of Vision from Cerebral Lesions, with Special Reference to the Cortical Representation of the Macula. *Proc. R. Soc. Med.* 9, 57–96. Available at: <http://www.pubmedcentral.nih.gov/articlerender.fcgi?artid=2017232&tool=pmcentrez&rendertype=abstract> [Accessed July 12, 2015].
- Liu, A., Devinsky, O., Bryant, A., Jefferson, A., Friedman, D., Shafi, M., Barr, W., Press, D., Herman, S., O'Connor, M., et al. (2014). Efficacy of Transcranial Direct Current Stimulation on Working Memory and Mood in Patients with Temporal Lobe Epilepsy (S43.006). *Neurology* 82, S43.006–. Available at: [http://www.neurology.org/content/82/10\\_Supplement/S43.006.short](http://www.neurology.org/content/82/10_Supplement/S43.006.short) [Accessed August 25, 2015].
- Livingstone, M. S., and Hubel, D. H. (1984). Anatomy and physiology of a color system in the primate visual cortex. *J. Neurosci.* 4, 309–56. Available at: <http://www.ncbi.nlm.nih.gov/pubmed/6198495> [Accessed June 17, 2015].
- Lund, J. S. (1988). Anatomical organization of macaque monkey striate visual cortex. *Annu. Rev. Neurosci.* 11, 253–88. doi:10.1146/annurev.ne.11.030188.001345.
- Lustenberger, C., Boyle, M. R., Foulser, A. A., Mellin, J. M., and Fröhlich, F. (2015). Functional role of frontal alpha oscillations in creativity. *Cortex* 67, 74–82. doi:10.1016/j.cortex.2015.03.012.
- Maitra, R., Roys, S. R., and Gullapalli, R. P. (2002). Test-retest reliability estimation of functional MRI data. *Magn. Reson. Med.* 48, 62–70. doi:10.1002/mrm.10191.
- Mang, C. S., Campbell, K. L., Ross, C. J. D., and Boyd, L. A. (2013). Promoting neuroplasticity for motor rehabilitation after stroke: considering the effects of aerobic exercise and genetic variation on brain-derived neurotrophic factor. *Phys. Ther.* 93, 1707–16. doi:10.2522/ptj.20130053.
- Martin, P. R. (1998). Colour processing in the primate retina: recent progress. *J. Physiol.* 513 ( Pt 3, 631–8. Available at: <http://www.pubmedcentral.nih.gov/articlerender.fcgi?artid=2231327&tool=pmcentrez&rendertype=abstract> [Accessed July 12, 2015].
- Meinzer, M., Lindenberg, R., Darkow, R., Ulm, L., Copland, D., and Flöel, A. (2014).

- Transcranial direct current stimulation and simultaneous functional magnetic resonance imaging. *J. Vis. Exp.* doi:10.3791/51730.
- Miller, J., Berger, B., and Sauseng, P. (2015). Anodal transcranial direct current stimulation (tDCS) increases frontal–midline theta activity in the human EEG: A preliminary investigation of non-invasive stimulation. *Neurosci. Lett.* 588, 114–119. doi:10.1016/j.neulet.2015.01.014.
- Milner, D., and Goodale, M. (2006). *The Visual Brain in Action (Oxford Psychology Series)*. 2nd ed. New York: Oxford University Press.
- Miniussi, C., Harris, J. A., and Ruzzoli, M. (2013). Modelling non-invasive brain stimulation in cognitive neuroscience. *Neurosci. Biobehav. Rev.* 37, 1702–1712. doi:10.1016/j.neubiorev.2013.06.014.
- Moliadze, V., Antal, A., and Paulus, W. (2010). Boosting brain excitability by transcranial high frequency stimulation in the ripple range. *J. Physiol.* 588, 4891–904. doi:10.1113/jphysiol.2010.196998.
- De Monasterio, F. M., and Gouras, P. (1975). Functional properties of ganglion cells of the rhesus monkey retina. *J. Physiol.* 251, 167–95. Available at: <http://www.pubmedcentral.nih.gov/articlerender.fcgi?artid=1348381&tool=pmcentrez&rendertype=abstract> [Accessed July 12, 2015].
- Van de Moortele, P.-F., Auerbach, E. J., Olman, C., Yacoub, E., Uğurbil, K., and Moeller, S. (2009). T1 weighted brain images at 7 Tesla unbiased for Proton Density, T2\* contrast and RF coil receive B1 sensitivity with simultaneous vessel visualization. *Neuroimage* 46, 432–46. doi:10.1016/j.neuroimage.2009.02.009.
- Morgan, P. S., Bowtell, R. W., McIntyre, D. J. O., and Worthington, B. S. (2004). Correction of spatial distortion in EPI due to inhomogeneous static magnetic fields using the reversed gradient method. *J. Magn. Reson. Imaging* 19, 499–507. doi:10.1002/jmri.20032.
- Morland, A. B., Baseler, H. A., Hoffmann, M. B., Sharpe, L. T., and Wandell, B. A. (2001). Abnormal retinotopic representations in human visual cortex revealed by fMRI. *Acta Psychol. (Amst)*. 107, 229–47. Available at: <http://www.ncbi.nlm.nih.gov/pubmed/11388137> [Accessed July 12, 2015].
- Moseley, M. E., and Glover, G. H. (1995). Functional MR imaging. Capabilities and limitations. *Neuroimaging Clin. N. Am.* 5, 161–91. Available at: <http://www.ncbi.nlm.nih.gov/pubmed/7640883> [Accessed July 13, 2015].
- Mueller, I., Mast, H., and Sabel, B. A. (2007). Recovery of visual field defects: A large clinical observational study using vision restoration therapy. *Restor. Neurol. Neurosci.* 25, 563–572. Available at: <http://content.iospress.com/articles/restorative-neurology-and-neuroscience/rnn00412?resultNumber=0&totalResults=421&start=0&q=Recovery+of+visual+field+defects%3A+a+large+clinical+observational+study+using+vision+restoration+therapy&resultsPageSize=10&rows=10> [Accessed September 2, 2015].
- Musso, M. (1999). Training-induced brain plasticity in aphasia. *Brain* 122, 1781–1790. doi:10.1093/brain/122.9.1781.
- Nardone, R., Höller, Y., Leis, S., Höller, P., Thon, N., Thomschewski, A., Golaszewski, S., Brigo, F., and Trinka, E. (2014). Invasive and non-invasive brain stimulation for treatment

- of neuropathic pain in patients with spinal cord injury: a review. *J. Spinal Cord Med.* 37, 19–31. doi:10.1179/2045772313Y.0000000140.
- Neuling, T., Rach, S., and Herrmann, C. S. (2013). Orchestrating neuronal networks: sustained after-effects of transcranial alternating current stimulation depend upon brain states. *Front. Hum. Neurosci.* 7, 161. doi:10.3389/fnhum.2013.00161.
- Nitsche, M. a, Cohen, L. G., Wassermann, E. M., Priori, A., Lang, N., Antal, A., Paulus, W., Hummel, F., Boggio, P. S., Fregni, F., et al. (2008). Transcranial direct current stimulation: State of the art 2008. *Brain Stimul.* 1, 206–23. doi:10.1016/j.brs.2008.06.004.
- Nitsche, M. A., Liebetanz, D., Lang, N., Antal, A., Tergau, F., and Paulus, W. (2003). Safety criteria for transcranial direct current stimulation (tDCS) in humans. *Clin. Neurophysiol.* 114, 2220–2; author reply 2222–3. Available at: <http://www.ncbi.nlm.nih.gov/pubmed/14580622> [Accessed November 7, 2014].
- Nitsche, M. A., and Paulus, W. (2000). Excitability changes induced in the human motor cortex by weak transcranial direct current stimulation. *J. Physiol.* 527 Pt 3, 633–9. doi:10.1111/j.1469-7793.2000.t01-1-00633.x.
- Nizard, J., Raoul, S., Nguyen, J.-P., and Lefaucheur, J.-P. (2012). Invasive stimulation therapies for the treatment of refractory pain. *Discov. Med.* 14, 237–46. Available at: <http://www.ncbi.nlm.nih.gov/pubmed/23114579> [Accessed November 7, 2014].
- Ogawa, S., and Lee, T. M. (1990). Magnetic resonance imaging of blood vessels at high fields: in vivo and in vitro measurements and image simulation. *Magn. Reson. Med.* 16, 9–18. Available at: <http://www.ncbi.nlm.nih.gov/pubmed/2255240> [Accessed July 13, 2015].
- Ogawa, S., Lee, T. M., Kay, A. R., and Tank, D. W. (1990a). Brain magnetic resonance imaging with contrast dependent on blood oxygenation. *Proc. Natl. Acad. Sci. U. S. A.* 87, 9868–72. Available at: [http://www.pubmedcentral.nih.gov/articlerender.fcgi?artid=55275&tool=pmcentrez&render\\_type=abstract](http://www.pubmedcentral.nih.gov/articlerender.fcgi?artid=55275&tool=pmcentrez&render_type=abstract) [Accessed April 10, 2015].
- Ogawa, S., Lee, T. M., Nayak, A. S., and Glynn, P. (1990b). Oxygenation-sensitive contrast in magnetic resonance image of rodent brain at high magnetic fields. *Magn. Reson. Med.* 14, 68–78. Available at: <http://www.ncbi.nlm.nih.gov/pubmed/2161986> [Accessed July 13, 2015].
- Ogawa, S., Tank, D. W., Menon, R., Ellermann, J. M., Kim, S. G., Merkle, H., and Ugurbil, K. (1992). Intrinsic signal changes accompanying sensory stimulation: functional brain mapping with magnetic resonance imaging. *Proc. Natl. Acad. Sci. U. S. A.* 89, 5951–5. Available at: <http://www.pubmedcentral.nih.gov/articlerender.fcgi?artid=402116&tool=pmcentrez&rendertype=abstract> [Accessed July 12, 2015].
- Oliveri, M., Rossini, P. M., Traversa, R., Cicinelli, P., Filippi, M. M., Pasqualetti, P., Tomaiuolo, F., and Caltagirone, C. (1999). Left frontal transcranial magnetic stimulation reduces contralesional extinction in patients with unilateral right brain damage. *Brain* 122, 1731–9. doi:10.1093/brain/122.9.1731.
- Ozen, S., Sirota, A., Belluscio, M. A., Anastassiou, C. A., Stark, E., Koch, C., and Buzsáki, G. (2010). Transcranial electric stimulation entrains cortical neuronal populations in rats. *J.*

- Neurosci.* 30, 11476–85. doi:10.1523/JNEUROSCI.5252-09.2010.
- Paulus, W. (2010). On the difficulties of separating retinal from cortical origins of phosphenes when using transcranial alternating current stimulation (tACS). *Clin. Neurophysiol.* 121, 987–91. doi:10.1016/j.clinph.2010.01.029.
- Pereira, J. B., Junqué, C., Bartrés-Faz, D., Martí, M. J., Sala-Llloch, R., Compta, Y., Falcón, C., Vendrell, P., Pascual-Leone, A., Valls-Solé, J., et al. (2013). Modulation of verbal fluency networks by transcranial direct current stimulation (tDCS) in Parkinson's disease. *Brain Stimul.* 6, 16–24. doi:10.1016/j.brs.2012.01.006.
- Perrey, S. (2013). Promoting motor function by exercising the brain. *Brain Sci.* 3, 101–22. doi:10.3390/brainsci3010101.
- Philipp, B. (2009). CircStat: A MATLAB Toolbox for Circular Statistics. *J. Stat. Softw.* 31, 1–22. Available at: <http://www.jstatsoft.org/v31/i10> [Accessed December 17, 2014].
- Pinel, J. P. J. (2011). *Biopsychology*. 8th ed. Boston: Allyn and Bacon.
- Pitzalis, S., Galletti, C., Huang, R.-S., Patria, F., Committeri, G., Galati, G., Fattori, P., and Sereno, M. I. (2006). Wide-field retinotopy defines human cortical visual area v6. *J. Neurosci.* 26, 7962–73. doi:10.1523/JNEUROSCI.0178-06.2006.
- Pleger, B., Foerster, A.-F., Widdig, W., Henschel, M., Nicolas, V., Jansen, A., Frank, A., Knecht, S., Schwenkreis, P., and Tegenthoff, M. (2003). Functional magnetic resonance imaging mirrors recovery of visual perception after repetitive tachistoscopic stimulation in patients with partial cortical blindness. *Neurosci. Lett.* 335, 192–196. doi:10.1016/S0304-3940(02)01153-9.
- Plichta, M. M., Schwarz, A. J., Grimm, O., Morgen, K., Mier, D., Haddad, L., Gerdes, A. B. M., Sauer, C., Tost, H., Esslinger, C., et al. (2012). Test-retest reliability of evoked BOLD signals from a cognitive-emotive fMRI test battery. *Neuroimage* 60, 1746–58. doi:10.1016/j.neuroimage.2012.01.129.
- Plow, E. B., Obretenova, S. N., Halko, M. A., Kenkel, S., Jackson, M. Lou, Pascual-Leone, A., and Merabet, L. B. (2011). Combining visual rehabilitative training and noninvasive brain stimulation to enhance visual function in patients with hemianopia: a comparative case study. *PMR* 3, 825–35. doi:10.1016/j.pmrj.2011.05.026.
- Plow, E. B., Obretenova, S. N., Jackson, M. Lou, and Merabet, L. B. (2012). Temporal profile of functional visual rehabilitative outcomes modulated by transcranial direct current stimulation. *Neuromodulation* 15, 367–73. doi:10.1111/j.1525-1403.2012.00440.x.
- Poggel, D. A., Treutwein, B., and Strasburger, H. (2011). Time will tell: deficits of temporal information processing in patients with visual field loss. *Brain Res.* 1368, 196–207. doi:10.1016/j.brainres.2010.10.065.
- Pogosyan, A., Gaynor, L. D., Eusebio, A., and Brown, P. (2009). Boosting cortical activity at Beta-band frequencies slows movement in humans. *Curr. Biol.* 19, 1637–41. doi:10.1016/j.cub.2009.07.074.
- Polanía, R., Nitsche, M. A., Korman, C., Batsikadze, G., and Paulus, W. (2012a). The importance of timing in segregated theta phase-coupling for cognitive performance. *Curr. Biol.* 22, 1314–8. doi:10.1016/j.cub.2012.05.021.

- Polanía, R., Paulus, W., and Nitsche, M. A. (2012b). Reorganizing the intrinsic functional architecture of the human primary motor cortex during rest with non-invasive cortical stimulation. *PLoS One* 7, e30971. doi:10.1371/journal.pone.0030971.
- Poldrack, R. A. (2000). Imaging brain plasticity: conceptual and methodological issues--a theoretical review. *Neuroimage* 12, 1–13. doi:10.1006/nimg.2000.0596.
- Poreisz, C., Boros, K., Antal, A., and Paulus, W. (2007). Safety aspects of transcranial direct current stimulation concerning healthy subjects and patients. *Brain Res. Bull.* 72, 208–14. doi:10.1016/j.brainresbull.2007.01.004.
- Prasad, S., and Galetta, S. L. (2011). Anatomy and physiology of the afferent visual system. *Handb. Clin. Neurol.* 102, 3–19. doi:10.1016/B978-0-444-52903-9.00007-8.
- Purves, D., Augustine, G. J., Fitzpatrick, D., Hall, W. C., LaMantia, A.-S., and White, L. E. (2012). *Neuroscience*. 5th ed. Sunderland, Massachusetts U.S.A: Sinauer Associates.
- Raemaekers, M., Bergsma, D. P., van Wezel, R. J. a, van der Wildt, G. J., and van den Berg, a V (2011). Effects of vision restoration training on early visual cortex in patients with cerebral blindness investigated with functional magnetic resonance imaging. *J. Neurophysiol.* 105, 872–82. doi:10.1152/jn.00308.2010.
- Raemaekers, M., Vink, M., Zandbelt, B., van Wezel, R. J. A., Kahn, R. S., and Ramsey, N. F. (2007). Test-retest reliability of fMRI activation during prosaccades and antisaccades. *Neuroimage* 36, 532–42. doi:10.1016/j.neuroimage.2007.03.061.
- Reato, D., Rahman, A., Bikson, M., and Parra, L. C. (2013). Effects of weak transcranial alternating current stimulation on brain activity-a review of known mechanisms from animal studies. *Front. Hum. Neurosci.* 7, 687. doi:10.3389/fnhum.2013.00687.
- Reato, D., Rahman, A., Bikson, M., and Parra, L. C. (2010a). Low-intensity electrical stimulation affects network dynamics by modulating population rate and spike timing. *J. Neurosci.* 30, 15067–79. doi:10.1523/JNEUROSCI.2059-10.2010.
- Reato, D., Rahman, A., Bikson, M., and Parra, L. C. (2010b). Low-intensity electrical stimulation affects network dynamics by modulating population rate and spike timing. *J. Neurosci.* 30, 15067–79. doi:10.1523/JNEUROSCI.2059-10.2010.
- Reitsma, D. C., Mathis, J., Ulmer, J. L., Mueller, W., Maciejewski, M. J., and DeYoe, E. A. (2013a). Atypical retinotopic organization of visual cortex in patients with central brain damage: congenital and adult onset. *J. Neurosci.* 33, 13010–24. doi:10.1523/JNEUROSCI.0240-13.2013.
- Reitsma, D. C., Mathis, J., Ulmer, J. L., Mueller, W., Maciejewski, M. J., and DeYoe, E. A. (2013b). Atypical retinotopic organization of visual cortex in patients with central brain damage: congenital and adult onset. *J. Neurosci.* 33, 13010–24. doi:10.1523/JNEUROSCI.0240-13.2013.
- Rogde, K., Hagen, Å. M., Melby-Lervåg, M., Lervåg, A., Hagen, Å. M., Melby-Lervåg, M., and Lervåg, A. (2013). The Effect of Language Comprehension Training on Standardized Tests: A Systematic Review. Available at: <http://campbellcollaboration.org/lib/project/302/> [Accessed November 7, 2014].
- Romanska, A., Rezlescu, C., Susilo, T., Duchaine, B., and Banissy, M. J. (2015). High-Frequency Transcranial Random Noise Stimulation Enhances Perception of Facial Identity.

*Cereb. Cortex*, bhv016–. doi:10.1093/cercor/bhv016.

- Rosa, M. G. P., Tweedale, R., and Elston, G. N. (2000). Visual Responses of Neurons in the Middle Temporal Area of New World Monkeys after Lesions of Striate Cortex. *J. Neurosci.* 20, 5552–5563. Available at: <http://www.jneurosci.org/content/20/14/5552.short> [Accessed July 6, 2015].
- Sabel, B. A., Fedorov, A. B., Naue, N., Borrmann, A., Herrmann, C., and Gall, C. (2011a). Non-invasive alternating current stimulation improves vision in optic neuropathy. *Restor. Neurol. Neurosci.* 29, 493–505. doi:10.3233/RNN-2011-0624.
- Sabel, B. A., and Gudlin, J. (2014). Vision restoration training for glaucoma: a randomized clinical trial. *JAMA Ophthalmol.* 132, 381–9. doi:10.1001/jamaophthalmol.2013.7963.
- Sabel, B. A., Henrich-Noack, P., Fedorov, A., and Gall, C. (2011b). Vision restoration after brain and retina damage: the “residual vision activation theory”. *Prog. Brain Res.* 192, 199–262. doi:10.1016/B978-0-444-53355-5.00013-0.
- Sabel, B. A., and Kasten, E. (2000). Restoration of vision by training of residual functions. *Curr. Opin. Ophthalmol.* 11, 430–436. Available at: <http://www.ncbi.nlm.nih.gov/pubmed/12671238>.
- Santaracchi, E., Brem, A.-K., Levenbaum, E., Thompson, T., Kadosh, R. C., and Pascual-Leone, A. (2015). Enhancing cognition using transcranial electrical stimulation. *Curr. Opin. Behav. Sci.* 4, 171–178. doi:10.1016/j.cobeha.2015.06.003.
- Santaracchi, E., Polizzotto, N. R., Godone, M., Giovannelli, F., Feurra, M., Matzen, L., Rossi, A., and Rossi, S. (2013). Frequency-dependent enhancement of fluid intelligence induced by transcranial oscillatory potentials. *Curr. Biol.* 23, 1449–53. doi:10.1016/j.cub.2013.06.022.
- Savoy, R. L. (2005). Experimental design in brain activation MRI: cautionary tales. *Brain Res. Bull.* 67, 361–7. doi:10.1016/j.brainresbull.2005.06.008.
- Schluppeck, D., Glimcher, P., and Heeger, D. J. (2005). Topographic organization for delayed saccades in human posterior parietal cortex. *J. Neurophysiol.* 94, 1372–84. doi:10.1152/jn.01290.2004.
- Schmidt, S., Mante, A., Rönnefarth, M., Fleischmann, R., Gall, C., and Brandt, S. A. (2013). Progressive enhancement of alpha activity and visual function in patients with optic neuropathy: a two-week repeated session alternating current stimulation study. *Brain Stimul.* 6, 87–93. doi:10.1016/j.brs.2012.03.008.
- Schneider, K. A., and Kastner, S. (2005). Visual responses of the human superior colliculus: a high-resolution functional magnetic resonance imaging study. *J. Neurophysiol.* 94, 2491–503. doi:10.1152/jn.00288.2005.
- Schneider, K. A., Richter, M. C., and Kastner, S. (2004). Retinotopic organization and functional subdivisions of the human lateral geniculate nucleus: a high-resolution functional magnetic resonance imaging study. *J. Neurosci.* 24, 8975–85. doi:10.1523/JNEUROSCI.2413-04.2004.
- Schnitzler, A., and Gross, J. (2005). Normal and pathological oscillatory communication in the brain. *Nat. Rev. Neurosci.* 6, 285–96. doi:10.1038/nrn1650.



- Schutter, D. J. L. G., and Hortensius, R. (2011). Brain oscillations and frequency-dependent modulation of cortical excitability. *Brain Stimul.* 4, 97–103. doi:10.1016/j.brs.2010.07.002.
- Schutter, D. J. L. G., and Hortensius, R. (2010). Retinal origin of phosphenes to transcranial alternating current stimulation. *Clin. Neurophysiol.* 121, 1080–4. doi:10.1016/j.clinph.2009.10.038.
- Seibert, T. M., Majid, D. S. A., Aron, A. R., Corey-Bloom, J., and Brewer, J. B. (2012). Stability of resting fMRI interregional correlations analyzed in subject-native space: a one-year longitudinal study in healthy adults and premanifest Huntington’s disease. *Neuroimage* 59, 2452–63. doi:10.1016/j.neuroimage.2011.08.105.
- Sela, T., Kilim, A., and Lavidor, M. (2012). Transcranial alternating current stimulation increases risk-taking behavior in the balloon analog risk task. *Front. Neurosci.* 6, 22. doi:10.3389/fnins.2012.00022.
- Sereno, M. I., and Allmann, J. M. (1991). Cortical visual areas in mammals. Available at: <http://discovery.ucl.ac.uk/81499/> [Accessed July 12, 2015].
- Sereno, M. I., Dale, A. M., Reppas, J. B., Kwong, K. K., Belliveau, J. W., Brady, T. J., Rosen, B. R., and Tootell, R. B. (1995). Borders of multiple visual areas in humans revealed by functional magnetic resonance imaging. *Science* 268, 889–93. doi:10.1126/science.7754376.
- Sereno, M. I., McDonald, C. T., and Allman, J. M. (1994). Analysis of retinotopic maps in extrastriate cortex. *Cereb. Cortex* 4, 601–20. doi:10.1093/cercor/4.6.601.
- Sereno, M. I., Pitzalis, S., and Martinez, A. (2001). Mapping of contralateral space in retinotopic coordinates by a parietal cortical area in humans. *Science* (80- ). 294, 1350–1354. Available at: <http://www.ncbi.nlm.nih.gov/pubmed/11701930>.
- Sergeeva, E. G., Fedorov, A. B., Henrich-Noack, P., and Sabel, B. A. (2012). Transcorneal alternating current stimulation induces EEG “aftereffects” only in rats with an intact visual system but not after severe optic nerve damage. *J. Neurophysiol.* 108, 2494–500. doi:10.1152/jn.00341.2012.
- Shah, P. P., Szaflarski, J. P., Allendorfer, J., and Hamilton, R. H. (2013). Induction of neuroplasticity and recovery in post-stroke aphasia by non-invasive brain stimulation. *Front. Hum. Neurosci.* 7, 888. doi:10.3389/fnhum.2013.00888.
- Silver, M. A., Ress, D., and Heeger, D. J. (2005). Topographic maps of visual spatial attention in human parietal cortex. *J. Neurophysiol.* 94, 1358–71. doi:10.1152/jn.01316.2004.
- Sincich, L. C., and Horton, J. C. (2005). The circuitry of V1 and V2: integration of color, form, and motion. *Annu. Rev. Neurosci.* 28, 303–26. doi:10.1146/annurev.neuro.28.061604.135731.
- Slotnick, S. D., Moo, L. R., Krauss, G., and Hart, J. (2002). Large-scale cortical displacement of a human retinotopic map. *Neuroreport* 13, 41–6. Available at: <http://www.ncbi.nlm.nih.gov/pubmed/11924891> [Accessed July 12, 2015].
- Slotnick, S. D., and Yantis, S. (2003). Efficient acquisition of human retinotopic maps. *Hum. Brain Mapp.* 18, 22–9. doi:10.1002/hbm.10077.
- Smith, A. T., Greenlee, M. W., Singh, K. D., Kraemer, F. M., and Hennig, J. (1998). The

- Processing of First- and Second-Order Motion in Human Visual Cortex Assessed by Functional Magnetic Resonance Imaging (fMRI). *J. Neurosci.* 18, 3816–3830. Available at: <http://www.jneurosci.org/content/18/10/3816.long> [Accessed December 14, 2014].
- Sparing, R., Thimm, M., Hesse, M. D., Küst, J., Karbe, H., and Fink, G. R. (2009). Bidirectional alterations of interhemispheric parietal balance by non-invasive cortical stimulation. *Brain* 132, 3011–20. doi:10.1093/brain/awp154.
- Specht, K., Willmes, K., Shah, N. J., and Jäncke, L. (2003). Assessment of reliability in functional imaging studies. *J. Magn. Reson. Imaging* 17, 463–71. doi:10.1002/jmri.10277.
- Spector, R. H. (1990). “Visual Fields,” in *Clinical Methods: The History, Physical, and Laboratory Examinations.*, eds. H. K. Walker, W. D. Hall, and J. W. Hurst (Boston: Butterworths), 565–572.
- Starr, C., Evers, C. A., and Starr, L. (2006). *Biology: Concepts and Applications*. 6th ed. Thomson Brooks/Cole.
- Stuart, C. (1997). Functional MRI: Methods and Applications. Available at: <http://users.fmrib.ox.ac.uk/~stuart/thesis/>.
- Swisher, J. D., Halko, M. A., Merabet, L. B., McMains, S. A., and Somers, D. C. (2007a). Visual topography of human intraparietal sulcus. *J. Neurosci.* 27, 5326–37. doi:10.1523/JNEUROSCI.0991-07.2007.
- Swisher, J. D., Halko, M. A., Merabet, L. B., McMains, S. A., and Somers, D. C. (2007b). Visual topography of human intraparietal sulcus. *J. Neurosci.* 27, 5326–37. doi:10.1523/JNEUROSCI.0991-07.2007.
- Teller, D. Y. (2013). *Vision and the Visual System.*, ed. J. Palmer Available at: <http://faculty.washington.edu/jpalmer/files/Teller/ByChapter/>.
- Teo, P. C., Sapiro, G., and Wandell, B. A. (1997). Creating connected representations of cortical gray matter for functional MRI visualization. *IEEE Trans. Med. Imaging* 16, 852–63. doi:10.1109/42.650881.
- Terney, D., Chaieb, L., Moliadze, V., Antal, A., and Paulus, W. (2008). Increasing human brain excitability by transcranial high-frequency random noise stimulation. *J. Neurosci.* 28, 14147–55. doi:10.1523/JNEUROSCI.4248-08.2008.
- Vossen, A., Gross, J., and Thut, G. (2015). Alpha power increase after transcranial alternating current stimulation at alpha-frequency ( $\alpha$ -tACS) reflects plastic changes rather than entrainment. *Brain Stimul.* 8, 499–508. doi:10.1016/j.brs.2014.12.004.
- Wach, C., Krause, V., Moliadze, V., Paulus, W., Schnitzler, A., and Pollok, B. (2013). The effect of 10 Hz transcranial alternating current stimulation (tACS) on corticomuscular coherence. *Front. Hum. Neurosci.* 7, 511. doi:10.3389/fnhum.2013.00511.
- Wandell, B. A., Brewer, A. A., and Dougherty, R. F. (2005). Visual field map clusters in human cortex. *Philos. Trans. R. Soc. Lond. B. Biol. Sci.* 360, 693–707. doi:10.1098/rstb.2005.1628.
- Wandell, B. A., Chial, S., and Backus, B. T. (2000). Visualization and measurement of the cortical surface. *J. Cogn. Neurosci.* 12, 739–52. doi:10.1162/089892900562561.
- Wandell, B. A., Dumoulin, S. O., and Brewer, A. A. (2007). Visual field maps in human cortex. *Neuron* 56, 366–83. doi:10.1016/j.neuron.2007.10.012.

- Wandell, B. A., and Wade, A. R. (2003). Functional imaging of the visual pathways. *Neurol. Clin.* 21, 417–43, vi. Available at: <http://www.ncbi.nlm.nih.gov/pubmed/12916486> [Accessed July 12, 2015].
- Wandell, B. A., and Winawer, J. (2011). Imaging retinotopic maps in the human brain. *Vision Res.* 51, 718–37. doi:10.1016/j.visres.2010.08.004.
- Wang, H.-P., Spencer, D., Fellous, J.-M., and Sejnowski, T. J. (2010). Synchrony of thalamocortical inputs maximizes cortical reliability. *Science* 328, 106–9. doi:10.1126/science.1183108.
- Warnking, J., Dojat, M., Guérin-Dugué, A., Delon-Martin, C., Olympieff, S., Richard, N., Chéhikian, A., and Segebarth, C. (2002). fMRI retinotopic mapping--step by step. *Neuroimage* 17, 1665–83. Available at: <http://www.ncbi.nlm.nih.gov/pubmed/12498741> [Accessed May 29, 2015].
- Wilson-Pauwels, L., Stewart, P., Akesson, E. J., and Spacey, S. D. (2013). *Cranial nerves illustrated*. 3rd ed. Available at: <http://www.bmc.med.utoronto.ca/cranialnerves/>.
- Wirth, M., Rahman, R. A., Kuenecke, J., Koenig, T., Horn, H., Sommer, W., and Dierks, T. (2011). Effects of transcranial direct current stimulation (tDCS) on behaviour and electrophysiology of language production. *Neuropsychologia* 49, 3989–98. doi:10.1016/j.neuropsychologia.2011.10.015.
- Woldorff, M. G., Fox, P. T., Matzke, M., Lancaster, J. L., Veeraswamy, S., Zamarripa, F., Seabolt, M., Glass, T., Gao, J. H., Martin, C. C., et al. (1997). Retinotopic organization of early visual spatial attention effects as revealed by PET and ERPs. in *Human Brain Mapping*, 280–6. doi:10.1002/(SICI)1097-0193(1997)5:4<280::AID-HBM13>3.0.CO;2-I.
- World Medical Association Declaration of Helsinki: ethical principles for medical research involving human subjects. (2000). *JAMA* 284, 3043–5. Available at: <http://www.ncbi.nlm.nih.gov/pubmed/11122593> [Accessed October 17, 2014].
- Yamada, E. S., Bordt, A. S., and Marshak, D. W. (2005). Wide-field ganglion cells in macaque retinas. *Vis. Neurosci.* 22, 383–93. doi:10.1017/S095252380522401X.
- Zaehle, T., Rach, S., and Herrmann, C. S. (2010). Transcranial Alternating Current Stimulation Enhances Individual Alpha Activity in Human EEG. *PLoS One* 5, 7. Available at: <http://dx.plos.org/10.1371/journal.pone.0013766>.
- Zaghi, S., Acar, M., Hultgren, B., Boggio, P. S., and Fregni, F. (2010). Noninvasive brain stimulation with low-intensity electrical currents: putative mechanisms of action for direct and alternating current stimulation. *Neuroscientist* 16, 285–307. doi:10.1177/1073858409336227.
- Zandbelt, B. B., Gladwin, T. E., Raemaekers, M., van Buuren, M., Neggers, S. F., Kahn, R. S., Ramsey, N. F., and Vink, M. (2008). Within-subject variation in BOLD-fMRI signal changes across repeated measurements: quantification and implications for sample size. *Neuroimage* 42, 196–206. doi:10.1016/j.neuroimage.2008.04.183.
- Zeki, S., and Bartels, A. (1998). The asynchrony of consciousness. *Proc. R. Soc. B Biol. Sci.* 265, 1583–1585. doi:10.1098/rspb.1998.0475.
- Zeki, S., and Bartels, A. (1999). Toward a theory of visual consciousness. *Conscious. Cogn.* 8, 225–59. doi:10.1006/ccog.1999.0390.

- Zeki, S., and Shipp, S. (1988). The functional logic of cortical connections. *Nature* 335, 311–7. doi:10.1038/335311a0.
- Zeng, H., and Constable, R. T. (2002). Image distortion correction in EPI: comparison of field mapping with point spread function mapping. *Magn. Reson. Med.* 48, 137–46. doi:10.1002/mrm.10200.
- Zhang, X., Kedar, S., Lynn, M. J., Newman, N. J., and Biouesse, V. (2006). Natural history of homonymous hemianopia. *Neurology* 66, 901–905. doi:10.1212/01.wnl.0000203338.54323.22.

# SELBSTÄNDIGKEITSERKLÄRUNG

Hiermit erkläre ich, dass ich die von mir eingereichte Dissertation zum dem Thema

## **“Modulations of Visual Cortex Organization Investigated with 7 Tesla fMRI”**

selbständig verfasst, nicht schon als Dissertation verwendet habe und die benutzten Hilfsmittel und Quellen vollständig angegeben wurden.

Weiterhin erkläre ich, dass ich weder diese noch eine andere Arbeit zur Erlangung des akademischen Grades doctor rerum naturalium (Dr. rer. nat.) an anderen Einrichtungen eingereicht habe.

Magdeburg, 29. September 2015  
Aini Ismafairus Binti Abd Hamid

# CURRICULUM VITAE

AINI ISMAFAIRUS BINTI ABD HAMID

M.HSc

## PERSONAL DETAILS

**Date of Birth:** 17. October 1985

**Nationality:** Malaysia

**Address:** Universitätsplatz 1/608  
39106 Magdeburg

**Email:** isma.abdhamid@ovgu.de, aini\_ismafairus@yahoo.com.my

## EDUCATION

**Otto-von-Guericke Universität Magdeburg**, Magdeburg, Germany, 2012-present  
Doctoral candidate in the Faculty of Natural Sciences

**Universiti Kebangsaan Malaysia**, Kuala Lumpur, Malaysia, 2009-2011  
Master of Health Science (Biomedical Science)

**Universiti Sains Malaysia**, Penang, Malaysia, 2004-2007  
Bachelor of Applied Sciences (Hons) in Medical Physics (2007)

## RESEARCH EXPERIENCE

**Department of Biomedical Resonance Imaging**, Institute for Experimental Physics, Otto-von-Guericke Universität Magdeburg, Magdeburg, Germany, 2012-2015

Doctoral student

*“Retinotopic Mapping with high resolution 7 Tesla fMRI”*

**Functional Image Processing Lab**, Diagnostic Imaging and Radiotherapy Program, School of Diagnostic and Allied Health Science, Faculty of Health Sciences, Universiti Kebangsaan Malaysia, Kuala Lumpur, Malaysia, 2008-2011

Research assistant, Master’s degree research project

*“Brain activation during addition and subtraction task in-noise and in-quiet”*,

*“Brain activation in motor cortex during finger tapping task”*

Advisor: Associates Professor Dr. Ahmad Nazlim Yusoff, Professor Dr. Siti Zamratol-Mai Sarah Mukari

**Health Outcome Research Division**, Institute for Health Systems Research, Kuala Lumpur, Malaysia, 2007- 2008

Assistant Research Officer

*“Improving patients and health system outcomes”*

Advisor: Dr. Sondi Sararaks, Dr. Lim Wei-Yin

**School of Physics**, Universiti Sains Malaysia, Penang, Malaysia, 2006-2007

Bachelor’s degree research project

*“Study in bone orientation and filter types on x-ray image magnification”.*

Advisor: Professor Dr. Suhaimi Jaafar

## PUBLICATIONS

\***Aini Ismafairus Abd Hamid**, Oliver Speck, Michael B. Hoffmann. 2015. Quantitative assessment of visual cortex function with fMRI at 7 Tesla – test-retest reliability. *Front. Hum. Neurosci.* 9.

\***Aini Ismafairus Abd Hamid**, Carolin Gall, Oliver Speck, Andrea Antal, and Bernhard Sabel. 2015. Effects of alternating current stimulation on the healthy and diseased brain. *Front. Neurosci.* 9, 391.

Ahmad Nazlim Yusoff, Ng Sok Bee, Teng Xin Ling, **Aini Ismafairus Abd Hamid**. 2014. Investigating Brain Activation and Neural Efficacy during Simple Arithmetic Addition Task in Quiet and in Noise: An fMRI Study. *Malaysian Journal of Health Science.* 12(1):23-33.

Mazlyfarina Mohamad, Ahmad Nazlim Yusoff, Siti-Zamratol Maisarah Mukari, A. Abdullah, **Aini Ismafairus Abd Hamid**. 2014. The effects of background noise on brain activation during a verbal working memory task. *Malaysian Journal of Medical Health Sciences.* 10(1): 29-38.

Khairiah Abdul Hamid, Ahmad Nazlim Yusoff, Siti-Zamratol Maisarah Mukari, Mazlyfarina Mohamad, **Aini Ismafairus Abd Hamid**. 2012. Effective connectivity between superior temporal gyrus and Heschl's gyrus during white noise listening: Linear versus non-linear models. *Biomed Imaging Interv J.* 8(2): e13

Win Mar Jalaluddin @ Salmah, Ahmad Helmy Abdul Karim, Munirah Che Abdullah, Shafie Mohd Abdullah, Siti Afidah, Wan Nazyrah Abdul Halim, Alwani Liyana Ahmad, Nor Safira Elaina Mohd Noor, **Aini Ismafairus Abd Hamid**, Hoshiang Chueh. 2012. Letter to the editor: a new start with fMRI. *Malaysian J Med Sci.* 19(2): 96-97.

**Aini Ismafairus Abd Hamid**, Ahmad Nazlim Yusoff, Siti Zamratol-Mai Sarah Mukari, Mazlyfarina Mohamad. 2011. Brain activation during addition and subtraction task in-noise and in-quiet. *Malaysian J Med Sci.* 18(2): 3-15.

Ahmad Nazlim Yusoff, Mazlyfarina Mohamad, Khairiah Abdul Hamid, **Aini Ismafairus Abd Hamid**, Hanani Abdul Manan, Mohd Harith Hashim. 2010. Activation characteristics of the primary motor (M1) and supplementary motor area (SMA) during robust unilateral finger tapping task. *Malaysian Journal of Health Sciences* 8(2): 43 – 49.

Ahmad Nazlim Yusoff, Mazlyfarina Mohamad, **Aini Ismafairus Abd Hamid**, Wan Ahmad Kamil Wan Abdullah, Mohd Harith Hashim, Nurul Zafirah Zulkifli. 2010. Functional specialisation and effective connectivity in cerebral motor cortices: An fMRI study on seven right handed female subjects. *Malaysian Journal of Medicine and Health Sciences* 6(2): 71 – 92.



Ahmad Nazlim Yusoff, Mazlyfarina Mohamad, Khairiah Abdul Hamid, ***Aini Ismafairus Abd Hamid***, Hanani Abdul Manan, Mohd Harith Hashim. 2010. Intrinsic Couplings between the primary motor area and supplementary motor areas during unilateral finger tapping task. *ASM Science Journal*. 4(2): 158-172.

***Aini Ismafairus Abd Hamid***, Ahmad Nazlim Yusoff, Siti Zamratol-Mai Sarah Mukari & Mazlyfarina Mohamad, Hanani Abdul Manan, Khairiah Abdul Hamid. Modeling brain responses in an arithmetic working memory task. *AIP Conference Proceeding*. 1250 (1): 520-523.

Khairiah Abdul Hamid, Ahmad Nazlim Yusoff, Mazlyfarina Mohamad, ***Aini Ismafairus Abd Hamid***, Hanani Abdul Manan. Modeling brain responses in an arithmetic working memory task. *AIP Conference Proceeding*. 1250 (1): 389-392.

\*Publication related to this thesis.

